SOIL MECHANICS FUNDAMENTALS

Isao Ishibashi • Hemanta Hazarika

CRC Press
Taylor & Francis Group

SOIL MECHANICS FUNDAMENTALS

SOIL MECHANICS FUNDAMENTALS

Isao Ishibashi, Ph.D., P.E.
Old Dominion University, Norfolk, VA, USA

Hemanta Hazarika, D. Eng.
Kyushu University, Fukuoka, Japan

CRC Press
Taylor & Francis Group
Boca Raton London New York

CRC Press is an imprint of the
Taylor & Francis Group, an **informa** business

CRC Press
Taylor & Francis Group
6000 Broken Sound Parkway NW, Suite 300
Boca Raton, FL 33487-2742

Version Date: 20140124

International Standard Book Number-13: 978-1-4398-9125-4 (eBook - PDF)

Dedication

To our parents and families

Contents

Preface

Soil Mechanics Fundamentals is written with the intention of providing a very basic, yet essential concept of soil mechanics to students and engineers who are learning the fundamentals of soil mechanics for the first time. This book is meant mainly for college students who have completed key engineering science courses such as basic calculus, physics, chemistry, statics, mechanics of solids, and engineering materials and are ready to enter into one of the specialty areas of civil, architectural, and **geotechnical engineering**. This book is intended to provide a thorough, fundamental knowledge of soil mechanics in a simple and yet comprehensive way, based on the students' knowledge of the basic engineering sciences. Special emphasis is placed on giving the reader an understanding of ***what soil is***, ***how it behaves***, ***why it behaves that way***, and ***what the engineering significance is of such behavior***.

There are many books on soil mechanics, geotechnical engineering, and the foundation engineering field. Through our experience in teaching introductory soil mechanics courses to college students for more than 20 years, we have come to realize that most of these textbooks are either lacking comprehensive explanations of soil behavior or contain massive information without clear and organized contents. We always felt the need for a better introductory textbook for our students. For us, the ideal first textbook on soil mechanics should be presented on a firm basis of the knowledge of the engineering sciences. Firstly, the varied behavior of soils shall be well explained, based on mathematics, physics, and chemistry in a simple and yet comprehensive way. Secondly, the rather complex phenomena of soil mechanics shall be better organized and presented in a systematic way with a smooth flow of information. Lastly, students who have finished the first course of soil mechanics shall be ready to apply the learned concepts into field applications such as foundation engineering with a full comprehension of the fundamentals of soil behavior. In other words, students shall not simply memorize equations and numbers, but also understand why and how soil mechanics works. We believe that only then students and engineers can confidently face challenging situations in well-thought-out, logical, and innovative ways.

This book was written in such a way that the above ideal introduction of soil mechanics concepts could be approached as closely and as smoothly as possible. For example, plasticity of soils is rather easily understood after learning clay minerals and the interactions of clay and water. Similarly, quick sand phenomenon in front of sheet pile and heaving at the bottom of excavation come after flow of water and effective stress concepts. Also, Mohr's circle is presented just before the shear strength and the lateral earth pressure theory. At the same time, we intentionally avoided including too much information in each subject area. The same goes for the presentation of equations, too. There are always exceptions and many empirical correlations available in the field of soil mechanics. However, this book includes only the essential ones to emphasize the importance of fundamentals.

To summarize, this book is not meant to cover the full spectrum of the geotechnical engineering discipline, but rather to provide the simplest yet most comprehensive first textbook in soil mechanics for students and engineers in the field of civil engineering as well as architecture to understand what is soil, how it works, and why it works that way.

Isao Ishibashi
Hemanta Hazarika
2010

The Authors

Dr. Isao Ishibashi is professor in the department of Civil and Environmental Engineering, Old Dominion University, Norfolk, Virginia. He was born in Japan, where he obtained bachelor's and master's degrees from Nagoya University. After earning his Ph.D. from the University of Washington, Seattle, he taught and was on the research faculty at the University of Washington and Cornell University before moving to Old Dominion University in 1986. Professor Ishibashi has been involved in research in many areas such as soil liquefaction, dynamic soil properties, and static and dynamic earth pressures, as well as seismic water pressure, granular mechanics, slope stability, used tire application to embankment, and many others in geotechnical and earthquake engineering areas. He is the author or co-author of more than 100 published technical papers in journals and proceedings in these areas. He is a member of ASCE, ISSMFE, ASTM, EERI, and JGS.

Dr. Hemanta Hazarika is professor in the department of Civil and Structural Engineering, Kyushu University, Fukuoka, Japan. Born in India, Professor Hazarika obtained his Bachelor of Technology degree in Civil Engineering from Indian Institute of Technology (IIT), Madras, India and his Ph. D. in Geotechnical Engineering from Nagoya University, Nagoya, Japan. Before moving to his present position, he served few years as a practicing engineer in industry as well as several years in teaching and research in academia and public sector research institute in Japan. Professor Hazarika's present research activities include Soil-Structure Interaction, Seismic Stability of Soil-Structure, Ground Improvement Geosystem, Applications of Recycled Waste and Lightweight Geomaterials, and Stability of Cut Slopes, Landslides and Their Protection. Professor Hazarika has more than 100 technical publications in reputed international journals, proceedings of international conferences, and symposia, including contributed chapters in several books. He is also credited as editor of two books in his research fields. He served and has also been serving presently as member of various technical committees of the International Society of Soil Mechanics and Geotechnical Engineering (ISSMGE), the Japanese Geotechnical Society (JGS), the Kyushu Branch of Japanese Geotechnical Society, the Kanto Branch of Japanese Geotechnical Society, and the Japan Landslide Society. He was also secretary of the Technical Committee No. 4 (Earthquake Geotechnical Engineering and Associated Problems) of ISSMGE. He is a member of many professional societies in both Japan and abroad, such as ASCE, ISSMGE, IACMAG, IGS, JSCE, and JGS.

1 Introduction

1.1 SOIL MECHANICS AND RELATED FIELDS

Soil Mechanics is one of the engineering disciplines that deals with soils as an engineering material. Since ancient ages, engineers have been handling soils as an engineering material for various construction projects. Construction of the Egyptian pyramids, Mesopotamian ziggurats, Roman aqueducts, and China's Great Wall are few of such magnificent historical achievements. However, those ancient projects were mostly accomplished by accumulated experiences of ancient engineers. During the 18th and 19th centuries, some modern engineering theories have been employed in this field, following the development of Newtonian mechanics. Coulomb's and Rankine's lateral earth pressure theories (Chapter 12) are some examples of such theories.

The modern era of soil mechanics had to wait until 1925, when **Dr. Karl von Terzaghi** had published a book called **Erdbaumechanik** (***Terzaghi 1925***). Especially, his new concept of "effective stress," which deals with interaction with pore water, has revolutionized the mechanics of soils. The development of modern soil mechanics is due to his great contribution. He is now regarded as the **father of soil mechanics.**

Related terminologies of soil mechanics are foundation engineering, geotechnical engineering, and geoenvironmental engineering. **Foundation engineering** is the field of designing safe foundations, including building footings and retaining structures, and the construction of earth structures such as embankments, earth or rockfill dams, and safe earth slopes, etc., based on the knowledge of soil mechanics. Thus, the discipline has been called **soil mechanics and foundation engineering** for many years. The new term **geotechnical engineering** was coined around 1970 to merge rock mechanics into soil mechanics and foundation engineering, and is the

most popularly used terminology in this field at present. In the 1980s, environmental-related geotechnical engineering became a great engineering concern, and the term **geoenvironmental engineering** was created, which includes the design and construction of solid and liquid waste containment facilities, and any other environmentally related geotechnical engineering problems.

1.2 DR. KARL VON TERZAGHI

Dr. Karl von Terzaghi (Figure 1.1), the father of modern soil mechanics, was born in Prague, Austria, in 1883. At the age of 10, Terzaghi was sent to a military boarding school. He developed an interest in astronomy and geography. He entered the Technical University in Graz to study mechanical engineering in 1900. He graduated with honors in 1904. Terzaghi then fulfilled a compulsory year long military service. He returned to the university for 1 year after this and combined the study of geology with courses on subjects such as highway and railway engineering.

His first job was as a junior design engineer for a firm in Vienna. The firm was becoming more involved in the relatively new field of hydroelectric power generation, and Karl became involved in the geological problems the firm faced. He embarked on an ambitious and challenging project to construct a hydroelectric dam in Croatia and an even more chaotic project in St. Petersburg, Russia. During 6 months in Russia, he developed some novel graphical methods for the design of industrial tanks, which he submitted as a thesis for his Ph.D. at the university. His growing list of achievements began to open more opportunities to him. He then resolved to go to the United States in 1912.

There, he undertook an engineering tour of major dam construction sites in the West Coast. This was no ordinary tour, but was his opportunity to gather reports and firsthand knowledge of the problems of many different projects, and he used it to the fullest before returning to Austria in December 1913. When World War I broke out, he found himself drafted into the army. He faced combat in Serbia and witnessed

FIGURE 1.1 Karl Terzaghi at age 43. (Photo permission by EJGE.)

the fall of Belgrade. After a short stint managing an airfield, he became a professor in the Royal Ottoman College of Engineering in Istanbul (now Istanbul Technical University). He began a very productive period, in which he began his lifelong work of bringing true engineering understanding to the subject of soil as an engineering material. He set up a laboratory for measurements of the force on retaining walls. The results were first published in English in 1919 and were quickly recognized as an important new contribution to the scientific understanding of the fundamental behavior of soils.

At the end of the war, he was forced to resign his post at the university, but managed to find a new post at Robert College in Istanbul. This time he studied various experimental and quantitative aspects of the permeability of soils and was able to work out some theories to explain the observations. In 1925, he published much of this in **Erdbaumechanik** that revolutionized the field to great acclaim. It resulted in the offer of a position from the Massachusetts Institute of Technology (MIT), which he immediately accepted.

One of his first tasks in the United States was to bring his work to the attention of engineers. He entered a new phase of prolific publication, and a rapidly growing and lucrative involvement as an engineering consultant on many large-scale projects.

In 1928, Terzaghi was determined to return to Europe. He accepted a chair at the Vienna Technische Hochshule in the winter of 1929. Using Austria as his base, he traveled ceaselessly throughout Europe, consulting and lecturing, and making new professional contacts and collaborations. Terzaghi then returned to America where he gave a plenary lecture at the First International Conference on Soil Mechanics and Foundation Engineering at Harvard University in 1936. He served as the first president of International Society of Soil Mechanics and Foundation Engineering from 1936 to 1957.

He made a lecture tour of many other universities but discovered that prospects for employment were dim. He returned to Vienna in November 1936. There, was caught up in a nasty professional and political controversy. He escaped from Vienna frequently by extended consulting trips to major construction projects in England, Italy, France, Algeria, and Latvia, adding greatly to his store of practical engineering experience.

In 1938, Terzaghi immigrated to the United States and took up a post at Harvard University. Before the end of the war, he consulted on the Chicago subway system and the Newport News Shipways construction among others. He became an American citizen in March 1943. He remained as a part-timer at Harvard University until his retirement in 1953 at the mandatory age of 70. In July of the next year, he became the chairman of the consulting board for the construction of the Aswan High Dam. He resigned this post in 1959 after coming into conflict with the Russian engineers in charge of the project, but continued to consult on various hydroelectric projects, especially in British Columbia. He died in 1963.

In honor of his great contribution in the field, the American Society of Civil Engineers (ASCE) established the Karl Terzaghi Award in 1960 to an "author of outstanding contributions to knowledge in the fields of soil mechanics, subsurface and earthwork engineering, and subsurface and earthwork construction," and the Terzaghi lectures are delivered and published annually as a highest honor in the field (abbreviated and modified from Wikipedia).

The reference (***Goodman 1999***) provides a detailed biography of Dr. Karl Terzaghi and is strongly recommended for all geotechnical engineers and geologists to learn more about his great contributions and many lessons on professional practice. His contribution is throughout this book, including effective stress, consolidation, and shear strength.

1.3 UNIQUENESS OF SOILS

As this book shows, soil is a very unique material and complex in nature. The unique characteristics of soils are as follows:

1. It is not a solid continuous material, but is rather composed of three different constituents—solid (grain), water, and air—and is thus an aggregated material.
2. Particle sizes have significant influence on soil behavior from granular soil to clay.
3. The amount of water also plays a very important role in soil behavior.
4. Its stress–strain relation is not linear from the small strain levels.
5. Its pore spaces possess the capability of water flow.
6. It has time-dependant characteristics; that is, it is creep susceptible.
7. It swells when wetted or shrinks when dried.
8. It is an anisotropic material due to the particle shapes and the depositional direction under gravity.
9. It is also spatially nonhomogeneous.

To handle this unique nature, the discipline utilizes many different areas of mechanics. For the various phases, it uses solid mechanics as well as discrete mechanics. The water flow characteristics are explained by a knowledge of fluid mechanics such as Darcy's law and Bernoulli's law. Physicochemical knowledge is required to understand swell and shrinkage characteristics. Understanding its anisotropic characteristics requires a high level of knowledge in mechanics and material science. Some statistical approaches are also needed to treat the nonhomogeneity of soils.

As briefly seen earlier, soil is a very unique material, and its engineering properties vary a lot depending on the particle sizes, origins, and many other factors. Their constitutive models are not as simple as Hooke's law used in some other materials.

1.4 APPROACHES TO SOIL MECHANICS PROBLEMS

Complexity and spatial variation of soil makes the field observation and laboratory testing very significant. **Field observation** ranges from geological study of the site to soil sampling and sometimes in situ testing of properties, such as well test for permeability, vane shear test for strength determination, etc. Sampled specimens are brought back to **laboratories** for various physical and mechanical tests. The former includes the grain size test, Atterberg limits tests, specific gravity test, etc., and the latter includes a compaction test, permeability test, consolidation test, and various shear strength tests.

Based on field observations and laboratory test data, geotechnical engineers classify soils, determine design properties, and **design** safe foundations and earth structures, by fully utilizing modern soil mechanics knowledge and foundation engineering concepts. Construction companies carry out **construction** of the project according to specifications made by design engineers. Usually, design engineers monitor construction practices carefully for proper execution.

The last stage is **field monitoring** of the performance of earth structures. At present, large construction projects always come with instrumentation and performance monitoring. Simple or complex theories are available in most cases. However, those are not always perfect due to complexity of soils and variations in material properties. And thus, the monitoring and reevaluation of design based on the feedback of the data are very crucial for successful projects.

1.5 EXAMPLES OF SOIL MECHANICS PROBLEMS

Engineers have to deal with many challenging soil mechanics problems even now, as well as in the past. A few historical and interesting cases are presented in the following section.

1.5.1 Leaning Tower of Pisa

This famous building illustrates historical soil mechanics problems. The 56-m-high bell tower at Pisa, Italy, leans about 3.97° or 3.9 m at top toward the south at present. The construction of the tower started in 1173 and was completed in 1372. It was reported that the tower started to sink after the construction progressed to the third floor in 1178 and more floors were built up to accommodate for the tilt.

The lean is obviously due to uneven settlement of the foundation soil. This time-dependent settlement phenomenon is called **consolidation** settlement of clay and is discussed later in this book. In March 1990, the tower was closed to the public due to the possibility of collapse in the near future. Engineering remediation procedures were discussed to stop further leaning. The earlier attempt was made to put heavy load (800 metric ton of lead counterweight) on the north side of the tower foundation to compensate for the larger settlement on the south. A more drastic measure was taken later to extract soil mass (38 m^3) under the north side of foundation soil by angled auger holes so that the north side experienced extra settlement. In December 2001, the tower was reopened to the public and has been declared stable for at least another 300 years (Figures 1.2 and 1.3).

1.5.2 Sinking of Kansai International Airport

The first-phase construction of **Kansai International Airport** near Osaka, Japan, a human-made island, 4.5 km long and 1.1 km wide, began in 1987, and the airport became operational in 1994. It was an amazingly fast-paced construction for this magnitude. The massive earth filling at an average water depth of 12 m on Osaka Bay required 208,000,000 m^3 of reclaimed soil and rock (82 times the volume of great Giza's pyramid). The filling materials were brought from three excavated nearby

FIGURE 1.2 Leaning Tower of Pisa.

FIGURE 1.3 Lead counterweight.

mountains. Geotechnical engineers anticipated quite a large consolidation settlement due to this massive fill over a large area on soft bay foundation soil. Settlement immediately started, was carefully monitored, and results were compared with computed values. It sank 50 cm in 1994; settlement was reduced to 20 cm in 1999, and was 9 cm in 2006. Originally, engineers estimated 12 m total settlement in 50 years, but, in fact, it had already settled 11.5 m by 2001. Because of anticipated uneven ground settlement, the terminal building was equipped with jacks in each column so

FIGURE 1.4 Kansai International Airport during Phase-II construction in 2002. (Photo courtesy by Kansai International Airport Land Development Co.)

that uneven settlement could be adjusted not to have extra stress on individual columns. It is still sinking. Amazingly, the phase II runway, the second island on deeper water, has been constructed (Figure 1.4 in 2002 and the cover page picture in 2003) and opened to operation in 2007. This is a magnificent megaconstruction project in recent years with very challenging geotechnical engineering problems.

1.5.3 Liquefaction—Sand Becomes Liquid during Earthquake

Can you believe that soil transforms into liquid? Yes, it does. During the 1964 Niigata Earthquake, Japan, with a Richter magnitude of 7.5, apartment buildings lost their foundation support and sank and tilted (Figure 1.5). Foundation soil was transformed into viscous liquid due to earthquake vibration. Similar phenomenon was

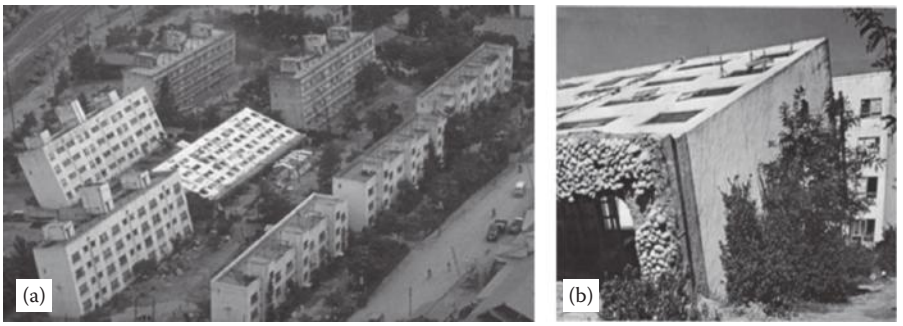

FIGURE 1.5 Building tilt and settlement due to liquefaction during 1964 Niigata Earthquake. ([a] Photo by Joseph Penzien, Courtesy of National Information Service for Earthquake Engineering, EERC, University of California, Berkeley, [b] Courtesy of Yoshiaki Yoshimi.)

also observed in the Alaska earthquake that occurred in August 1964. This phenomenon is called **soil liquefaction**. Soil liquefaction describes the behavior of soils that, when cyclically loaded, suddenly go from a solid state to a liquefied state, or having the consistency of a heavy liquid and cannot support foundation load any more. Liquefaction is more likely to occur in loose to medium dense saturated granular soils with poor drainage, such as sand or silty sand. During loading, usually cyclic undrained loading—for example, earthquake loading—loose sand tends to decrease in volume, which produces an increase in its pore water pressure and consequently a decrease in shear strength, that is, reduction in effective stress (Chapter 7).

Liquefaction is one of the major geotechnical engineering problems during earthquakes. It causes the settlement and tilting of buildings, catastrophic slope failures, and massive lateral movement of the ground. Although this topic is not covered in this book, it is one of the major topics in advanced soil mechanics field, **soil dynamics** or **earthquake engineering**.

1.6 ORGANIZATION OF CONTENTS

Chapters and contents are carefully placed in an order so that the understanding level of the subject matters increases gradually chapter by chapter. It is, therefore, recommended to follow the sequence of the materials presented.

After the introductory **Chapter 1** about soil mechanics, **Chapter 2** (Physical Properties of Soils) deals with the origin and the description of soils. The major terms used in soil mechanics are defined by using the three-phase diagram. Soil shapes and gradations are discussed also in Chapter 2. **Chapter 3** (Clays and Their Behavior) presents unique characteristics of clays from their mineral origins, sizes, shapes, electrical properties, behavior in water, and interaction among particles. Based on this knowledge, its plastic behavior, swelling, and shrinkage properties, sensitivity, and quick clays are discussed.

Based on the knowledge gained in Chapters 2 and 3, soil classifications by Unified Soil Classification System (ASTM) and the AASHTO are presented in **Chapter 4**. **Chapter 5** handles laboratory and field compaction techniques, including description of the relative density and the CBR (California Bearing Ratio) method.

Chapter 6 presents the flow of water through soils. Definitions of various hydraulic heads and the coefficient of permeability are presented, as well as the two-dimensional flow net technique, introduced as a simple one-dimensional water flow mechanism without using the Laplace equation. Finally, a systematic method to compute the boundary water pressures is demonstrated.

In **Chapter 7,** the concept of effective stress and its applications to various important soil mechanics problems, including capillary rise, quick sand, and heave at the bottom of excavation, are discussed. The concept is later used in consolidation theory (Chapter 9) and shear strength (Chapter 11).

Chapter 8 is a preparation chapter to Chapter 9 (Settlements). Stress increments in a soil mass due to various types of footing load on ground are presented. Most of those solutions are based on Boussinesq's elastic solution, and those are needed as the major source of consolidation settlements in Chapter 9.

In **Chapter 9**, Terzaghi's one-dimensional consolidation theory and its application are presented. To simplify the discussions, the consolidation problems are categorized into two parts—"how soon" (rate) problems and "how much" (amount of final settlement) problems—so that readers can clearly avoid confusion while handling the thickness (H or 2H) of the clay layer.

Chapter 10 deals with Mohr's circle, which is utilized in chapters relating to shear strength and lateral earth pressure. In particular, a clear definition of the shear stress sign convention is made, so that the concept of the pole of Mohr's circle (the origin of the planes) can be utilized effectively without any chance of mistakes.

Chapter 11 is related to the shear strength of soils. Failure criteria are introduced, and laboratory as well as field shear strength determination techniques are presented. Clear definitions are made on consolidated, unconsolidated, drained, and undrained shear strength parameters, and usages of those different shear strength parameters are critically evaluated.

Chapters 12 and **13** are introductory chapters to foundation engineering. In Chapter 12, at-rest earth pressure and the classical Rankine and Coulomb active and passive pressure theories are presented. Those classic theories are critically reviewed in terms of their assumptions and limitations, and appropriate applications of those theories into practice are discussed. In Chapter 13, fundamental bearing capacity theories are introduced as a gateway to foundation design practice.

In most of the chapters, many **exercise problems** were carefully selected for readers to practice use of the learned concepts. Spreadsheet techniques are often employed in those exercise problems. At the end of each chapter, many **problems** are selected, and those can be utilized by students to further exercise their skills in problem solving, or they could be presented as homework assignments by instructors. Numerical values of solutions for the problem sections are shown at the end of the book for the convenience of self-studying readers.

Throughout the book, key words are highlighted with **bold letters** and those also appear in the **subject index** at the end of the book; thus, readers can easily search the locations of those key words in the main section of the book.

Some sentences are highlighted with bold and italic letters, emphasizing the importance of the concepts.

References appear in ***bold and italic letters*** in the text and are listed at the end of each chapter and in the **author index** at the end of the book.

This book basically uses the **SI units** except the ones cited from original references. The key **unit conventions** are also summarized at the end of the book.

REFERENCES

Goodman, R. E. (1999), *Karl Terzaghi—The Engineer as Artist*, ASCE Press, 340 pp.
Terzaghi, K. (1925), *Erdbaumechanik*, Franz Deuticke.

2 Physical Properties of Soils

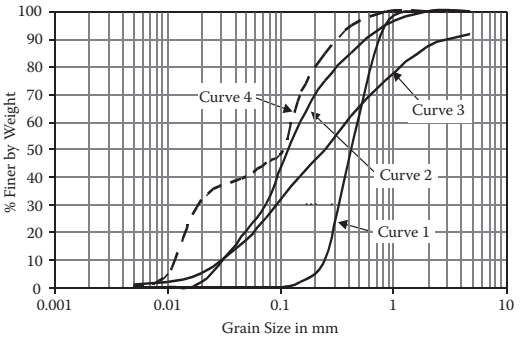

2.1 INTRODUCTION

In this chapter, "What is soil?" and "How is it formed?" are presented first. Key terms used in soil mechanics are then defined by using the three-phase diagram (i.e., solid, water, and air phases). Lastly, soil grain shapes, sizes, and grain size distribution are discussed. Laboratory methods to determine the grain size distribution are presented.

2.2 ORIGIN OF SOILS

Soil can be defined as ***an assemblage of nonmetallic solid particles (mineral grains)***, and it consists of three phases: **solid, liquid (water), and gas (air)**. Commonly used terms such as gravel, sand, silt, and clay are the names of soils based on their particle grain sizes. Quartz, mica, feldspar, etc., are based on their crystal names.

The rock cycle in Figure 2.1 illustrates the origins of a variety of soils on the earth. Most original rock starts forming from molten magma (liquid) in the deep earth (to the depth of 2885 km from the base of crust). Magma cools down and solidifies when it approaches the earth's crust (about 4–6 km thick under the deep oceans and 25–60 km thick on the continent) due to tectonic and volcanic activities. Thus, **igneous rocks** are formed such as basalt, granite, pumice, olivine, etc. The next process is **weathering**. Solid igneous rocks on the earth surface are subjected

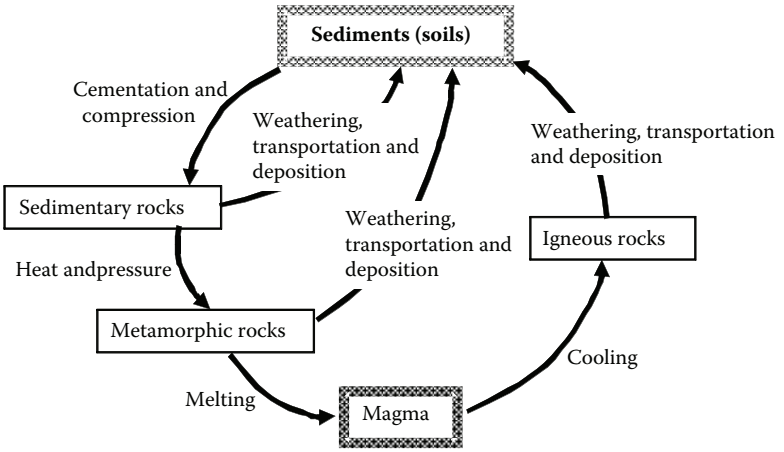

FIGURE 2.1 Rock cycle.

to all kinds of attacks in the environment such as erosion by water and air, thermal expansion and contraction, intrusion of plant roots in the cracks, icing on the cracks, chemical attack on the surface, etc. The surface of igneous rocks is weathered and broken down to smaller sizes. The next process in the cycle is **transportation**. Broken fragments of rock are displaced by means of water run, glacier, and sometimes by wind, and they eventually settle down at a certain distance from the original location (**deposition**). During the transportation process, particles further suffer physical and chemical attacks, and they become smaller and rounder. Deposited materials (**sediments**) are one type of soils. Thus, this type of soil originates from igneous rocks, and particles have crystals similar to those in igneous rocks.

Deposited soils on many occasions are subjected to many geological years of cementation and compression that transform those to **sedimentary rocks**, such as sandstone, shale, limestone, dolomite, and many others. Rocks might go through further transformation due to high heat and pressure in a deeper earth but without melting. This process is called **metamorphism,** and **metamorphic rocks** are formed. Transformation of marble from limestone by metamorphism is a good example of this. Metamorphic rocks could be melted into magma to complete a rock cycle when they go more deeply in the earth.

Sedimentary rocks and metamorphic rocks are also subjected to weathering, transportation, and deposition processes to form sediments (soils) as shown in Figure 2.1. Thus, those rocks can become the origins of soil particles in addition to the ones from igneous rocks. All the preceding processes, including origin of soils, weathering, transportation, and deposition, make different types of soil in terms of particle sizes, shapes, mineral compositions, etc. Note that the particle size becomes smaller and smaller, and thus it yields a larger surface area per the same weight of soils. Smaller particles with larger surface area will be more vulnerable to chemical attack, and their original crystal structures may be changed to form different clay minerals as will be discussed in Chapter 3.

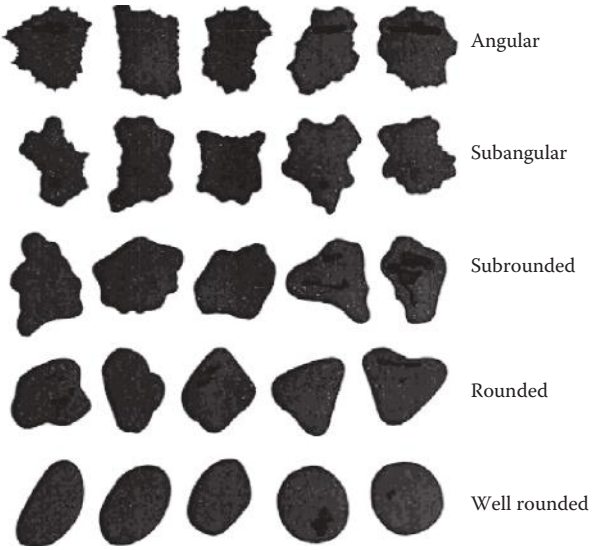

FIGURE 2.2 Soil's angularity (Müller, G. (1967). Methods in Sedimentary Petrology, Hafner.).

2.3 SOIL PARTICLE SHAPES

Weathering and transportation processes produce a variety of particle shapes from angular to rounded as shown in Figure 2.2 (***Müller 1967***). Since soil is an assemblage of particles, interlocking of those particles and their contact mechanism, in particular, for larger particles, determine many important mechanical properties of soils such as strength, rigidity, permeability, and compaction. For example, angular particle assembly will give more resistance to sliding deformation (higher rigidity and strength) as compared to round particle assembly. Soil **angularity** can be determined by comparing particle shape (under a microscope, if needed) with the sample shapes shown in Figure 2.2.

For smaller particle assemblies like in clay minerals, particle shapes are much flatter and sometimes flaky as shown in Figure 2.3, as an example. In those smaller particle soils, short-range interparticle forces play an important role to determine the behavior of soils. The details of clay minerals will be discussed in Chapter 3.

2.4 DEFINITIONS OF TERMS WITH THREE-PHASE DIAGRAM

Soil is an assemblage of particles, and, thus, there are separate volumes of solid and void. The voids are occupied with air and water. To define many key parameters in soil mechanics, soil assemblage with spaces of solid (grain) and void (air and water) is modeled into a **three-phase diagram,** as shown in Figure 2.4. Volume side and weight side are drawn in three phases (solid, water, and air), and individual components are designated as V_s, V_w, V_a and W_s, W_w, W_a. The total volume and the total weight are also designated as V and W, respectively. The volume of void V_v is the volume of

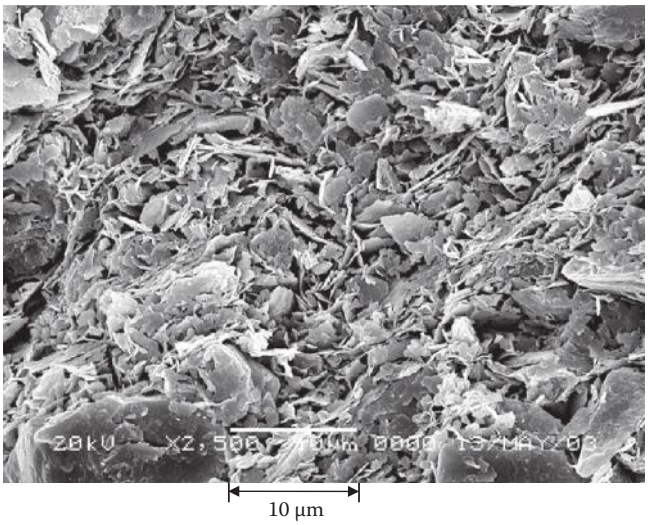

FIGURE 2.3 Scanned electron microscope (SEM) picture of clay particle assembly. (Hai-Phong (Vietnam) clay: 50% Kaolinite and 50% Illite.) (From ***Watabe et al. 2004***. Proceedings of the 2nd International Conference on Site Characterization, Porto, pp. 1765–1772; Photo courtesy of Y. Watabe.)

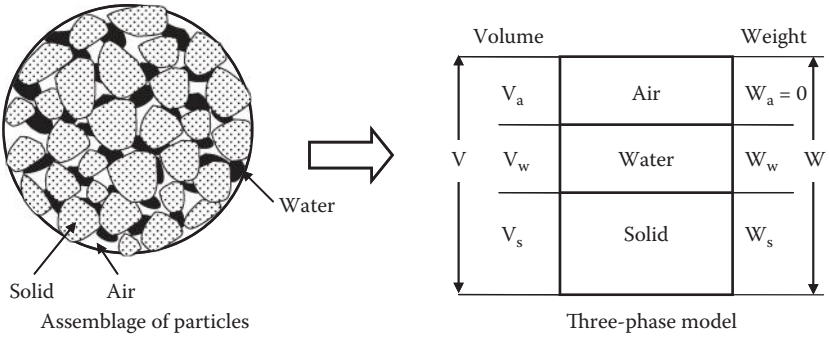

FIGURE 2.4 Three-phase diagram of soil.

water V_w plus the volume of air V_a. Note that the weight of air W_a is assigned as zero since it is negligible relative to other weights of the element. The following definitions are made based on the three-phase diagram:

$$\textbf{Porosity}: \; n = \frac{\text{volume of void}}{\text{total volume}} = \frac{V_v}{V} = \frac{V_a + V_w}{V} \tag{2.1}$$

$$\textbf{Void ratio}: \; e = \frac{\text{volume of void}}{\text{volume of solid}} = \frac{V_v}{V_s} \tag{2.2}$$

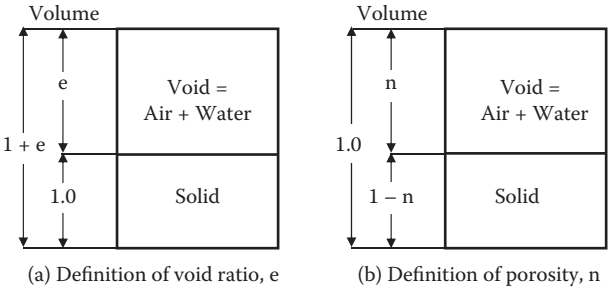

FIGURE 2.5 Relationship between porosity, n, and void ratio, e.

Referring to Figure 2.5 and applying the definitions of n and e to Figure 2.5a and b, respectively, the following relationships are obtained:

$$n = \frac{e}{1+e} \qquad \text{or} \qquad e = \frac{n}{1-n} \tag{2.3}$$

Void ratio ranges from around 0.3 for **glacial tills** (highly compacted mixture of gravel to clay under glacial load) to 1.4 for very soft clay. For **organic clay,** the value could go to around 3.0 or more as a special case. Corresponding (e = 0.3 to 1.4) porosity, n values are about 0.23 to 0.58, respectively.

$$\textbf{Water content}:\ w = \frac{\text{weight of water}}{\text{weight of solid}} = \frac{W_w}{W_s}\ (\times 100\%) \tag{2.4}$$

The water content for completely **dry soil** is 0% and normally up to several tens % for **fully saturated** soils. However, the value may go up to more than 200% for highly open-structured clay formed under marine environment and for **organic soils** as unusual cases.

$$\textbf{Degree of saturation}:\ S = \frac{\text{volume of water}}{\text{volume of void}} = \frac{V_w}{V_v}\ (\times 100\%) \tag{2.5}$$

S value changes from 0% for completely **dry soil** condition to 100% for **fully saturated** soil. The soils with $0 < S < 100\%$ are called **partially saturated** soils. Note that in many occasions, "saturated" soils are interpreted as "fully saturated" without spelling out "fully."

$$\textbf{Specific gravity}:\ G_S = \frac{\text{unit weight of solid}}{\text{unit weight of water}} = \frac{W_s/V_s}{\gamma_w} \tag{2.6}$$

where γ_w is the unit weight of water and is 9.81 kN/m^3 or 62.4 lb/ft^3. Most soils have a rather narrow range of G_s value: 2.65 to 2.70. This implies that solid particle is about 2.65 to 2.70 times heavier than the weight of water for the same volume. If specific

gravity test was not performed during the initial evaluation of geotechnical engineering problems, assuming G_s as a value between 2.65 or 2.70 would not provide a major error in the results.

There are several definitions of **unit weights** of soil:

$$\textbf{Total unit weight: } \gamma_t = \frac{\text{total weight}}{\text{total volume}} = \frac{W}{V} = \frac{W_s + W_w}{V_s + V_w + V_a} \tag{2.7}$$

$$\textbf{Dry unit weight: } \gamma_d = \frac{\text{weight of solid}}{\text{total volume}} = \frac{W_s}{V} \tag{2.8}$$

Note that $\boldsymbol{\gamma_d}$ ***is not necessarily physically dry unit weight of soils, but it rather is treated as a case by mathematically removing water while maintaining constant total volume*** **V** ***without shrinkage***, which takes place during the physical drying process. From Exercise 2.1, the following relation is obtained:

$$\gamma_t = \frac{(1+w)G_s}{1+e}\gamma_w = \frac{G_s + Se}{1+e}\gamma_w \tag{2.9}$$

The dry unit weight γ_d can be obtained by substituting S = 0 in the last term in Equation 2.9. Thus, for mathematically dry soil, the following equation is obtained:

$$\gamma_t = (1+w)\frac{G_s\gamma_w}{1+e} = (1+w)\gamma_d \quad \text{or} \quad \gamma_d = \frac{G_s\gamma_w}{1+e} = \frac{\gamma_t}{1+w} \tag{2.10}$$

This relationship is conveniently used to compare the effectiveness of compaction by the dry unit weight in **compaction test** analysis (Chapter 5). ***The total unit weight does not measure the effectiveness of compaction directly since the weight of water in void will increase the total unit weight. In either cases, the void ratio increases (less compaction) or decreases (more compaction)***.

The last important definition is the **submerged unit weight γ'** (or **buoyant unit weight**), which is the soil's unit weight under water.

$$\gamma' = \gamma_t - \gamma_w = \frac{G_s + Se}{1+e}\gamma_w - \gamma_w = \frac{G_s - 1 - e(1-S)}{1+e}\gamma_w \text{ (for } \textbf{partially saturated}\text{)} \tag{2.11}$$

In the last-term expression in Equation 2.11, the degree of saturation S could be other than 1.0 (full saturated) even though soils are under water. It is possible shortly after soils were submerged in water. However, eventually, soils under the water table will be fully saturated (S = 1.0) and thus:

$$\gamma' = \gamma_t - \gamma_w = \frac{G_s + e}{1+e}\gamma_w - \gamma_w = \frac{G_s - 1}{1+e}\gamma_w \text{ (for } \textbf{fully saturated}\text{)} \tag{2.12}$$

As will be discussed in detail in Chapter 7 (effective stress), stresses in a soil mass due to its own weight are given by the total unit weight γ_t times the thickness of the soil when soil is above the ground water table, while it is given by submerged unit weight γ' times the thickness when soil is below the ground water table. A range of γ_t is about 15 to 20 kN/m^3 (or 90 to 130 lb/ft^3). Since γ_w is 9.81 kN/m^3 (or 62.4 lb/ft^3), γ' becomes about a half of γ_t. This is a significant reduction in the stress induced in soil mass.

Exercise 2.1

Using the three-phase diagram for a general soil, derive a formula to determine γ_t from the known values of S, e, w, and G_s.

Solution:

Referring to Figure 2.6, first assume that $W_s = 1$, then $W_w = w$

$$\text{From the definition, } G_s = \frac{W_s}{V_s}/\gamma_w, \quad \text{thus } V_s = \frac{W_s}{G_s\gamma_w} = \frac{1}{G_s\gamma_w} \tag{2.13}$$

$$\text{From the definition, } \gamma_w = \frac{W_w}{V_w}, \quad \text{thus } V_w = \frac{W_w}{\gamma_w} = \frac{w}{\gamma_w} \tag{2.14}$$

$$\text{From the definition, } S = \frac{V_w}{V_a + V_w}, \text{thus } V_a = \frac{(1-S)V_w}{S} = \frac{(1-S)w}{S\gamma_w} \tag{2.15}$$

$$\text{From the definition, } e = \frac{V_a + V_w}{V_s} = \frac{V_a + V_w}{1/G_s\gamma_w}, \text{ thus } V_a + V_w = \frac{e}{G_s\gamma_w} \tag{2.16}$$

From Equations 2.14 through 2.16,

$$S = \frac{V_w}{V_a + V_w} = \frac{w/\gamma_w}{e/G_s\gamma_w} = \frac{wG_s}{e}, \quad \text{then} \quad Se = wG_s \tag{2.17}$$

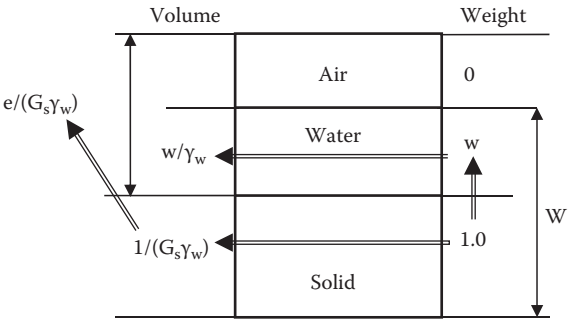

FIGURE 2.6 Exercise 2.1.

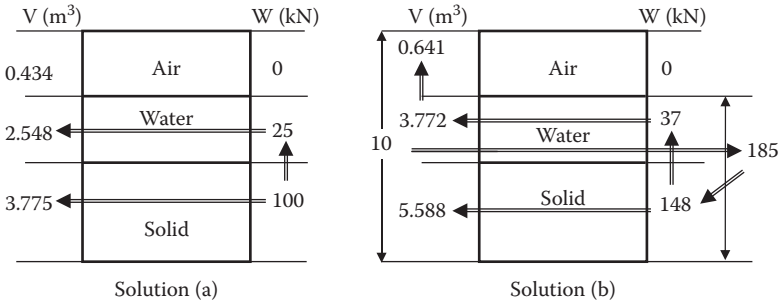

FIGURE 2.7 Exercise 2.2.

Now, using Equations 2.13 through 2.17 and applying the definition of γ_t ,

$$\gamma_t = \frac{W_s + W_w}{V_a + V_w + V_s} = \frac{1+w}{e/G_s\gamma_w + 1/G_s\gamma_w} = \frac{(1+w)G_s}{1+e}\gamma_w = \frac{G_s + wG_s}{1+e}\gamma_w = \frac{G_s + Se}{1+e}\gamma_w \tag{2.18}$$

In Exercise 2.1, the weight of solid W_s was first assumed as 1.0, and then other components in the three phases were computed. ***Any one component can be assumed with any value such as 100 or 1000*** since all definitions of w, S, e, n, γ_t, etc., are the ratios of components, and thus the same results can be obtained. Note that $\mathbf{G_s}$ ***and*** $\boldsymbol{\gamma_w}$ ***always work as key bridge values to connect the weight side and the volume side*** as shown in Exercise 2.1. Exercise 2.2 demonstrates that the two different initial assumptions yield the same solutions.

Exercise 2.2

For a given soil, w = 25% and γ_t = 18.5 kN/m³ are measured. Determine void ratio e and degree of saturation S. Assume that G_s is 2.70.

Solution (a):

First assume W_s = 100 kN as shown in Figure 2.7a. Then, $W_w = 100 \times 0.25 = 25$ kN.

Calculate $V_s = W_s/G_s\gamma_w = 100/(2.7 \times 9.81) = 3.775$ m³.

Calculate $V_w = W_w/\gamma_w = 25/9.81 = 2.548$ m³.

Since $\gamma_t = 18.5$ kN/m³ $= (W_s + W_a)/(V_s + V_w + V_a) = (100 + 25)/(3.775 + 2.548 + V_a)$, thus, $V_a = 0.434$ m³.

Now, all components in the three phases are obtained as shown in Figure 2.7a and,

$e = (V_w + V_a)/V_s = (2.548 + 0.434)/3.775 =$ **0.790** ←

$S = V_w/(V_w + V_a) = 2.548/(2.548 + 0.434) = 0.854 =$ **85.4%**. ←

Solution (b):

First assume $V = 10\ m^3$ as seen in Figure 2.7b.

From $W_s + W_w = W_s + wW_s = (1 + w)W_s = V\gamma_t = 10 \times 18.5 = 1\ 85\ kN$,

$W_s = 185/(1 + 0.25) = 148\ kN$, and $W_w = 185 - 148 = 37\ kN$.

Using Gs as a bridge value, $V_s = W_s/G_s\gamma_w = 148/(2.7 \times 9.81) = 5.588\ m^3$.

Using γ_w as a bridge value, $V_w = W_w/\gamma_w = 37/9.81 = 3.772\ m^3$.

Thus $V_a = V - (V_s + V_w) = 10 - (5.588 - 3.772) = 0.641\ m^3$.

Now, all components in the three phase are obtained as shown in Figure 2.7b and,

$e = (V_w + V_a)/V_s = (3.772 + 0.641)/5.588 =$ **0.789.** ←

$S = V_w/(V_w + V_a) = 3.772/(3.772 + 0.641) = 0.855 =$ **85.5%**. ←

In Solutions (a) and (b) of Exercise 2.2, the same results were obtained even though all components had different values. First assumed values ($W_s = 100$ kN or $V = 10\ m^3$ in the example) are arbitrary so that any convenient number can be assumed.

The three-phase diagram is also a convenient tool to handle many real-world problems that relate soils weight, water content, and volume. Exercise 2.3 shows one such problem.

Exercise 2.3

In a fill section of a construction site, 1500 m^3 of moist compacted soils is required. The design water content of the fill is 15%, and the design unit weight of the compacted soil is 18.5 kN/m^3. Necessary soil is brought from a borrow site, with the soil having 12% natural water content, 17.5 kN/m^3 wet unit weight of the soil, and $G_s = 2.65$. How much (in cubic meters) of the borrow material is required to fill the construction fill section? And how heavy is it?

Solution:

Draw three-phase diagrams of the fill site and the borrow site in Figure 2.8a and b, respectively.

First for the fill site in Figure 2.8a, $V = 1500\ m^3$ so that $W_s + W_w = V\gamma_t = 1500 \times 18.5 = 27750$ kN.

$W_s + W_w = (1 + w)W_s = 27750$ kN, so that $W_s = 27750/(1 + 0.15) = 24130$ kN.

This much solid weight of the soil is required at the fill site.

At the borrow site, the same solid weight 24130 kN is needed as shown in Figure 2.8b.

Thus, $W_w = wW_s = 0.12 \times 24130 = 2897$ kN, and $W_s + W_w = 24130 + 2897 =$ **27026 kN**. ←

Since $\gamma_t = (W_s + W_w)/V = 17.5\ kN/m^3$, $V = 27026/17.5 =$ **1545 m^3**. ←

Thus, 1545 m^3 of the borrow material is needed for the project carrying a total weight of 27026 kN.

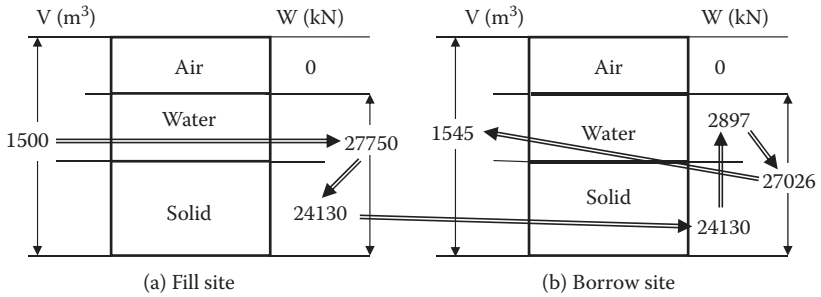

FIGURE 2.8 Exercise 2.3.

2.5 PARTICLE SIZE AND GRADATION

Particle size plays a dominant role in distinguishing soil types. Commonly used names of soil such as **gravel**, **sand**, **silt**, and **clay** are based on their grain sizes. Figure 2.9 shows those names with ranges of grain size. The boundary particle sizes are slightly different, depending on the standards. two mm in **AASHTO** or 4.75 mm in **USCS (Unified Soil Classification System)** or in **ASTM Soil Classification System** are the boundary particle size between gravel and sand. seventy five μm (0.075 mm) is the boundary between sand and silt in both standards, and 5 μm is the one between silt and clay in AASHTO. In USCS (ASTM), materials that are finer than 75 μm are called "**fine**." Note that in some other standard such as British soil classification (***BS8004, 1986***), 2 μm is used as the boundary between silt and clay.

In order to separate grain sizes of soil assembly, a set of sieves is used for larger grain sizes. In particular, the boundary of 75 μm grain size is important; 75 μm is the opening size of No. 200 sieve, which is practically the smallest size of sieves. Particles that are smaller than No. 200 sieve (**minus No. 200 material**) cannot be mechanically sieved due to developed static electricity on the surface of particles. If water is poured on dry minus No. 200 material, particles are easily suspended in the water and the water gets dirty. That is a good indication of an existence of minus No. 200 or "fine" material in it. Gravel and sand are called **cohesionless (granular) soils,**

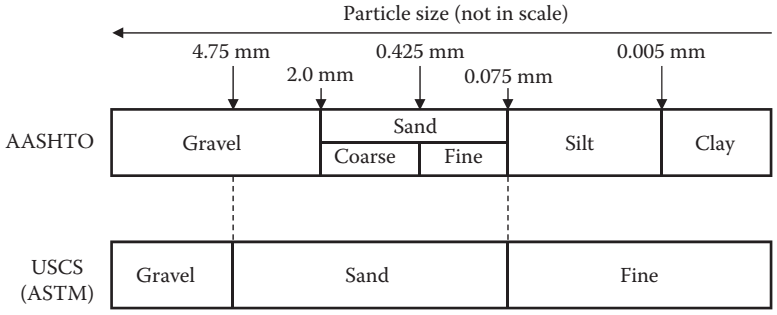

FIGURE 2.9 Soil's names with grain sizes.

TABLE 2.1
U.S. Standard Sieve Numbers and Openings

U.S. Standard Sieve No.	Opening in mm
4	4.75
10	2.00
20	0.85
40	0.425
60	0.25
100	0.15
140	0.106
200	0.075

and clay is called **cohesive soils**. Silt is a transitional material between granular and cohesive soils. Those two soil groups have distinguished differences in engineering behavior. Granular soils' resistance upon shearing mostly comes from their surface friction and interlocking mechanisms. On the other hand, cohesive soils' resistance comes from short-range particle-to-particle interactive forces, as will be discussed in Chapter 3. The former is less compressive than the latter, and the former has much higher capacity of water flow through it than the latter, etc.

To identify grain size characteristics of soils, **grain size distribution curve** is developed. First, **sieve analysis** is conducted. A variety of sieves with different openings are stacked, with the largest opening sieve on the top and smaller on the lower sections. The smallest (usually No. 200 sieve) is placed at the second from the bottom and a pan with no opening at the bottom. Table 2.1 shows **U.S. Standard Sieve Numbers** and their corresponding openings.

Note that the sieve number is designated as the number of meshes in a 1 in. (25.4 mm) spacing. For example, No. 4 sieve's opening is calculated from 1 in. (25.4 mm) divided by 4 minus 4 wire thicknesses. Oven-dried specimen (ASTM D-422) with a known weight is placed on the top of the sieve stack, and a cover is placed on the top of the sieve. The whole stack is vibrated vertically and horizontally until no more weight change in each sieve occurs (less than 1% change in 1 min shaking). Weights of soils retained on each sieve are carefully measured on a balance. Confirm that the initial weight and the summation of weights on each sieve after sieving are nearly equal.

Table 2.2 shows an example computation of the sieve analysis. The values in Column C of Table 2.2 are measured during the experiment, and the rests are completed by a spreadsheet setup as seen at the bottom of the table. The percent (%) finer implies that the percentage of the soil passes the corresponding sieve or that the percentage of soil weight is finer than the corresponding sieve opening. For example, in F(6) data of Table 2.2, 63.6 implies that 63.6% of the soil passes through a No. 100 sieve, or 63.6% of soil is finer than 0.15 mm.

When a relatively large percent passing through No. 200 sieve (e.g., more than 10% as a guideline) is obtained from the sieve analysis, a **hydrometer analysis** is conducted. **A hydrometer** is a float with a bulb in the middle as seen in Figure 2.10.

TABLE 2.2
Example Computation of Sieve Analysis

	A	B	C	D	E	F
i	U.S. Standard Sieve No.	Opening mm	Weight Retained, gf	% Weight Retained	% Cumulative Retained	% Finer
1	4	4.75	0	0.0	0.0	100
2	10	2.00	16.8	3.1	3.1	96.9
3	20	0.85	37.8	7.0	10.1	89.9
4	40	0.425	45.9	8.4	18.5	81.5
5	60	0.25	44.4	8.2	26.7	73.3
6	100	0.15	52.5	9.7	36.4	63.6
7	140	0.106	50.7	9.3	45.7	54.3
8	200	0.075	39.0	7.2	52.9	47.1
9	Pan		255.6	47.1	100	0
10		Summation	542.7	100		

Note: Column D(i) = C(i)/C(10) × 100; column E(1) = D(1) and E(i) = E(i − 1) + D(i); column F(i) = 100 − E(i).

Since larger (heavier) particles settle quicker than the finer (lighter) ones in the suspension, the density of the suspension reduces with time. A hydrometer reading at the surface of the suspension reflects this density change around the bulb section. In theory, it assumes that the soil particles are spheres, and individual particles settle in the water solution with a certain velocity, which is a function of particle diameter and the time passing after the agitation.

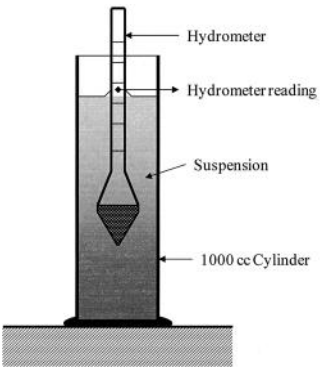

FIGURE 2.10 Hydrometer test setup.

TABLE 2.3
Example of Hydrometer Test Result

A	B	C
Particle Diameter D, mm	**% Finer**	**Modified % Finer**
0.066	84.5	45.7
0.045	74.3	40.2
0.036	68.3	37.0
0.025	58.2	31.5
0.015	48.4	26.2
0.011	42.3	22.9
0.007	34.6	18.7
0.005	28.1	15.2
0.004	24.3	13.2
0.003	20.1	10.9
0.0018	16.2	8.8
0.0012	12.3	6.7

Note: Column C = column B $\times F_{200(\text{Curve 1})}/F_{200(\text{Curve 2})}$.

Hydrometer analysis (***ASTM, D-422***) is performed for the material collected in the pan (minus No. 200 material) during the sieve analysis. Take exactly 50 g of oven-dried well-pulverized soil in a mixing beaker, and thoroughly mix the soil with 125 cc of **Calgon solution** (or other **deflocculation agent**). Note that the purpose of the deflocculation agent is to change the chemical environment of the solution so that its clay structures start dispersing. This makes the lumped particles break down to individual particles for accurate particle size measurement. Detailed discussions on clay structures (flocculated or dispersed) will be given in Chapter 3.

Using distilled water, transfer the soil–water slurry completely into a 1000 cc hydrometer cylinder exactly to its 1000 cc mark. By using the palm of the hand over the open end of the cylinder (or with a rubber stopper), the cylinder is then turned upside down and back for 1 min for a full agitation of the suspension. At the end of 1 min agitation, place it on a flat table. Set the time as zero when the cylinder is placed on the table and, then, insert the hydrometer immediately into the suspension. Read the hydrometer at 0.25, 0.5, 1, and 2 min while it is immersed in the suspension. Then the hydrometer is removed and immersed back at each reading of 4, 8, 16, and 30 min, 1, 2, 4, 8, and 24 h from the initial time. Record the exact times and the corresponding hydrometer readings.

This determines the relationship between the particle size and the corresponding percentage of weight settled. Refer the details of hydrometer test procedure, theory, and computation in soil testing manuals such as ASTM D-422.

The columns A and B in Table 2.3 show a set of data obtained from a hydrometer test. Test data from the sieve analysis and hydrometer test are then combined (**combined grain size analysis**). The relationship between the sieve opening and

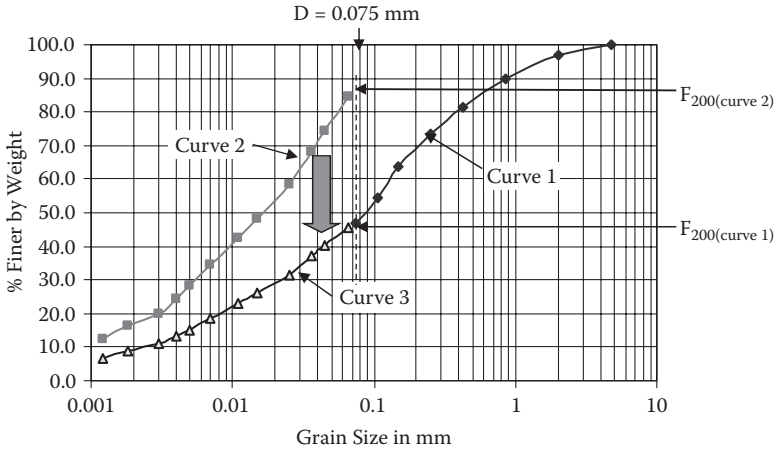

FIGURE 2.11 Combined grain size analysis.

the percent finer are plotted in semi-log scale to generate the grain size distribution curve as shown in Figure 2.11. The data in Table 2.2 are plotted as Curve 1. The hydrometer test result from columns A and B of Table 2.3 is also plotted as Curve 2. The latter data were obtained on the minus No. 200 material and is an enlarged curve of minus No. 200 section of Curve 1. Thus, the vertical values of Curve 2 are proportionally reduced by multiplying by $F_{200(\text{Curve 1})}/F_{200(\text{Curve 2})}$ as shown in the Figure 2.11, where $F_{200(\text{Curve 1})}$ is the percent finer with the No. 200 sieve from the sieve analysis and $F_{200(\text{Curve 2})}$ is that from the hydrometer test. Column C in Table 2.3 shows those modified percent finer used in this combined analysis. The modified Curve 3 is considered as an extension of Curve 1 to cover the finer section (D < 74 μm) to complete the entire domain of the grain-size distribution curve.

Referring to a grain size distribution curve in Figure 2.12, since the boundary grain sizes defining gravel, sand, silt, and clay were given earlier in Figure 2.9, the percentages of individual constituent of soil can be obtained as seen in the figure. In this example, 9% gravel, 63% sand, 21% silt, and 7% clay are obtained. Also, in the grain-size distribution curve, several key grain sizes are utilized: D_{10}, D_{30}, D_{50}, and D_{60}, which are the grain sizes corresponding to 10%, 30%, 50%, and 60% finer by weight, respectively.

D_{50} is called the **mean grain size,** and D_{10} is called the **effective grain size**. The latter is the grain size at a finer portion of the soil assembly and is rather influential with such water flow characteristics as permeability (Chapter 6), capillary rise (Chapter 7), etc.; thus, it is called the effective size.

The **coefficient of uniformity** C_u is defined as

$$C_u = D_{60}/D_{10} \tag{2.19}$$

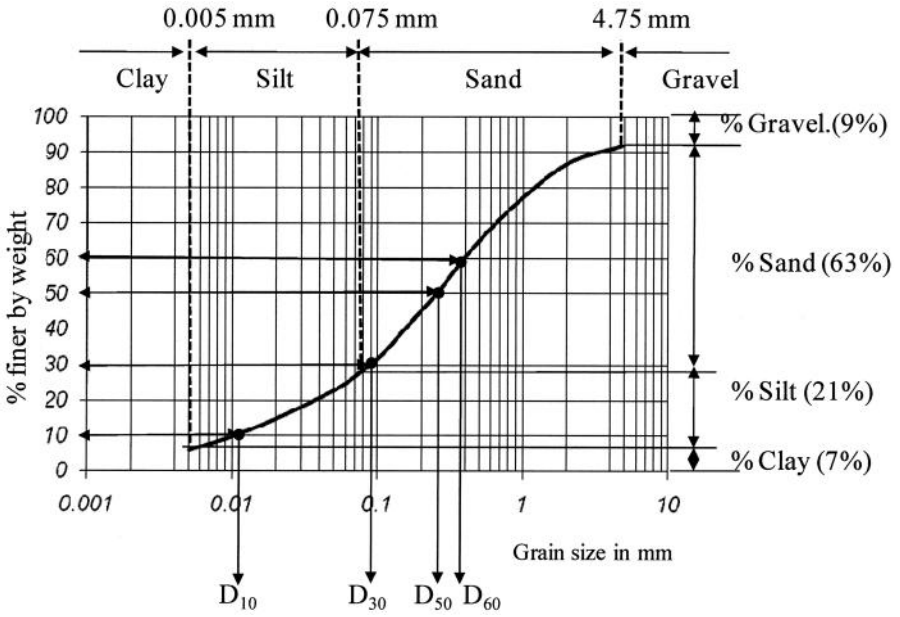

FIGURE 2.12 Grain size distribution curve.

Figure 2.13 shows a variety of grain size distribution curves. Curves 1, 2, and 3 have different C_u values (2.0, 4.7, and 13, respectively). Curve 1 soil is a **uniformly graded** (or **poorly graded**) **soil**, while Curve 3 soil is a **well-graded soil**. In the Unified Soil Classification System, C_u less than 4 for gravels and C_u less than 6 for sands are classified as uniformly graded soils, and those with higher than 4 for gravels and 6 for sands are classified as well-graded soils.

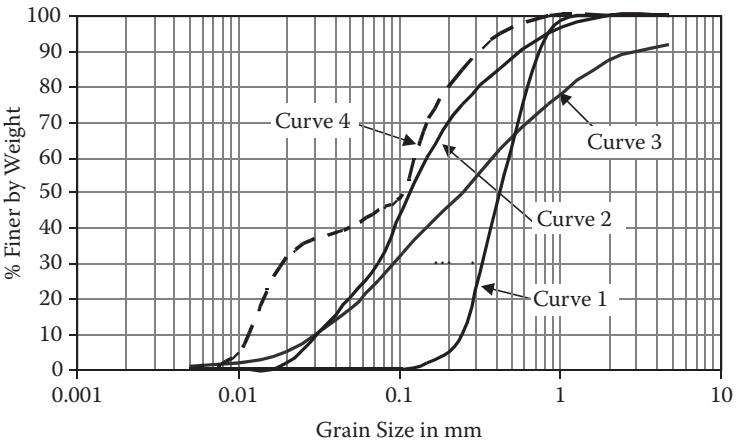

FIGURE 2.13 Various grain size distribution curves.

Coefficient of gradation C_g is defined from the gradation curve as

$$C_g = \frac{D_{30}/D_{10}}{D_{60}/D_{30}} = \frac{(D_{30})^2}{D_{60}\,D_{10}} \tag{2.20}$$

For smooth gradation curves, the range of C_g values is between 1 and 3. The Curve 4 in Figure 2.13 shows rather low C_g value (= 0.29) in comparison with other soils (e.g., $C_g = 1.33$ for Curve 2). Soils with $1 < C_g < 3$ are considered as well graded as long as $C_u > 4$ for gravels and $C_u > 6$ for sands, according to Unified Soil Classification System (USCS). On the other hand, soils with $C_g > 3$ or $C_g < 1$ are called **gap-graded soils**.

The coefficient of uniformity and the coefficient of gradation affect the soil packing arrangement. Well-graded soils make more stable packing since finer particles fill voids made by larger particle assemblages. On the other hand, uniformly graded soils make rather ordinary arrangement of packing and thus less interlocking mechanism. Soil classification systems use C_u and C_g as key parameters in their methods.

2.6 SUMMARY

In this chapter, starting with the origin of soils, soil formation processes were studied. Soil was then modeled by the three phases (solid, water, and air), and key definitions were made on unit weight (γ), void ratio (e), porosity (n), water content (w), degree of saturation (S), specific gravity (G_s), etc., based on the three-phase diagram. Those terms are used throughout the book hereafter. Some of their interrelationships are derived for convenient uses later. It was also demonstrated that the three-phase diagram is a convenient tool to solve field problems with volume and weight determinations in the exercises. At the end, grain shape, size, and its distribution were discussed. From grain size distribution curve, several key parameters can be obtained such as the effective grain size (D_{10}), the mean grain size (D_{50}), the coefficient of uniformity (C_u), and the coefficient of gradation (C_g). Those parameters will be used in soil classification practices in Chapter 4 and also will be correlated with many engineering properties of soils such as in compaction (Chapter 5), permeability (Chapter 6), etc.

REFERENCES

ASTM (2002), Standard Test Method for Particle-Size Analysis of Soils, *Annual Book of ASTM Standards*, Vol. 04.08, Designation D422-63.

BS8004 (1986), *Code of Practice for Site Investigation*, British Standard Institution.

Müller, G. (1967), *Methods in Sedimentary Petrology*, Hafner.

Watabe, Y., Tanaka, M., and Takemura, J. (2004), Evaluation of in situ K_0 for Ariake, Bangkok and Hai-Phong clays, *Proceedings of the 2nd International Conference on Site Characterization*, Porto, pp. 1765–1772.

Problems

2.1 For a given soil, derive the following relation by drawing the three-phase diagram.

$$\gamma_t = G_s \gamma_w (1 - n) (1 + w)$$

2.2 For a given soil, derive the following relation by drawing the three-phase diagram.

$$\gamma_t = G_s \gamma_w (1 - n) + n S \gamma_w$$

2.3 For an organic soil, the void ratio e is found to be 10.0, and G_s is 2.35. If this soil is fully saturated, find
(a) Total unit weight of the soil γ_t.
(b) Water content w.
(c) Does this soil sink in water?

2.4 For a given soil, the void ratio e, water content w, and specific gravity G_s are found to be 0.50, 15%, and 2.65, respectively. Find
(a) Total unit weight of the soil γ_t.
(b) Degree of saturation S.
(c) Dry unit weight γ_d if the water in the void is removed.

2.5 For a given soil, $G_s = 2.70$, $\gamma_t = 19.0$ kN/m^3, and w = 12.5% were measured. Determine
(a) Degree of saturation S.
(b) Dry unit weight of the soil γ_d.
(c) Submerged unit weight of the soil γ' as is.
(d) Total unit weight of the soil γ_t if the air void is filled with water.

2.6 The dry unit weight of a soil is found to be 15.8 kN/m^3, and its porosity n = 0.40. Determine
(a) The total unit weight of the soil γ_t when the soil's degree of saturation S is increased to 50%.
(b) The total unit weight of the soil γ_t when the soil is fully saturated.
(c) The specific gravity G_s of this soil.

2.7 Soil collected from the site is found to have $\gamma_t = 18.5$ kN/m^3, w = 8.6%, and $G_s = 2.67$. After a heavy rainfall overnight, 10% increase in the degree of saturation S was observed. Determine
(a) The degree of saturation S of the soil before the rainfall.
(b) The void ratio e of the soil before the rainfall.
(c) The water content w after 10% increase in S.
(d) The total unit weight γ_t after 10% increase in S.

2.8 In a construction site, 100 m^3 of the volume is excavated. γ_t, G_s, and w of the excavated soil are 18.5 kN/m^3, 2.68, and 8.2%, respectively.
(a) How heavy is the whole excavated soil?
(b) What is the porosity of the soil?

(c) If the excavated soil is dried out to a 5% water content at the site, how heavy does it become?

2.9 Table below shows a data set from a sieve analysis:

U.S. sieve no.	Opening, mm	Weight retained, gf
4	4.75	135.9
10	2	97.5
20	0.85	108
40	0.425	67.8
60	0.25	41.4
100	0.15	15
140	0.106	0
200	0.075	0
Pan		0

(a) Complete the rest of the table using a spreadsheet as in Table 2.2
(b) Plot the grain size distribution curve.
(c) Determine D_{10}, D_{30}, D_{50}, and D_{60}.
(d) Compute C_u and C_g.
(e) Report the % gravel, % sand, % silt, and % clay according to AASHTO.

2.10 Table below shows a data set from a sieve analysis.

U.S. sieve no.	Opening, mm	Weight retained, gf
4	4.75	16.8
10	2	38.4
20	0.85	54.9
40	0.425	67.8
60	0.25	101.7
100	0.15	94.2
140	0.106	77.4
200	0.075	61.8
Pan		70.5

(a) Complete the rest of the table using a spreadsheet as in Table 2.2.
(b) Plot the grain size distribution curve.
(c) Determine D_{10}, D_{30}, D_{50}, and D_{60}.
(d) Compute C_u and C_g.
(e) Report the % gravel, % sand, % silt, and % clay according to AASHTO.

2.11 Table below shows a data set from a sieve analysis.

U.S. sieve no.	Opening, mm	Weight retained, gf
4	4.75	0
10	2	0
20	0.85	6.9
40	0.425	71.7
60	0.25	109.2
100	0.15	126.9
140	0.106	147.6
200	0.075	115.8
Pan		110.7

(a) Complete the rest of the table using a spreadsheet as in Table 2.2.
(b) Plot the grain size distribution curve.
(c) Determine D_{10}, D_{30}, D_{50}, and D_{60}.
(d) Compute C_u and C_g.
(e) Report the percentages of gravel, sand, silt, and clay according to AASHTO.

2.12 Table below shows a data set from a sieve analysis.

U.S. sieve no.	Opening, mm	Weight retained, gf
4	4.75	15.6
10	2	35.4
20	0.85	121.8
40	0.425	102.3
60	0.25	82.8
100	0.15	50.4
140	0.106	37.8
200	0.075	30.6
Pan		56.7

(a) Complete the rest of the table using a spreadsheet as in Table 2.2.
(b) Plot the grain size distribution curve.
(c) Determine D_{10}, D_{30}, D_{50}, and D_{60}.
(d) Compute C_u and C_g.
(e) Report the percentages of gravel, sand, silt, and clay according to AASHTO.

2.13 The table below shows the sieve analysis data on the left and a hydrometer test data on the right for the minus #200 sieve material for a given soil.
(a) Plot grain size distribution curves for both tests individually on a graph.

(b) Combine two curves into a combined grain size distribution curve for the soil.

Sieve analysis			Hydrometer analysis	
U.S. sieve no.	Opening, mm	Weight retained, gf	Particle diameter, mm	% finer
4	4.75	0	0.072	78.2
10	2	0	0.046	58.2
20	0.85	0	0.034	50.4
40	0.425	13.5	0.026	42.8
60	0.25	45.3	0.017	38.1
100	0.15	75.4	0.012	35.4
140	0.106	147.6	0.007	30.2
200	0.075	168.2	0.004	25.7
Pan		230.5	0.0032	22.9
			0.0024	20.9
			0.0017	18.2
			0.0012	14.5

2.14 The table below shows the sieve analysis data on the left and a hydrometer test data on the right for the minus #200 sieve material for a given soil.
(a) Plot grain size distribution curves for both tests individually on a graph.
(b) Combine two curves into a combined grain size distribution curve for the soil.

Sieve analysis			Hydrometer analysis	
U.S. sieve no.	Opening, mm	Weight retained, gf	Particle diameter, mm	% finer
4	4.75	0	0.071	67.8
10	2	0	0.05	57.2
20	0.85	11.2	0.03	48.2
40	0.425	14.5	0.024	43.5
60	0.25	51.8	0.015	39.2
100	0.15	81.3	0.011	37.1
140	0.106	189.3	0.0072	35.2
200	0.075	152.1	0.0046	31.5
Pan		280.3	0.0035	30.2
			0.0025	29.1
			0.0016	27.2
			0.0012	26.2

3 Clays and Their Behavior

3.1 INTRODUCTION

Clay needs special attention because of its small particle size. As discussed in the grain size distribution section, soils with their particle diameters less than 5 μm (2 μm in some definition) are classified as clay or clay size particle. In such a small size, **electrical interactive forces** become more significant as compared to the physical **frictional interactive forces** in the case of larger grain soils (sand and gravel).

3.2 CLAY MINERALS

To understand various unique engineering behavior of clay, it is most beneficial to study microstructures of clay particles first. The microstructural observation greatly helps to understand their macrobehavior.

In the nature, basically there are three types of clay minerals, namely, **kaolinite** clay, **illite** clay, and **montmorillonite** clay. Those clays have different atomic structures and behave differently. Those clay minerals are all made of two basic atomic sheets, namely, **silica tetrahedral sheet** and **aluminum octahedron sheet,** as seen in Figure 3.1. Naturally abundant atom silica (Si) and aluminum atom (Al) occupy the center positions of the sheets, and oxygen atom (O) and hydroxyl (OH^-) are strongly bonded to those core atoms, respectively. Those bonds are either **ionic bond** or **covalent bond**, and actual bonds in silica sheet and aluminum sheet are combinations of those two types of bonds.

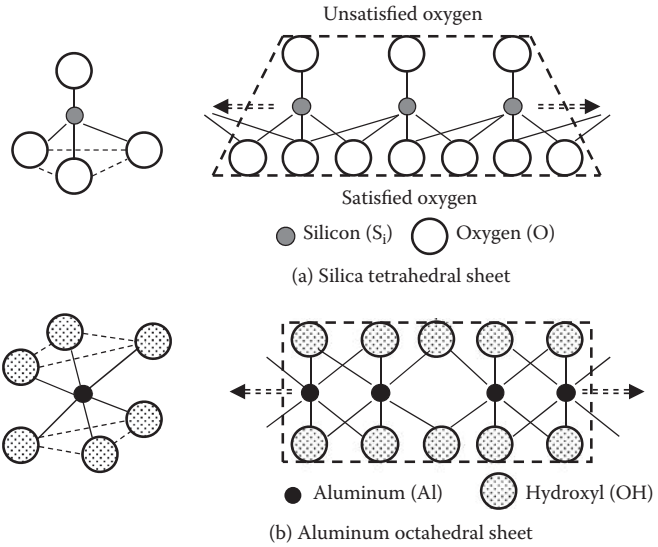

FIGURE 3.1 Silica and aluminum sheets.

Note that the ionic bond is due to exchange of orbiting electrons of two atoms such as Na^+ (sodium ion) and Cl^- (chlorine ion) to make NaCl (sodium chloride = salt), and the covalent bond is due to sharing electrons in their orbits such as two H^+ (hydrogen ions) to form H_2 (hydrogen gas). Those atomic bonds are very strong and never to be broken by ordinary physical forces. Those are called the **primary bonds**.

Silica tetrahedral sheet is symbolized with a trapezoid, of which the shorter face holds electrically unsatisfied oxygen atoms and the longer face holds electrically satisfied oxygen atoms. Aluminum octahedron sheet is symbolized with a rectangle with top and bottom faces having the same characteristics of exposed hydroxyl (OH^-). In most instances in nature, sheets further are bonded together, basically due to the unsatisfied face of silica sheet to form various clay minerals.

3.2.1 Kaolinite Clay

The basic unit of this type of clay is formed by atomic bond of the unsatisfied face of silica sheet and either face of aluminum sheet as seen in Figure 3.2. The bond between two sheets is strong and, also, it is the primary bond. However, the stack of two sheets (with thickness 7.2 Å [Angstrom]) is not a form of clay yet. Many layers of this basic kaolinite unit make a kaolinite clay particle. Figure 3.3 shows an electron photomicrograph of well-crystallized kaolinite clay particles. From the picture, it can be estimated that the diameter of a particle is about 5 μm, and the thickness of the particle is about one-tenth of that (i.e., 0.5 μm). Thus, it is required to have about 700 layers of the basic unit to make a kaolinite clay particle in the picture. The bond between each basic silica and aluminum sheet unit is the one between exposed OH^- and satisfied O^{2-} and is called a **hydrogen bond**. This bond is not as strong as

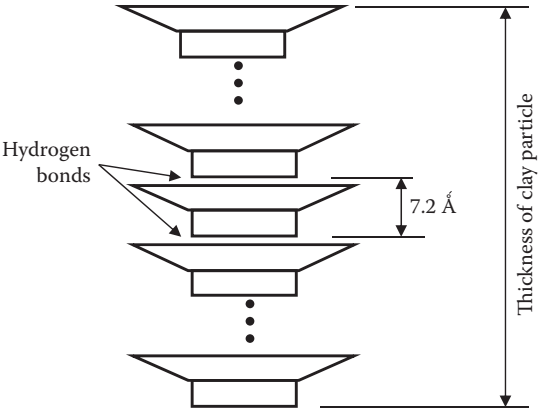

FIGURE 3.2 Kaolinite clay formation.

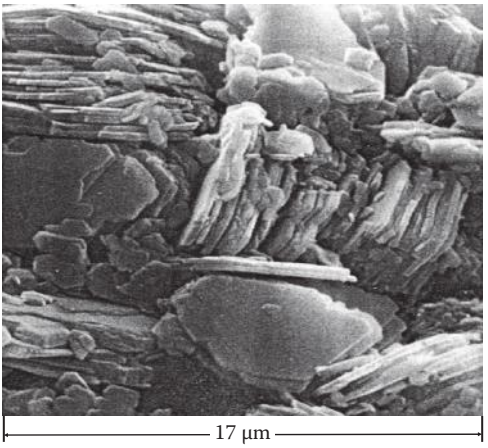

FIGURE 3.3 Electron photomicrograph of kaolinite clay. (From Tovey, N. K. (1971), *CUED/C-SOILS/TR5a*, University of Cambridge, Department of Engineering. Photo courtesy by N. K. Tovey.)

the previous atomic bond (primary bond) but much stronger than the bond between exposed O^{2-} and O^{2-} in case of montmorillonite clay, which will be discussed later. Hydrogen bond is categorized as a primary bond in many literatures, but it shall be noted that this is a marginally strong bond. Because of its nature of bonds within the kaolinite particle, this clay is rather stable, has less swelling and shrinking characteristics, and is less problematic.

3.2.2 Montmorillonite Clay

The unused OH^- face of aluminum sheet of the silica and aluminum sheet unit in the Kaolinite clay structure may attract the unsatisfied face of another silica sheet to make

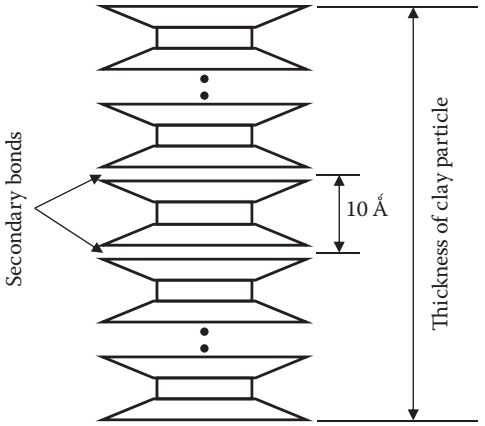

FIGURE 3.4 Montmorillonite clay formation.

a three-layer stack, as shown in Figure 3.4. This makes the basic unit of montmorillonite clay structure with the thickness of about 10 Å. Figure 3.5 shows an electron photomicrograph of this type of clay. The picture shows a flaky nature of this clay. The diameter to thickness ratio is much larger (more than 100), and thus, the thickness of a particle in the picture may be as small as 0.05 μm. Therefore, it is required to have about 50 layers of stack of this basic three-sheet unit to make a single clay particle of montmorillonite clay. The bonds between individual three-sheet units are due to facing surfaces of satisfied O^{2-} and O^{2-} of silica sheets and much weaker (**secondary bond**) than the primary bonds previously discussed. In many occasions, water easily goes in and comes out between those basic sheets due to very weak bond between exposed O^{2-} and O^{2-} surfaces. That makes this type of clay highly vulnerable to large swell and shrinkage.

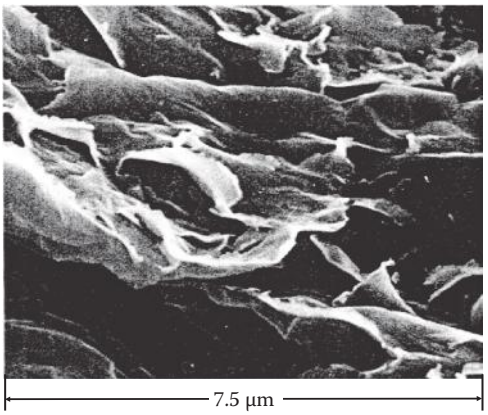

FIGURE 3.5 Electron photomicrograph of montmorillonite clay. (From Tovey, N. K. (1971), *CUED/C-SOILS/TR5a*, University of Cambridge, Department of Engineering. Photo courtesy of N. K. Tovey.)

Montmorillonite clay and similar group of clays (**Semectite**) are very unstable and problematic clays. If houses are built on this type of clay, severe differential settlements and cracks in the wall would be developed due to cycles of drying and wetting. On the other hand, in some occasions, geotechnical engineers exploit this problematic characteristic (high swell) toward a positive application. **Bentonite** (one of Semectite) is a highly swelling soil, and its slurry is filled in drilled bore holes, excavated trenches, and so on to temporarily support the bare soil walls against caving.

3.2.3 Illite Clay

Basic structure of this clay is the same as the one of montmorillonite (three-layer sheet stack). However, potassium ions (K^+) are filled in between facing O^{2-} and O^{2-} surfaces of silica sheets as seen in Figure 3.6. This secondary bond is not so strong in comparison with the hydrogen bond of kaolinite but much stronger than that of montmorillonite clay. Figure 3.7 shows an electron photomicrograph of illite clay. The characteristics of this clay are classified as in between those of kaolinite and montmorillonite.

Formation of various types of clays in natural environment depends upon the availability of basic atoms, temperature, drainage condition, etc. For example, from its composition, kaolinite requires more aluminum or less silica relative to other types of clays and, thus, it favors relatively high precipitation and good drainage condition to form. On the other hand, montmorillonite requires abundant of silica, and it favors a climate condition of high evaporation over precipitation (arid regions). Obviously, illite needs potassium in its structure so that parent rocks such as muscovite (common mica, $KAl_2(AlSi_3O_{10})(F,OH)_2$), biotite (dark mica, $K(Mg, Fe)_3AlSi_3O_{10}(F, OH)_2$) are favored as origins of illite. The readers can study the details of **clay genesis** in other references (e.g., ***Mitchell and Soga 2005***).

A scanned electron microscope (SEM) picture of a clay assemblage seen in Figure 2.3 was from Hai-Phong, Vietnam, and it was reported that it consisted of about 50% kaolinite and about 50% illite (***Watabe et al. 2004***).

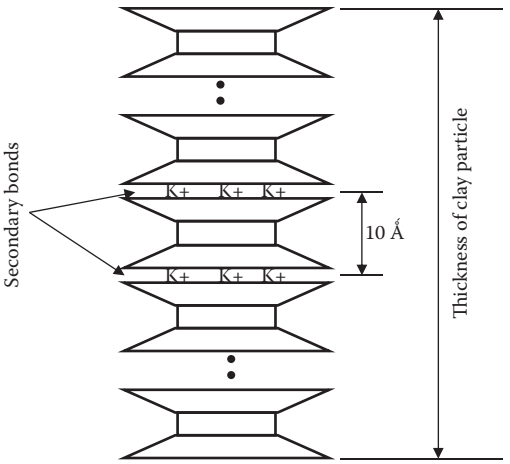

FIGURE 3.6 Illite clay formation.

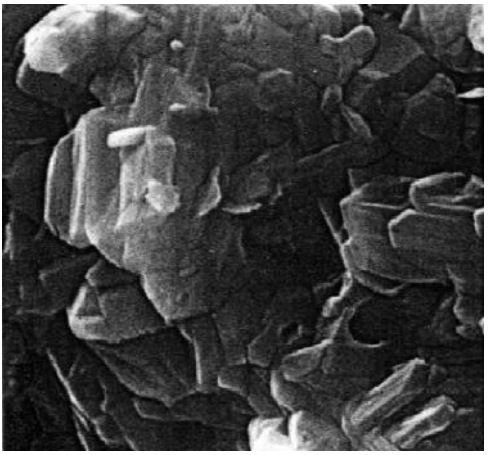

FIGURE 3.7 Electron photomicrograph of illite clay. (From Tovey, N. K. (1971), *CUED/C-SOILS/TR5a*, University of Cambridge, Department of Engineering. Photo courtesy by N. K. Tovey.)

3.3 CLAY SHAPES AND SURFACE AREAS

Clays are formed in stack of several layers of basic sheet units as discussed in the previous section. These are generally flat and smaller in size, and thus, their surface areas per weight are very large. Table 3.1 compares the types of clay with their general shapes, general dimensions, and surface areas. The **specific surface** is defined as the surface area of clay per 1 gm of dry clay particles. In addition, for a comparison purpose, those values of spheres with 1 μm and 0.1 μm diameters are included in the table. Those two spheres are called **clay-size particles.** They are not clay minerals, since their compositions reveal that, unlike flat clay minerals, they are spherical in shape and are rather simply smaller sizes of sands or gravels.

It shall be noted that the flatness and particle sizes are the major factors in determining the surface area, which contributes to many unique aspects of clay behavior such as water adsorption, plasticity, etc., as will be discussed later in this chapter.

TABLE 3.1
Comparison of Shapes and Surface Areas of Clays and Clay-Size Particles

Clay Type	Typical Length (L), μm	Typical Thickness (T), μm	Typical Dimensional Ratio (L × L × T)	Specific Surface, m^2/g
Kaolinite	0.3–3	0.05–1	10 × 10 × 1	10–20
Illite	0.1–2	0.01–0.2	20 × 20 × 1	80–100
Montmorillonite	0.1–1	0.001–0.01	100 × 100 × 1	800
Sphere (1 μm dia.)	1	1	1 × 1 × 1	3
Sphere (0.1 μm dia.)	0.1	0.1	1 × 1 × 1	10

Thus, ***it is very important to distinguish the differences between clay minerals and clay-size particles, even though their particle sizes are similar.***

3.4 SURFACE CHARGE OF CLAY PARTICLES

Another unique and important characteristic of clay is their electrical surface charge. The surface of clays is generally negatively charged, even though the resultant charge in a particle is neutral. First, as seen in clays' atomic composition, O^{2-} and OH^{-} are exposed on the surface. Secondly, due to availability of other types of atoms in the environment, such as aluminum ion (Al^{3+}), ferrous ion (Fe^{2+}), magnesium ion (Mg^{2+}), etc., Si^{4+} atoms in the center of tetrahedral silica sheet are replaced by lower valence ions Al^{3+}, and Al^{3+} atoms in the octahedral sheet are replaced by Fe^{2+} and Mg^{2+} without changing their crystal structures. These atomic substitutions are called **isomorphous substitution**. Replaced lower-valence cations (positive charge) make the whole clay particle negatively charged and, thus, its surface is more negatively charged.

Thirdly, the linkage of octahedral and tetrahedral sheets must end with a certain length that determines the clay size. The **broken edge** of the clay particle is complex in nature. Figure 3.8 shows probable mechanisms of breaking link of kaolinite (***Yong and Warkentin 1975***). Based on the acidity (pH), the edge attracts $OH^{-1/2}$ in pH = 7 environment or attracts $OH_2^{+1/2}$ and $H^{+1/2}$ in pH < 5. For increasing pH, the edge of clay

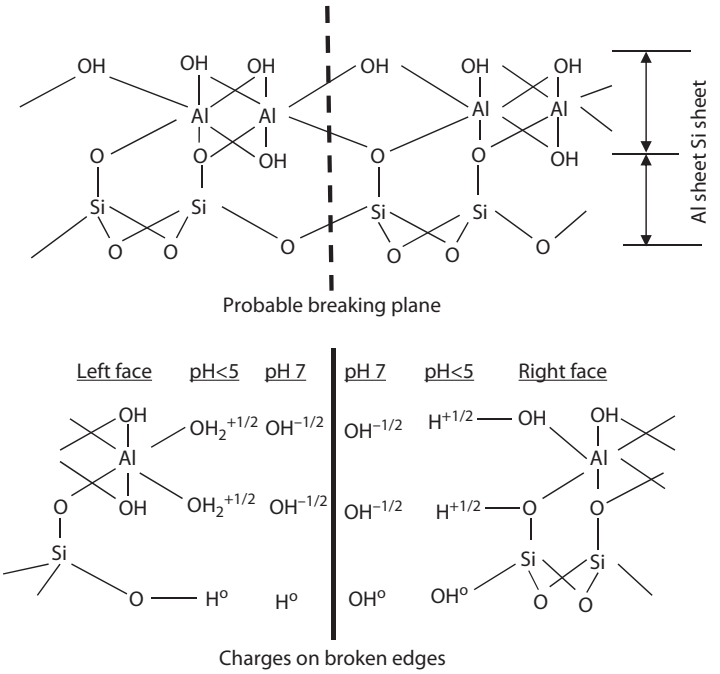

FIGURE 3.8 Probable mechanism of breaking link of kaolinite clay. (After Yong, R. and Warkentin, B. P. [1975], *Soil Properties and Behavior*, Elsevier.)

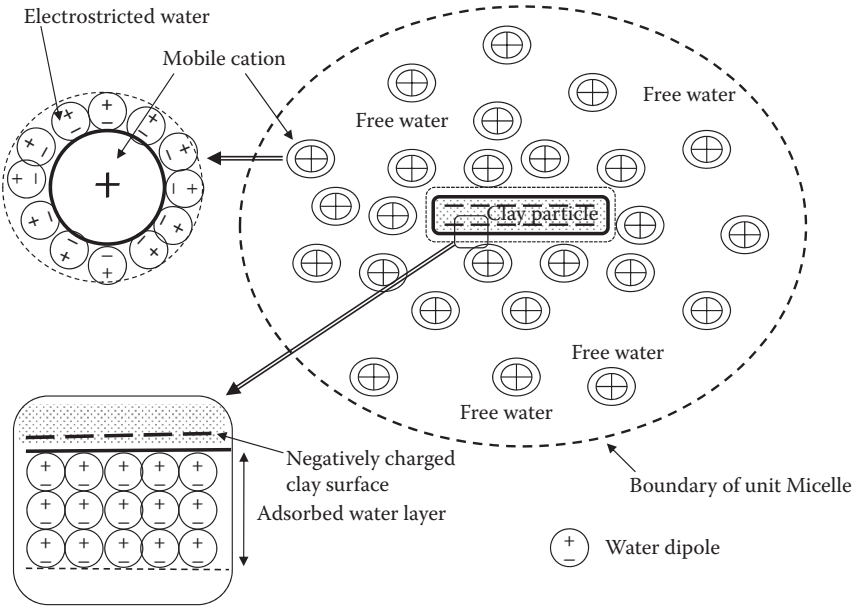

FIGURE 3.9 A clay particle in water (unit Micelle).

particles may be negatively charged due to this mechanism. For low pH environment, however, the edges of kaolinite may be positively charged.

All the preceding conditions contribute to make the clay surface be negatively charged and to have possibly positive edge in some conditions. The electrical surface and edge charges of clays play an important role in forming the clay structures.

3.5 CLAY–WATER SYSTEM

In the natural environment, clays are often formed under water. Consider first, a situation, where a clay particle is placed in a pool of water, as shown in Figure 3.9. Because of relatively strong negative surface charge of the particle, positively charged ions (**cations**) and positive edges of **dipoles** (water molecules) are attracted to its surface. Note that water molecule due to its atomic structure makes a small magnet (dipole) with positive and negative charges on the opposite sides as shown in Figure 3.10. Several

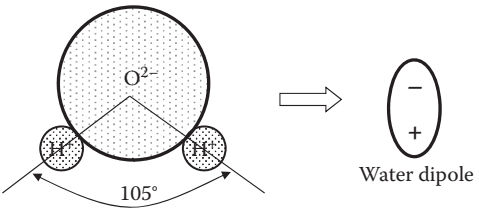

FIGURE 3.10 Water molecule as a dipole.

layers of water molecules are attracted on the clay surface in a very ordinary way. This water layer with the thickness of about 10Å is called **adsorbed water layer.** The layer is very rigidly, electrically attracted to the clay surface and behaves as if a part of the particle itself.

In the outer part of water, there are distributions of mobile **cations** (+) and **anions** (–). Those cations and anions are from resolved minerals and other matters in natural water. Cations distribute more near the clay surface and less at the outermost part of the water. The anion distribution is opposite to the cation distribution. Because of the negative charge on clay surface, cations' influence dominates the anions'. Therefore, Figure 3.9 shows only the presence of cation distributions. Those cations further attract dipoles (water molecules) around them. This type of water is called **electrostricted water,** and they move together when a cation moves. The rest of the space is filled with regular water, which is called **free water**. There is a boundary within which a clay particle has an influence electrically. The boundary is called the **boundary of unit Micelle**. Thus, there are three different types of water in a **unit Micelle**: adsorbed water rigidly attached to the surface of clay particle, electrostricted water around cations, and free water in the rest of the space.

Electro-osmosis is a good example of utilizing unique characteristics of electrostricted water in the field of soil mechanics. A direct current is applied in soil field through terminals (cathode (+) and anode (–)) as seen in Figure 3.11. Mobile cations with electrostricted water are attracted to the anode, where water is collected and pumped out for drainage to reduce water content in the field. This is a quiet operation of soft soil remediation. Further details of this can be found in other references (e.g., ***Scott 1963***).

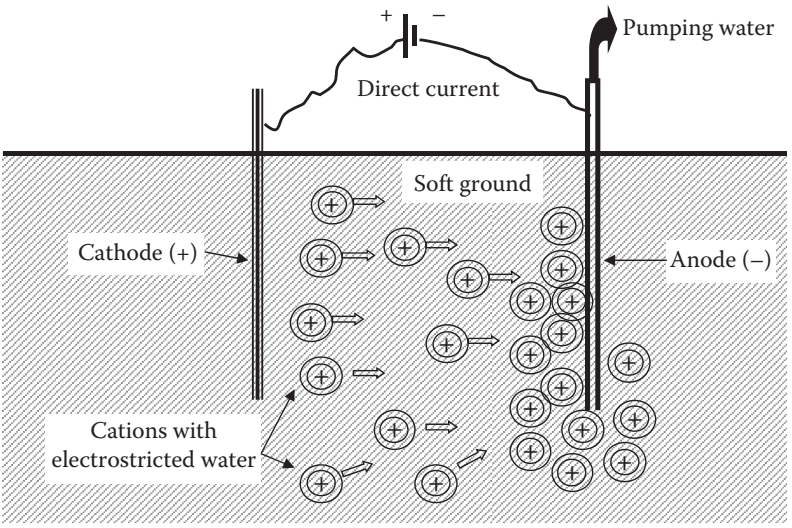

FIGURE 3.11 Principle of electro-osmosis.

3.6 INTERACTION OF CLAY PARTICLES

When many clay particles are mixed together in water, particles interact and their unit Micelles overlap each other. There exist several interactive forces (attractive or repulsive) between particles when those particles are brought closer.

3.6.1 Van der Waal's Force (Attractive)

Overlapping of electrons' motion on their orbits of atoms creates this close-range attractive force. It is believed that the magnitude of the force (F_{vdw}) is inversely proportional to approximately the third power of the spacing (r) between particles (i.e., $F_{vdw} = k/r^3$, where k is a proportional constant).

3.6.2 Dipole–Cation–Dipole Attraction

A negatively charged clay surface attracts the positive side of a dipole (water), and the opposite side (–) of the dipole attracts cation (+), that attracts negative side of another dipole and so on, as seen in Figure 3.12a.

3.6.3 Cation Linkage (Attractive)

As it has been seen in the case of illite clay, cations act as the intermediate charge between the particles (Figure 3.12b).

3.6.4 Cation–Cation Repulsive Force

Cations repel each other if they are brought closer, as seen in Figure 3.12c.

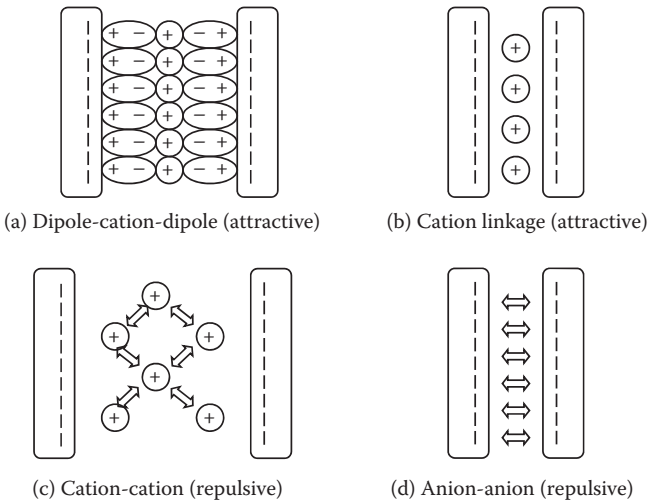

FIGURE 3.12 Interactive forces between clay particles.

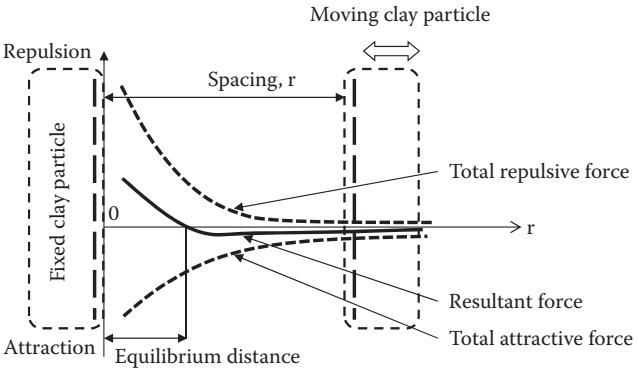

FIGURE 3.13 Interactive forces versus parallel particle spacing.

3.6.5 Anion–Anion Repulsive Force

Two adjacent clay surfaces (both negatively charged) repel each other when they are in close encounter (Figure 3.12(d)).

The resultant force between adjacent particles is the sum of potentially all the preceding attractive and repulsive forces. The magnitude of the force depends on many factors such as the level of surface change, relative spacing, existence and amount of cations and anions, cation valence, etc. Figure 3.13 shows a schematic relationship between interactive forces and the relative spacing of two parallel particles. When the space is too close, the resultant is very large repulsive forces due to repelling of both the clay surfaces. The resultant force curve passes through the zero resultant value. This spacing is called the **equilibrium distance**, at which two parallel particles are in balance and establish their stable relative position. The equilibrium distance also depends on many factors, such as electrolyte concentration, ion valence, dielectric constant, temperature, pH of the solution, etc., and thus, relative distance of clay particles are influenced by these factors in the environment. The **double-layer theory** provides the detailed discussions of the preceding, and the readers are referred to other literatures such as in ***Mitchell and Soga* (*2005*)**.

3.7 CLAY STRUCTURES

The final structures of clay are established from the balance of interactive forces and external forces applied to the clay assemblage, as seen in Figure 3.14. The external forces are due to the stress induced in a soil element, including its gravitational weight. The external forces move particles' position away from their equilibrium distance, and, thus, the final interparticle forces among adjacent particles could be either attractive or repulsive.

If the final interparticle forces are repulsive, the particles want to separate from each other when the boundary confinements are removed. This is a situation of **dispersed clay**. On the contrary, if the interparticle forces are attractive, then particles

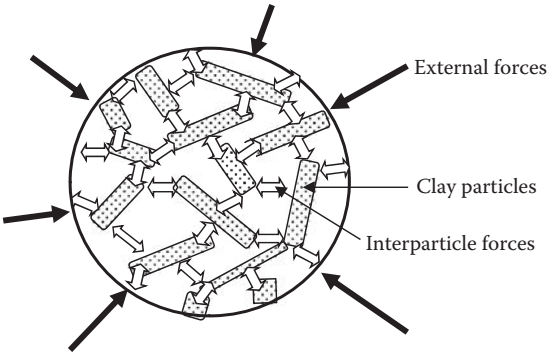

FIGURE 3.14 Final clay structure with particles' interactive and external forces.

want to come together, making **flocculated clay**. In flocculated clays, surface and edge charges play an important role. If the edge charges are positive, most likely, the edges are attracted to the flat surfaces of other clay particles. This makes a **card-house structure** of flocculated clay, most commonly in saltwater environments. In freshwater environments, more **face-to-face flocculated structures** are formed due to negative charges at the edges. Those models of various clay structures are shown in Figure 3.15.

The relative particle positions are dependent on various environmental factors as discussed earlier. If the environmental factors change after the formation of the original clay structure, clay will possess a potentially different structure. In hydrometer test to determine finer particle sizes (Chapter 2, Section 2.5), **Calgon solution** (or other **deflocculation agents**) is added to soil and water solution to break down lumped soil particles. The solution is to change a chemical condition of the suspension from flocculated to dispersed, so that individual particles diameters are measured. **Quick clay** is another good example of this and will be discussed later in this chapter in details.

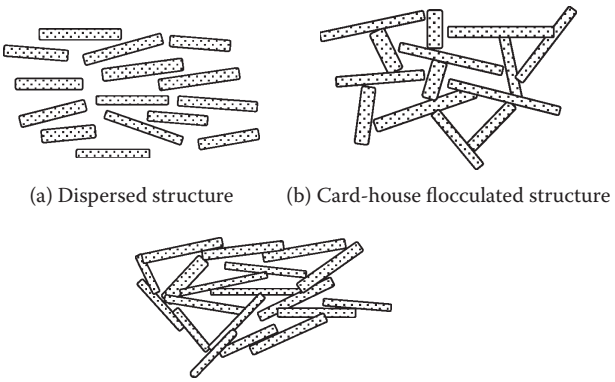

FIGURE 3.15 Clay structures.

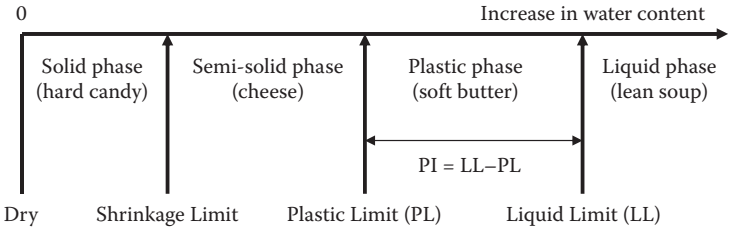

FIGURE 3.16 Phase change of clay with water content.

3.8 ATTERBERG LIMITS AND INDICES

Water plays a very significant role in the engineering behavior of clays. When the water content changes, clay changes its character in a surprising manner. When it is subjected to a large amount of water, it is similar to a lean soup (**liquid**), and, at a little drier state, it becomes similar to a soft butter (**plastic**). At further dried stage, it behaves like a cheese (**semi-solid**). At a very dry stage, it is like a hard candy (**solid**). As seen in Figure 3.16, **liquid limit** (LL) is defined as the water content between liquid phase and plastic phases, **plastic limit** (PL) as the boundary water content between plastic and semisolid phases, and **shrinkage limit** (SL) as the maximum water content below which no further volume change of the clay will occur, as demonstrated in Figure 3.17. Note that at this point, the soil is still fully saturated.

LL and SL can be understood from the study of the clay–water system. Adsorbed water layer is considered as an integral part of clay particle. As shown in Figure 3.18, when clay particles contain enough water, adsorbed water layers are not at all in contact with each other, and thus, there is no frictional resistance. It is at a liquid stage (Figure 3.18a). Now, if water is removed to a certain level at which all the adsorbed water layers are just in contact, frictional resistance will be developed at the contact points. This is considered to be the stage of LL (Figure 3.18b). When it is further dried, overlapping of adsorbed water layer will take place. The limiting stage of this overlapping is the level at which all particles themselves touch each other and no

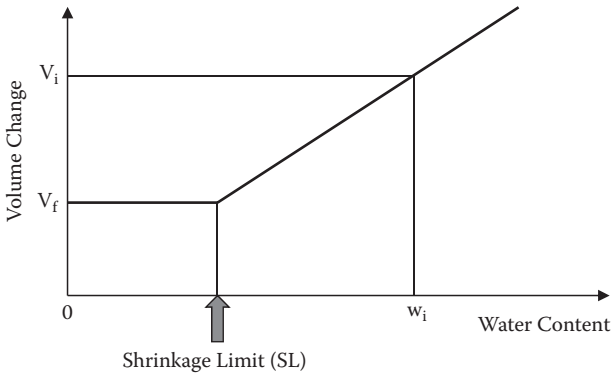

FIGURE 3.17 Definition of shrinkage limit.

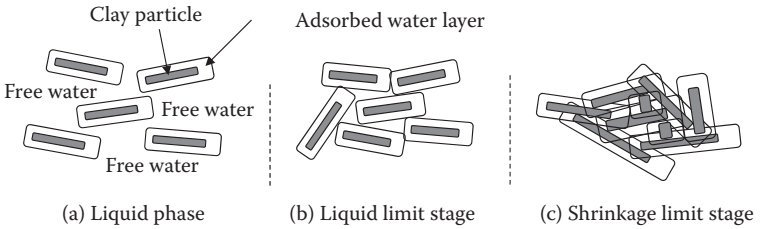

FIGURE 3.18 Clay particles with adsorbed water layers in water.

further overlapping will be possible (Figure 3.18c). This stage is considered as the SL. PL may have some degree of overlapping of adsorbed water layers.

Those three limits are called the **Atterberg limits**, named after a Swedish scientist, A. Atterberg, who defined those limits in the early 1900s. Current standard liquid limit test (***ASTM D-4318***) uses a small semispherical cup as seen in Figure 3.19. A thoroughly mixed wet clay specimen is filled into a portion of the cap, and a groove is cut with a special grooving tool on the center portion of the specimen. The cranking handle, which lifts and drops the cup, is then rotated with two revolutions per second until the opening of the groove closes with 13 mm (1/2 in.) length. The number of revolution (**blow counts**) is recorded, and the water content at this stage is measured. Several trials with slightly different (usually few percentages) water content specimens are performed. **Flow curve**, which plots the blow counts and the corresponding measured water contents in a semi-log scale, is prepared, as shown in Figure 3.20. LL is then defined as the water content with 25 blows in the flow curve.

PL test is run in a more primitive way (***ASTM D-4318***). A drier specimen is rolled into a thread by human palms on a glass plate. PL is defined as the water content

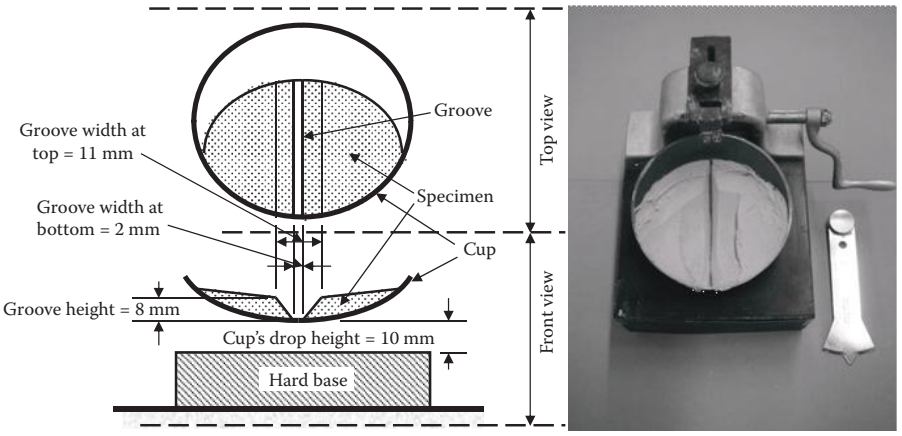

FIGURE 3.19 Liquid limit apparatus.

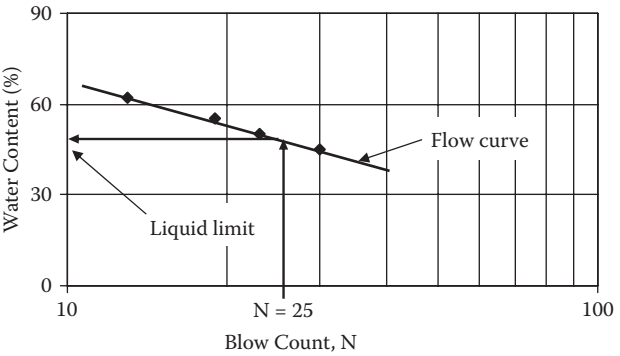

FIGURE 3.20 Flow curve to determine liquid limit.

at which a rolled thread just crumbles with 3 mm (1/8 in.) diameter, as shown in Figure 3.21. Several trials shall be made to take an average water contents at that stage to get the PL value.

Referring to Figure 3.17, the SL test is run by measuring the water content w_i and the volume V_i of a saturated specimen (slightly above its LL) and the oven-dried volume V_f and weight W_f of the same specimen. Since the volume change (due to shrinkage) from V_i to V_f is simply due to loss of water from w_i to SL, weight loss of specimen $(V_i - V_f) \bullet \gamma_w$ is equal to $(w_i - SL) \bullet (100) \bullet W_f$, and thus:

$$SL = w_i - \frac{(V_i - V_f)\gamma_w}{W_f} \tag{3.1}$$

Detailed procedures of SL determination can be seen in ASTM D-427 by the **mercury method** or D-4943 by the **wax method**.

From these limits, various important parameters are developed. The **plasticity index** (PI) is defined as

$$PI = LL - PL \tag{3.2}$$

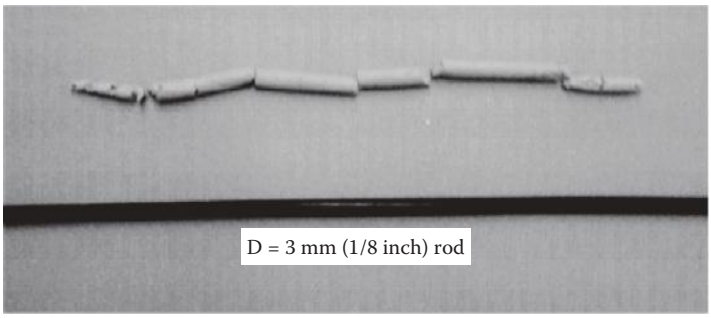

FIGURE 3.21 Plastic limit determination.

TABLE 3.2
Atterberg Limits and Plasticity Index of Clay Minerals

Mineral	Exchangeable Ion	LL	PL	PI	SL
Montmorillonite	Na	710	54	656	9.9
	K	660	98	562	9.3
	Ca	510	81	429	10.5
	Mg	410	60	350	14.7
	Fe	290	75	215	10.3
	Fe[a]	140	73	67	—
Illite	Na	120	53	67	15.4
	K	120	60	60	17.5
	Ca	100	45	55	16.8
	Mg	95	46	49	14.7
	Fe	110	49	61	15.3
	Fe[a]	79	46	33	—
Kaolinite	Na	53	32	21	26.8
	K	49	29	20	—
	Ca	38	27	11	24.5
	Mg	54	31	23	28.7
	Fe	59	37	22	29.2
	Fe[a]	56	35	21	—

Source: Data from Cornell University (1951). *Final Report on Soil Solidification Research*, Ithaca, New York.

[a] After five cycles of wetting and drying (after Lambe, T. W. and Whitman, R. V. (1969). *Soil Mechanics*, John Wiley and Sons).

It indicates the range of water content of a material for its plastic behavior, and many engineering behaviors of clays are related to PI. Table 3.2 summarizes measured LL, PL, PI, and SL values for variety of clays. LL varies from very large (140–710) for montmorillonite to relatively small values (38–59) for kaolinite. It makes sense by recognizing that the stage of the LL is as the moment of adsorbed water layers being just in contact as shown in Figure 3.18b and that a large surface area of montmorillonite (Table 3.1) carries large amount of adsorbed water at that stage of water content in comparison with that of kaolinite.

Another parameter called the **liquidity index** (LI) is defined as

$$\text{LI} = \frac{w_n - \text{PL}}{\text{PI}} \quad (\times 100\%) \tag{3.3}$$

where w_n is the natural water content of soil. The liquidity index shows the position of the current water content above the PL relative to PI. In most in situ soils, LI ranges

from 0% (w_n at PL) to 100% (w_n at LL). In very unusual situations, LI is higher than 100, which implies that the in situ water content is higher than its LL. It is impossible for ordinary soils that were formed under their own gravitational forces. This unique case will be discussed in the section of **quick clay** in this chapter.

3.9 ACTIVITY

When PI and clay fraction (the percentage of particles less than 2 μm) relations for various types of clays are plotted as in Figure 3.22, it was found that there were unique linear correlations between them for each of the different clays (***Skempton 1953***). The slope of those straight line correlations is defined as the **activity,** and thus:

$$A = \frac{PI}{\text{clay fraction } (\leq 2\,\mu m)} \tag{3.4}$$

where PI and clay fraction are expressed in the percentage. The higher the activity, the more influence of clay fraction is to PI. Typical values of activity for various clays are shown in Table 3.3. Activity is highly related to soils' swelling and shrinkage potentials.

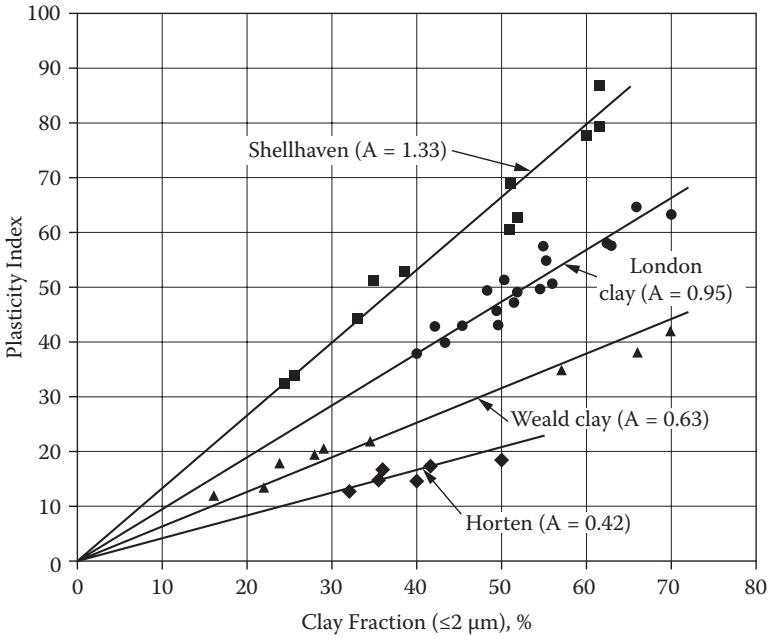

FIGURE 3.22 Relationship between % fraction (≤ 2 μm) of clay and Plasticity Index. (After Skempton, A. W. (1953). *Proceedings of the Third International Conference of Soil Mechanics and Foundation Engineering*, Vol. 1, pp. 57–61.)

TABLE 3.3
Activities for Various Clay Minerals

Mineral	Activity
Montmorillonite	1–7
Illite	0.5–1
Kaolinite	0.5

Source: After Mitchell, J. K. and Soga, K. (2005). *Fundamentals of Soil Behavior*, 3rd ed., John Wiley & Sons, New York.

3.10 SWELLING AND SHRINKAGE OF CLAYS

When clay specimen is in process of increasing the water content, clay swells mainly due to weak secondary bonds between exposed OH^- and OH^- surfaces of facing sheets, as shown in Figure 3.4, in particular, in the case of montmorillonite. When water content is decreased, it shrinks due to the reversed phenomenon of swelling. A large amount of swelling upon wetting or shrinkage upon drying would cause devastating damages to buildings and foundations. The swelling and shrinkage potentials are closely related to the types of clays and their activities. Figure 3.23 shows a classification chart of **swelling potential** based on many experimental data. The higher the activity and the clay fraction (≤ 2 μm), the higher the swelling potential. This

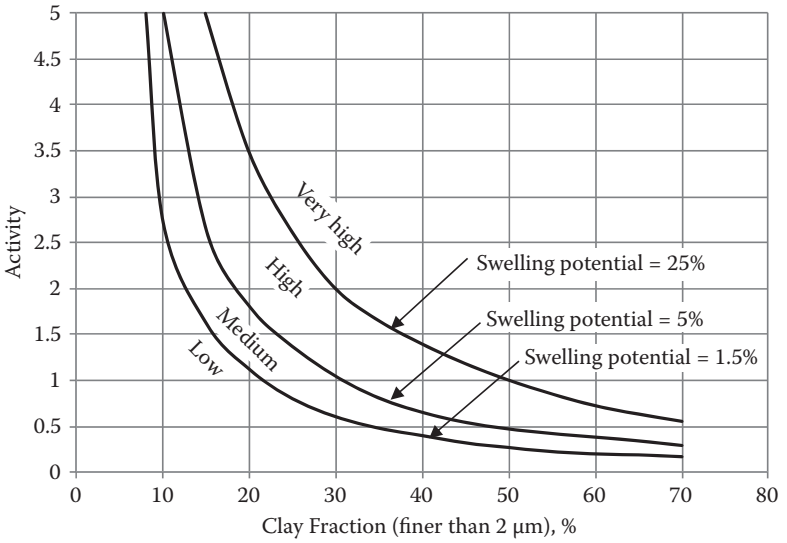

FIGURE 3.23 Classification chart for swelling potential. (After Seed, H. B., Woodward, R. J., and Lundgren, R. (1962). Prediction of swelling potential for compacted clays, *Journal of Soil Mechanics and Foundations Division*, ASCE, Vol. 88, No. SM3, pp. 53–87.)

chart is a useful guidance for classifying a given soil for potential swelling by simply knowing few key soil parameters: LL, PL, and clay fraction.

3.11 SENSITIVITY AND QUICK CLAY

When naturally formed clays are **disturbed** or **remolded,** their original clay structures will be destroyed. Since they cannot easily recover their original formation, they will lose the strengths. The degree of recovery depends on its new environment and also takes time due to viscoelastic nature of clay (**thixotropy**). Thixotropy is defined as a time-dependent change of clay's strength upon remolding and sitting since the rearrangement of particle positions under interparticle forces and ion movement in the system requires some time. Detailed discussion on thixotropy can be seen in other references (e.g., ***Scott 1963; Mitchell and Soga 2005***).

Sensitivity is defined as the clay's **shear strength** (detailed discussions in Chapter 11) before remolding to that after remolding:

$$S_t = \frac{\text{shear strength before remolding}}{\text{shear strength after remolding}} \tag{3.5}$$

S_t value ranges from 2 to 4 for low sensitive clays to more than 100 for extra quick clays, as summarized in Table 3.4.

Sensitivity is found to be very much related to the soils' LI. Figure 3.24 plots relationship between LI and S_t. The higher the LI, the higher the S_t. Note that LI > 1.0 (100%) implies that their natural water content is higher than their LL (see Equation 3.3) and, for ordinary clays, it is less than 1.0 (100%). However, it is possible for some unique circumstances and is explained in case of Scandinavian quick clay in the following.

A very unique type of clay called the **quick clay** is commonly abundant in Scandinavian countries (i.e., Norway and Sweden). It has very high value of S_t as seen in Table 3.4. Figure 3.25 demonstrates a dramatic change of its strength from a

TABLE 3.4
Typical Values of Sensitivity

	Range of S_t	
Sensitivity	**U.S.**	**Sweden**
Low sensitive	2–4	<10
Medium sensitive	4–8	10–30
Highly sensitive	8–16	>30
Quick	16	>50
Extra quick	—	>100

Source: After Holtz, R. D. and Kovacs, W. D. (1981), *An Introduction to Geotechnical Engineering*, Prentice Hall, Englewood Cliffs, NJ.

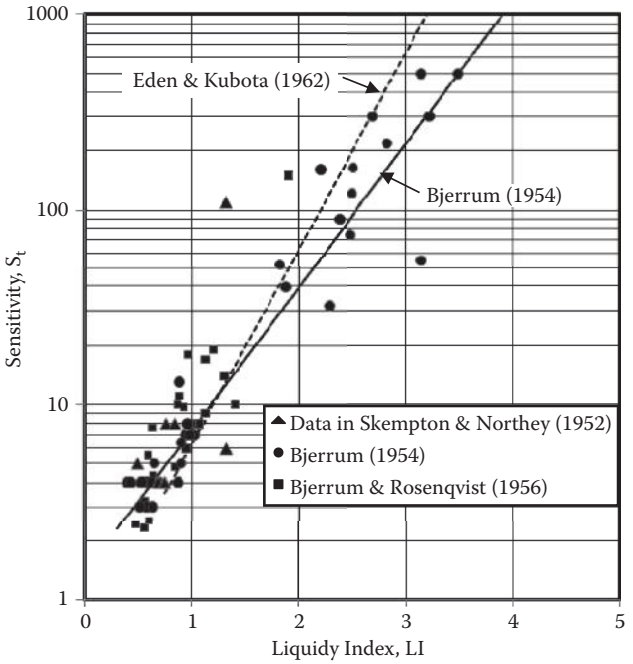

FIGURE 3.24 Relationship between liquidity index and sensitivity.

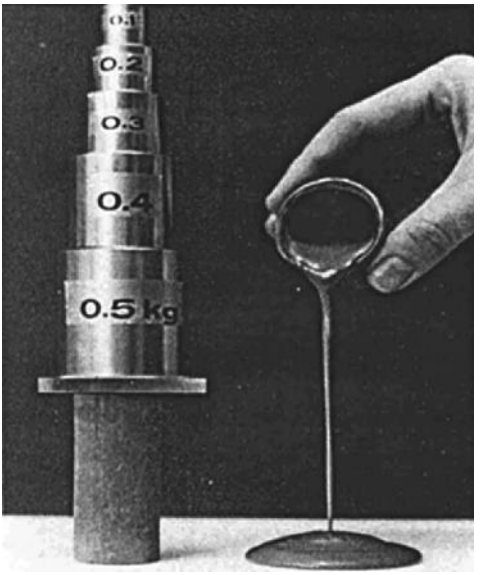

FIGURE 3.25 Quick clay before and after remolding. (Photo courtesy of Haley and Aldrich, Inc.)

solid undisturbed specimen (left) to liquid stage of remolded specimen (right). Since the shear strength of liquid is nearly zero, S_t is extremely high from Equation 3.5.

Scandinavian clay was formed under a marine environment and had open-clay structures such as the one in Figure 3.15b. The area was then uplifted due to the retreat of glacier and tectonic movement, and formed land over the sea level. Fresh rainwater and groundwater then leached out the salt content in the system, but it still maintained the original rather stable open structure. The current environment is not the one of the original saltwater (marine), but rather the one of freshwater environment. When it is remolded (or disturbed), the original flocculated structure is destroyed and tries to restore its structural balance in a new environment, which happened to be a dispersed structure. And clay loses the strength in a great deal. The original open structure is stable without disturbance, but has rather high water contents. The LL test is conducted on totally remolded specimen by using freshwater and, thus, the measured LL could be much less than its water content that makes LI much higher than 100 (%).

In August 1978, near Rissa, Norway, 0.34 km^2 of farm land, including seven farms (5–6 million cubic meters of soil mass) slid into a lake (**Rissa's landslide**). The site was made of quick clay, and the initial landslide was triggered by an excavation and stockpiling of 700 cubic meters of soil placed along the shoreline of the lake. The stockpiling disturbed the balance of quick clay formation initially, and it progressively spread over the large area (***USC 2008***).

3.12 CLAY VERSUS SAND

Clays as studied in this chapter are quite different from sand (granular soils) in their characteristics and behaviors. Those are summarized in Table 3.5.

Most of properties and behavior of clay in Table 3.5 have been presented in this chapter. It is important to recognize these differences to understand the differences in their engineering behaviors. The remaining differences such as volume change characteristics and shear resistance will be discussed in detail in Chapters 9 and 11, respectively.

TABLE 3.5
Comparisons between Clay and Sand

Properties and Behavior	Clay	Sand
Particle size	Small (<0.005 or 0.002 mm)	Large (>0.075 mm)
Structure	Clay structures	Crystal formations
Shape	Flat	Angular to round
Surface charge	Negative and sometimes positive at edge	Negligible
Specific surface	Large	Small
Interactive forces	Strong	Negligible
Plasticity	Plastic	Nonplastic
Shear resistance	By cohesion	By friction
Volume change	Large, time dependent	Small, instantaneous

3.13 SUMMARY

The microstructural study of clays helps us to understand their macrobehavior. Many unique behaviors of clays, such as plasticity, swelling, shrinkage, sensitivity, and the nature of quick clay, were reviewed based on observations of atomic structures, surface charges, particles in water, and interactive forces. The understanding of the subject in this chapter will further enhance the studies of effective stress, consolidation, and shear strength in later chapters.

REFERENCES

ASTM (2002), Standard Test Methods for Liquid Limit, Plastic Limit, and Plasticity Index of Soils, *Annual Book of ASTM Standards*, Vol. 04.08, Designation D4318-00.

Bjerrum, L. (1954), Geotechnical Properties of Norwegian Marine Clays, *Geotechnique*, Vol. 4, pp. 49–69.

Bjerrum, L. and Rosenqvist, I. Th. (1956), Some Experiments with Artificially Sedimented Clays, *Geotechnique*, Vol. 6, pp. 124–136.

Cornell University (1951), *Final Report on Soil Solidification Research*, Ithaca, New York.

Eden, W. J. and Kubota, J. K. (1962), Some Observations on the Measurement of Sensitivity of Clays, *Proceedings of American Society for Testing and Materials*, Vol. 61, pp. 1239–1249.

Holtz, R. D. and Kovacs, W. D. (1981), *An Introduction to Geotechnical Engineering*, Prentice Hall, Englewood Cliffs, NJ.

Lambe, T. W. and Whitman, R. V. (1969), *Soil Mechanics*, John Wiley & Sons, New York.

Mitchell, J. K. and Soga, K. (2005), *Fundamentals of Soil Behavior*, 3rd ed., John Wiley & Sons, New York.

Scott, R. F. (1963), *Principles of Soil Mechanics*, Addison-Wesley.

Seed, H. B., Woodward, R. J., and Lundgren, R. (1962), Prediction of swelling potential for compacted clays, *Journal of Soil Mechanics and Foundations Division*, ASCE, Vol. 88, No. SM3, pp. 53–87.

Skempton, A. W. and Northey, R. D. (1952), The Sensitivity of Clays, *Geotechnique*, Vol. 3, pp. 30–53.

Skempton, A. W. (1953), The Colloidal Activity of Clays, *Proceedings of the Third International Conference of Soil Mechanics and Foundation Engineering*, Vol. 1, pp. 57–61.

Tovey, N. K. (1971), A Selection of Scanning Electron Micrographs of Clays, *CUED/C-SOILS/TR5a*, University of Cambridge, Department of Engineering.

University of Southern California (2008), http://gees.usc.edu/ce467/Fall2006/Material/2_Characterization/quick_clay_landslide_in_rissa.htm

Watabe, Y., Tanaka, M., and Takamura, J. (2004), Evaluation of in-situ K_0 for Ariake, Bangkok and Hai-Phong clays, *Proceedings of the 2nd International Conference on Site Characterization*, Porto, pp. 1765–1772.

Yong, R. and Warkentin, B. P. (1975), *Soil Properties and Behavior*, Elsevier.

Problems

3.1 What are the key differences between clay minerals and 0.1-μm-diameter silica spheres?
3.2 Why are the clay surfaces charged negatively?
3.3 What is the importance of the adsorbed water layer around clay surface?
3.4 Why does montmorillonite clay swell more than kaolinite clay?
3.5 How does the specific surface of clays affect the properties of clays?

3.6 Why do some clays flocculate and some disperse?

3.7 How are the edge-to-face flocculated clays formed?

3.8 The following data are obtained from a liquid limit test. Draw the flow curve and determine LL value of the soil.

Blow Count, N	Water Content, %
55	23.5
43	27.9
22	36.4
15	45.3

3.9 The following water content data are from several plastic limit tests for a soil. Determine PL of the soil as the average of those values.

Test 1		Test 2		Test 3		Test 4	
Wet wt. + tare wt., gf	25.3	Wet wt. + tare wt., gf	28.3	Wet wt. + tare wt., gf	22.3	Wet wt. + tare wt., gf	26.3
Dry wt. + tare wt., gf	22.3	Dry wt. + tare wt., gf	24.5	Dry wt. + tare wt., gf	19.5	Dry wt. + tare wt., gf	23.2
Tare wt., gf	1.8	Tare wt., gf	1.8	Tare wt., gf	1.8	Tare wt., gf	1.8

3.10 Problems 3.8 and 3.9 are for a same soil and its natural water content at in situ was 32.5%. Determine
(a) Plasticity index of the soil.
(b) Liquidity index of the soil.

3.11 A shrinkage limit test for a saturated specimen had the initial volume V_i = 21.35 cm^3 and initial weight W_i = 37 gf (= 37 × 0.00981 = 0.363 N). After drying, it became V_f = 14.3 cm^3 and W_f = 26 gf (26 × 0.00981 =0.255 N). Compute the shrinkage limit (SL) of this soil.

3.12 Atterberg limits (LL and PL) and % clay fraction (<2 μm) are obtained for the following soils. For each soil
(a) Compute activity.
(b) Evaluate the severity for swelling potential.

	Soil 1	Soil 2	Soil 3
LL	140	53	38
PL	73	32	27
% Clay fraction	50	50	50

3.13 How was the Scandinavian quick clay formed? Was it sensitive when it was originally formed?

3.14 Explain what LI > 1.0 (100%) mean. Is it possible? If so, what will be such a situation?

4 Soil Classification

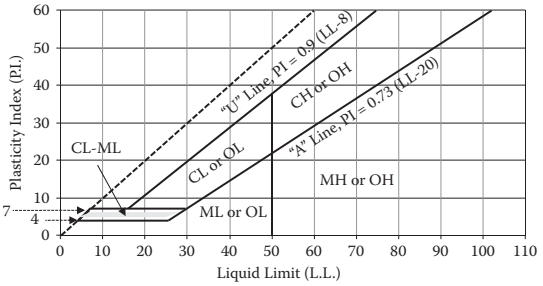

4.1 INTRODUCTION

Soils are all different, depending on their origins, compositions, locations, geological histories, and many other factors. Two soils may be quite different, even though they were obtained from nearby boring holes on the same construction site. And thus, in situ and laboratory tests on soil specimens are very important to obtain their index parameters and engineering characteristics. However, it is more convenient for engineers when soils are categorized into several groups with similar engineering behaviors. Engineers can understand approximate engineering characteristics of those grouped soils without actual laboratory or field tests. This process is called **soil classification,** and it helps engineers in the preliminary design stage of geotechnical engineering problems.

Most soil classification standards use soil indices such as Atterberg limits (liquid limit, plastic limit), soil gradation information (D_{10}, D_{50}, C_u, C_g), etc. In current geotechnical engineering practice, two standards are widely used in the United States: The **Unified Soil Classification System (USCS)** and **AASHTO (**American Association of State Highway and Transportation Officials) method.

4.2 UNIFIED SOIL CLASSIFICATION SYSTEM (USCS)

First, developed by Arthur Casagrande for wartime airfields construction in 1942, the system was modified and adopted for regular use by the Army Corps of Engineers and then by the Bureau of Reclamation in 1952 as the **Unified Soil Classification System** (***Casagrande 1948***). Currently, it is adapted in ASTM (Designation D-2487) and periodically updated. This is the most widely used classification system by geotechnical engineers.

The system uses simple six major symbols and four modifiers as in the following:

Major symbols:
- **G** Gravel
- **S** Sand
- **M** Silt
- **C** Clay
- **O** Organic
- **Pt** Peat

Modifiers:
- **W** Well graded (for gravel and sand)
- **P** Poorly graded (for gravel and sand)
- **H** High plasticity (for silt, clay, and organic soils)
- **L** Low plasticity (for silt, clay, and organic soils)

Classified group names are combinations of these characters. For example, GP for poorly graded gravel, SW for well-graded sand, CH for high-plasticity clay, SM for silty sand, etc. And thus, GW, GP, GM, and GC are possible group names for gravelly soil; SW, SP, SM, and SC are for sandy soils; MH and ML are for silty soils; CH and CL for clayey soils; OH and OL for organic soils; and Pt stands alone for peat. Dual naming is also possible for several boundary soils, such as GW–GM (well-graded gravel with silt), GC–GM (silty clayey gravel), SW–SM (well-graded sand with silt), etc.

This system uses LL, PL, and PI (= LL − PL), and soils' gradation information. First, from a grain size distribution curve, the percentages of each component (gravel [$d > 4.75$ mm], sand [$4.75 \text{ mm} \geq d \geq 0.075$ mm], and fine [$d < 0.075$ mm]) are identified as shown in Figure 4.1.

From this, the values of F_{200}, R_{200}, F_4, and R_4 are obtained as

F_{200}: % finer than No. 200 Sieve (0.075 mm) = % of fine content
R_{200}: % retained on No. 200 Sieve (0.075 mm) = % of sand and gravel content
F_4: % finer than No. 4 Sieve (4.75 mm) = % of sand and fine content
R_4: % retained on No. 4 Sieve (4.75 mm) = % of gravel content

Note that in USCS, clay and silt are categorized as "**fine**."

Next, the coefficient of uniformity C_u (= D_{60}/D_{10}) and the coefficient of gradation C_g (= $(D_{30})^2/(D_{60} \times D_{10})$) are calculated.

Based on those values, the classification procedure is summarized in a flowchart in Figure 4.2. The chart starts from F_{200} information as far left in the following steps.

4.2.1 For G or S

1. If $F_{200} < 50\%$ (or $R_{200} \geq 50\%$, i.e., gravel and sand content is more than 50%), then soil is G or S.
2. Then, if $R_4 \geq \frac{1}{2}F_{200}$ (gravel content ≥ sand content), it is G, or if $R_4 < \frac{1}{2}F_{200}$ (gravel content < sand content), it is S.

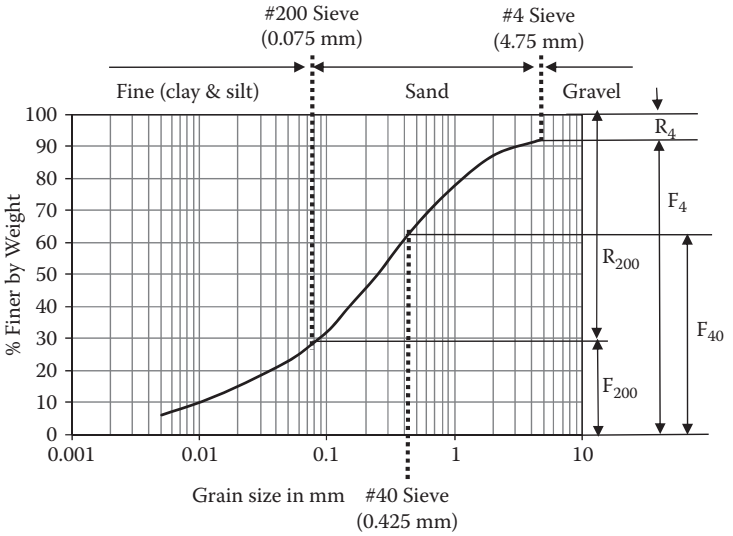

FIGURE 4.1 Definitions of F_{200}, R_{200}, F_{40}, F_4, and R_4.

3. In the next step, F_{200} (fine content) is checked for G and S. If $F_{200} < 5\%$, naming fine content is ignored and soils will be GW, GP, SW, or SP. If $F_{200} > 12\%$, soils will be GM, GC, SM, or SC. When $5\% \leq F_{200} \leq 12\%$, double naming comes in as GW–GM, GW–GC, GP–GM, and GP–GC for gravel or SW–SM, SW–SC, SP–SM, and SP–SC for sand.
4. In the final step for gravel and sand, C_u and C_g values are evaluated for modifiers W or P. For gravel, $C_u \geq 4$ and $1 \leq C_g \leq 3$ are conditions for W and the other values of those are for P. For sand, the condition for W is $C_u \geq 6$ and $1 \leq C_g \leq 3$ and the other values are for P.
5. For GW and GP soils, if % sand content is at or more than 15%, it is named as GW or GP with sand.
6. Similarly, for SW and SP soils, if % gravel content is at or more than 15%, it is named as SW or SP with gravel.

4.2.2 For C, M, O, or Pt

1. Going back to the F_{200} value in Figure 4.2, if $F_{200} \geq 50\%$ (i.e., fine contents are at or more than 50%), then soil is either M or C (or possibly O or Pt).
2. To classify M or C, **plasticity chart** (Figure 4.3) is used. It utilizes LL and PI (= LL − PL) values. LL and PL tests shall be performed on F_{40} specimen (soil passed No. 40 sieve (0.425 mm)), and LL and PI data point of the soil tested is plotted on the plasticity chart to identify soil type (CH, CL, MH, ML, or CL-ML) by the zone on which the data point falls.

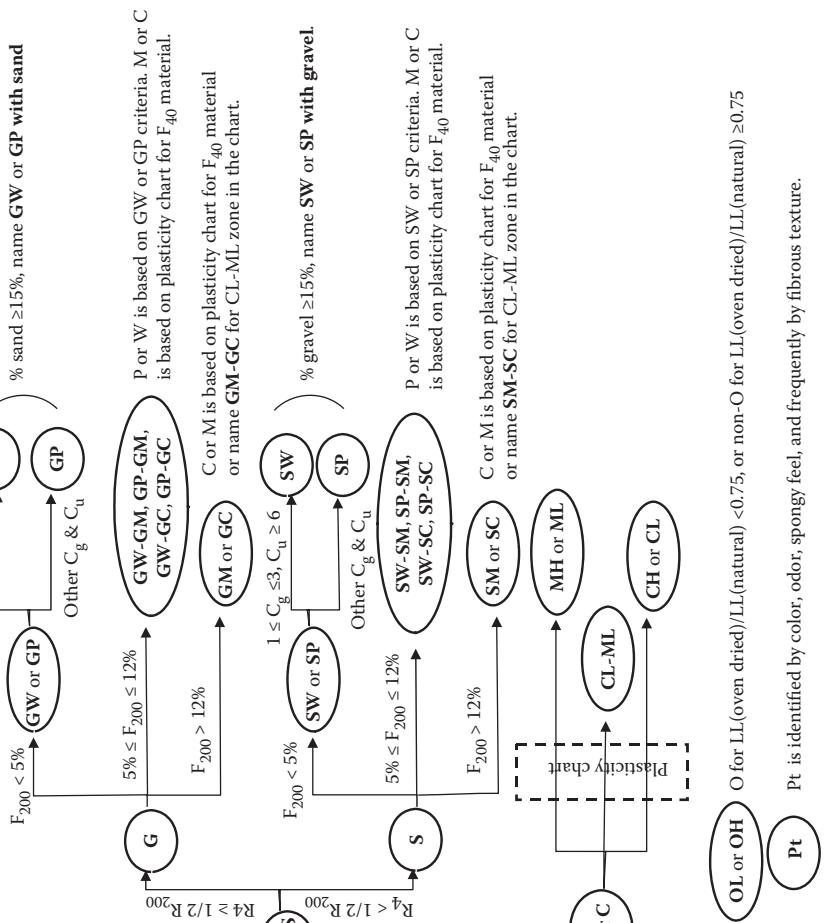

FIGURE 4.2 Flowchart for USCS.

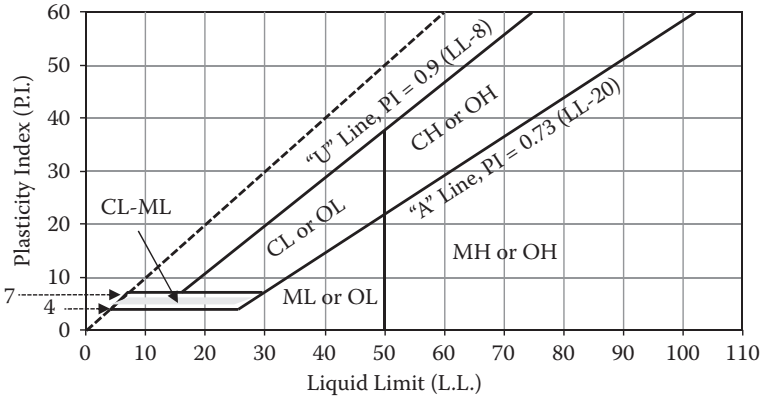

FIGURE 4.3 Plasticity chart for USCS.

3. On the plasticity chart, most natural soils fall below "U" line and around "A" line or CL-ML zone. It shall be noted that LL = 50 is the boundary LL for high-plastic (LL > 50) or low-plastic (LL < 50) soils.
4. These M or C classification method by the plasticity chart is also used in subgroup names in gravel and sand category soils with their fine contents between 5% and 12%. These are GM, GC, SM, SC, and dual named soils GW–GM, GW–GC, GP–GM, and GP–GC for gravel or SW–SM, SW–SC, SP–SM, and SP–SC for sand. Note that for gravels and sands, it also uses only F_{40} specimen for LL and PL determination as mentioned before.
5. Pt (**peat**) shall be identified by its color, odor, spongy feeling, and frequently by fibrous texture by testing engineers. O (**organic soil**) can be identified by observing the change in LL values from natural soil to oven-dried (burns some organic) soil. If LL (oven dried)/LL (natural) < 0.75, it is classified as O. If the ratio ≥0.75, it is nonorganic.

Since USCS uses simple symbols with their meanings, it is easy to understand the nature of soils from classified group names. Also, it requires only LL and PL tests and sieve analysis. Hydrometer test is not required since the silt and clay are treated as "fine," and it uses the plasticity chart to identify the clay and silt. USCS and its modified versions are the most widely used soil classification system around the world today. Engineers provided useful general guidelines for those classified soils in different applications such as roadway construction, compaction practice, etc. Table 4.1 shows such an example for roads and airfields.

TABLE 4.1
USCS Group and its Relations to Various Engineering Properties

Symbols		Value as Subbase or Subgrade	Value as Base Course	Potential Frost Action	Compressibility and Expansion	Drainage Characteristics	Dry Unit Weight pcf[c]	Field CBR	Subgrade modulus K, pci[d]
GW		Excellent	Good	None to very slight	Almost none	Excellent	125–140	60–80	>300
GP		Good to excellent	Poor to fair	None to very slight	Almost none	Excellent	110–130	25–60	>300
GM	d[a]	Good to excellent	Fair to good	Slight to medium	Very slight	Fair to good	130–145	40–80	>300
	u[b]	Good	Poor	Slight to medium	Slight	Poor to impervious	120–140	20–40	200–300
GC		Fair to good	Poor	Slight to medium	Slight	Poor to impervious	120–140	20–40	200–300
SW		Good	Poor	None to very slight	Almost none	Excellent	110–130	20–40	200–300
SP		Fair to good	Poor to not suitable	None to very slight	Almost none	Excellent	100–120	10–25	200–300
SM	d[a]	Good	Poor	Slight to high	Very slight	Fair to poor	120–135	20–40	200–300
	u[b]	Fair to good	Not suitable	Slight to high	Slight to medium	Poor to impervious	105–130	10–20	200–300
SC		Fair to good	Not suitable	Slight to high	Slight to medium	Poor to impervious	105–130	10–20	200–300
ML		Fair to poor	Not suitable	Medium to very high	Slight to medium	Fair to poor	100–125	5–15	100–200
CL		Fair to poor	Not suitable	Medium to high	Medium	Impervious	100–125	5–15	100–200
OL		Poor	Not suitable	Medium to high	Medium to high	Poor	90–105	4–8	100–200
MH		Poor	Not suitable	Medium to very high	High	Fair to poor	80–100	4–8	100–200
CH		Poor to very poor	Not suitable	Medium	High	Impervious	90–110	3–5	50–100
OH		Poor to very poor	Not suitable	Medium	High	Impervious	80–105	3–5	50–100
Pt		Not suitable	Not suitable	Slight	Very high	Fair to poor	—	—	—

[a] *d for LL ≤ 28 and PI ≤ 6.*

[b] *u for LL > 28.*

[c] *1 pcf (lb/ft³) = 0.1572 kN/m³.*

[d] *1 pci (lb/in³) = 271.43 kN/m³.*

Source: After U.S. Air Force Engineering Support Agency/Civil Engineering Squad (AFCESA/CES)(1997), Criteria and Guidance for C-17 Contingency and Training on Semi-Prepared Airfields, *Engineering Technical Letter 97–9.*

4.3 AASHTO CLASSIFICATION SYSTEM

AASHTO soil classification was developed in the late 1920s by the U.S. Bureau of Public Roads (now the Federal Highway Administration) for road constructions. The current version, which was revised in 1945, is used for extended applications in road bases, subbases, subgrades, and embankment constructions (***AASHTO 1995***). As a reference, the terminology of road construction materials such as **base**, **subbase**, **subgrade**, etc., are shown in Figure 4.4 for typical rigid (concrete) and flexible (asphalt cement) pavement systems.

AASHTO method uses Atterberg limits (LL and PL), and information on grain size distribution curve (F_{10}, F_{40}, and F_{200}), which are the percent passing on No. 10 sieve, No. 40 sieve, and No. 200 sieve, respectively. The procedure uses an elimination process of columns in Table 4.2, from the upper left corner (F_{10}) toward downward and right. If the condition on the row is not satisfied, the entire column is eliminated and it is never referred back. After the last row check for PI, one or possibly more than one column may survive this elimination process.

If more than one column survived, the first column from the left is selected as a group or subgroup name. The group names are A-1 through A-7 with some subgroups. In general, the left-side group is better than the right side one as roadway construction materials.

In addition, **Group Index** (GI), as defined in the following, shall be calculated and reported in the AASHTO system.

$$GI = (F_{200} - 35)\,[0.2 + 0.005(LL - 40)] + 0.01(F_{200} - 15)(PI - 10) \tag{4.1}$$

There are some rules in Equation 4.1:

1. When GI is calculated as negative values, report GI = 0.
2. GI is reported in rounded integer numbers. For example, GI = 4.4 shall be reported as 4 and GI = 4.5 shall be reported as 5.
3. For A-2-6 and A-2-7 subgroups, use only the second term of Equation 4.1 and assign the first term always zero, that is,

$$GI = 0.01(F_{200} - 15)(PI - 10) \tag{4.2}$$

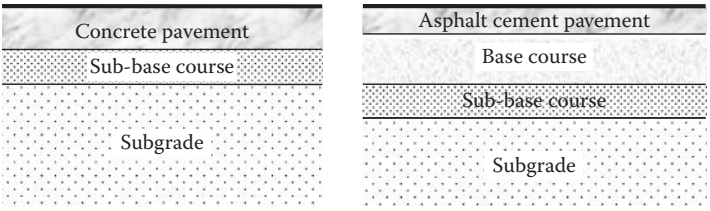

(a) Rigid pavement system (concrete)

(b) Flexible pavement system (asphalt cement)

FIGURE 4.4 Typical road pavement systems.

TABLE 4.2
Classification of Soils and Soil Aggregate Mixtures

General Classification	Granular Materials (35% or Less Passing 0.075 mm)							Silt–Clay Materials (More than 35% Passing 0.075 mm)			
Group Classification	A-1			A-2							A-7
	A-1-a	A-1-b	A-3	A-2-4	A-2-5	A-2-6	A-2-7	A-4	A-5	A-6	A-7-5[a] A-7-6[b]
Sieve analysis, % passing											
No.10 (2.00 mm)	50 max	—	—	—	—	—	—	—	—	—	—
No.40 (0.425 mm)	30 max	50 max	51 min	—	—	—	—	—	—	—	—
No. 200 (0.075 mm)	15 max	25 max	10 max	35 max	35 max	35 max	35 max	36 min	36 min	36 min	36 min
For F_{40} materials											
Liquid limit	—		—	40 max	41 min	40 max	41 min	40 max	41 min	40 max	41 min
Plasticity index	6 max		N.P.	10 max	10 max	11 min	11 min	10 max	10 max	11 min	11 min[a]
Usual types of significant constituent materials	Stone fragments, gravel, and sand		Fine sand	Silty or clayey gravel and sand				Silty soils		Clayey soils	
General ratings as subgrade	Excellent to good							Fair to poor			

a: *For A-7-5, PI ≤ LL – 30.*

b: *For A-7-6, PI> LL- 30.*

Source: After AASHTO 1995.

The standard says that under average conditions of good drainage and thorough compaction process, the supporting value of a material as subgrade may be assumed as an inverse ratio to the group index; that is, a group index of zero (0) indicates a "good" subgrade material and a group index of 20 or greater indicates a "very poor" subgrade material.

Exercise 4.1

Soil gradation curve is shown in Figure 4.5. Classify the soil (a) by USCS and (b) by AASHTO classification methods. LL = 46% and PL = 35% were obtained for F_{40} material of the specimen.

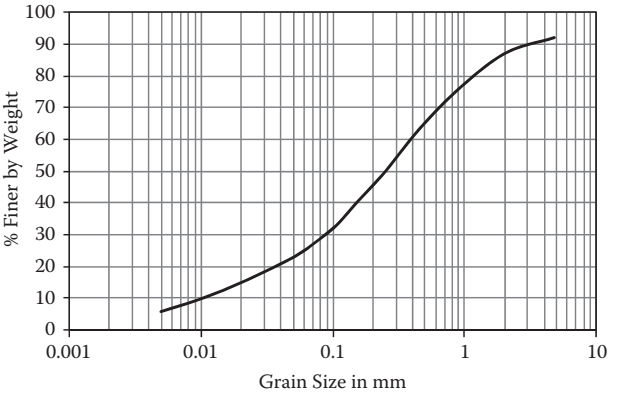

FIGURE 4.5 Gradation curve for Exercise 4.1.

Solution:

From the gradation curve, the following values can be read:

% passing No. 4 (4.75 mm) = 92%
% passing No. 10 (2.0 mm) = 87%
% passing No. 40 (0.425 mm) = 63%
% passing No. 200 (0.075 mm) = 28%
$F_{200} = 28\%$, and thus $R_{200} = 72\%$
$F_4 = 92\%$, and thus $R_4 = 8\%$
$D_{10} = 0.01$ mm
$D_{30} = 0.090$ mm
$D_{60} = 0.39$ mm
$C_u = D_{60}/D_{10} = 0.39/0.01 = 39$
$C_g = (D_{30})^2/(D_{60} \times D_{10}) = (0.090)^2/(0.01 \times 0.39) = 2.08$

and

LL = 46
PI = 46 − 35 = 11

(*a*) *USCS Method*

By using the flowchart in Figure 4.2, since F_{200} (28) < 50%, it shall be G or S.
$R_4(8) < ½R_{200}(72) = 36$, and thus, it shall be S.
$F_{200}(28) > 12\%$ and it shall be SM or SC.
LL(46) and PL(11) falls in the region of ML or OL in the plasticity chart (Figure 4.3).
And thus, the soil is classified as **SM (silty sand).** ←

(*b*) *AASHTO Method*

By using elimination process in Table 4.2 from top left,

(% passing No. 10 = 87) eliminates A-1-a
(% passing No. 40 = 63) eliminate A-1-b, but A-3 survives
(% passing No. 200 = 28) eliminates A-3, A-4, A-5, A-6 and A-7
LL = 46 eliminates A-2-4 and A-2-6
PI = 11 eliminates A-2-5

And thus, survived subgroup is **A-2-7 (silty or clayey gravel and sand)**. ←
Since it is A-2-7, Equation 4.2 is used for group index computation.
GI = 0.01(F_{200} − 15)(PI − 10) = 0.01(28 − 15)(11 − 10) = 0.13 → 0 (rounded integer). **GI = 0**
And thus, this soil is classified as **A-2-7 (GI = 0).** ←

4.4 SUMMARY

Widely used soil classification systems, namely, USCS and AASHTO, were presented in this chapter. Classification systems provide general guidelines of soil types based on the results of rather simple sieve analysis and Atterberg limits tests. Based on the accumulated data for many years, many convenient relationships between classified soil groups and many engineering properties have been prepared. Table 4.1 is such an example. Geotechnical engineers could use those properties for the primary phase of engineering design and analysis if needed. For detailed and later design phases, however, undisturbed specimens shall be tested in the field (in situ test), or sampled and tested in laboratories to obtain more reliable soils' properties and engineering design values.

REFERENCES

AASHTO (1995), *Standard Specifications for Transportation Materials and Methods of Sampling and Testing*, 17th ed., Part I Specifications, Designation M 145.

Casagrande, A. (1948), Classification and Identification of Soils, *Transaction of ASCE*, Vol. 113, pp. 901–991.

U.S. Air Force Engineering Support Agency/Civil Engineering Squad (AFCESA/CES) (1997), Criteria and Guidance for C-17 Contingency and Training on Semi-Prepared Airfields, *Engineering Technical Letter 97–9*.

Problems

4.1–4.4 Figure below shows grain size distribution curves for soils A, B, C, and D with their LL and PL values. For each soil,

(a) Classify the soil according to USCS
(b) Classify the soil according to AASHTO including GI computation
(c) Discuss the suitability of the soil as subgrade material

Problem	Soil	LL	PL
4.1	A	55	25
4.2	B	45	26
4.3	C	25	19
4.4	D	42	33

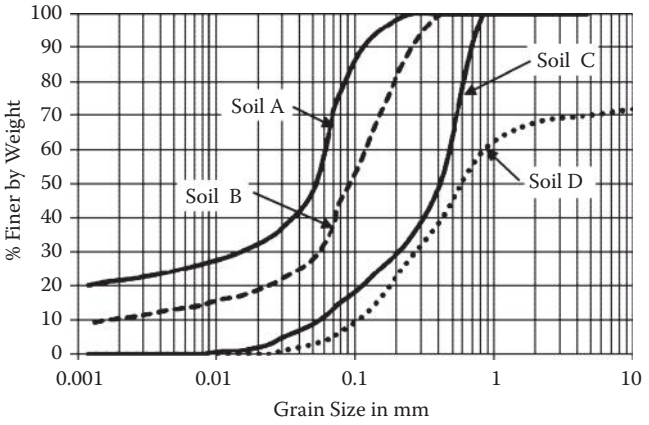

4.5–4.8 Figure below shows grain size distribution curves for soils E, F, G, and H with their LL and PL values. For each soil,

(a) Classify the soil according to USCS
(b) Classify the soil according to AASHTO including GI computation
(c) Discuss the suitability of the soil as subgrade material

Problem	Soil	LL	PL
4.5	E	55	27
4.6	F	43	22
4.7	G	46	28
4.8	H	41	32

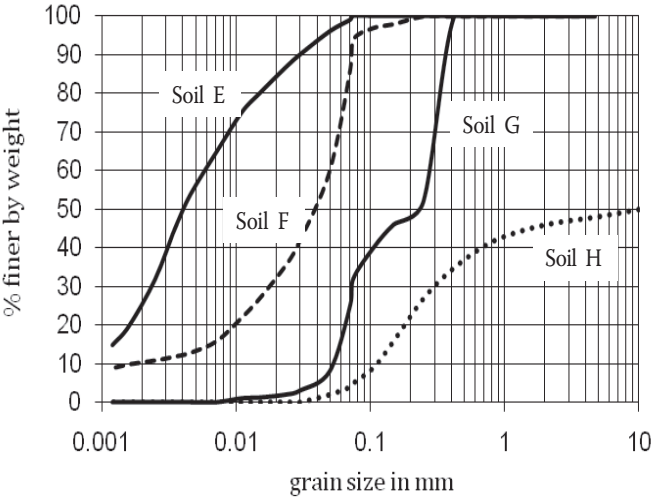

5 Compaction

5.1 INTRODUCTION

The soil's footing supporting capacity (bearing capacity), settlement, shear strength, etc., all depend on how well the soil is compacted. Compaction increases the soil's strength and decreases compressibility and permeability. It may also control characteristics of swelling and shrinkage and frost susceptibility. Compaction is a physical process to decrease the voids of soil by static or dynamic loading. For example, granular soils are easily compacted by vibration, while saturated cohesive soils cannot be well compacted by dynamic loads because of viscous resistance of pore water pressure to transient loadings. Compaction characteristics are first discussed based on the laboratory compaction test. Then compaction specification in the field, field compaction techniques, and field inspection methods are discussed. Related subjects, such as relative density and California Bearing Ratio (CBR), are also presented in this chapter.

5.2 RELATIVE DENSITY

It is important to know the level of compaction that has been achieved on earth works or on existing earth. Soil's unit weight value (either dry or wet condition) alone cannot tell its compaction level since the ranges of unit weight vary

depending on the type of soils. For example, well-graded gravelly soil may have the unit weight ranging from 18 to 20 kN/m^3 (or 115 to 127 lb/ft^3). On the other hand, for soils with more cohesive materials, the range may be 15 to 18 kN/m^3 (or 96 to 115 lb/ft^3). In order to indicate the level of compaction relative to the densest and the loosest compaction level for a given specific soil, mostly for granular soils, **relative density** (D_r) is introduced and is defined in the following equation:

$$D_r = \frac{e_{max} - e}{e_{max} - e_{min}} \times (100\%) \tag{5.1}$$

Where e_{max}, e_{min}, and e are the **maximum**, **minimum,** and in-situ soil's **void ratios**, respectively. When the in-situ soil's void ratio is in its loosest ($e = e_{max}$) state, then, $D_r = 0\%$. If it is in its densest ($e = e_{min}$), $D_r = 100\%$. D_r values of most in-situ soils are between 0% and 100%. Table 5.1 shows some guidelines of relationships among the relative densities, level of denseness, SPT (Standard Penetration Test) N_{60} value, and the effective friction angle of soils (Chapter 12). The $\mathbf{N_{60}}$ **value** is the modified SPT blow count adjusted to 60% hammer drop energy and is directed to many practical design values in foundation engineering practice. Readers are directed to other references on SPT (e.g., ***Peck et al. 1974***).

e_{min} and e_{max} are determined in the laboratory as follows (ASTM D-4253) for dry granular soils. As shown in Figure 5.1, dry granular soil is poured gently (without any vibration) into a rigid mold through a funnel. The funnel is moved up in a spiral motion to distribute grains evenly over the entire cross section of the mold and the drop heights of particles are maintained at about 25.4 mm (1 in.) till the top of the mold. The top surface is leveled by a straight edge to coincide exactly with the level of the top edge of the mold. The specimen in the mold is weighed, and the unit weight of the loosest specimen γ_{min} is calculated from the weight and inside volume of the mold.

TABLE 5.1
Relative Density with Soil Parameters

Relative Density, Dr (%)	Level of Denseness	Standard Penetration Resistance, N_{60} (*Terzaghi and Peck 1967*)	Effective Friction Angle, φ′ (Degree) (*Peck et al. 1974*)
<20	Very loose	<4	<29
20–40	Loose	4–10	29–30
40–60	Medium	10–30	30–36
60–80	Dense	30–50	36–41
>80	Very dense	>50	>41

Source: After U.S. Army Corps of Engineers (1992), *Engineer Manual*, EM 1110-1-1905.

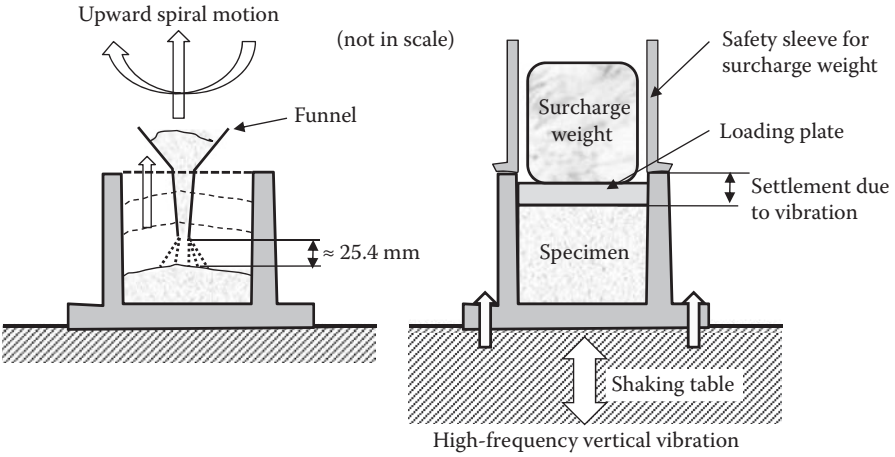

FIGURE 5.1 Maximum and minimum void ratio determination.

From Equation 2.9 (by substituting S = 0 for dry soil),

$$\gamma_{min} = \frac{G_s \gamma_w}{1 + e_{max}}, \quad \text{and thus} \quad e_{max} = \frac{G_s \gamma_w}{\gamma_{min}} - 1 \tag{5.2}$$

To determine e_{min}, the loosest specimen after the γ_{min} determination test is used. A surcharged weight, which applies 13.8 kN/m^2 (2 psi) on the specimen, is placed on the top of the specimen in the mold. The whole mold is firmly bolted on a shaking table and shaken vertically for 8 min with 60 Hz (cycle/second) and 0.33 mm peak-to-peak displacement, or for 12 min with 50 Hz and 0.48 mm peak-to-peak displacement. After shaking, the settlement of the specimen is carefully measured by a dial gauge, and the volume of the densified specimen is computed. The value of γ_{max} is calculated as the weight of soil divided by its volume in the mold. The void ratio e_{min} is then obtained as

$$e_{min} = \frac{G_s \gamma_w}{\gamma_{max}} - 1 \tag{5.3}$$

After several experimental trials, the mean values are reported as γ_{min} (or e_{max}) and γ_{max} (or e_{min}).

By substituting Equations 5.2 and 5.3 into Equation 5.1, the relative density, D_r, can also be defined as

$$Dr = \frac{\gamma - \gamma_{min}}{\gamma_{max} - \gamma_{min}} \bullet \frac{\gamma_{max}}{\gamma} \quad (\times 100\%) \tag{5.4}$$

5.3 LABORATORY COMPACTION TEST

In the laboratory, specimens with different water contents are compacted with the same level of compaction energy. Water contents versus compacted soil's dry densities are then plotted to determine the optimum compaction effort. In the early 1930s, ***Proctor (1933)*** developed a standard compaction procedure during earth dam construction projects. This method is called the **Proctor method**, and its original version and some modified versions are currently used in ASTM (D-698 and D-1557) and AASHTO (T-99 and T-180).

5.3.1 Standard Proctor Test Procedure

The Standard Proctor method follows the following steps:

1. Mix dry soil thoroughly with water to prepare a uniform specimen with designed water content.
2. Pour the specimen at a little over one-third depth into a standard-size mold 101.6 mm (4 in.) diameter, 116.43 mm (4.584 in.) high without an extension collar, with 944 cm^3 (1/30 ft^3) volume as seen in Figure 5.2a.
3. Compact the specimen by 25 free drops of a rammer (W 24.5 N (2.5 kgf or 5.5 lbf)) from 304.8 mm (12 in.) high as seen in Figure 5.2b. The mold should be placed on a hard ground to avoid possible compaction energy loss.
4. Repeat Steps 1 to 3 for the second and thirds layers to fill the mold with soil slightly above the top level of the mold. For the third-layer compaction, an extension collar is attached.
5. Remove the extension collar and trim the specimen surface by a straight edge to get exactly 944 cm^3 (1/30 ft^3) volume of the specimen.

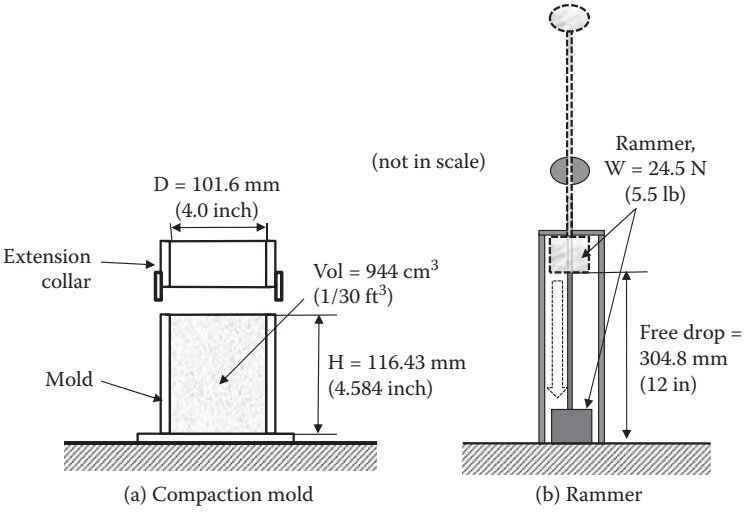

FIGURE 5.2 Standard Proctor compaction device.

6. Weigh the whole mold with soil in it to obtain the wet weight of the specimen.
7. Extrude the specimen from the mold and obtain a representative soil specimen in a container for water content determination.
8. Repeat Steps 1 to 7 for several different water content. In general, soils from the previous experiment could be reused for the next test by breaking down to particles and remixing with additional water.

5.3.2 Compaction Curve

After the experiment, a set of wet (total) unit weight (γ_t) and water content (w) are measured. The compaction effectiveness, however, is compared in terms of increased **dry unit weight** (γ_d) of the specimen instead of total unit weight (γ_t). Equation 2.10 (as Equation 5.5) is used to explain this.

$$\gamma_t = (1+w)\frac{G_s \gamma_w}{1+e} = (1+w)\gamma_d \quad \text{or} \quad \gamma_d = \frac{G_s \gamma_w}{1+e} = \frac{\gamma_t}{1+w} \tag{5.5}$$

As seen in the first term of the γ_t expression, increasing *w* increases γ_t for a same value of void ratio *e*, which is a measure of compaction effectiveness. ***Thus γ_t cannot be used to evaluate the effectiveness of compaction. The γ_d expression in Equation 5.5 shows a direct relationship between "e" and "γ_d." Accordingly, $\gamma_d = \gamma_t/(1 + w)$ in Equation 5.5 is used in the compaction analysis.*** Note that the obtained γ_d is for a mathematically dried-out specimen (the weight of water was eliminated in its three-phase diagram by keeping the same volume for the void) without any shrinkage, which occurs in the physical drying process. Accordingly, γ_d and w relations are plotted. Table 5.2 shows an example computation of test data, and the results are plotted in Figure 5.3.

TABLE 5.2
Example Computation of Compaction Test Data

A	B	C
Water Content, w (%)	Total (wet) Unit Weight, γ_t (kN/m^3)	Dry Unit Weight, γ_d (kN/m^3) (= γ_t/(1+w))
2.3	15.80	15.45
4.5	17.18	16.44
6.7	18.83	17.65
8.5	19.72	18.18
10.8	20.04	18.08
13.1	19.34	17.10
15	18.45	16.04

Note: C(i) = B(i)/(1+A(i)/100).

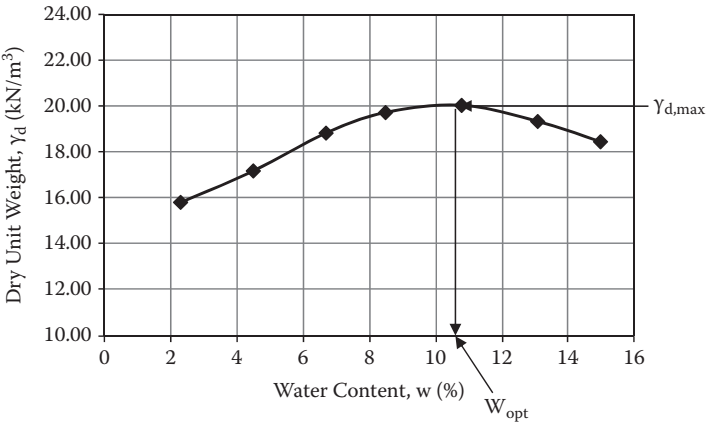

FIGURE 5.3 Example compaction curve.

In Figure 5.3, γ_d increases with increase of *w* in the beginning, reaches the peak at w ≈ 10.6%, and drops thereafter. The peak γ_d is defined as the **maximum dry unit weight** $\gamma_{d,max}$, and the corresponding water content is called the **optimum water content**, w_{opt}. In the beginning, the addition of water works as a lubricant between particles to reduce the void and then to increase the unit weight. However, when the void is highly saturated with water, water starts to work as a cushion against compaction energy and does not work anymore to increase the soil's unit weight, but rather to decease it with increased water content due to reduced compaction energy to the soil's skeleton. Thus, there is an optimum amount of water to transmit the most compaction energy to soil grain structures. During compaction experiment, the optimum water content can be felt by pushing the surface of compacted soil by a thumb. Until the optimum water content has been reached, the surface is hard to push. After passing the optimum level, the surface becomes soft and spongy.

5.3.3 Zero Air Void (ZAV) Curve

From Equation 5.5 and using $Se = G_s w$ relation in Equation 2.17, γ_d can be rewritten as

$$\gamma_d = \frac{G_s \gamma_w}{1+e} = \frac{G_s \gamma_w}{1+\frac{G_s w}{S}} \tag{5.6}$$

Equation 5.6 shows a unique relationship between γ_d and w for a fixed S (degree of saturation) value and for a given G_s value. Figure 5.4 plots a group of curves from Equation 5.6 for various S values (40%, 60%, 80%, and 100%) with $G_s = 2.7$.

It can be seen that, when w increases, S increases. At $\gamma_{d\,max}$, S reaches more than 90% and S approaches nearly 100% (full saturation) when the water content passes w_{opt}. The S = 100% curve is called the **ZAV curve**, and compaction curves approach the ZAV curve at high water content as seen. Therefore, this curve is often used as a guideline to construct a proper compaction curve for a higher-water-content zone.

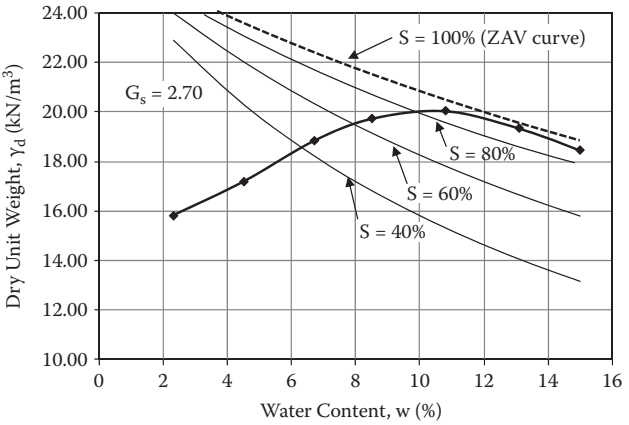

FIGURE 5.4 Compaction curve with various S (degree of saturation) values.

5.3.4 Compaction Energy

The Proctor test is a standard test with compaction energy of

$$\begin{aligned} E &= \sum[W \text{ (weight of rammer)} \times h \text{ (height of drop)/volume of specimen}] \\ &= 24.5 \text{ N} \times 0.3048 \text{ m} \times 3 \text{ (layers)} \times 25 \text{ (drops)}/944 \times 10^{-6} \text{ m}^3 \\ &= 594 \text{ kN-m/m}^3 \rightarrow 600 \text{ kN-m/m}^3 \end{aligned} \tag{5.7}$$

There are several other modified versions of compaction energy obtained by changing the mold size, the weight of the rammer, the drop height, the number of drops, and the number of layers. Table 5.3 summarizes some of those modified versions.

TABLE 5.3
Various Compaction Energies in Laboratory Tests

Tests	Mold Size (D × H) (mm)	Mold Volume (cm^3)	Weight of Rammer (N)	Drop Height (m)	No. of Drops/ Layer	No. of Layers	Total Energy/Vol. (kN-m/m^3)
Standard Proctor	101.6 × 116.4	944	24.5	0.3048	25	3	593 ≈ 600
ASTM, D-698, Method C	152.4 × 116.4	2124	24.5	0.3048	56	3	591 ≈ 600
ASTM, D-1557, AASHTO, T-180, Method A	101.6 × 116.4	944	44.5	0.4572	25	5	2694 ≈ 2700
ASTM, D-1557, Method C, and AASHTO, T-180, Method D	152.4 × 116.4	2124	44.5	0.4572	56	5	2682 ≈ 2700

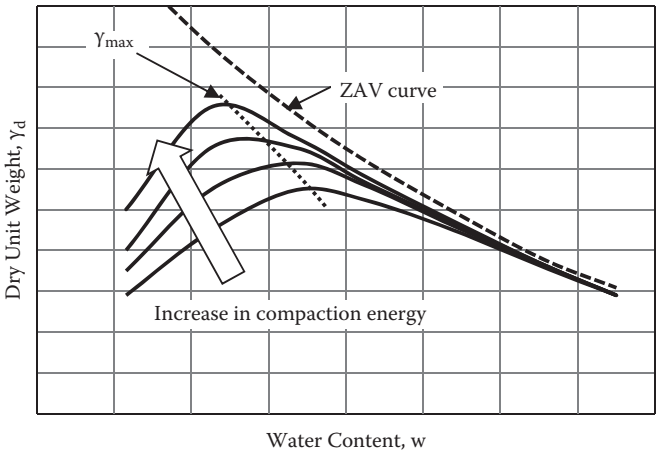

FIGURE 5.5 Compaction curves with various compaction energies.

When the compaction energy is increased, $\gamma_{d,max}$ increases. Since the ZAV curve confines the upper limit of the compaction curve, the corresponding w_{opt} decreases slightly as seen in an example in Figure 5.5. This observation suggests that, when a higher unit weight is required in the field, the field compaction energy shall be increased and, at the same time, water content shall be adjusted to have a slightly lower value to obtain the maximum effect of the increased compaction energy.

5.4 SPECIFICATION OF COMPACTION IN THE FIELD

After the compaction curve for a given soil is obtained from laboratory tests, the specification of compaction in the field is made. **Relative compaction** (R.C.) is defined as

$$\text{R. C.} = \frac{\gamma_{d,field}}{\gamma_{d,max}} \quad (\times 100\%) \tag{5.8}$$

where $\gamma_{d,field}$ is the specified dry unit weight, that shall be achieved in the field, and $\gamma_{d,max}$ is the maximum dry unit weight obtained from the laboratory compaction test. Since $\gamma_{d,max}$ varies depending on the compaction energy level or test method such as standard Proctor, etc., it shall be noted that R.C. could be more than 100% if the compaction energy in the laboratory was low. That implies that if a higher R.C. value (>100%) is required in the field, higher field compaction energy than the laboratory energy level is required to achieve the specified requirement. Table 5.4 provides a guide for tentative R.C. requirement for various types of soils in USCS and the importance of earthworks.

As can be seen in Table 5.4, the poorer the type of soil or the higher the importance of the earthwork, the higher the required R.C. values. It is noted again that those R.C. values are based on the standard Proctor test and so, if other the standards with different energy level are used, the required R.C. values may change.

TABLE 5.4
Tentative Requirements for Compaction Based on USCS

	Required R.C.—% of Standard Proctor Maximum		
Soil Group in USCS	**Class 1**	**Class 2**	**Class 3**
GW	97	94	90
GP	97	94	90
GM	98	94	90
GC	98	94	90
SW	97	95	91
SP	98	95	91
SM	98	95	91
SC	99	96	92
ML	100+	96	92
CL	100	96	92
OL	—	96	93
MH	—	97	93
CH	—	—	93
OH	—	97	93

Class 1: Upper 8 ft of fills supporting 1- or 2-story buildings
Upper 3 ft of subgrade under pavement
Upper 1 ft of subgrade under floors
Earth dams over 100 ft high
Class 2: Deeper parts of fills under buildings
Deeper parts (to 30 ft) of fills under pavements, floors
Earth dams less than 100 ft high
Class 3: All other fills requiring some degree of strength or incompressibility
Source: After Sowers, G. F. (1979), *Introductory Soil Mechanics and Foundations: Geotechnical Engineering*, 4th ed., Macmillan New York.

It is cautioned that the relative compaction R.C. in Equation 5.8 and the relative density D_r in Equation 5.1 (or Equation 5.4) shall not be mixed up since γ_{max} in Equation 5.8 is obtained from the compaction test at its optimum water content, while γ_{max} in Equation 5.4 for D_r is obtained from a standard maximum unit weight test for dry granular specimen. Those values are not necessarily the same.

Exercise 5.1

A soil sample is tested by the standard Proctor test, and the compaction curve obtained is shown in Figure 5.3. The specification says that the in-situ soil shall be compacted with 95% of R.C. and above of the maximum dry unit weight from the standard Proctor test. Determine the range of field water content to achieve the above specification.

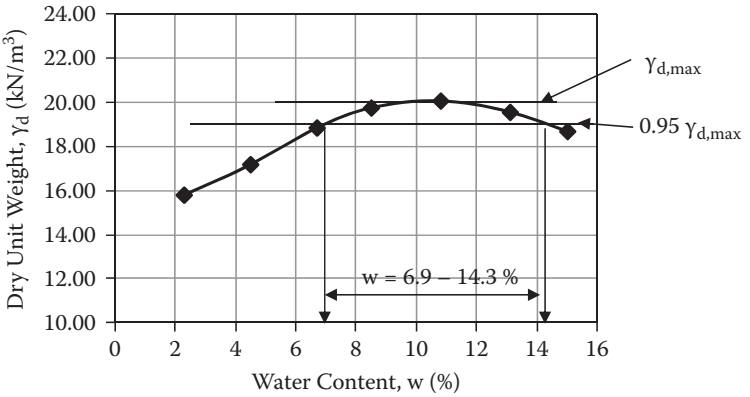

FIGURE 5.6 Solution to Exercise 5.1.

Solution:

From Figure 5.6, $\gamma_{d,max} = 20.0$ kN/m^3, and thus $\gamma_{d,\ field} = 0.95 \times 20.0$ kN/m^3 = 19.0 kN/m^3.

In Figure 5.6, $\gamma_{d,max} = 20.0$ kN/m^3 and $\gamma_{d,field} = 19.0$ kN/m^3 lines are drawn, and the corresponding range of water content, which satisfies $\gamma_{d,\ field} = 19.0$ kN/m^3 and above, is obtained as 6.9 to 14.4%.

5.5 FIELD COMPACTION METHODS

5.5.1 Compaction Equipments

After the compaction specification is given at the site, contractors are required to achieve its specified unit weight as the minimum in the field with proper equipments. For small jobs such as filling excavated small trenches, hand-operated vibratory tampers (Figure 5.7a) may be used. For larger job sites, several different types of heavy-duty compaction rollers are available. The commonly used compaction equipments are

Pneumatic rubber tire rollers (Figure 5.7b): The pneumatic rubber tire roller can be used for both sandy soils and as clayey soils. Soils are compacted with both tire pressure and kneading action.

Sheep's-foot rollers (Figure 5.7c): This unique wheel surface can effectively compact the clayey soils and the deeper part of soils in earlier passes.

Smooth-wheel (drum) rollers (Figure 5.7d): This is mostly used for both sandy and clayey soils for the finishing and smoothing process. The compaction pressure is not as high as in the former two rollers, and, therefore, it is not used to compact thicker layers.

Vibratory wheels: All the foregoing rollers are usually equipped with vibratory wheels, which are especially effective in compacting granular soils.

(a) Hand-operated vibratory tamper

(b) Pneumatic rubber tire roller

(c) Sheep's-foot roller

(d) Smooth wheel drum roller

FIGURE 5.7 Field compaction equipments.

Table 5.5 provides some guideline on the type of soils and applicable compaction equipments.

There are several key parameters that influence field compaction in addition to the level of compaction energy and controlling the water content as close as possible to its optimum water content. They are as follows:

Number of passes: In general construction practice, several or more passes of rollers are required to obtain a specified unit weight. The more number of passes is applied, the higher unit weight is obtained. Figure 5.8 plots γ_d versus depth with various number of passes from 2 to 45 of a single 2.44 m lift (8 ft) fill by 55.6 kN (12.5 kips) smooth roller (***D'Appolonia et al. 1969***). After five passes, a large increase is needed in the number of passes to achieve significant increase in compaction. In general, it is considered that more than 10 to 15 rolls may not be effective and not an economical way to compact fills.

Amount of lift: The amount of lift is also significant. Figure 5.8 also shows that only the upper section at 0.3–0.5 m (1–1.5 ft) deep is effectively compacted. The lift should be small enough to get the maximum compaction effect over the entire depth, but not be too small, since the very top portion of the layer also cannot be well compacted because of particle segregation upon vibration application. In general applications, a loose lift is limited to about 0.5 m (20 in.).

TABLE 5.5
Soil Compaction Characteristics and Recommended Equipment

General Soil Description	USCS Group	Compaction Characteristics	Recommended Equipments
Sand and sand–gravel mixture (no silt and clay)	SW, SP, GW, GP	Good	Vibratory drum roller, vibratory rubber tire, or pneumatic tire equipment
Sand or gravel–sand with silt	SM, GM	Good	Vibratory drum roller, vibratory rubber tire, or pneumatic tire equipment
Sand or sand–gravel with clay	SC, GC	Good to fair	Pneumatic tire, vibratory rubber tire, or vibratory sheep's-foot equipment
Silt	ML	Good to poor	Pneumatic tire, vibratory rubber tire, or vibratory sheep's-foot equipment
Silt	MH	Fair to poor	Pneumatic tire, vibratory rubber tire, or vibratory sheep's-foot, sheep's-foot-type equipment
Clay	CL	Good to fair	Pneumatic tire, sheep's-foot, vibratory rubber tire, or vibratory sheep's-foot equipment
Organic soil	CH, OL, OH, Pt	Not recommended structural earth fill	—

Source: After McCarthy, D. (2008).

5.5.2 Dynamic Compaction

Recently, this simple yet effective compaction technique was introduced. The **dynamic compaction** method involves dropping a heavy weight repeatedly on the ground at regularly spaced intervals as seen in Figure 5.9. The weight is typically between 80 and to 360 kN, and the height changes from 10 to 30 m. The impact of the free drop of weight creates stress waves that densify the soil to a relatively large depth. The method is effectively used for sandy soils but is also applied to silt and clay soils. This is a rather economical way to compact the site if such operations with vibration and noise can be tolerated.

5.6 FIELD DENSITY DETERMINATIONS

The final important step in compaction is field monitoring and inspection of compaction practice. Since after the completion of compaction it is not easy to tell whether

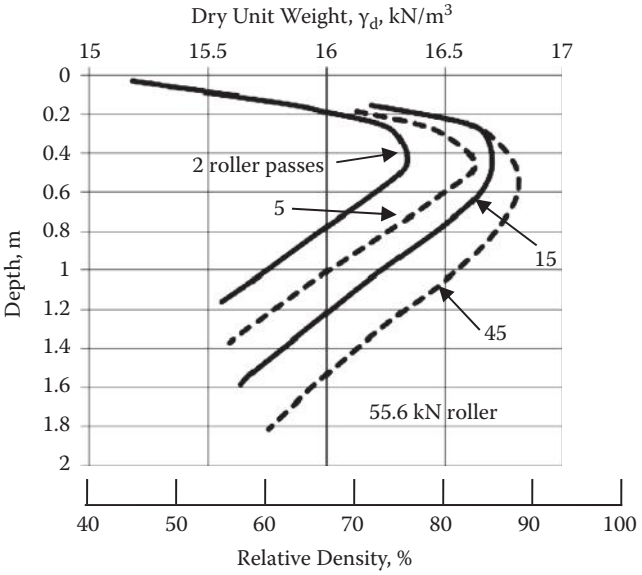

FIGURE 5.8 Effect of field compaction with depth and number of passes. (After D'Appolonia et al. 1969, *Journal of Soil Mechanics and Foundation Division*, Vol. 95, No. SM1, pp. 263–284.)

FIGURE 5.9 Dynamic compaction. (Photo courtesy of Terra Systems, Inc.)

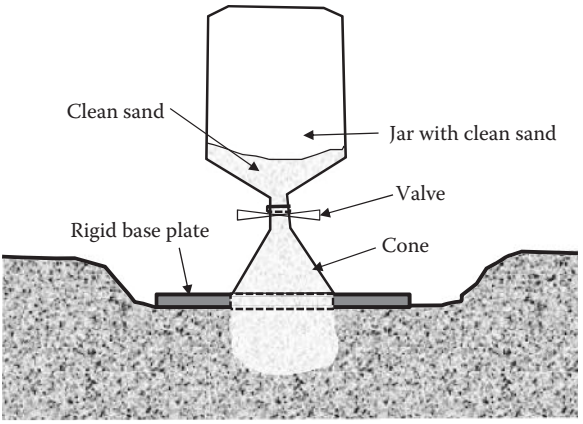

FIGURE 5.10 Sand cone method.

the site is properly compacted or not according to the specification, monitoring during compaction practice, and inspection after compaction are needed.

A preliminary check can be made by an inspector who can observe penetration of a probe (typically 13 mm diameter steel rod) pushed by the inspector's own weight to find any abnormal spots over the entire site. However, in most cases, the field unit weight is measured after the completion of compaction. There are several methods available, such as the sand cone method (ASTM D-1556 and AASHTO T-191), rubber balloon method (ASTM D-2167 and AASHTO T-205), nuclear density method (ASTM D-2922 and AASHTO T-238), etc. The **sand cone method** is widely used and is described in the following text.

5.6.1 Sand Cone Method

As shown in Figure 5.10, the method uses free-flowing sand to fill a field-excavated hole to measure its volume and thus calculate the field total unit weight as well as the dry unit weight with the measured water content of the excavated soil. Uniformly graded, dry, clean sand with gradation between 2 mm (passing No. 10 Sieve) and 0.25 mm (retaining No. 60 Sieve) are used for this purpose. Calibration is made to determine the sand's dry unit weight, $\gamma_{d,sand}$, with free drop in the laboratory prior to the field measurement. The field procedure involves the following steps:

1. Prior to fieldwork, $\gamma_{d,sand}$ shall be calibrated. Several jars with identification numbers for each are filled with the sand, and their total weights are recorded.
2. At a site selected for field density determination, the surface of the ground is flattened and leveled by the edge of the rigid base plate. The surface level is typically located at a certain depth since the compacted top surface does not necessarily represent the true compaction result of the soil layer.
3. Through the circular opening at the center of the base plate, the ground is carefully excavated by using a spoon, and all soil from the excavated hole shall be collected in a plastic bag.

4. The jar filled with sand is placed upside down so that the top of the cone engages into the inner edge of the opening in the base plate. At this stage, the valve in the jar is kept closed.
5. After the jar with the cone is securely placed on the base plate, the valve is carefully opened to allow free flow of sand into the excavated hole and the cone section of the device.
6. After the observation of completion of sand flow into the space, the valve is carefully closed. The total weight of the jar and the remaining sand is measured later. This weight is subtracted from the original weight of the jar of sand, and then the weight that filled the space of the hole and cone is obtained as $W_{sand,cone+hole}$.
7. The field wet (total) specimens from the excavated holes are weighted and their water contents are determined as $W_{t,hole}$ and w, respectively. These measurements could be done either in the field by using a balance and a quick-drying microwave oven or in the laboratory.

The calculation is as follows:

$$\gamma_{d,sand} = W_{sand,cone+hole}/V_{hole+cone} \text{ and thus} \tag{5.9}$$

$$V_{hole+cone} = W_{sand,cone+hole}/\gamma_{d,sand} \tag{5.10}$$

$$V_{hole} = V_{hole+cone} - V_{cone} \tag{5.11}$$

$$\gamma_{t,hole} = W_{t,hole}/V_{hole} \tag{5.12}$$

$$\gamma_{d,hole} = \gamma_{t,hole}/(1+w) = \gamma_d \tag{5.13}$$

In the foregoing computation of γ_d, the volume of the cone V_{cone} and $\gamma_{d,sand}$ shall be calibrated with the sand used. The values of $W_{sand,cone+hole}$, $W_{t,hole}$, and w are field-measured properties.

The measured γ_d value is compared with the specified $\gamma_{d,field}$. When the measured values do not satisfy the requirement, the field inspector shall direct recompaction of the site to the contractor.

Exercise 5.2

The following data are obtained from a field sand cone test. Determine $\gamma_{d,field}$ and the relative compaction R.C. The $\gamma_{d,max}$ value from the standard Proctor test for the soil was 18.8 kN/m^3.

$\gamma_{d,sand}$ = 15.5 kN/m^3 (calibrated dry unit weight of sand)

$W_{sand,cone}$ = 1.539 kgf (weight of sand to fill sand cone only)

Weight of jar + cone + sand (before the test) = 7.394 kgf

Weight of jar + cone + sand (after the test) = 2.812 kgf

$W_{t,\ hole}$ = 3.512 kgf (wet weight of soil obtained from the hole)

w = 10.6% (water content of in-situ soil after laboratory determination)

Solution:

$V_{cone} = W_{sand,cone}/\gamma_{d,sand} = 1.539 \times 9.81 \times 10^{-3}/15.5 = 0.974 \times 10^{-3}$ m^3

$W_{sand,cone+hole} = 7.394 - 2.812 = 4.582$ kgf

$V_{sand,cone+hole} = W_{sand,cone+hole}/\gamma_{d,sand} = 4.582 \times 9.81 \times 10^{-3}/15.5 = 2.900 \times 10^{-3}$m^3

$V_{sand,hole} = V_{sand,cone+hole} - V_{cone} = 2.900 \times 10^{-3} - 0.974 \times 10^{-3}$ m^3 $= 1.926 \times 10^{-3}$ m^3

$\gamma_{t,hole} = \gamma_t = W_{t,\ hole}/V_{sand,hole} = 3.512 \times 9.81 \times 10^{-3}/1.926 \times 10^{-3} = 17.89$ kN/m^3

$\gamma_d = \gamma_t/(1+w) = 17.89/(1 + 0.106) =$ **16.18 kN/m^3** ←

R.C. $= \gamma_d/\gamma_{d,max} = 16.18/18.8 = 0.860 =$ **86.0%** ←

5.6.2 Other Field Density Methods

Regarding other popular field density determination methods, the **rubber balloon method** uses a similar principle as the sand cone method. Instead of dry clean sand, it uses the rubber balloon to fill the excavated hole, and the hole is replaced with water to measure the volume.

In recent years, the **nuclear density method** (ASTM D-2922) became a popular method to determine the field density and the water content. It uses gamma radiation for density determination. It measures the scatter of radiation, which is proportional to the density, while the scatter of alpha particles detects water content. Both need prior calibrations to establish empirical correlations. This quick and nondestructive test is handy, but it requires specially trained technicians and careful handling of low-level radioactive materials.

5.7 CALIFORNIA BEARING RATIO (CBR) TEST

CBR is a penetration test for evaluating the strength of road subgrade and base course materials. This is originally developed by the California Department of Transportation and became standards in ASTM (D1883) and AASHTO (T193). As seen in Figure 5.11, the test uses 152.4 mm (6 in.) diameter mold, and 24.4 N (5.5 lb.) or 44.5 N (10 lb) rammers are used as in standard or modified Proctor tests. The specimen is compacted in the mold to have a specified dry unit weight, which simulates the field situation. To achieve selected conditions, a proper compaction energy level is chosen by adjusting the numbers of drops and layers and the drop height. Water content could be at its optimum or as desired. A selected surcharge load, which simulates the field situation, is applied on top of the specimen with metal discs, and the specimen could be soaked or unsoaked in water to simulate the in situ condition. The vertical load then is applied on the surface of the specimen by the penetration piston. The penetration value and load are recorded.

The CBR value is defined as

$$CBR = (P/P_s) \times 100 \tag{5.14}$$

where P is the load intensity on the penetrometer at 2.54 mm (0.1 in.) penetration in the specimen, and P_s is the load intensity on the penetrometer at 2.54 mm (0.1 in.) penetration in the standard crushed stone. The value of P is obtained from the

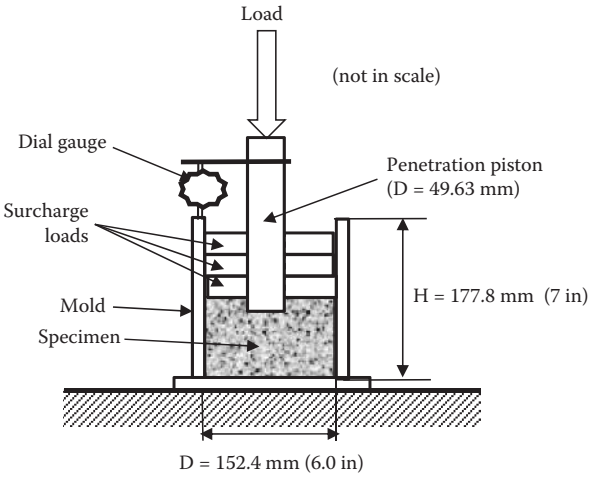

FIGURE 5.11 California Bearing Ratio (CBR) test device.

load-penetration curve of the test, and P_s is given as 6900 kN/m^2. As seen in the definition, CBR is the percentage of load level at 2.54 mm penetration on a given soil to that of the best available material (crushed stone). The standard material for this test is crushed California limestone for which the CBR value is 100. The harder the surface, the higher the CBR rating.

The CBR rating was developed for measuring the load-bearing capacity of soils used for building roads, and it can also be used for measuring the load-bearing capacity of unimproved airstrips or for soils in underpaved airstrips. CBR is incorporated in many pavement design charts, and it is also related to other useful engineering properties. Table 4.1 in Chapter 4 includes typical CBR values with USCS group names.

5.8 SUMMARY

Compaction is a very important practice for the proper placement of fills. Without proper compactions, ground surface may settle in the future and cause many problems. Laboratory and field compaction methods were presented in this chapter. Proper utilization of laboratory compaction result in field practice with an adequate compaction machine was studied. Also the importance of in-situ density inspection was emphasized. The CBR method, which is popularly used in the pavement design practice, was also presented.

REFERENCES

D'Appolonia, D. J., Whitman, R. V., and D'Appolonia, E. D. (1969), Sand compaction with vibratory rollers, *Journal of Soil Mechanics and Foundation Division*, Vol. 95, No. SM1, pp. 263–284.

McCarthy, D. (2008), *Essentials of Soil Mechanics and Foundations:Basic Geotechnics*, 7th ed., Pearson/Prentice Hall, Upper Saddle River, NJ.

Peck, R. B., Hanson, W. E., and Thornburn, T. H. (1974), *Foundation Engineering*, 2nd ed., John Wiley & Sons, New York.
Proctor, R. R. (1933), Fundamental principals of soil mechanics, *Engineering News Record*, Vol. 111, Nos. 9, 10, 12, and 13.
Sowers, G. F. (1979), *Introductory Soil Mechanics and Foundations: Geotechnical Engineering*, 4th ed., Macmillan, New York.
Terzaghi, K., and Peck, R. B. (1967), *Soil Mechanics in Engineering Practice*, 2nd ed., John Wiley & Sons, New York.
U.S. Army Corps of Engineers (1992), *Engineer Manual*, EM 1110-1-1905.

Problems

5.1 At a borrow site, sandy soil was excavated. The soil had $\gamma_t = 19.3$ kN/m^3, $w = 12.3\%$, and $G_s = 2.66$. The soil was dried, the maximum and minimum void ratio tests were performed, and $e_{max} = 0.564$ and $e_{min} = 0.497$ were obtained. Determine the relative density of the soil at the borrow site.

5.2 The soil in Problem 5.1 is used to fill an earthwork, and 75% of relative density is required in the field compaction with 10% water content. Determine the required unit weight of the soil γ_t for this earthwork.

5.3 For a given soil with $G_s = 2.65$, plot the γ_d versus w relations for S = 40%, 60%, 80%, and 100% for a range of w = 0% to 20%.

5.4 The standard Proctor test was performed for a soil with Gs = 2.66, and the results are as follows:

Water Content, %	Wet Weight in Mold, gf
5.6	1420
7.9	1683
10.8	1932
13.3	1964
14.8	1830
16.2	1630

(a) Plot the γ_d versus w relation.
(b) Determine $\gamma_{d,max}$ and w_{opt}.
(c) Calculate S and e at the maximum dry unit weight point.
(d) What is γ_t at w_{opt}?
(e) What is the range of water content if the relative compaction (R.C.) is required to be 90% of the standard Proctor $\gamma_{d,max}$?

5.5 The modified Proctor test (ASTM D-698, Method C) was performed for a soil with Gs = 2.70, and the results are as follows:

Water Content, %	Wet Weight in Mold, gf
6.5	3250
9.3	3826
12.6	4293

14.9	4362
17.2	4035
18.6	3685

(a) Plot the γ_d versus w relation.
(b) Determine $\gamma_{d,max}$ and w_{opt}.
(c) Calculate S and e at the maximum dry unit weight point.
(d) What is γ_t at w_{opt}?
(e) What is the range of water content if the relative compaction (R.C.) is required to be 95% of the standard Proctor $\gamma_{d,max}$?

5.6 The following table shows a standard Proctor test result. Soil type was SW according to USCS. The soil is used for filling a small trench that was excavated in a parking lot. Determine the required γ_d and the range of water content for this job. Use Table 5.4 as a guideline.

Water Content, %	Dry Unit Weight γ_d, kN/m^3
3.5	14.3
6.2	16.8
9.2	18.6
12.5	18.7
15.3	17.6
18.6	14.6

5.7 The same soil as in Problem 5.6 is used for the upper section of subgrade under a pavement. Determine the required γ_d and the range of water content for this job. Use Table 5.4 as a guideline.

5.8 A planned fill site requires 2500 m^3 of fill material with $\gamma_d = 18.5$ kN/m^3 and w = 14%. The material is brought from a borrow site that has $\gamma_t = 19.5$ kN/m^3 with w = 16.5% and Gs = 2.70.
(a) How much of the borrow material (in cubic meters) is required to fill the site?
(b) How heavy is it?

(Hint: use the three-phase diagrams for the fill site and the borrow site.)

5.9 The field sand cone test was performed, and the following data were obtained. Determine the field dry unit weight of the soil.

γ_{sand} = calibrated unit weight of sand = 16.2 kN/m^3
V_{cone} = calibrated volume of cone = 0.974×10^{-3} m^3
$W_{wet\ soil}$ = wet soil obtained from the hole = 3.425 kgf
$W_{sand\ to\ fill\ cone+hole}$ = 4.621 kgf
$W_{dry\ soil}$ = oven-dried soil obtained from the hole = 3.017 kgf

5.10 The CBR penetration data (stress versus penetration) for a given soil as follows:

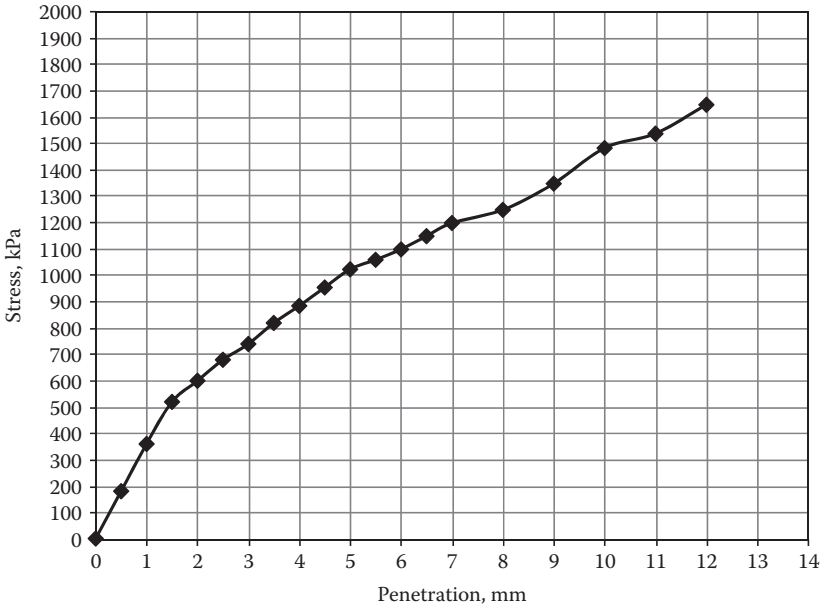

(a) Determine the CBR value.
(b) Evaluate the suitability of the soil as pavement subgrade material.

6 Flow of Water through Soils

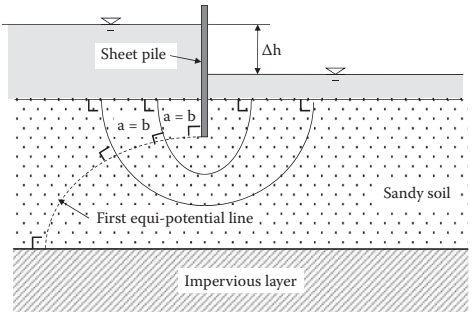

6.1 INTRODUCTION

Among construction materials, soil is very unique. Because of a relatively large space of void in its constituent, water can flow through soil. The water flow (**seepage**) characteristics are very important in many applications of earthworks and structures such as earth dams, levees, embankments, underground structures, excavations, etc.

6.2 HYDRAULIC HEADS AND WATER FLOW

Consider a water flow through a soil specimen filled in a clean pipe as seen in Figure 6.1. Because of the water-level difference between the left side and the right side of the pipe, water flows from left to right. The water-level difference is called **total head loss** Δh, which is the source of energy to create the flow. Classic **Bernoulli's equation** (Equation 6.1) is used to define the flow of water through soil masses:

$$h_t = h_z + h_p + h_v = z + \frac{u}{\gamma_w} + \frac{v^2}{2g} \tag{6.1}$$

where

h_t: **total head**
h_z: **elevation head**
h_p: **pressure head**

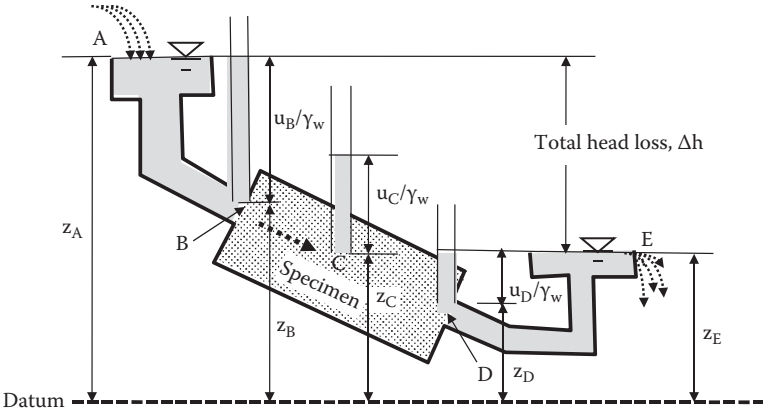

FIGURE 6.1 Water flow through a pipe.

h_v: **velocity head**
u: **pore water pressure**
v: **flow velocity**

The velocity head term $v^2/2g$ is neglected in most soil mechanics problems since this value is quite small in comparison with the values of other terms, and thus Equation 6.1 becomes

$$h_t = h_z + h_p = z + \frac{u}{\gamma_w} \tag{6.2}$$

It is very important to define the **datum** ***to use Equation 6.2. The datum could be chosen at any elevation, and all the heads are defined relative to the datum.*** As seen in Figure 6.1, u/γ_w ($=h_p$) is the height of water in a standpipe with water pressure u, and z is the height at that point from the datum. The total head h_t is the level of water in standpipes relative to the datum, and it constitutes a variety of combinations of h_z and h_p. The values of the parameters appear in Figure 6.1 and are summarized in Table 6.1.

TABLE 6.1
Heads h_z, h_p, and h_t at Various Points in Figure 6.1

Point	h_z	h_p	$h_t = h_z + h_p$
A	z_A	0	z_A ($=h_t$ at B)
B	z_B	u_B/γ_w	$z_B + u_B/\gamma_w$ ($=h_t$ at A)
C	z_C	u_C/γ_w	$z_C + u_C/\gamma_w$
D	z_D	u_D/γ_w	$z_D + u_D/\gamma_w$ ($=h_t$ at E)
E	z_E	0	z_E ($=h_t$ at D)

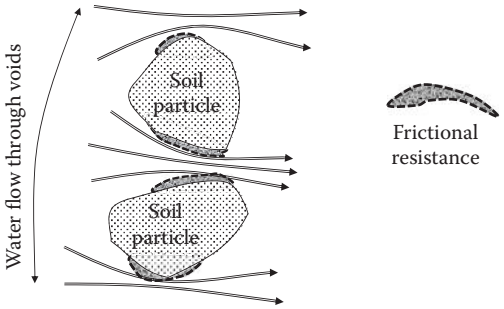

FIGURE 6.2 Frictional energy loss around particles due to water flow.

Table 6.1 demonstrates that h_t values are the same at Points A and B and at Points D and E, although h_z and h_p are different at all the points. If there are no changes in h_t, it implies "no (total) head loss." As seen in Figure 6.1 and Table 6.1, the only head loss occurs from Points B to D, where water flows through the soil.

Head loss is an energy loss. When water flows in soils, it must flow through many small passages in void sections of soils as illustrated in Figure 6.2. This creates frictional resistance on the surfaces of particles. Flow energy is transmitted to frictional resistance on particle surfaces and then may be lost in heat generation, although it may not be easy to measure the temperature rise due to this energy transfer.

6.3 DARCY'S EQUATION

The energy of water flow comes from the total head loss as described in the previous section, and it follows Darcy's law in Equation 6.3.

$$v = k\, i \tag{6.3}$$

$$q = v\, A = k\, i\, A = k\, (\Delta h/L)A \tag{6.4}$$

$$Q = q\, t = k\, i\, A\, t = (k\, \Delta h\, A\, t)/L \tag{6.5}$$

where

v: **discharge velocity** of water flow through porous media (m/s)
k: **coefficient of permeability** (m/s)
i: **hydraulic gradient** (head loss/flow length = $\Delta h/L$)
A: cross-sectional area of specimen perpendicular to flow direction (m^2)
q: **flow rate** of water (m^3/s)
Q: total amount of flow (m^3) for a period t (second)

Note that the discharge velocity v (or simply, velocity) in Equation 6.3 is not the true velocity of water flow but is rather an average velocity in the flow direction through the porous media. Since water can flow only in the void section of the media, the true velocity of water (still in average in the direction of an average flow direction) must

be faster than v to carry the same quantity of water. The true velocity through the void is called **seepage velocity** v_s and is computed as

$$v_s = \frac{v}{n} \tag{6.6}$$

where n is the porosity of soils, in which area water can only flow relative to gross cross-sectional area 1 (one) for discharge velocity v. The real velocity of water molecules are even faster than v_s since real water passages are not straight but rather meandering with longer passages around the particles. ***The discharge velocity v, however, has an engineering significance since it is a gross measure of velocity for a cross section of soils in an average flow direction***. Discharge velocity is simply termed as ***velocity*** and is used in the following discussions.

Exercise 6.1

Figure 6.3 shows water flow though soil the specimen in a cylinder. The specimen's k value is 3.4×10^{-4} cm/s

(a) Calculate pressure heads h_p at Points A, B, C, and D and draw the levels of water height in standpipes.
(b) Compute the amount of water flow q through the specimen.

Solution:

(a) Based on the datum selected in the figure and using Equation 6.2, a computation table is constructed in Table 6.2.

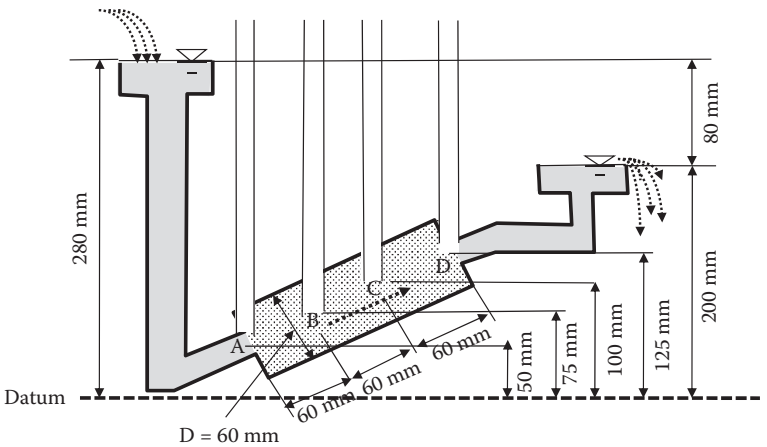

FIGURE 6.3 Exercise 6.1 problem.

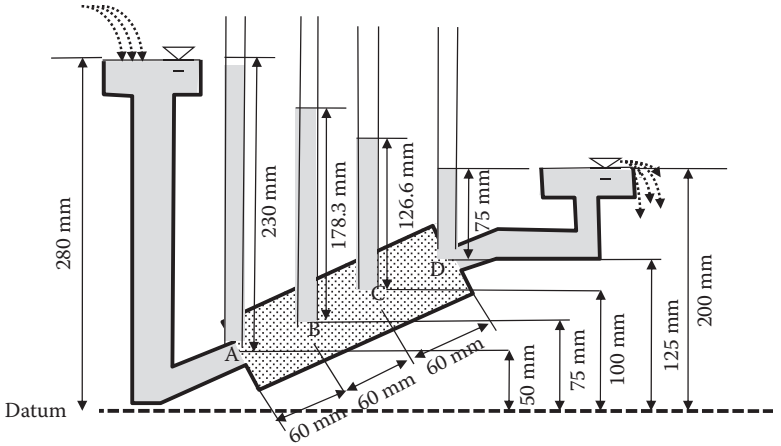

FIGURE 6.4 Solution to Exercise 6.1.

TABLE 6.2
Heads, h_z, h_t, and h_p at Various Points in Figure 6.3

Point	h_z (mm)	h_t (mm)	$h_p = h_t - h_z$ (mm)
A	50	280	230
B	75	280–80/3 = 253.3	178.3
C	100	253.3–80/3 = 226.6	126.6
D	125	226.6–80/3 = 200	75

In the h_t computation in the table, the head loss from A to B is one-third of the total head loss (80 mm). The same loss occurs from B to C and from C to D. The heights of water in standpipes are plotted in Figure 6.4.

(b) From Equation 6.4,

$$q = k\,(\Delta h/L)A = 3.4 \times 10^{-4} \times (8/18) \times \pi(6/2)^2 = \mathbf{4.27 \times 10^{-3}}\ \mathbf{cm^3/s} \leftarrow$$

6.4 COEFFICIENT OF PERMEABILITY

In Darcy's equation (Equations 6.3, 6.4, and 6.5), the coefficient of permeability k is the sole material parameter and shall be determined. The value of k changes in a logarithmic way. For example, the k value is more than 1×10^{-1} cm/s for gravels, and it is less than 1×10^{-7} cm/s for clayey soils. Table 6.3 shows a general guide for k values with different type of soils.

From Table 6.3, clays still have a capability to pass water through. However, it is practically impervious to water in most applications. For example, in one of **geosynthetic** applications (***Koerner 2005***), **bentonite clay** (one type of Montmorillonite

TABLE 6.3
Typical Coefficient of Permeability k Values for Different Soils

Relative Permeability	Coefficient of Permeability, k (cm/sec)	Typical Soils
Very permeable	$> 1 \times 10^{-1}$	Coarse gravel
Medium permeable	$1 \times 10^{-1} - 1 \times 10^{-3}$	Sand, fine sand
Low permeable	$1 \times 10^{-3} - 1 \times 10^{-5}$	Silty sand, dirty sand
Very low permeable	$1 \times 10^{-5} - 1 \times 10^{-7}$	Silt, fine sandstone
Impervious	$< 1 \times 10^{-7}$	Clay

clays) is used to contain contaminated water in landfill sites. Its k value is in the range of 2×10^{-9} to 2×10^{-10} cm/s, which is practically impervious to water. Core sections of earth and rockfill dams also utilize clay materials as impervious layers to control seepage. On the other hand, high-permeable gravels and sands are used as filtering materials in many applications.

Researchers tried to make correlations between k value and other handy material properties of soils. A few are shown in the following text.

6.4.1 Hazen's Formula

Hazen's empirical formula (***Hazen 1911***) is most widely used for saturated sandy soils.

$$k = C\,(D_{10})^2 \tag{6.7}$$

where

k: coefficient of permeability (cm/s)
D_{10}: particle size for which 10% of the soil is finer (or effective grain size) (mm)
C: Hazen's empirical coefficient, which takes a value between 0.4 and 10.0 (mostly 0.4 to 1.5), depending on literatures (***Carrier 2003***), with the average value of 1.0.

This is a very simple and useful equation. However, because of its wide range of C value, this equation shall be used only as a very rough estimate of k.

6.4.2 Chapuis's Formula

Another similar empirical type of correlation is given by ***Chapuis (2004)***:

$$k = 2.4622\left[D_{10}^{\,2}\,\frac{e^3}{1+e}\right]^{0.7825} \tag{6.8}$$

where

k: coefficient of permeability (cm/s)
D_{10}: particle size for which 10% of the soil is finer (or effective grain size) (mm)
e: void ratio of soil

6.4.3 Kozeny and Carman's Formula

A more reliable semitheoretical and semiempirical formula is given by Kozeny and Carman (***Kozeny 1927,*** and ***Carman 1938, 1956***) as

$$k = \frac{\gamma_w}{\eta_w} \frac{1}{C_{k-c} S_s^2} \frac{e^3}{1+e} \tag{6.9}$$

where

k: coefficient of permeability (cm/s)

γ_w: unit weight of water (9.81 kN/m^3)

η_w: viscosity of water (1.307×10^{-3} N sec/m^2 for t = 10°C, 1.002×10^{-3} N s/m^2 for t = 20°C)

C_{k-c}: Kozeny–Carman's empirical constant (4.8 ± 0.3 for uniform spheres, and usually 5.0 is used)

S_s: **specific surface** area per unit volume of particles (1/cm)

e: void ratio of soil

When γ_w = 9.81 kN/m^3, $\eta_w = 1.0 \times 10^{-3}$ N s/m^2, and C_{k-c} = 5 are substituted into Equation 6.9,

$$k = 1.96 \times 10^4 \frac{1}{S_s^2} \frac{e^3}{1+e} \tag{6.10}$$

Estimation of S_s values is not straightforward. It is 6/D for uniform spheres with D as the diameter of the spheres. ***Carrier (2003)*** gave estimation of S_s for distributed soils from effective diameter D_{eff}:

$$S_s = SF/D_{eff} \tag{6.11}$$

$$D_{eff} = \frac{100\ \%}{\sum \left(\frac{f_i}{D_{avg,i}} \right)} \tag{6.12}$$

$$D_{avg,i} = D_{l,i}^{0.5}\, D_{s,i}^{0.5} \tag{6.13}$$

where

f_i: fraction (in percent) of particles between two sieve sizes with $D_{l,i}$ as larger and $D_{s,i}$ as smaller sieve sizes.

SF: **shape factor** (spherical—6: rounded—6.1: worn—6.4: sharp—7.4, and angular—7.7 by ***Fair and Hatch (1933),*** or rounded—6.6: medium angularity—7.5, and angular—8.4 by ***London (1952)***.

In all the above equations, it can be seen that the particle diameter and void ratio play important roles in the determination of k values.

Note that the aforementioned equations are applicable to gravels and sands. Also, these empirical equations shall be used with caution, only to obtain a rough estimate of k values. More reliable values of k shall be obtained from laboratory permeability tests or field techniques.

6.5 LABORATORY DETERMINATION OF COEFFICIENT OF PERMEABILITY

There are two laboratory methods available: **constant head permeability test** (ASTM D-2434) and **falling head permeability test**.

6.5.1 Constant Head Permeability Test

As seen in Figure 6.5, the soil specimen is prepared in a vertical standing cylindrical mold, and a constant hydraulic head is applied. Under a steady-state flow condition, discharged water at the exit is collected in a cylinder as Q for a time period t. From Equation 6.5, k is computed as

$$k = \frac{QL}{A\,\Delta h\,t} \tag{6.14}$$

where

Q: collected amounts of water for a time period t
L: length of soil specimen in the flow direction
A: cross-sectional area of a soil specimen
Δh: hydraulic head loss in constant head test setup

An average value from several trails is reported as the measured k value.

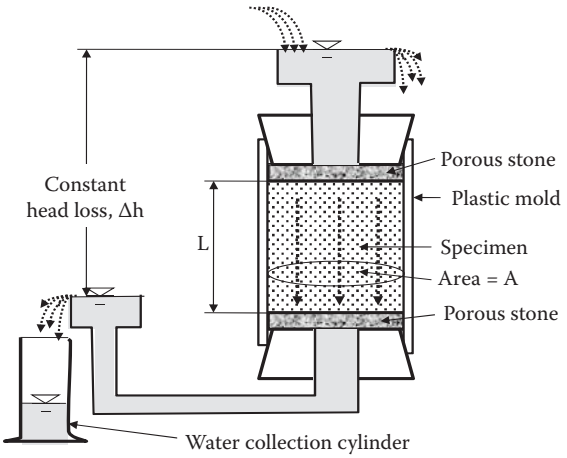

FIGURE 6.5 Constant head permeability test.

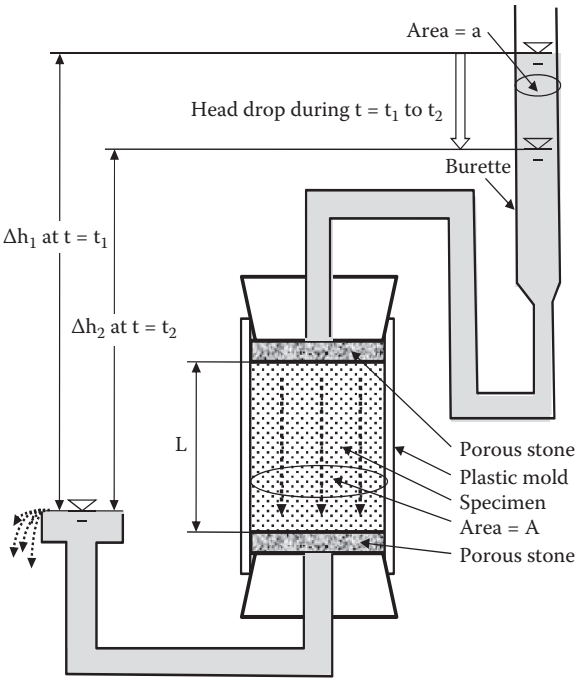

FIGURE 6.6 Falling head permeability test.

6.5.2 Falling Head Permeability Test

Figure 6.6 shows a setup for this test. The specimen is prepared similarly as in the constant head test. The higher head is applied through a burette in which the head changes with time. The head at the discharging side is constant as seen. At initial time ($t = t_1$), head loss is Δh_1, and at $t = t_2$, head loss is Δh_2. The amount of water flow "q" (per unit time) is equal to the change in head loss ($d\Delta h$) multiplied by the burette's cross-sectional area "a" per time "dt." Thus,

$$q = -a\frac{d\Delta h}{dt} = k\frac{\Delta h}{L}A, \text{ or } dt = \frac{aL}{Ak}\left(\frac{-d\Delta h}{\Delta h}\right) \tag{6.15}$$

Equation 6.15 is integrated from t_1 to t_2, and for the corresponding Δh_1 to Δh_2,

$$\int_{t_1}^{t_2} dt = (t_2 - t_1) = \frac{aL}{Ak}\int_{\Delta h_1}^{\Delta h_2}\left(\frac{-d\Delta h}{\Delta h}\right)$$

$$= \frac{aL}{Ak}\ln\frac{\Delta h_1}{\Delta h_2} \tag{6.16}$$

And then, k is obtained as

$$k = \frac{a\,L}{A(t_2 - t_1)} \ln \frac{\Delta h_1}{\Delta h_2} \tag{6.17}$$

The constant head test is usually used for coarse-grained soils and the falling head test for finer soils for rather accurate measurements with an effective use of testing time.

The laboratory permeability test is rather simple and is a cost-effective way to determine k values. However, it should be realized that samples are reconstituted mostly for sand and gravels, and for cohesive soils, some degree of disturbance cannot be avoided during a sampling process, transporting to the laboratory, and inserting it into the test mold. In particular, a specimen shall be perfectly fitted into the inside of the mold to avoid any water flow through possible spaces between the inner wall of mold and the specimen itself. For that reason, cohesive soils are often tested in an enclosed and pressurized membrane in the triaxial chamber (see Chapter 11) for k value determination.

6.6 FIELD DETERMINATION OF COEFFICIENT OF PERMEABILITY

Laboratory permeability tests have some shortcomings as mentioned earlier, and the sample size is so small that the measured values may not be necessarily true representatives of field conditions, which may include nonuniformity and fissures. An alternative way to obtain a more representative and reliable k value is using field methods, although these may be relatively expensive. The classic field permeability test methods involve pumping water from a well and observing water table changes in two observation wells. For idealized in-situ situations, rigorous analytical solutions are available, although these are not shown here. Readers can refer to other literature (e.g., ***Murthy 2003***). The results of two idealized field cases are introduced here. Readers can also refer to ***Daniel (1989)***, which summarizes other field techniques in detail.

6.6.1 Unconfined Permeable Layer Underlain by Impervious Layer

As seen in Figure 6.7, a well is excavated through the permeable layer, and two observation wells are installed at r_1 and r_2 distances from the center of the well hole. Water is pumped out with a steady rate until the height of the water level at the well and also at the two observation wells become stable. The theory for this idealized situation gives

$$k = \frac{q}{\pi(h_2^{\,2} - h_1^{\,2})} \ln \frac{r_2}{r_1} \tag{6.18}$$

Where

q: amount of pumped water per unit time

r_1 and r_2: distances of observation wells from the center of well hole

h_1 and h_2: observed water heights at observation wells as defined in Figure 6.7

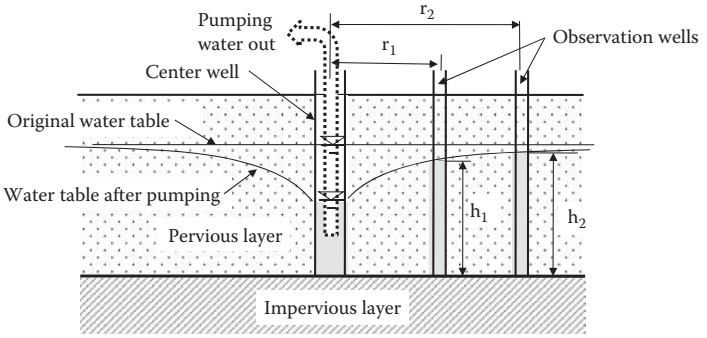

FIGURE 6.7 Field permeability test for unconfined permeable layer underlain by the impervious layer.

6.6.2 Confined Aquifer

Figure 6.8 shows an idealized case with a pervious layer that is sandwiched by two impervious layers. The water table is in the upper impervious layer. This situation is called **confined aquifer**. A well is dug into the lower impervious layer and two observation wells are installed. A steady-state flow is established as before. The solution to compute the k value for the pervious layer in this case is given by

$$k = \frac{q}{2\pi H(h_2 - h_1)} \ln \frac{r_2}{r_1} \tag{6.19}$$

Where

q: amount of pumped water per unit time
H: thickness of permeable layer
r_1 and r_2: distances of observation wells from the center of well hole
h_1 and h_2: observed water heights at observation wells as defined in Figure 6.8.

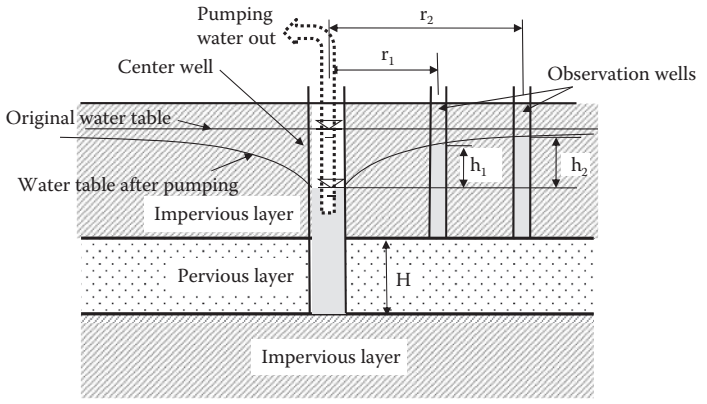

FIGURE 6.8 Field permeability test for confined aquifer.

6.7 FLOW NET

Flow net is a convenient graphical tool to compute hydraulic properties such as the amount of water flow, water pressure on flow boundaries, etc., for two-dimensional flow problems with complex geometries. Although the theory of the flow net can be demonstrated mathematically by using the **Laplace equation** for the hydraulic potential (e.g., ***Terzaghi 1943***), a simple one-dimensional model is first introduced here to help understand the principle of the flow net.

6.7.1 One-Dimensional Flow Net

Figure 6.9 shows a water flow through soil in a vertical cylinder with length L and cross-sectional area A. The flow is downward due to the total head loss of Δh. The cylinder is equally divided into three (or N_f in general) **flow channels**, which are parallel to the direction of the flow. Those imaginary boundaries of the flow channels are called **flow lines,** and water flow never crosses the flow lines. The total head loss Δh occurs from the top of the specimen to the bottom of the specimen as seen in the water levels in the standpipes. The specimen length L is equally divided by 4 (or N_d in general) as seen with dotted horizontal lines. Since the head loss occurs linearly through the specimen depth in this case, the head losses between adjacent horizontal lines are all Δh/4 (or $\Delta h/N_d$ in general). The total heads on individual horizontal lines are constant since they have the same elevation heads and the same pressure heads and, and thus, those lines are called **equipotential lines**. Flow lines and equipotential lines make a net (mesh) geometry, which is called **flow net**.

An enlarged rectangular on the right side of Figure 6.9 is bordered by two equipotential lines on the top and bottom, and by two flow lines at the left and right sides. It should be noted that water flows only in parallel direction to the flow line (vertical direction in this case) in the rectangular. Also, there is no waterflow along the

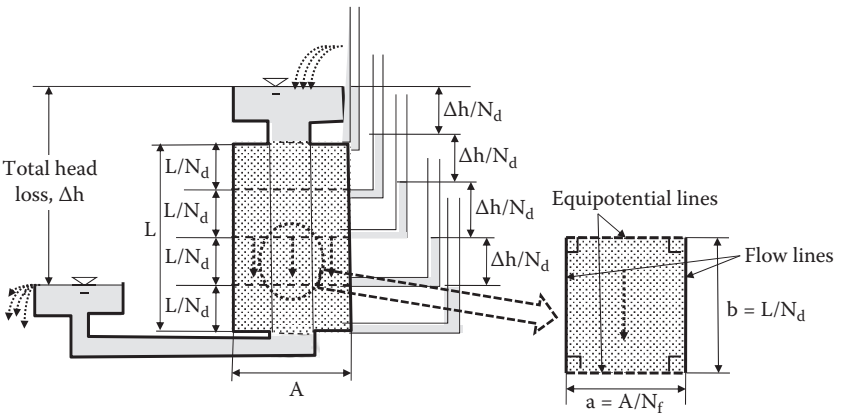

FIGURE 6.9 One-dimensional flow net concept.

direction of equipotential lines since the total head is constant (that is, no head loss) along the equipotential line. These two rules dictate that ***equipotential lines and the flow lines intersect each other at 90°***.

The amount of water flow q_a through a × b rectangular section is calculated as

$$q_a = k\,i\,a = k\,\frac{\frac{\Delta h}{N_d}}{b}\,a = k\,\Delta h\,\frac{1}{N_d}\,\frac{a}{b} \tag{6.20}$$

Thus, the total amount of water flow q_A through the entire cross section of the cylinder is

$$q_A = q_a N_f = k\,\Delta h\,\frac{N_f}{N_d}\,\frac{a}{b} \tag{6.21}$$

The selections of n_d (number of total equipotential line drops) and n_f (number of flow channels) are arbitrary, and thus, ***a = b is chosen*** in Equation 6.21. It makes Equation 6.21 much simpler as

$$q_A = k\,\Delta h\,\frac{N_f}{N_d} \tag{6.22}$$

Equation 6.22 is used to compute flow rate in earth structures using flow nets, and N_f/N_d is called the **shape factor**. The flow rate computation thus becomes simply a multiplication of material property k (coefficient of permeability), total head loss Δh, and a geometry parameter N_f/N_d (shape factor).

6.7.2 Flow Net for Two-Dimensional Problems with Isotropic Soils

From the foregoing one-dimensional flow-net discussion, two important criteria for flow net construction emerge:

1. Flow lines and equipotential lines intersect each other at a 90° degree angle.
2. Each opening of the net shall be drawn to have a square shape or close to it (i.e., a = b requirement) to utilize Equation 6.22.

Associated rules from item 1 are

3. Flow lines themselves never merge. If it occurs, it closes a passage of flow.
4. Equipotential lines never merge except at special points such as at corners of boundaries.
5. Flow lines and equipotential lines shall be smooth curves.

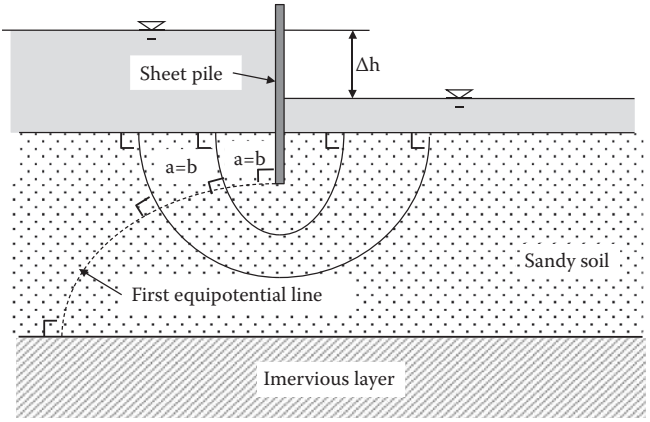

FIGURE 6.10 Flow net construction.

Based on the foregoing rules, the following steps are recommended for flow-net constructions:

1. Draw the geometry of structure correctly on the paper. It implies that the horizontal and vertical scales shall be the same. Otherwise, the square shape requirement cannot be met.
2. Select proper N_f values. Normally, N_f of 3 or 4 is adequate for the first trial.
3. Identify the boundary flow lines and boundary equipotential lines in the drawing. In an example in Figure 6.10, the upstream ground surface and downstream ground surface are the initial and the final equipotential lines, respectively. The front and back sides of the sheet pile and the surface of the impervious layer are the boundary flow lines.
4. First draw trial flow lines with selected N_f for the entire earth structures (Figure 6.10). This must be done based on the engineers' best instinct on how water flows. It should be noted that there are equal amounts of water flow through all flow channels.
5. By starting from the upstream site, draw the first equipotential line to have all net openings squares or near-squares with 90° intersections. In two-dimensional problems, however, it is impossible to have all net openings to be squares. Figure 6.11 shows examples of acceptable near-squares in the flow net. In Figure 6.11d and e, triangle or pentagon openings may be the only available net openings at the corners of the structural boundaries. In such cases, margining of two equipotential lines is allowed as seen in the triangle case. Similarly, merging of two flow lines is allowed in Figure 6.11e as a special case. Make the necessary corrections on originally drawn flow lines to satisfy near-square and 90° intersection requirements as close as possible. Note that, at locations that are far away from the major water flow, such as at the far-left element in Figure 6.10, there is no possibility to have near-square elements. These are exceptions to the rules.

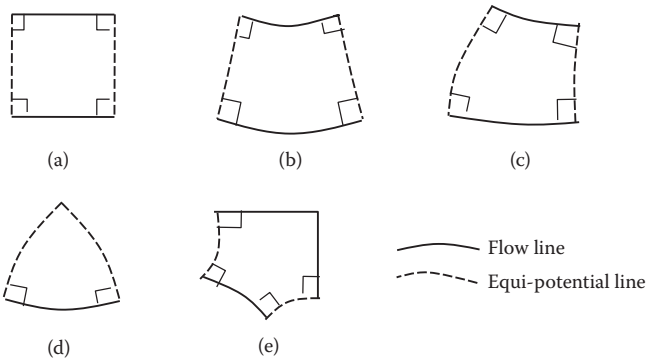

FIGURE 6.11 Acceptable near-squares in flow net construction.

6. Continue the foregoing step for the second and third equipotential lines and so on till it reaches the downstream exit as seen in Figure 6.12.
7. At the downstream exit point, it may not get to full squares with the last equipotential line. In such a case, draw an imaginary equipotential line beyond the last physical equipotential line to have full near-square sections. Based on partial squares for the last elements, obtain an average fractional number for the last equipotential line, such as 5.4 in Figure 6.12.

In Figure 6.12, $N_f = 3$ is chosen and $N_d = 5.4$ is obtained, and thus, shape factor N_f/N_d of this geometry is 0.556. If a larger number of N_f is chosen, a proportionally larger N_d value will be obtained when the square rule is carefully followed, and thus, the similar shape factor should be obtained. In Figure 6.13, several examples of flow net under concrete dams and through earth dams are shown (***Terzaghi 1943***).

Note that the two-dimensional flow-net technique with the square (a = b) requirement is based on the assumption that soil is an isotropic material; that is, permeability

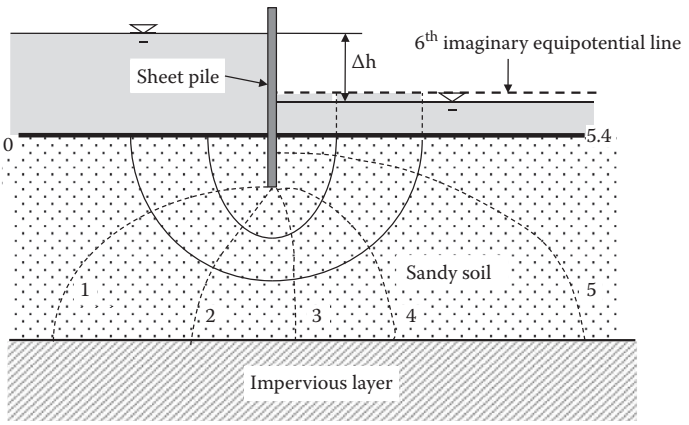

FIGURE 6.12 Completion of flow-net construction.

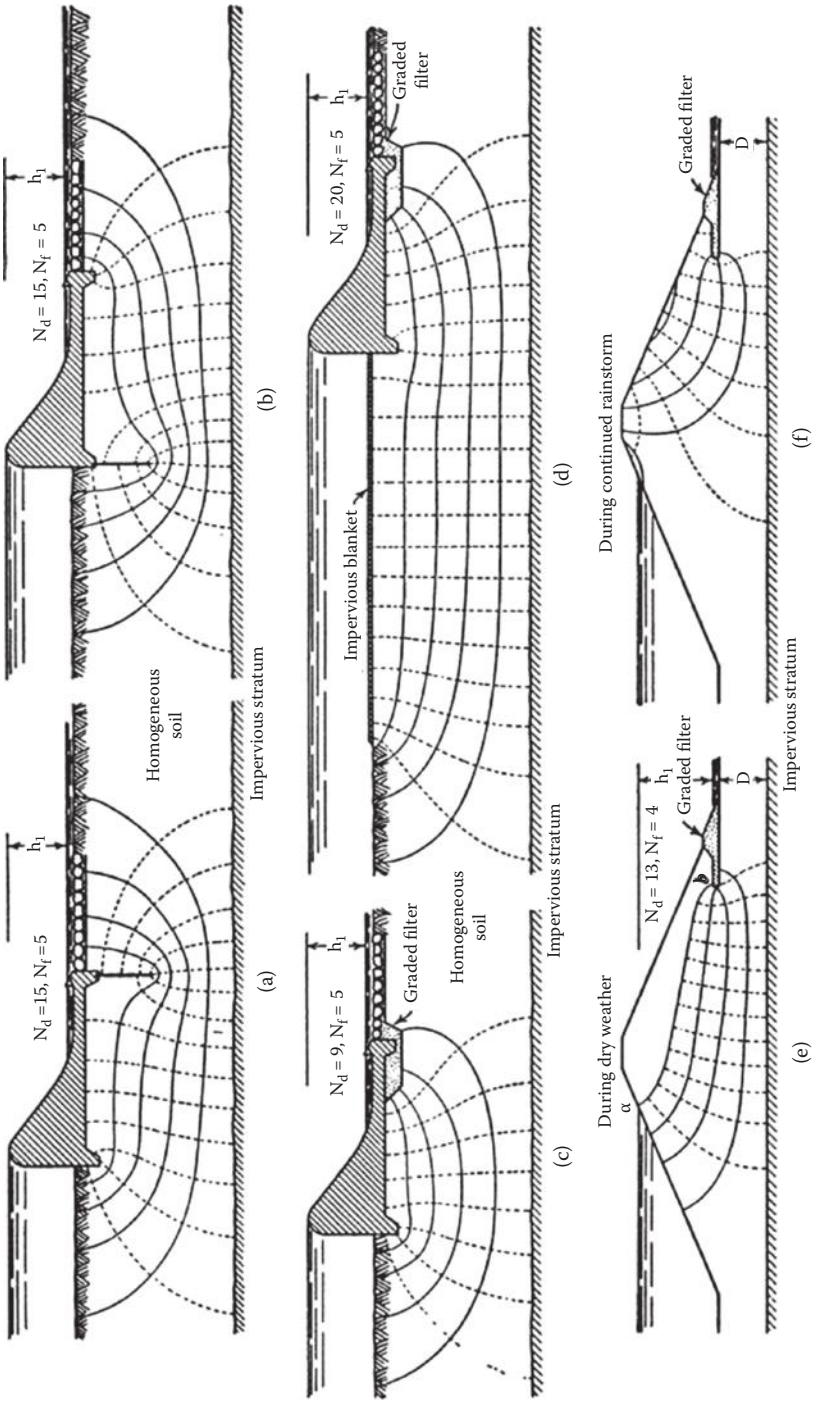

FIGURE 6.13 Examples of flow net for dams. (From Terzaghi 1943, *Theoretical Soil Mechanics*, John Wiley & Sons, New York.)

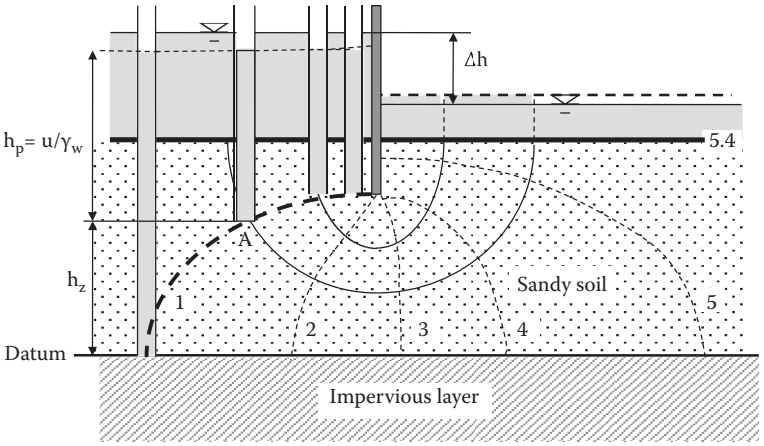

FIGURE 6.14 Pressure heads in flow net.

in the horizontal direction (k_h) and that in the vertical direction (k_v) are equal. If k_h is not equal to k_v, rearrangement of the vertical and horizontal scales is needed. Readers can refer to other literatures on the subject (e.g., ***Terzaghi 1943***) for details.

6.7.3 Pressure Heads in Flow Net

Total heads at any points on the same equipotential line shall be the same. As seen in Figure 6.14, if standpipes are placed all along the first equipotential line, the water levels in the pipes are the same since the total head is expressed in Equation 6.2 (the water height in the pipe (h_p) + elevation head (h_z)).

6.8 BOUNDARY WATER PRESSURES

Flow net is effectively used to determine boundary water pressures. As seen in examples in Figure 6.15, water flow under a dam creates uplift pressure on the base

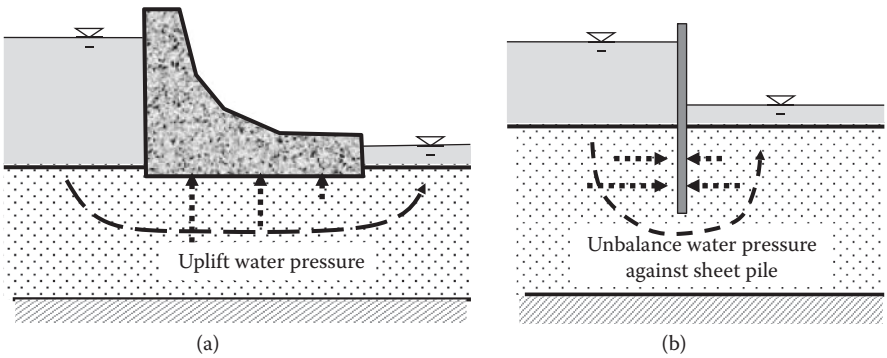

FIGURE 6.15 Boundary water pressure problems.

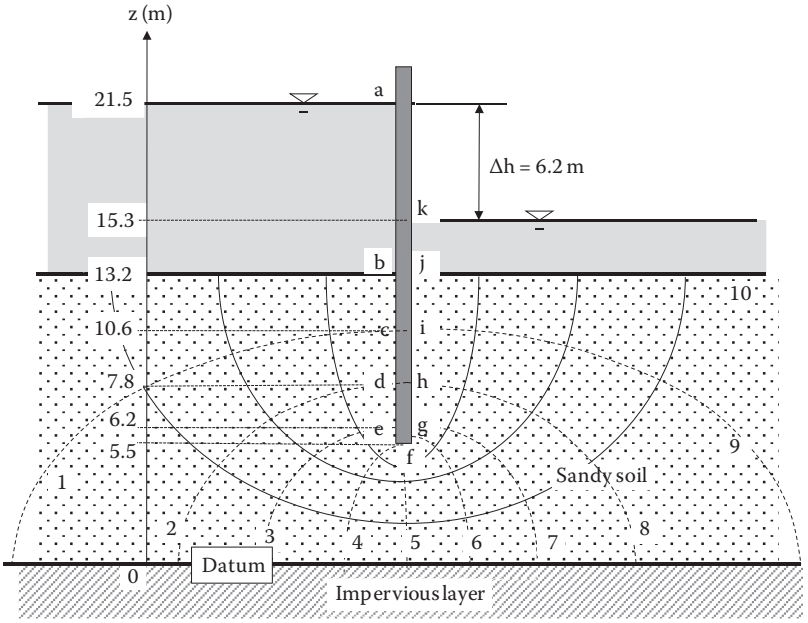

FIGURE 6.16 Boundary pressure head computation.

of the dam that may possibly cause a stability problem to the dam (Figure 6.15a). Because of water flow, the upstream side and the downstream side of a sheet pile are subjected to different water pressures (Figure 6.15b). The unbalanced water pressure is one of the key parameters for sheet pile section design.

Those boundary water pressures are computed systematically by using a flow net drawing and Equation 6.2 ($h_t = h_z + h_p$). Figure 6.16 shows a completed flow net around a sheet pile. Points "a" through "k" are labeled along the sheet pile. Water pressures at those points are required to compute. The elevations of those points are also shown alongside the figure. Table 6.4 demonstrates a systematic computation of the boundary water pressures against the sheet pile.

1. First, the datum must be chosen. It could be at any elevation. In this example, it is chosen at the top of the impervious layer.
2. Total head loss $\Delta h = 6.2$ m.
3. $N_d = 10$, so that head loss for one equipotential line drop Δh_i is $\Delta h_i = \Delta h/N_d = 6.2/10 = 0.62$ m.

In Table 6.4, Column D is computed by knowing that the total head loss in each equipotential line drop in the soil's section is Δh_i. By this procedure, h_t at Point "j" became 15.3 m, which is the same as the total head at point "k." The rest are systematic computations.

Figure 6.17 plots the obtained water pressure distribution along both sides of the sheet pile. From points "a" to "b" and "k" to "j" are hydrostatic water pressure

TABLE 6.4
Computation of Heads and Water Pressure for Figure 6.16

A	B	C	D	E	F
Point	No. on Equipotential Line (i)	h_z (m)	h_t (m)	h_p (m)	u (kN/m²)
a		21.5	21.5	0	0
b	0	13.2	21.5	8.3	81.4
c	1	10.6	21.5–1 × 0.62 = 20.88	10.28	100.8
d	2	7.8	21.5–2 × 0.62 = 20.26	12.46	122.2
e	3	6.2	21.5–3 × 0.62 = 19.64	13.44	131.8
f	5	5.5	21.5–5 × 0.62 = 18.4	12.9	126.5
g	7	6.2	21.5–7 × 0.62 = 17.16	10.96	107.5
h	8	7.8	21.5–8 × 0.62 = 16.54	8.74	85.7
i	9	10.6	21.5–9 × 0.62 = 15.92	5.32	52.2
j	10	13.2	21.5–10 × 0.62 = 15.3	2.1	20.6
k		15.3	15.3	0	0

Notes: Column: C: Read from the graph.
D: $h_t = h_{t,b} - i \bullet \Delta h_i$ for points "c" through "j" computation ($h_{t,b}$: total head at point "b").
E: D–C.
F: E • γ_w ($\gamma_w = 9.81$ kN/m³).

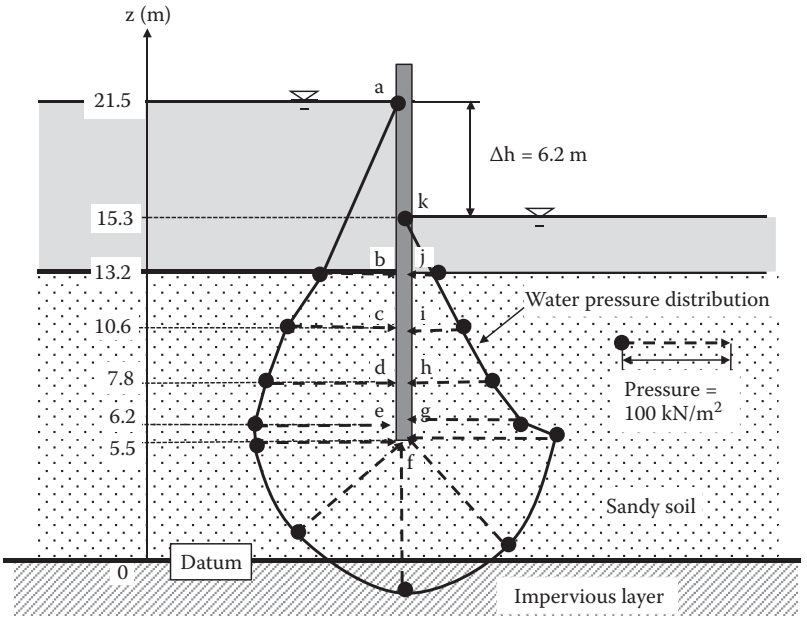

FIGURE 6.17 Pressure distribution along sheet pile.

distributions. The upstream side in the soil had a higher pressure than the hydrostatic pressure, and the downstream side in the soil had a pressure lower than the hydrostatic pressure. Thus, it makes the resultant water pressure act toward the right, which creates an extra bending moment on the pile. Note that, at Point "f" (tip of the pile), the same pressure (126.5 kN/m^2) acts toward "f" as seen.

Exercise 6.2

Flow net under a concrete dam is drawn in Figure 6.18.

(a) Calculate and plot the water pressure distribution along the base of the dam.
(b) Compute the resultant uplift force against the base of the dam.
(c) Calculate the point of application of the resultant uplift force.

Solution:

Datum is chosen at the top of the impervious layer.

$\Delta h = 17 - 12 = 5.0$ m.

$N_d = 8$

$\Delta h_i = \Delta h / N_d = 5.0/8 = 0.625$ m

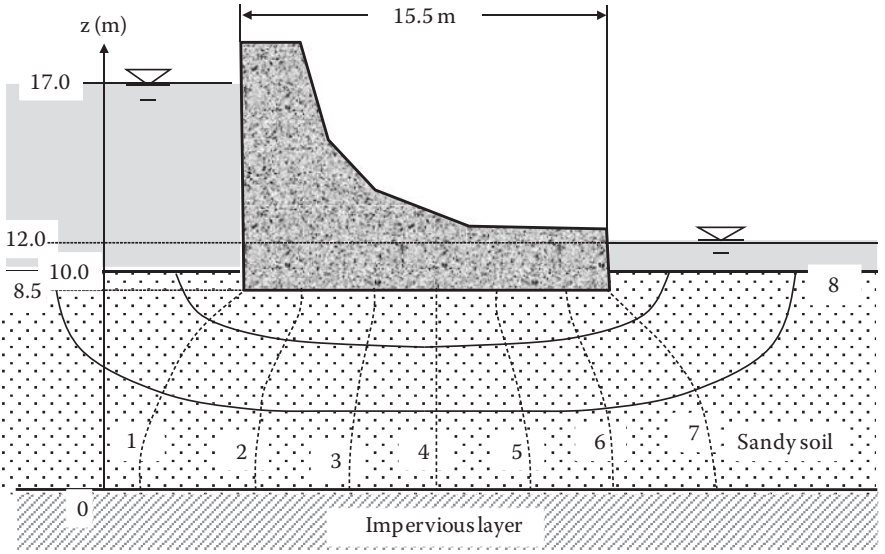

FIGURE 6.18 Exercise 6.2 problem.

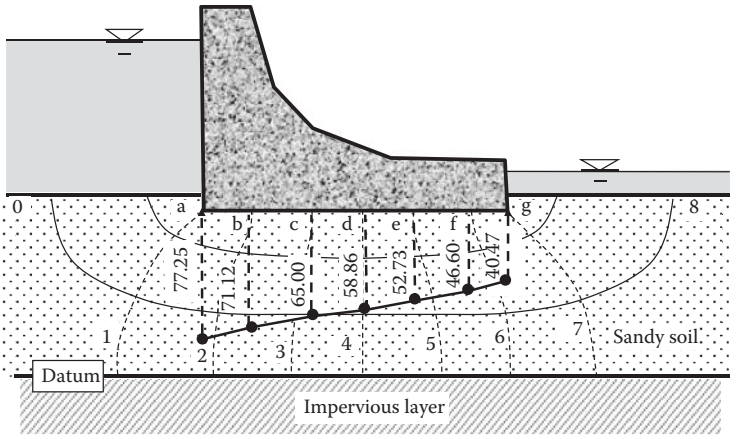

FIGURE 6.19 Solution to Exercise 6.2.

Points "a" through "g" at the base of the dam are labeled in Figure 6.19.

(a) Computation of the water pressures along the base is made in Table 6.5. The result is plotted in Figure 6.19.
(b) Horizontal distances "x" of those points from point "a" are read from the graph and shown in Column C in Table 6.6. Forces of trapezoids made by the two adjacent pressure readings (Column E), and the moment of the forces about point "a" (Column G), are also computed in Table 6.6.

TABLE 6.5
Computation of Heads and Water Pressure for Figure 6.19

A	B	C	D	E	F
Point	No. on Equipotential Line (i)	h_z (m)	h_t (m)	h_p (m)	p_w (kN/m^2)
a	1	8.5	17–1 × 0.625 = 16.375	7.875	77.25
b	2	8.5	17–2 × 0.625 = 15.75	7.25	71.12
c	3	8.5	17–3 × 0.625 = 15.125	6.625	65.00
d	4	8.5	17–4 × 0.625 = 14.5	6	58.86
e	5	8.5	17–5 × 0.625 = 13.875	5.375	52.73
f	6	8.5	17–6 × 0.625 = 13.25	4.75	46.60
g	7	8.5	17–7 × 0.625 = 12.625	4.125	40.47

Notes: Column C: Read from the graph
D: $h_t = h_{t,o} - i \bullet \Delta h_i$ ($h_{t,0}$: initial total head at the entry point).
E: D–C.
F: E • γ_w (γ_w = 9.81 kN/m^3).

TABLE 6.6
Computation of Forces and Moments from Pressure Distribution in Figure 6.19

A	B	C	D	E	F	G
Point	u (kN/m²)	Distance × from "a" (m)	Δ × (m)	Force P_i (kN/m)	Distance to Centroid from "a"(m)	Moment about "a" (kN/m-m)
a	77.25	0				
b	71.12	2.4	2.4	178.0	1.2	210.7
c	65.00	5.7	3.3	224.6	4.0	904.1
d	58.86	8.3	2.6	161.0	7.0	1123.7
e	52.73	10.8	2.5	139.5	9.5	1328.9
f	46.60	13.8	3	149.0	12.3	1828.0
g	40.47	15.5	1.7	74.0	14.6	1082.8
			Total	926.2		6478.2

Notes: Column D: C_i-C_{i-1} (distance between two adjacent pressures)
E: ½$(B_{i-1} + B_i) \times D_i$ (area of pressure diagram between two adjacent pressures)
F: $C_{i-1} + ⅓\ D_i \times (B_{i-1} + 2 \times B_i)/(B_{i-1} + B_i)$ (distance from "a" to the centroid* of each trapezoid)
G: $E_i \times F_i$ (moment of force of each trapezoid about "a")
*Centroid of trapezoid = ⅓ h (a + 2b)/(a + b) from length "a" side of the trapezoid; "b" is the other side length, and h is the height.

From the last row in Table 6.6,

Resultant uplift force **P = 926.2 kN/m** (per dam length). ←

(c) Point of application of P = ∑(moment)/P = 6478.2/926.2 = **6.99 m from Point "a"**. If a single trapezoid for the entire near-linear pressure distribution is used for the problem,

P= ½(77.25+40.47) × 15.5 = 912.3 kN/m² (1.5 % off from the above computation)

Point of application = 1/3 × 15.5 × (77.27 + 2 × 40.47)/(77.27 + 40.47) = 6.94 m (0.7% off from the above computation)

6.9 SUMMARY

The flow mechanism of water through soils was explained by Bernoulli's equation and Darcy's formula. Laboratory and field techniques for the determination of the coefficient of permeability were presented. Two-dimensional flownet technique is a convenient tool to compute the flow rate in problems involving complex geometries and was discussed in detail. Although many commercial computer flow rate computational programs are available at present, readers shall always be aware of the principal rules of the flow net when they are utilized.

REFERENCES

Carman, P. C. (1938), The determination of the specific surface of powders, *Journal of the Society of Chemical Industry Transactions*, Vol. 57, 225.

Carman, P. C. (1956), *Flow of Gases through Porous Media*, Butterworths Scientific, London.

Carrier III, W. D. (2003), Goodbye, Hazen; Hello, Kozeny-Carman, *Journal of Geotechnical and Geoenvironmental Engineering,* Vol. 129, No.11, 1054–1056.

Chapuis, R. P. (2004), Predicting the saturated hydraulic conductivity of sand and gravel using effective diameter and void ratio, *Canadian Geotechnical Journal*, Vol. 41, No. 5, 787–795.

Daniel, D. E. (1989), In Situ hydraulic conductivity tests for compacted clay, *Journal of Geotechnical Engineering*, Vol. 115, No. 9, 1205–1226.

Fair, G. M. and Hatch, L. P. (1933), Fundamental factors governing the stream-line flow of water through sand, *Journal of the American Water Works Association*, Vol. 25, 1551–1565.

Hazen, A. (1911), Discussion of "Dams on Sand Foundations" by A. C. Koenig, *Transactions*, ASCE, Vol. 73, 199–203.

Koerner, R. M. (2005), *Designing with Geosynthetics*, 5th ed., Pearson/Prentice Hall, Upper Saddle River, NJ.

Kozeny, J. (1927), Ueber kapillare leitung des wassers im boden, *Wien, Akad. Wiss.*, Vol. 136, No. 2a, 271.

London, A. G. (1952), The computation of permeability from simple soil tests, *Geotechniques*, Vol. 3, 165–183.

Murthy, V. N. S. (2003), *Geotechnical Engineering*, Marcel Dekker, New York.

Terzaghi, K. (1943), *Theoretical Soil Mechanics*, John Wiley & Sons, New York.

Problems

6.1. In Fig. 6.1, BC = 3.0 m, CD = 3.0 m, z_A = 10.0 m, z_B = 6.0 m, z_C = 4.0 m, z_D = 2.0 m, z_E = 5.0 m, and the diameter of the specimen pipe D = 2.0 m are given.
   (a) Compute h_p and h_t at points A, B, C, D, and E.
   (b) Compute the flow rate of water q in m^3/day. The coefficient of permeability k is given as 2.0×10^{-3} cm/sec.

6.2. Soil's gradation data are given below. The void ratio e was 0.550 at the site, and its particle shape was found to be round.

U.S. Sieve No.	D, mm	% Finer
	10	100.00
4	4.75	88.83
10	2	66.92
20	0.85	43.73
40	0.425	26.98
60	0.25	13.45
100	0.15	6.57
140	0.106	2.28
200	0.075	0.13

Estimate the approximate values of coefficient of permeability by
(a) Hazen's formula
(b) Chapuis's formula
(c) Kozeny and Carman's formula

6.3. Constant head permeability test was conducted and the following data was obtained. Compute the coefficient of permeability.
L = 15 cm
D (sample diameter) = 7.2 cm
Δh = 30 cm
Q = 32.5 cm^3 for a time period of 10 second

6.4. Constant head permeability test was conducted and the following data were obtained. Compute the coefficient of permeability.
L = 15 cm
D (sample diameter) = 7.2 cm
Δh = 45 cm
Q = 26.5 cm^3 for a time period of 20 second

6.5. Variable head permeability test was conducted and the following data were obtained. Compute the coefficient of permeability.
L = 15 cm
D (sample diameter) = 7.2 cm
Δh_1 (at t = 0) = 36.0 cm
Δh_2 (at t = 4 min.) = 28.3 cm
d (burette diameter) = 1.2 cm

6.6. Variable head permeability test was conducted and the following data were obtained. Compute the coefficient of permeability.
L = 15 cm
D (sample diameter) = 7.2 cm
Δh_1 (at t = 0) = 40.0 cm
Δh_2 (at t = 10 min.) = 22.9 cm
d (burette diameter) = 1.2 cm

6.7. Field well test was conducted for an unconfined permeable layer underlain by an impervious layer as idealized in Fig. 6.7 and the following data were obtained. Determine the coefficient of permeability from this field test.
r_1 = 3.2 m
r_2 = 6.0 m
h_1 = 6.24 m
h_2 = 7.12 m
q = 12500 cm^3/min

6.8. Field well test was conducted for a confined aquifer as idealized in Fig. 6.8 and the following data were obtained. Determine the coefficient of permeability from this field test.
r_1 = 3.2 m
r_2 = 6.0 m
h_1 = 2.34 m

$h_2 = 2.83$ m
H = 6.34 m
q = 3635 cm^3/min

6.9. For a given sheet pile which is driven into a permeable soil layer underlain by an impermeable clay layer,
(a) Draw the flow net by using $N_f = 3$.
(b) Compute the flow rate q around the sheet pile.

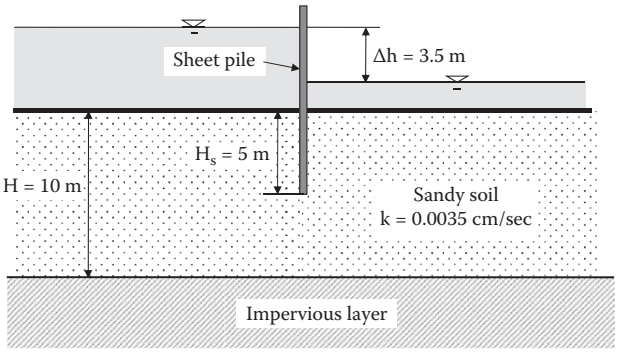

6.10. In problem 6.9 figure above, make the depth of the sheet pile H_s to 7.5 m and redraw the figure in a correct scale.
(a) Draw the flow net by using $N_f = 3$.
(b) Compute the flow rate q around the sheet pile.

6.11. For a given dam in the figure below,
(a) Draw the flow net by using $N_f = 3$.
(b) Compute the flow rate q under the dam.
(c) Compute the water pressures at the heel (A) and toe (B) sections of the dam base based on the drawn flow net.

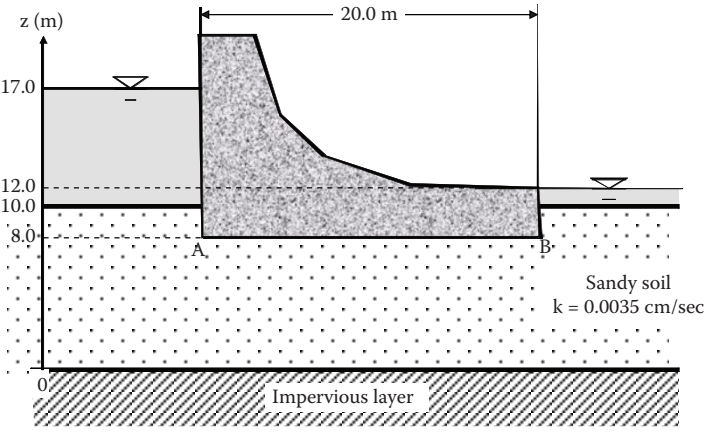

6.12 For the same dam and the same soil conditions as in Problem 6.11, a 4-meter-long vertical sheet pile is added at the left end of the dam base.
(a) Draw the flow net by using $N_f = 3$.
(b) Compute the flow rate q around under the dam.
(c) Compute the water pressures at the heel (A) and toe (B) sections of the dam base based on the drawn flow net.

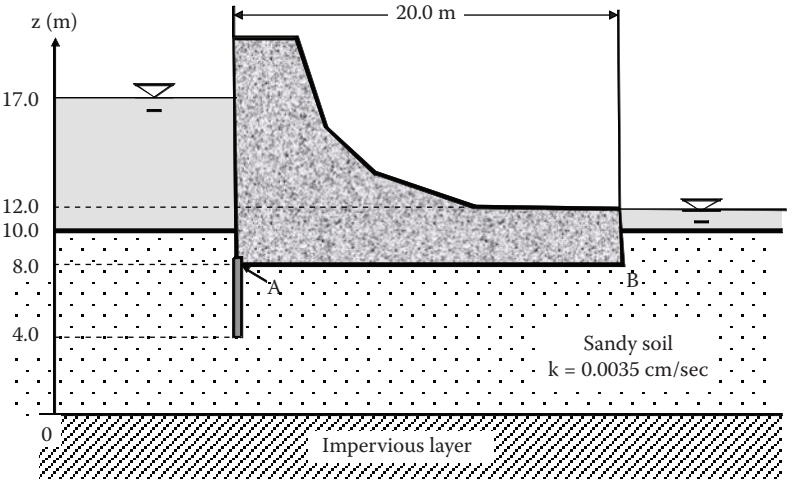

6.13 For the earth dam with a sheet pile at the heel section in problem 6.12,
(a) Compute and plot the water pressure distribution against the upstream face of the dam from z = 17.0 m to z = 4.0 m.
(b) Compute the resultant of the above pressures against the face of the dam, including sheet pile section.

6.14. For the earth dam with a sheet pile at the heel section in problem 6.12,
(a) Compute and plot the uplift water pressure distribution along the base of the dam.
(b) Compute the resultant of the above pressures against the base of the dam.

7 Effective Stress

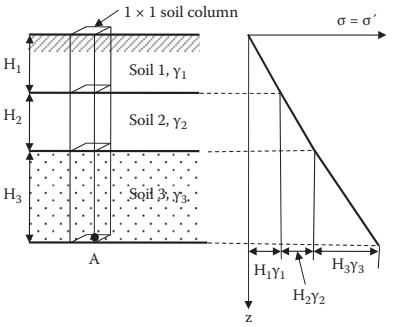

7.1 INTRODUCTION

Terzaghi (1925) developed the **effective stress concept**, which became a key concept in modern soil mechanics. Effective stress in soil contributes to its strength and volume change. It also influences the capillary rise, seepage force due to water flow, quicksand (sand boiling), and heaving at the bottom of the excavation. These are discussed in this chapter.

7.2 TOTAL STRESS VERSUS EFFECTIVE STRESS

Soil is an assemblage of particles, so that the soils' skeleton (particle connected structure) is a major body to resist against external forces as seen in Figure 7.1, in which two-headed arrow vectors indicate interparticle forces at contact points, including normal contact forces as well as shear contact forces. In a dry situation, interparticle forces are in equilibrium with the external forces as seen. However, if the soil is saturated or partially saturated, pore water pressure develops, and it also resists against some part of the external forces.

Figure 7.2 models the interparticle and pore water pressure resistances against the external stress σ. The model consists of a water-filled cylinder with a frictionless loading piston that is supported by a spring. In the piston, there is a small hole to allow drainage. The spring represents the skeleton's resistance, filled water represents the pore water of the soils, and a small hole in the piston reflects the permeability of the soil. Terzaghi defined **effective stress** σ' as

$$\sigma' = \sigma - u \tag{7.1}$$

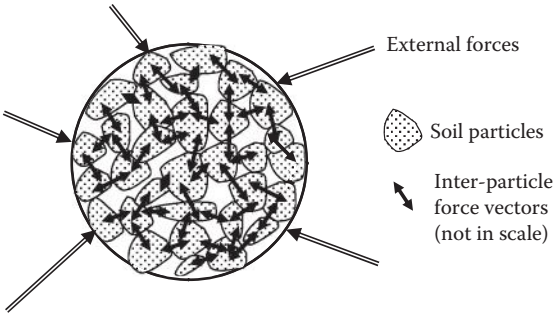

FIGURE 7.1 Inter-particle stresses in particle assemblage.

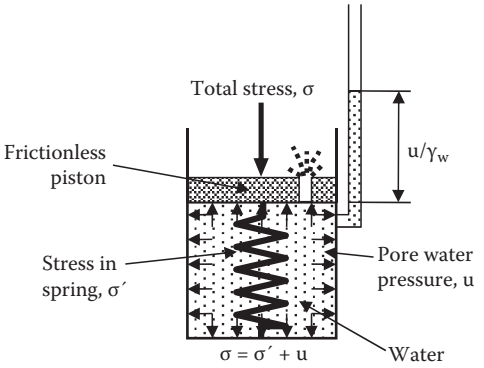

FIGURE 7.2 Terzaghi's effective stress model.

where σ is the applied **total stress** and u is the **pore water pressure**. In the model, the applied stress is carried partially by σ_{spring} and partially by the pore water pressure u. Thus, the skeleton's stress is closely related to the effective stress. When the volume change occurs (the spring is compressed), σ_{spring} (effective stress) develops, or vice versa, as demonstrated in the model. ***Total stress does not contribute any to the volume change of soils; rather, the effective stress is the one to cause the volume change of soils***.

7.3 EFFECTIVE STRESS COMPUTATIONS IN SOIL MASS

In-situ soil at a certain depth is subjected to an **overburden stress**, which generally determines the current formation of the soil. At a greater depth beneath the ground surface, the soil is more compacted because of its higher overburden stress. ***According to the effective stress concept, the stress that determines the current form of the skeleton is the effective stress***. In the following text, effective overburden stress computations are demonstrated for various situations.

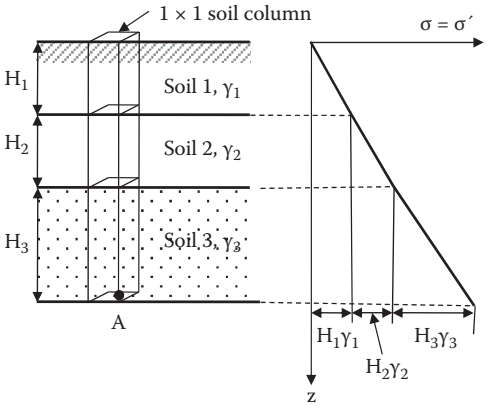

FIGURE 7.3 Effective stress computation for dry soil layers.

7.3.1 Dry Soil Layers

Figure 7.3 shows several layers of dry soil deposit. The total vertical (overburden) stress at point A is the weight of a soil column of 1 × 1 area above the point A, and thus,

$$\sigma = H_1\gamma_1 + H_2\gamma_2 + H_3\gamma_3 = \Sigma(H_i\gamma_i) \tag{7.2}$$

The vertical stress distribution σ with the depth is plotted alongside. In this case, u = 0, and thus, σ′ = σ throughout the depth.

7.3.2 Soil Layers with Steady Water Table

Figure 7.4 plots a situation with a steady groundwater table. The water table is at a midway of soil layer 2. In this case, the total vertical stress σ at point A is calculated

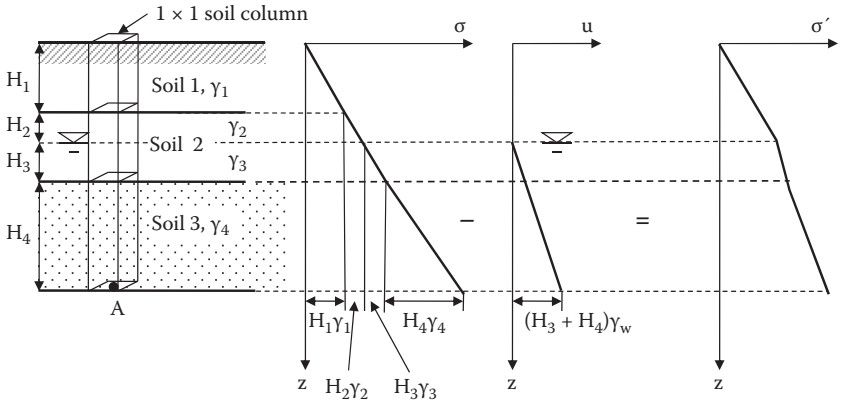

FIGURE 7.4 Effective stress computation for dry and wet soil layers.

first as the weight of a 1 × 1 soil column as before, and then the hydrostatic water pressure u is computed. Finally, the effective vertical stress σ′ is computed as follows:

$$\sigma = H_1\gamma_1 + H_2\,\gamma_2 + H_3\gamma_3 + H_4\gamma_4 = \Sigma(H_i\gamma_i) \tag{7.3}$$

$$u = (H_3 + H_4)\gamma_w \tag{7.4}$$

$$\sigma' = \sigma - u = [H_1\gamma_1 + H_2\gamma_2 + H_3\gamma_3 + H_4\gamma_4] - [(H_3 + H_4)\gamma_w]$$

$$= H_1\gamma_1 + H_2\gamma_2 + H_3(\gamma_3 - \gamma_w) + H_4(\gamma_4 - \gamma_w)$$

$$= \Sigma(H_i\gamma_i)_{\text{above W.T.}} + \Sigma[(H_j(\gamma_j - \gamma_w)]_{\text{below W.T.}} \tag{7.5}$$

where i and j donate the values for above the water table and below the water table, respectively. These individual distribution curves are also plotted in Figure 7.4. The effective stress distribution curve and Equation 7.5 suggest that ***σ′ can be directly calculated by a summation of soil layer thickness multiplied by the unit weight for all layers by assigning the total unit weight γ_t for soils above the water table and submerged unit weight γ' ($= \gamma_t - \gamma_w$) for soils below the water table***.

Exercise 7.1

Figure 7.5 shows soil conditions and water table elevation. Calculate the effective overburden stress at point A, (a) by computing σ and u individually, and (b) by directly using γ_t above the water table and γ' below the water table.

Solution:

Assume that for soil 2, γ_t values above and below the water table are the same.

Method (a): individual computations of σ and u, then σ′

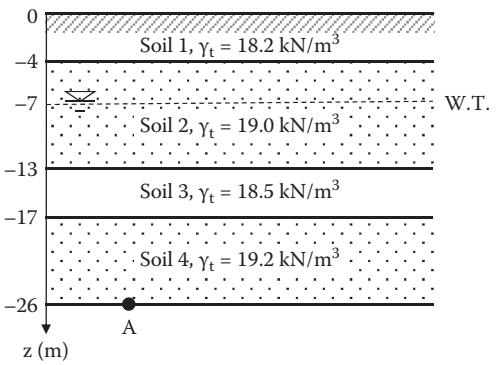

FIGURE 7.5 Exercise 7.1 problem.

$\sigma_A = \Sigma(H_i\gamma_t) = 4 \times 18.2 + 9 \times 19.0 + 4 \times 18.5 + 9 \times 19.2 = 490.6$ kPa

$u_A = (6 + 4 + 9) \times 9.81 = 186.4$ kPa

$\sigma'_A = \sigma_A - u_A = 490.6 - 186.4 =$ **304.2 kPa ←**

Method (b): direct computation of σ'

$\sigma'_A = \Sigma(H_i\gamma_i) + \Sigma(H_j\gamma'_j) = 4 \times 18.2 + 3 \times 19.0 + 6 \times (19.0 - 9.81) + 4 \times (18.5 - 9.81) + 9 \times (19.2 - 9.81)$

$=$ **304.2 kPa ←**

Both solutions yielded the same results.

7.3.3 Totally Submerged Soil Layers

To calculate the effective stress σ' for soils under lakes or at ocean bottom, it uses the same principles as before, that is, use of γ' for soils under the water table. Since all soils are under the water table, it is simply

$$\sigma' = \Sigma(H_j\gamma'_j)_{\text{below W.T.}} \tag{7.6}$$

Fig. 7.6 shows the distributions of σ, u, and σ' for this case. It can be seen that σ' is not affected by the depth of water H_w.

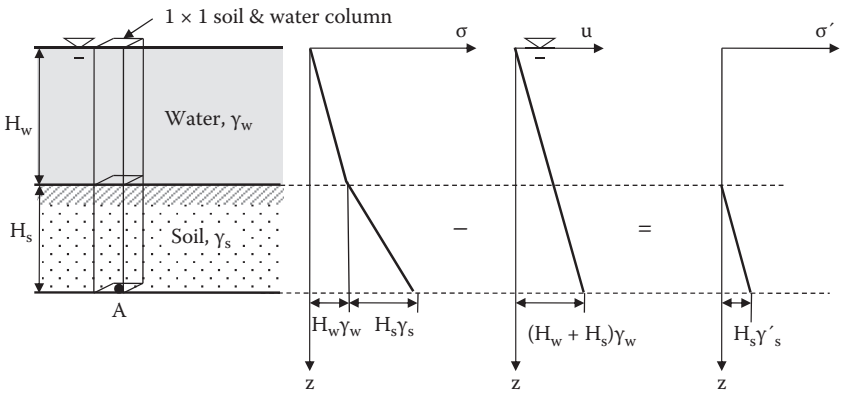

FIGURE 7.6 Effective stress computation for underwater soil layers.

Exercise 7.2

Calculate σ, u, and σ' on a soil element at 2 m depth from an ocean-bottom surface under 300 m deep water. The soil's unit weight is 17.5 kN/m^3. Does this high water pressure compress soil?

Solution

$\sigma = H_w\gamma_w + H_{soil}\gamma_{soil} = 300 \times 9.81 + 2 \times 17.5 = 2978$ kPa

$u = H_w\gamma_w = (300 + 2) \times 9.81 = 2963$ kPa

$\sigma' = \sigma - u = 2978 - 2963 = 15$ kPa

Total stress and pore water pressure are very high, but the effective stress is very low. Since the formation of the soil's skeleton is controlled by interparticle stress (effective stress), soils at the near surface of the ocean bottom are not compressed much because of the rather small effective overburden stress.

The foregoing exercise demonstrates that there exist very soft soils at deep ocean bottoms even though those soils are subjected to extremely high water pressures. ***High water pressure acts hydrostatically all around the surface of grain particles, and thus, it does not contribute any to increase in interparticle stresses***.

7.4 EFFECTIVE STRESS CHANGE DUE TO WATER TABLE CHANGE

When the water table changes, the effective overburden stress changes since the effective stress computation uses either γ_t or γ' depending on the water table elevation as seen in the previous section. In particular, when the water table drops, the effective stress increases. The effective stress increase implies higher grain skeleton stress, and thus, it causes volume decrease or settlement. In modern history, many urban industrial cities pumped up underground water for industrial uses and lowered the water table elevation permanently. The consequence was ground surface settlement in many cities around the world.

Exercise 7.3

For the site shown in Figure 7.7 (the same site as in Exercise 7.1), water table elevation was at –7 m originally, and lowered to 6 m to –13 m due to heavy industrial

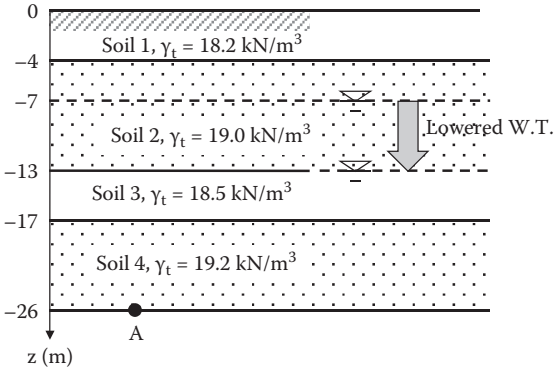

FIGURE 7.7 Exercise 7.3 problem.

water use. Calculate the change of the effective overburden stress at point A. What is a consequence of the lowering water table elevation?

Solution:

Assume that, for soil 2, γ_t values above and below the water table are the same. Before lowering the water table using the result in Exercise 7.1,

$$\sigma'_A = \Sigma(H_i\gamma_i) + \Sigma(H_j\gamma'_j) = 4 \times 18.2 + 3 \times 19.0 + 6 \times (19.0 - 9.81) + 4 \times (18.5 - 9.81) + 9 \times (19.2 - 9.81)$$

$$= 304.2 \text{ kPa}$$

After lowered water table to –13 m,

$$\sigma'_A = \Sigma(H_i\gamma_i) + \Sigma(H_j\gamma'_j) = 4 \times 18.2 + 9 \times 19.0 + 4 \times (18.5 - 9.81) + 9 \times (19.2 - 9.81)$$

$$= 363.1 \text{ kPa}$$

Thus the change in σ'; $\Delta\sigma' = 363.1 - 304.2$ **= +58.9 kPa increase.** ←

This increase in effective stress would cause ground settlement in the near future. ←

In contrast to cases with lowering water table elevation, its rise causes a reduction in effective stress. In such cases, some swell is possible, but it may not be as severe as in the case of settlement. One potential problem of this case is that, underground structures, including buried pipes as well as massive underground structures may be pushed upward due to increased buoyancy forces applied to such structures. In recent years, it was reported that the underground sections of the Tokyo railway station have been affected by increased upward pressure. This is due to the restriction of groundwater use in that area. As a result, in recent years, the water table has been rising gradually.

7.5 CAPILLARY RISE AND EFFECTIVE STRESS

Soils above the water table are, in general, not completely dry due to **capillary rise,** as seen in Figure 7.8a. The capillary zone affected by the rise depends on the size of the void opening of the soils. The smaller the void spacing, the higher the rise. Small void spaces in soil assemblages work as capillary tubes. ***Hazen (1930)*** empirically

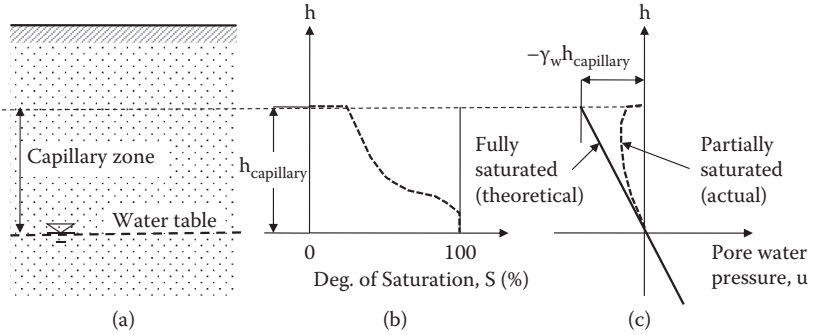

FIGURE 7.8 Capillary rise.

TABLE 7.1
Approximate Capillary Rise in Different Soils

Soil Type	Loose	Dense
Coarse sand	0.03–0.12 m	0.04–0.15 m
Medium sand	0.12–0.50 m	0.35–1.10 m
Fine sand	0.30–2.0 m	0.40–3.5 m
Silt	1.5–10 m	2.5–12 m
Clay	≥10 m	

Source: Hansbo, S. (1975), *Jordmateriallara*, Almqvist & Wiksell Forlag AB, Stockholm, 218 pp.

gave an approximate maximum height of capillary rise $h_{capillary}$ as a function of soil properties D_{10} and e as

$$h_{capillary}\ (\text{in mm}) = \frac{C}{e\,D_{10}} \tag{7.7}$$

where e is the void ratio, D_{10} is the effective grain size in mm, and C is a constant with a range of 10 to 50. Table 7.1 shows general values of those for different soils. As can be seen in the table, capillary rise is quite high for finer soils.

Capillary rise is due to suction created by the **surface tension** of water films around particles, as seen in Figure 7.9. This suction works as attractive particle-to-particle stress and creates negative pore water pressure. Thus, it increases the effective stress, according to Equation 7.1. Theoretically, the pore water pressure u in the capillary zone is $-\gamma_w h$ for fully saturated soils, as seen in Figure 7.8c. However, the degree of saturation in the capillary zone changes from nearly fully saturated condition at the water table level to very low at the highest rise, as shown in Figure 7.8b. Therefore, the actual u is smaller than the theoretical one. It is approximated by

$$u = -\left(\frac{S}{100}\right)\gamma_w h_{capillary} \tag{7.8}$$

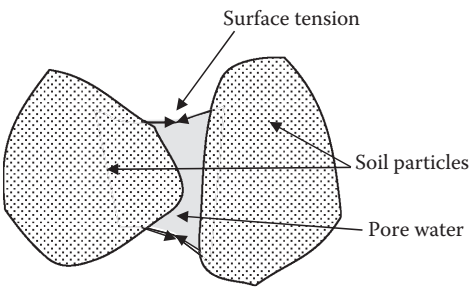

FIGURE 7.9 Surface tension between particles.

where S is the degree of saturation in percent and $h_{capillary}$ is the height from the water table level. Actual pore water pressure u in the capillary rise zone is also shown in Figure 7.8c with a dotted line.

Because of negative pore water pressure in the capillary zone, the effective stress in that zone needs to be modified from the one without capillary rise consideration, as demonstrated in Exercise 7.4.

Exercise 7.4

For the soil condition given in Figure 7.10, calculate and plot σ, u, and σ′ distributions with the depth considering the capillary rise. Assume that the average degree of saturation in the capillary zone is 50%.

Solution:

at −8 m without capillary rise,

$\sigma = 8 \times 18.2 = 145.6$ kPa

$u = 0$

$\sigma' = 145.6$ kPa

at −8 m with capillary rise,

$\sigma = 8 \times 18.2 = 145.6$ kPa

$u = -(S/100)\gamma_w h_{capillary} = -0.5 \times 9.81 \times 1.5 = -7.4$ kPa

$\sigma' = 145.6 - (-7.4) = 153.0$ kPa

at −9.5m

$\sigma = 8 \times 18.2 + 1.5 \times 18.5 = 173.4$ kPa

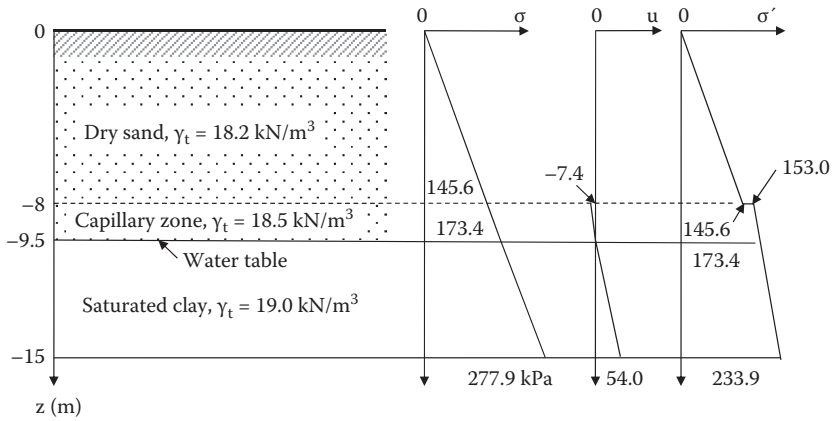

FIGURE 7.10 Effective stress computation with capillary tension.

$u = 0$

$\sigma' = 173.4$ kPa

at –15 m,

$\sigma = 8 \times 18.2 + 1.5 \times 18.5 + 5.5 \times 19.0 = 277.9$ kPa

$u = 5.5 \times 9.81 = 54.0$ kPa

$\sigma' = 277.9 - 54.0 = 223.9$ kPa

The foregoing distributions are plotted in Figure 7.10.

Note that, in Exercise 7.4, there is a discontinuity in the effective stress distribution curve at the top of capillary zone. It occurred due to using an average S value for the capillary zone in the exercise. In reality, that portion of the curve should change smoothly when the variation of S is properly accounted, though the precise estimation of S is not an easy task.

7.6 EFFECTIVE STRESS WITH WATER FLOW

When water flows through pores of soil mass, it drags the particle. The dragging action creates frictional force on the particle surface toward the direction of water flow, as seen in Figure 7.11. Those frictional forces that act on particles' surface work as **seepage force** and change the effective stress.

In Figure 7.12, a cylinder filled with soil is subjected to upward water flow due to the head difference at both ends of the soil column. Alongside, water pressure through the soil column is plotted. Point E is the water pressure from the supply side of water, and point F is the pressure from the discharge side of the system.

The pressure line AEB is a hydrostatic water pressure based on the left side of the water supply, while CFD is a hydrostatic water pressure from the right side of the water supply, both of which are parallel and have a slope of $1/\gamma_w$. On those two lines, only EB and CF sections with solid lines are real pressures, and AE and FD sections with dotted lines are just extensions of the EB and CF lines, respectively.

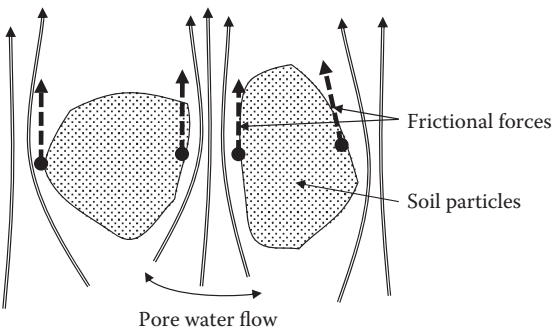

FIGURE 7.11 Upward seepage force.

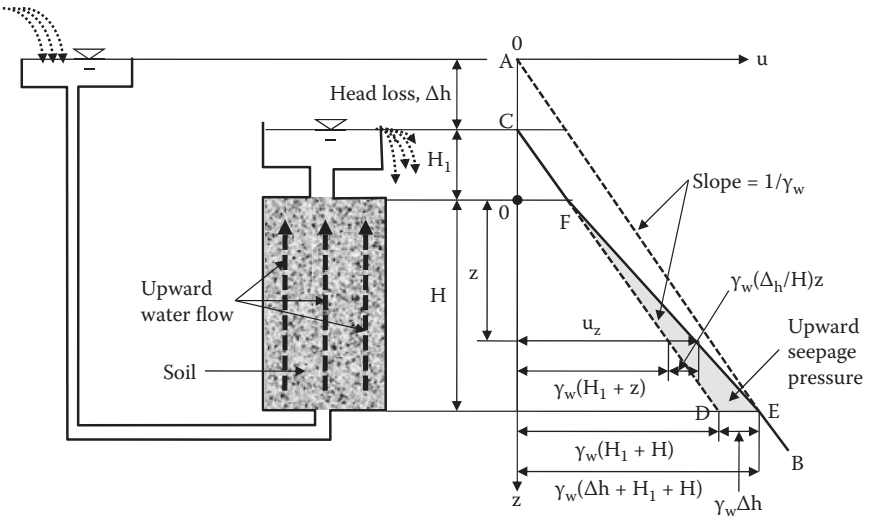

FIGURE 7.12 Water pressure with upward seepage flow.

Since the water pressure is continuous through the soil column, and the upward seepage force changes proportionally with hydraulic pressure loss through the specimen, it changes linearly with the depth in this case, and thus, Points F and E are connected with the solid straight line. Therefore, the real water pressure distribution of the system becomes CFEB in the figure.

Referring to Figure 7.12, at the bottom of the soil column (at E), the total water pressure is $\gamma_w(\Delta h + H_1 + H)$, which is higher than the hydrostatic pressure $\gamma_w(H_1 + H)$ without water flow (i.e., at D). This extra water pressure of $\gamma_w \Delta h$ is called upward **seepage pressure**. This is created by dragging the force of upward water flow through the soil. The triangle FDE in the figure is the upward seepage pressure due to upward water flow. At arbitrary depth z, the seepage pressure is calculated as $\gamma_w(\Delta h/H)\, z$ by using a proportionality in the triangle FDE. Thus, water pressure u_z at depth z is

$$\mu_z = \gamma_w(H_1 + z) + \gamma_w(\Delta h/H)z \tag{7.9}$$

and the total stress σ_z at depth z is

$$\sigma_z = \gamma_w H_1 + \gamma_t z = \gamma_w H_1 + (\gamma' + \gamma_w)z = \gamma_w (H_1 + z) + \gamma' z \tag{7.10}$$

and thus the effective stress σ'_z at depth z is

$$\sigma'_z = \sigma_z - u_z = [\gamma_w (H_1 + z) + \gamma' z] - [\gamma_w(H_1 + z) + \gamma_w(\Delta h/H)z] = \gamma' z - \gamma_w(\Delta h/H)z \tag{7.11}$$

Now, the condition of $\sigma' = 0$ in Equation 7.11 yields

$$\frac{\Delta h}{H} = \frac{\gamma'}{\gamma_w} = i_c \tag{7.12}$$

where i_c is called **critical hydraulic gradient**. Equation 7.12 implies that, when the $\Delta h/H$ ratio is equal to or higher than the i_c value (γ'/γ_w), the effective stress is zero or negative. The effective stress is the interparticle stress, and thus, zero or negative interparticle stress implies separation of the particles. This condition causes **quicksand** (or **sand boiling**) of granular soils and **heave** of cohesive soils.

The i_c value is approximately 1.0 since γ' ($=\gamma_t - \gamma_w$) is nearly equal to γ_w for many soils (e.g., $\gamma_t = 18 \sim 20$ kN/m^3, and $\gamma_w = 9.81$ kN/m^3). Thus, ***when the total head loss Δh exceeds approximately the length of the specimen H, those critical conditions would prevail***.

7.7 QUICKSAND (SAND BOILING)

Quicksand or sand boiling is best demonstrated in the case of the cut-off sheet pile situation as shown in Figure 7.13. In the figure, water flows from left to right due to the head difference. Soils near the BC section of the sheet pile are subjected to upward seepage pressure and potentially possess the quicksand condition. The **Factor of safety for the quicksand** condition can be measured by

$$FS = \frac{i_c}{i_{B\to C}} \tag{7.13}$$

where i_c is the critical hydraulic gradient defined in Equation 7.12, and $i_{B\to C}$ is the hydraulic gradient from Point B to Point C and computed by

$$i_{B\to C} = \frac{\Delta h_{B\to C}}{BC} = \frac{h_B - h_C}{BC} \tag{7.14}$$

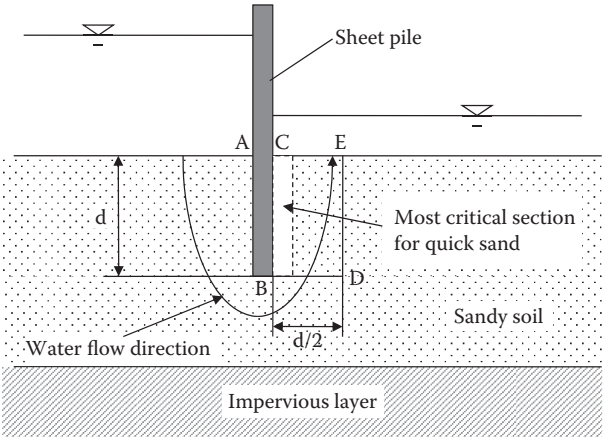

FIGURE 7.13 Critical section for quicksand on cut-off sheet pile.

where h_B and h_C are hydraulic heads at Points B and at C, respectively, and BC is the length of the water flow from Point B to Point C. The heads h_B and h_C can be read from equipotential lines of the flow net as discussed in Chapter 6. The zone along BC is the most critical section for the quick condition since H in Equation 7.12 is the smallest for the same interval of equipotential lines (Δh_i) in this sheet pile problem.

Terzaghi (1922) suggested evaluating the factor of safety against quicksand for the section of d × d/2 (area BCED) based on his experimental observation, which is also seen in Figure 7.13. The average head loss from B-D to C-E can be computed from $\Delta h_{BD \to CE} = h_{BD} - h_{CE}$, and the flow distance BD to CE is approximately as d (depth of sheet pile) in this case.

Exercise 7.5

For a given flow net of water flow around a sheet pile in Figure 7.14, compute the factor of safety against the quicksand condition, (a) at the most critical section along the downstream face of the sheet pile, and (b) by Terzaghi's method. In the figure, the total head loss $\Delta h = 7$ m, the sheet pile depth d = 10 m, and $\gamma_t = 19.0$ kN/m^3.

Solution:

Figure 7.15 is an enlarged drawing of the right side of the sheet pile where the quicksand condition is most likely to occur.

$N_d = 10.0$

$\Delta h_i = \Delta h / n_d = 7/10 = 0.7$ m

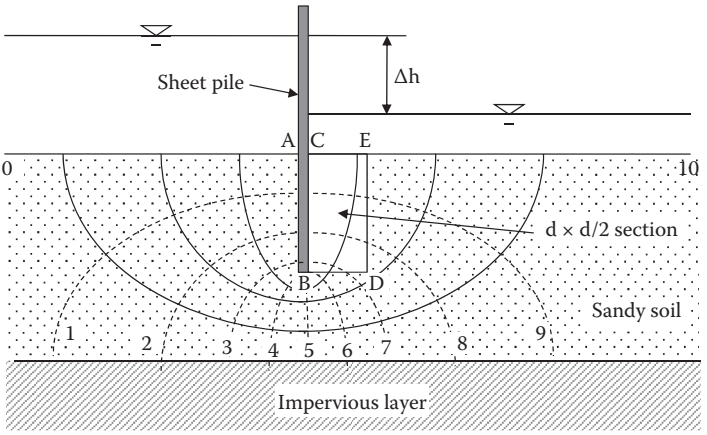

FIGURE 7.14 Exercise 7.5.

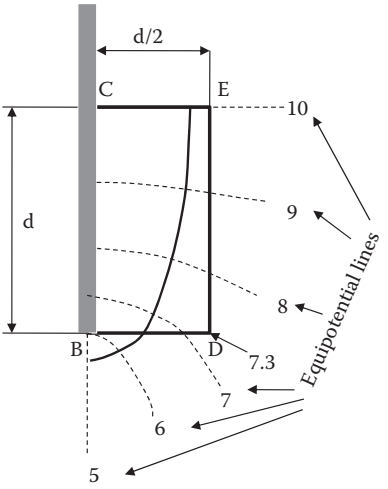

FIGURE 7.15 Enlarged picture of Terzaghi's quicksand computation zone.

a. Along the face BC, there are five equipotential drops from point B to point C, and thus,

$i_{B\to C} = \Delta h_i \times (10 - 5)/d = 0.7 \times 5/10 = 0.35$

$i_c = \gamma'/\gamma_w = (19 - 9.81)/9.81 = 0.937$

thus, $FS = i_c/i_{B\to C} = 0.937/0.35 = 2.68$ (>1.0, safe against the quicksand condition).

b. for BDEC section (d × d/2 section) by Terzaghi

Referring to Figure 7.15, point D is on nearly the 7.3th equipotential line. From points B to C, there are five equipotential drops, and from points D to E, there are 2.7 equipotential drops, and thus, the average equipotential drops from line BD to line CE is approximately (5 + 2.7)/2 = 3.85. Therefore, the average head drop from BD to CE is

$\Delta h_{BD\to CE} = \Delta h_i \times 3.85 = 0.7 \times 3.85 = 2.695$ m.

$i_{BD\to CE} = \Delta h_{BD\to CE}/d = 2.695/10 = 0.270$

Thus, $FS = i_c/i_{BD\to CE} = 0.937/0.270 = 3.47$ (>1.0, safe against the quicksand condition).

In Exercise 7.5, it should be noted that Terzaghi's d × d/2 section method provides a higher factor of safety than the critical section along the downstream face of the sheet pile.

7.8 HEAVE OF CLAY DUE TO EXCAVATION

When ground excavation is done on clay soil to a certain depth, the heave at the bottom of the excavation would pose a potential danger at construction sites.

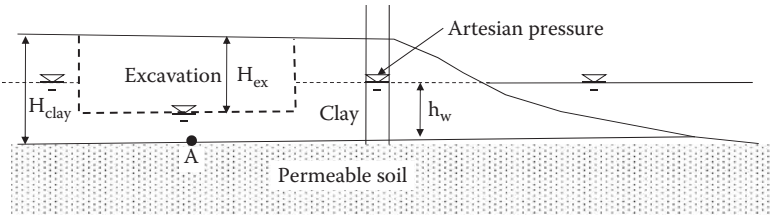

FIGURE 7.16 Heave of clay (dry excavation).

This bottom heave is due to reduction in effective stress. Depending on excavation procedures, there are two categories of the heave problem: **dry excavation** and **wet excavation**.

7.8.1 Dry Excavation

When excavation is done rather quickly or the water in the excavated pit is continuously pumped out, **dry excavation** may prevail. In this case, during excavation, the bottom of the excavated pit is rather dry. A typical situation is shown in Figure 7.16. The top clay layer is under an artesian water pressure. That is, due to a nearby lake or river, the water table in clay layer is steady, and a permeable layer underneath the clay layer is connected to the water supply from the lake or river. The effective stress at the bottom of clay layer, point A, is computed as

$$\sigma = (H_{clay} - H_{ex})\gamma_{clay} \tag{7.15}$$

$$u = h_w\gamma_w \tag{7.16}$$

$$\sigma' = \sigma - u = (H_{clay} - H_{ex})\gamma_{clay} - h_w\gamma_w \tag{7.17}$$

Note that the pore water pressure at point A is not $(H_{clay} - H_{ex})\gamma_w$ but rather $h_w\gamma_w$ due to the artesian water pressure. In Equation 7.17, $\sigma' > 0$ is the condition for safe excavation without heave. If $\sigma' < 0$ condition would prevail, the bottom of the excavation would heave, and the excavation site would be prone to disaster.

Exercise 7.6

As in Figure 7.16, the excavated pit is kept dry by continuous pumping of water. The clay layer thickness H_{clay} is 15 m, and the artesian pressure height h_w is 10 m. $\gamma_{clay} = 18.0$ kN/m^3. Determine the maximum excavation depth H_{ex} without heave.

Solution:

At the bottom of clay layer, point A, from Equation 7.17, the effective stress σ' is:

$$\sigma' = \sigma - u = (H_{clay} - H_{ex})\gamma_{clay} - h_w\gamma_w = (15 - H_{ex}) \times 18.0 - 10 \times 9.81 > 0$$

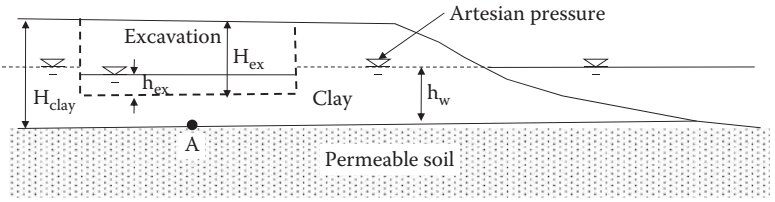

FIGURE 7.17 Heave of clay (wet excavation).

By solving this equation for H_{ex}, $H_{ex} < 9.55$ m, and thus, the maximum safe excavation depth without bottom heave is 9.55 m. ←

7.8.2 Wet Excavation

When excavation process is rather slow, water seeps out and fills the excavation site. This situation is called **wet excavation**. Figure 7.17 shows such a situation, in which h_{ex} is the water depth in the excavated pit. In this case, the effective stress at Point A is

$$\sigma = h_{ex}\gamma_w + (H_{clay} - H_{ex})\gamma_{clay} \tag{7.18}$$

$$u = h_w\gamma_w \tag{7.19}$$

$$\sigma' = \sigma - u = h_{ex}\gamma_w + (H_{clay} - H_{ex})\gamma_{clay} - h_w\gamma_w \tag{7.20}$$

Note again that the pore water pressure at A still remains the same as in dry excavation case due to the artesian water pressure. In Equation 7.20, $\sigma' > 0$ is the condition for safe excavation without heave.

Exercise 7.7

Referring to Figure 7.17, H_{clay} is 15 m, h_w is 10 m, and γ_{clay} =18.0 kN/m^3. First, wet excavation was done to 10 m (H_{ex} = 10 m), and the water level in the pit was 5 m (h_{ex} = 5 m).

(a) Check the excavation safety for this wet excavation.
(b) If (a) above is safe against heaving, by how much could the water level in the pit be lowered by pumping without heave?

Solution:

(a) From Equation 7.20, the effective stress at A is

$\sigma' = \sigma - u = h_{ex}\gamma_w + (H_{clay} - H_{ex})\gamma_{clay} - h_w\gamma_w = 5 \times 9.81 + (15–10) \times 18 - 10 \times 9.81$
$= \mathbf{+\ 40.95\ kPa}$

The σ' value is a positive number, and so the pit is safe against bottom heave. ←

(b) When the water level in the pit is further lowered with Δh_{ex}, $(h_{ex} - \Delta h_{ex})$ is substituted in h_{ex} in Equation 7.20 to compute the effective stress at A, and it becomes

$$\sigma' = \sigma - u = (h_{ex} - \Delta h_{ex})\gamma_w + (H_{clay} - H_{ex})\gamma_{clay} - h_w\gamma_w$$
$$= (5 - \Delta h_{ex}) \times 9.81 + (15 - 10) \times 18 - 10 \times 9.81$$

By solving $\sigma' > 0$ in the equation, the limit of Δh_{ex} value is obtained as

$$\mathbf{\Delta h_{ex} < 4.15\ m}\ \text{(or water depth in the pit} = 5.0 - 4.15 = \mathbf{0.85\ m)} \leftarrow$$

This is the lowest depth to which water could be pumped out without heave at the bottom.

By comparing Exercises 7.6 (dry excavation) and 7.7 (wet excavation), it can be observed that wet excavation can go a little deeper (i.e., 9.55 m in dry excavation versus 10 m with 0.85 m water depth in the pit). It should be noted that computation of the critical excavation depth is a purely theoretical one, and so, the actual safe excavation depth would be smaller than that of the computed value considering water level fluctuation, uncertainty in soil properties, etc.

7.9 SUMMARY

The effective stress concept is the most important contribution made by Terzaghi. The effective vertical stress is the one used to determine the current soil formation. It controls volume change (Chapter 9) and strength of soils (Chapter 11). Capillary rise, seepage force, quicksand or sand boiling, and heaving of clay at the bottom of the excavation are all related to effective stress. ***Understanding the concept and computation technique of effective stress is critically important in the modern soil mechanics of practice***.

REFERENCES

Hansbo, S. (1975), *Jordmateriallara*, Almqvist & Wiksell Forlag AB, Stockholm, 218 pp.
Hazen, A. (1930), Water supply, in *American Civil Engineering Handbook*, Wiley, New York.
Terzaghi, K. (1922), Der Groundbruch an Stauwerken und seine Verhutung, *Die Wasserkraft*, Vol. 17, pp. 445–449.
Terzaghi, K. (1925), *Erdbaumechanik*, Franz Deuticke.

Problems

7.1. Define effective stress and explain its importance in soil mechanics.

7.2. Compute the total vertical stress σ, pore water pressure u and then the effective vertical stress σ' at Points A, B, C, and D in the soil profile shown in Figure Problem 7.2. Plot those with the depth z.

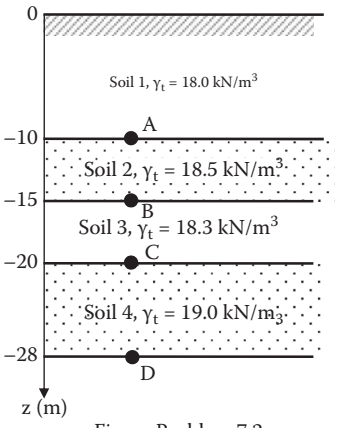

Figure Problem 7.2

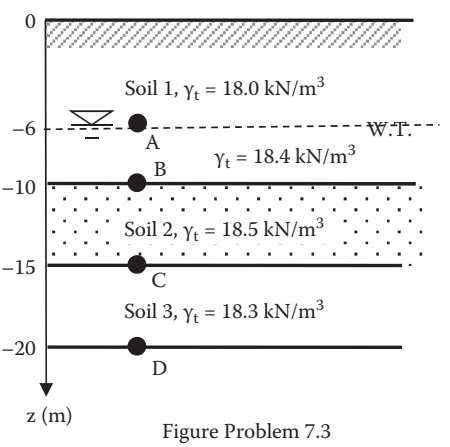

Figure Problem 7.3

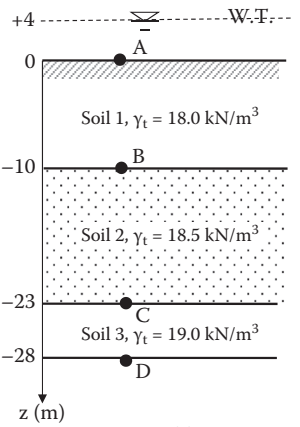

Figure Problem 7.4

7.3. Compute the total vertical stress σ, pore water pressure u, and then the effective vertical stress σ′ at Points A, B, C, and D in the soil profile shown in Figure Problem 7.3. Plot those with the depth z.

7.4. Compute the total vertical stress σ, pore water pressure u, and then the effective vertical stress σ′ at Points A, B, C, and D in the soil profile shown in Figure Problem 7.4. Plot those with the depth z.

7.5. Compute the vertical effective stress σ' at Points A, B, C, and D directly by using the submerged unit weight of soils γ' for the given soil's profile shown in Figure Problem 7.5, Plot those with the depth z.

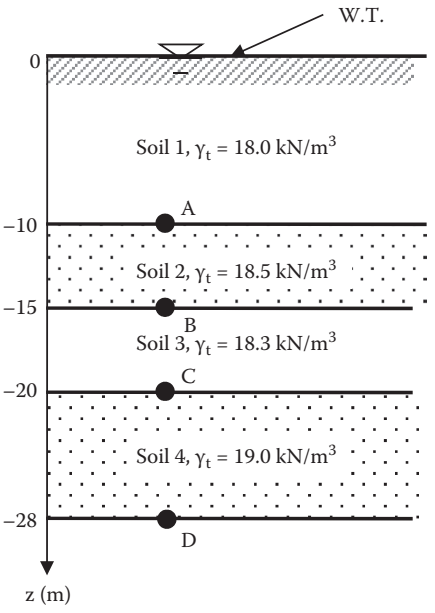

Figure Problem 7.5

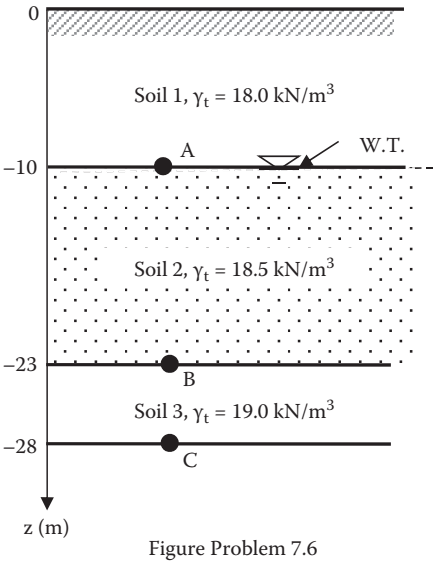

Figure Problem 7.6

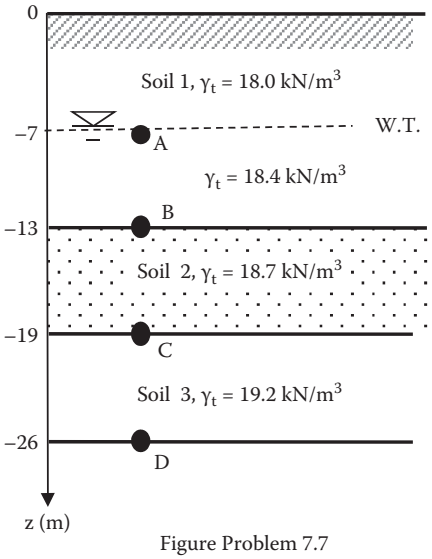

Figure Problem 7.7

7.6 Compute the vertical effective stress σ' at points A, B, and C directly by using the submerged unit weight of soils γ' for the given soil's profile shown in Figure Problem 7.6. Plot those with the depth z.

7.7 Compute the vertical effective stress σ' at Points A, B, C, and D directly by using the submerged unit weight of soils γ' for the given soil's profile shown in Figure Problem 7.7. Plot those with the depth z.

7.8 For the following soil's profile, when the water table elevation is lowered to the level shown,

(a) What is the change in the effective stress at Point A?

(b) What will be the consequence of the effective stress change?

Assume that the total unit weight γ_t of the sand layer above the water table will decrease 5% from its saturated unit weight after lowering the water table.

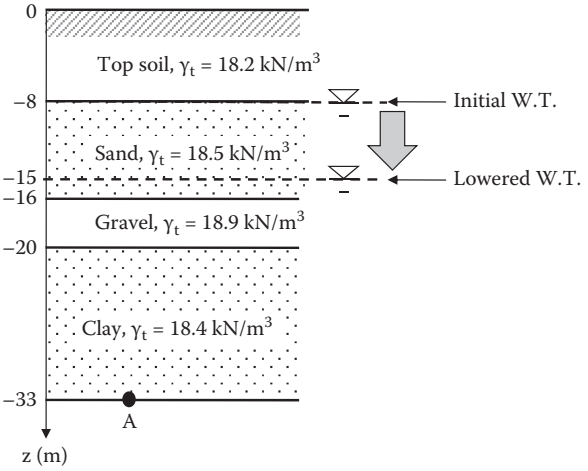

7.9. For the soil's profile shown in Figure Problem 7.8, when the water table elevation is raised to the top of the ground surface,

(a) What is the change in the effective stress at Point A?

(b) What will be the consequence of the effective stress change?

Assume that the total unit weight γ_t of the top soil below the water table will increase 5% from its moist unit weight after raising the water table.

7.10. Compute a range of capillary size according to Hazen's formula (Equation 7.7) for the following soils:

(a) Sandy soil with D_{10} = 0.1 mm and e = 0.50

(b) Silty soil with D_{10} = 0.01 mm and e = 0.50

(c) Clayey soil with D_{10} = 0.001 mm and e = 0.50

7.11 For the following given soil profile, there is an anticipated capillary zone above the groundwater table as shown. Assuming the degree of saturation S for the capillary zone to be 60%, compute the total vertical stress σ, pore water pressure u and then the effective vertical stress σ' at Points A, B, and C. Plot those with the depth z.

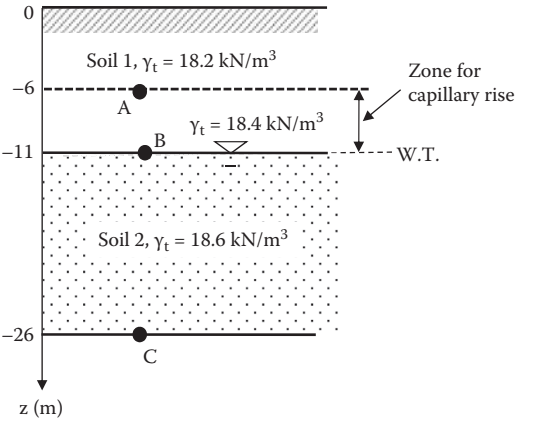

7.12 In Problem 7.11, when the degree of saturation S for the capillary zone is 40%, compute the total vertical stress σ, pore water pressure u and then the effective vertical stress σ' at Points A, B, and C. Plot those with the depth z.

7.13 In Figure 7.12, the following conditions are given: H = 300 mm, Δh = 200 mm, H_1 = 100 mm, and γ_t = 18.5 kN/m^3. Compute the following at the bottom of the specimen tube:

(a) Hydrostatic water pressure from the specimen side
(b) Seepage pressure
(c) Total pore water pressure at the bottom
(d) Critical hydraulic gradient i_c
(e) Factor of safety against quicksand
(f) Will this system be safe against quicksand?

7.14 The quicksand demonstration tank is planned to be built as shown in the figure, determine the minimum height of H_1 to create quicksand conditions in the tank. H_2 = 50 cm, H_3 = 55 cm, and the unit weight of sand γ_t = 16.8 kN/m^3 are used.

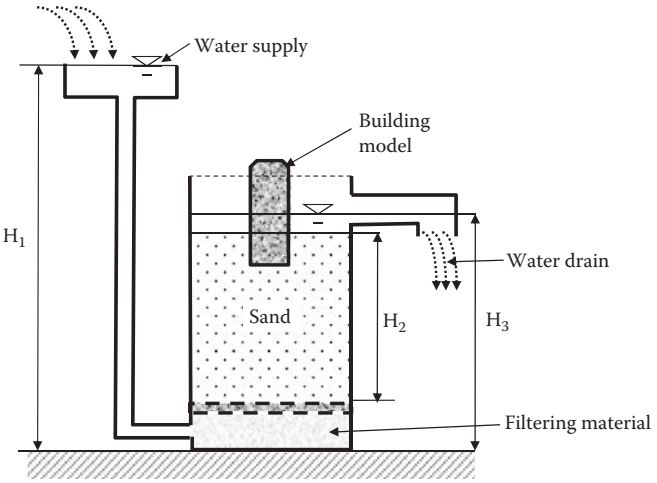

7.15. The following figure shows the flow net around a sheet pile. Determine
(a) The factor of safety against quicksand by Terzaghi's practical method
(b) The factor of safety against quicksand at the most critical section (downstream face of the sheet pile)

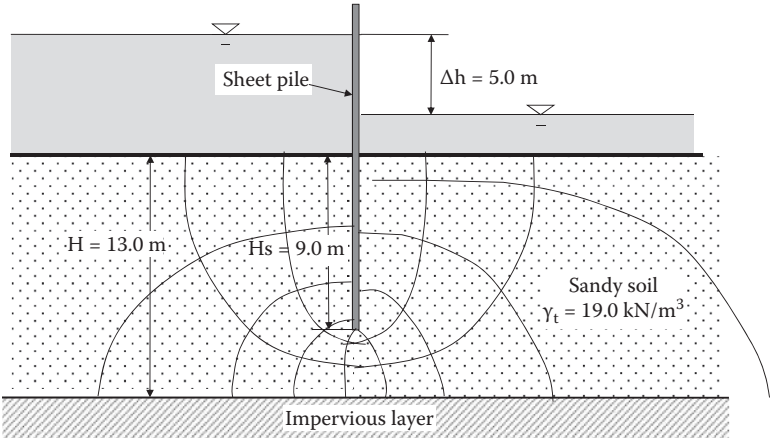

7.16. The soil condition in the following figure shows an artesian pressure. If an excavation is made in a rather short period of time in this clay layer (dry excavation), how deep can it go without causing heaving of the bottom clay layer?

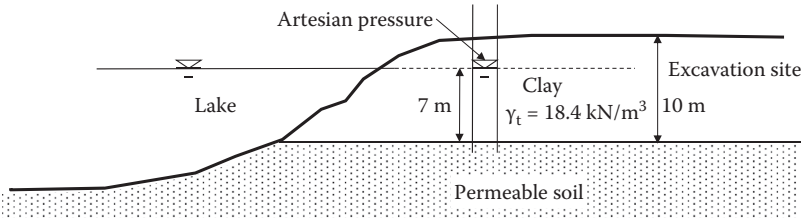

7.17. In Problem 7.16, if the excavation is a slow process, which allows water to seep into the hole (wet excavation), how deep can it go without causing heaving of the bottom clay layer? Assume that the water depth in the hole rises to 7 m above the permeable layer.

7.18. In Problem 7.16, the excavation is done safely up to 8 m depth by allowing the water to seep into the hole (wet excavation). The water is then pumped out from the hole. How deep can the water be pumped out without causing heaving of the bottom clay layer?

8 Stress Increments in Soil Mass

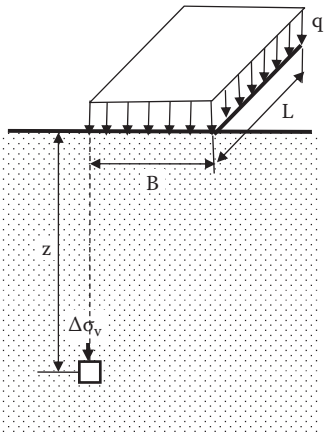

8.1 INTRODUCTION

Chapter 7 studies computational techniques of current effective vertical stress in soil mass and defines the current structure of soils in most cases. Soils are stable under the existing effective overburden stresses. However, when additional loads are placed on ground surface, such as by footings, traffic loads, etc., those additional loads increase the stresses in the soil mass. Those extra stresses are major sources of the settlement of soils. In this chapter equations for the vertical stress increments in soil mass due to various types of load on the ground surface are discussed. They will be used in settlement computation in Chapter 9.

8.2 2:1 APPROXIMATE SLOPE METHOD

Figure 8.1 shows a $B \times L$ rectangular footing on ground surface with a vertical force P, which is applied on the center of the footing. Vertical stress $\sigma_{v,0}$ on the ground surface is $P/(B \times L)$. This $\sigma_{v,0}$ is redistributed over a wider loading area with increasing depth z. A slope with 2 in vertical to 1 in horizontal defines spread loading areas within the soil mass. Stress is spread over an area of $(B + z) \times (L + z)$ at depth z. Accordingly, the vertical stress increment $\Delta\sigma_{v,z}$ at depth z can be calculated from:

$$\Delta\sigma_v = \frac{P}{(B+z)(L+z)} \tag{8.1}$$

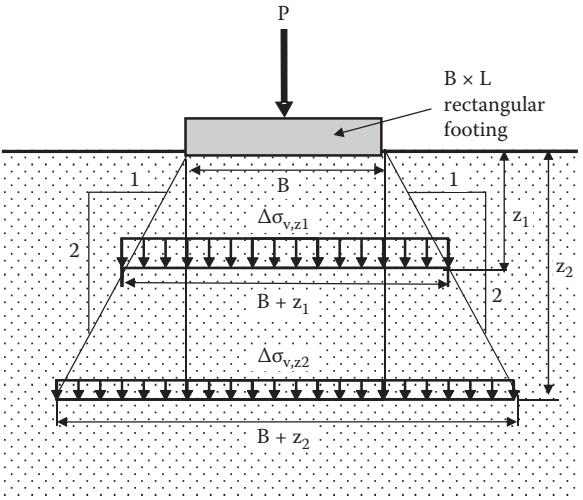

FIGURE 8.1 Vertical stress increment by approximate 2:1 slope method.

Vertical stress decreases with increasing depth z with increased distribution area as seen in Figure 8.1. In this method, it is assumed that the stress is uniformly distributed over (B + z) × (L + z) area, and it suddenly becomes zero beyond the zone defined by 2:1 slope. The real stress distribution is, however, a smooth change over the area under the footing with its maximum value directly under the center of the footing. This is a simple approximate method, and thus it could be used as a rough estimation of stress increment computation.

Exercise 8.1

A 5 kN point load is applied at the center of 1 m × 1 m square footing on the ground surface. Compute and plot the magnitudes of a vertical stress increment

TABLE 8.1
$\Delta\sigma_v$ by 2:1 Slope Method

A	B
z (m)	$\Delta\sigma_v$ (kN/m^2)
0	5.00
2	0.56
4	0.20
6	0.10
8	0.06
10	0.04

$B_i = P/(1 + A_i)(1 + A_i)$

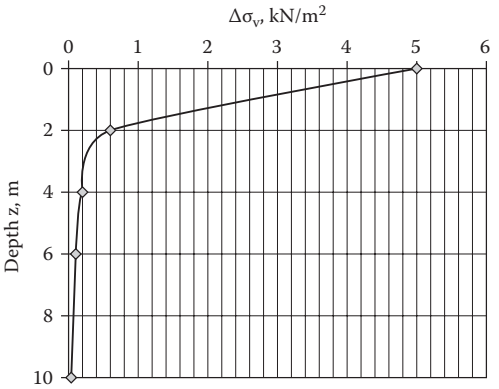

FIGURE 8.2 $\Delta\sigma_v$ distribution (Exercise 8.1).

under the center of the footing at the depths 2, 4, 6, 8, and 10 m from the ground surface. Use a 2:1 approximate slope method.

Solution:

P = 5 kN, B = L = 1 m, and a spreadsheet (Table 8.1) is prepared to obtain vertical stress distribution $\Delta\sigma_v$ with depth z using Equation 8.1. The result is plotted in Figure 8.2.

8.3 VERTICAL STRESS INCREMENT DUE TO A POINT LOAD

Boussinesq (1885) developed an elastic solution for stresses in an isotropic homogeneous elastic media due to a point load on the ground surface as shown in Figure 8.3.

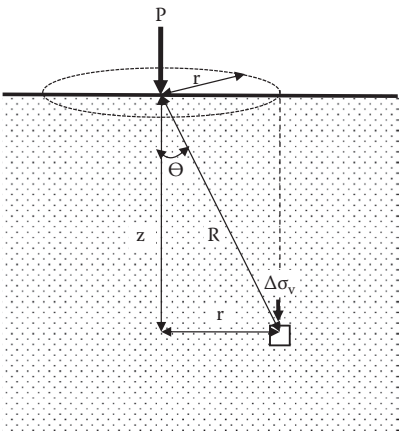

FIGURE 8.3 Boussinesq's point load problem.

TABLE 8.2
Influence Factor I_1 by Equation 8.3 (Boussinesq's Point Load)

r/z	I_1	r/z	I_1	r/z	I_1
0	0.4775	0.32	0.3742	0.85	0.1226
0.02	0.4770	0.34	0.3632	0.9	0.1083
0.04	0.4756	0.36	0.3521	0.95	0.0956
0.06	0.4732	0.38	0.3408	1	0.0844
0.08	0.4699	0.4	0.3295	1.2	0.0513
0.1	0.4657	0.42	0.3181	1.4	0.0317
0.12	0.4607	0.44	0.3068	1.6	0.0200
0.14	0.4548	0.46	0.2955	1.8	0.0129
0.16	0.4482	0.48	0.2843	2	0.0085
0.18	0.4409	0.5	0.2733	2.2	0.0058
0.2	0.4329	0.55	0.2466	2.4	0.0040
0.22	0.4243	0.6	0.2214	2.6	0.0028
0.24	0.4151	0.65	0.1978	2.8	0.0021
0.26	0.4054	0.7	0.1762	3	0.0015
0.28	0.3954	0.75	0.1565	4	0.0004
0.3	0.3849	0.8	0.1386	5	0.0001

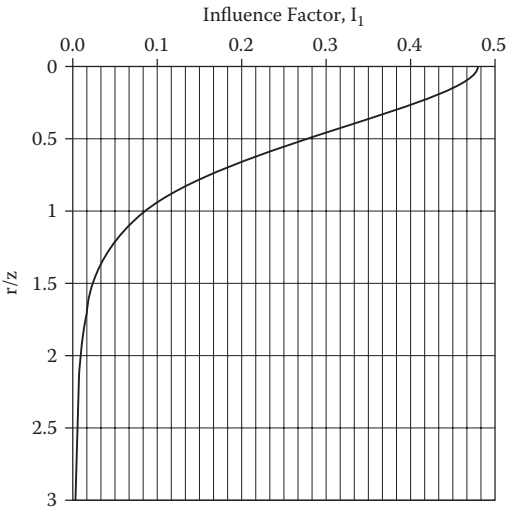

FIGURE 8.4 Influence factor, I_1 versus r/z (point load).

The vertical stress increment under radius r from the loading point is given by

$$\Delta\sigma_v = \frac{3}{2\pi}\frac{P}{z^2}\cos^5\theta = \frac{3Pz^3}{2\pi\left(r^2+z^2\right)^{5/2}} = \frac{P}{z^2}\frac{3}{2\pi}\frac{1}{\left[1+\left(r/z\right)^2\right]^{5/2}} = \frac{P}{z^2}I_1 \tag{8.2}$$

$$I_1 = \frac{3}{2\pi}\frac{1}{\left[1+\left(r/z\right)^2\right]^{5/2}} \tag{8.3}$$

where I_1 is called the **influence factor** for stress increment computation, and R, r, z, and θ are defined in Figure 8.3. I_1 is a sole function of r/z ratio, and the values are tabulated in Table 8.2 and plotted in Figure 8.4.

Exercise 8.2

A 5 kN point load is applied on the ground surface. Compute and plot the magnitudes of vertical stress increment, (a) under the point load at the depth z from 0 m to 10 m below the ground surface, and (b) under 1.0 m off from the load application point at the same depth as above. Use Boussinesq's method.

Solution:

(a) r/z = 0 and I_1 = 0.4775 is obtained from Equation 8.3 or Table 8.2.
(b) r = 1 m, and thus r/z varies with depth.

TABLE 8.3
$\Delta\sigma_v$ Computation under a Point Load

A	B	C	D	E	A	B	C	D	E
(1) r = 0 m					(2) r = 1 m				
z, m	r, m	r/z	I_1	$\Delta\sigma_v$	z, m	r, m	r/z	I_1	$\Delta\sigma_v$
0	0	0	0.4775	∞	0	1	∞	0	0
0.3	0	0	0.4775	26.53	0.3	1	3.33	0.0009	0.05
0.5	0	0	0.4775	9.55	0.5	1	2.00	0.0085	0.17
1	0	0	0.4775	2.39	1	1	1.00	0.0844	0.42
2	0	0	0.4775	0.60	2	1	0.50	0.2733	0.34
4	0	0	0.4775	0.15	4	1	0.25	0.4103	0.13
6	0	0	0.4775	0.07	6	1	0.17	0.4459	0.06
8	0	0	0.4775	0.04	8	1	0.13	0.4593	0.04
10	0	0	0.4775	0.02	10	1	0.10	0.4657	0.02

Note: Column $E_i = P/z^2 \times D_i$ (Equation 8.2)

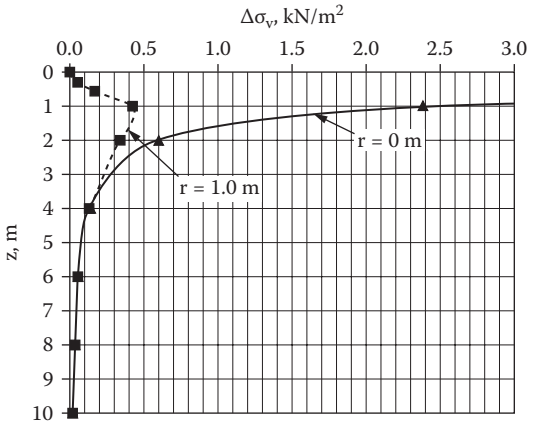

FIGURE 8.5 $\Delta\sigma_v$ distributions under a point load (Exercise 8.2).

A spreadsheet (Table 8.3) is created for the computation, and the results are plotted in Figure 8.5. Note that Equation 8.2 gives the infinitive $\Delta\sigma_v$ value directly underneath the point load (that is, r = 0 and z = 0) as a special case. When distance r takes a non-zero value, $\Delta\sigma_v$ value becomes zero at z = 0 as seen in Case (b).

8.4 VERTICAL STRESS INCREMENT DUE TO A LINE LOAD

The rest of the solutions are all from the integrations of Boussinesq's point load solution (Equation 8.2) over the area (or line) where the load is applied on the ground surface. As seen in Figure 8.6, line load q is applied on an infinitively long line on

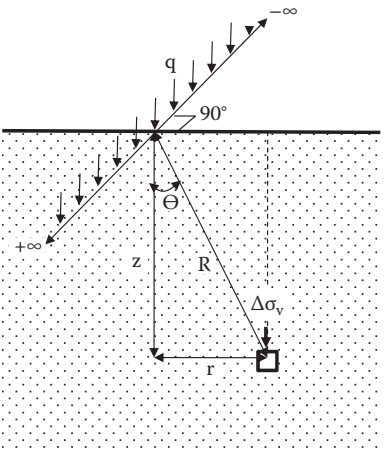

FIGURE 8.6 Vertical stress increment due to a line load.

TABLE 8.4
Influence Factor I_2 by Equation 8.5 (Line Load)

r/z	I_2	r/z	I_2	r/z	I_2
0	0.637	1.1	0.130	2.2	0.019
0.1	0.624	1.2	0.107	2.4	0.014
0.2	0.589	1.3	0.088	2.6	0.011
0.3	0.536	1.4	0.073	2.8	0.008
0.4	0.473	1.5	0.060	3	0.006
0.5	0.407	1.6	0.050	3.2	0.005
0.6	0.344	1.7	0.042	3.4	0.004
0.7	0.287	1.8	0.035	3.6	0.003
0.8	0.237	1.9	0.030	3.8	0.003
0.9	0.194	2	0.025	4	0.002
1	0.159			5	0.001

the ground, and $\Delta\sigma_v$ is obtained in a soil mass at (z, r), where distance r is measured perpendicular to the line of load. Integration of Equation 8.2 over a loaded line from $-\infty$ to $+\infty$ gives:

$$\Delta\sigma_v = \frac{2qz^3}{\pi R^4} = \frac{2q}{\pi z\left[\left(r/z\right)^2+1\right]^2} = \frac{q}{z}\frac{2}{\pi\left[\left(r/z\right)^2+1\right]^2} = \frac{q}{z}I_2 \tag{8.4}$$

$$I_2 = \frac{2}{\pi\left[\left(r/z\right)^2+1\right]^2} \tag{8.5}$$

Table 8.4 tabulates influence factor I_2 as a function of r/z.

8.5 VERTICAL STRESS INCREMENT DUE TO A STRIP LOAD

Uniformly distributed strip load q is applied on the ground with footing width B as seen in Figure 8.7. $\Delta\sigma_v$ at point (x, z) can be obtained by an integration of Equation 8.2 over x from –B/2 to +B/2 and y from $-\infty$ to $+\infty$.

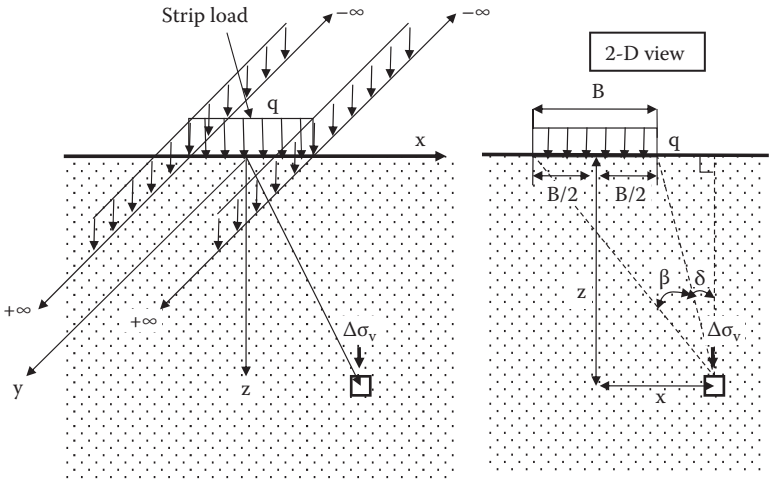

FIGURE 8.7 Vertical stress increment due to a strip load.

The integrated solution is given by:

$$\Delta\sigma_v = \frac{q}{\pi}\left[\beta + \sin\beta\cos(\beta + 2\delta)\right]$$

$$= \frac{q}{\pi}\left\{\left[\tan^{-1}\left(\frac{\frac{2z}{B}}{\frac{2x}{B}-1}\right) - \tan^{-1}\left(\frac{\frac{2z}{B}}{\frac{2x}{B}+1}\right)\right] - \frac{\frac{2z}{B}\left[\left(\frac{2x}{B}\right)^2 - \left(\frac{2z}{B}\right)^2 - 1\right]}{2\left[\frac{1}{4}\left\{\left(\frac{2x}{B}\right)^2 + \left(\frac{2z}{B}\right)^2 - 1\right\}^2 + \left(\frac{2z}{B}\right)^2\right]}\right\}$$

$$= q\, I_3 \tag{8.6}$$

Note that in Equation 8.6, when 2x/B<1 (point (x, z) is inside the foundation width B), the value in the first term of the second line becomes negative. To get the correct angle value in that case, π shall be added to it. That is, the first term of the second line of Equation 8.6 shall be replaced by:

$$\text{For } 2x/B<1,\ \tan^{-1}\left(\frac{\frac{2z}{B}}{\frac{2x}{B}-1}\right) + \pi \tag{8.7}$$

Table 8.5 shows the values of I_3 as function of 2x/B and 2z/B and Figure 8.8 plots those values near the footing.

TABLE 8.5
Influence factor I_3 by Eq. 8.6 (strip load)

	2x/B											
2z/B	**0**	**0.2**	**0.4**	**0.6**	**0.8**	**1**	**1.25**	**1.5**	**2**	**3**	**5**	**10**
0	1	1	1	1	1	0.5	0	0	0	0	0	0
0.1	1.000	0.999	0.999	0.997	0.980	0.500	0.011	0.002	0.000	0.000	0.000	0.000
0.2	0.997	0.996	0.992	0.979	0.909	0.500	0.059	0.011	0.002	0.000	0.000	0.000
0.4	0.977	0.973	0.955	0.906	0.773	0.498	0.178	0.059	0.011	0.001	0.000	0.000
0.6	0.937	0.928	0.896	0.825	0.691	0.495	0.258	0.120	0.030	0.004	0.000	0.000
0.8	0.881	0.869	0.829	0.755	0.638	0.489	0.305	0.173	0.056	0.010	0.001	0.000
1	0.818	0.805	0.766	0.696	0.598	0.480	0.332	0.214	0.084	0.017	0.002	0.000
1.2	0.755	0.743	0.707	0.646	0.564	0.468	0.347	0.243	0.111	0.026	0.004	0.000
1.4	0.696	0.685	0.653	0.602	0.534	0.455	0.354	0.263	0.135	0.037	0.005	0.000
1.6	0.642	0.633	0.605	0.562	0.506	0.440	0.356	0.276	0.155	0.048	0.008	0.001
1.8	0.593	0.585	0.563	0.526	0.479	0.425	0.353	0.284	0.172	0.060	0.010	0.001
2	0.550	0.543	0.524	0.494	0.455	0.409	0.348	0.288	0.185	0.071	0.013	0.001
2.5	0.462	0.458	0.445	0.426	0.400	0.370	0.328	0.285	0.205	0.095	0.022	0.002
3	0.396	0.393	0.385	0.372	0.355	0.334	0.305	0.274	0.211	0.114	0.032	0.003
3.5	0.345	0.343	0.338	0.329	0.317	0.302	0.281	0.258	0.210	0.127	0.042	0.004
4	0.306	0.304	0.301	0.294	0.285	0.275	0.259	0.242	0.205	0.134	0.051	0.006
5	0.248	0.247	0.245	0.242	0.237	0.231	0.222	0.212	0.188	0.139	0.065	0.010
6	0.208	0.208	0.207	0.205	0.202	0.198	0.192	0.186	0.171	0.136	0.075	0.015
8	0.158	0.157	0.157	0.156	0.155	0.153	0.150	0.147	0.140	0.122	0.083	0.025
10	0.126	0.126	0.126	0.126	0.125	0.124	0.123	0.121	0.117	0.107	0.082	0.032
15	0.085	0.085	0.085	0.084	0.084	0.084	0.083	0.083	0.082	0.078	0.069	0.041
20	0.064	0.064	0.064	0.063	0.063	0.063	0.063	0.063	0.062	0.061	0.056	0.041
50	0.025	0.025	0.025	0.025	0.025	0.025	0.025	0.025	0.025	0.025	0.025	0.024
100	0.013	0.013	0.013	0.013	0.013	0.013	0.013	0.013	0.013	0.013	0.013	0.012

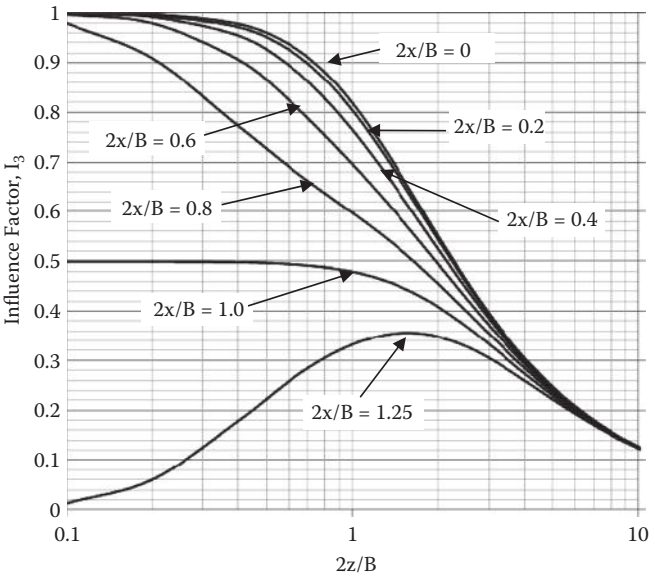

FIGURE 8.8 Influence factor I_3.

Exercise 8.3

A strip load q = 100 kN/m^2 is applied over a footing with width B = 5 m. Calculate and plot the vertical stress distribution over the x distance at z = 5 m and at z = 10 m under the footing.

TABLE 8.6
Computation for Exercise 8.3

At z = 5 m, 2z/B = 2

x, m	0	0.5	1	2	2.5	3.125	3.75	5	7.5	12.5
2x/B	0	0.2	0.4	0.8	1	1.25	1.5	2	3	5
I_3	0.550	0.543	0.524	0.455	0.409	0.348	0.288	0.185	0.071	0.013
$\Delta\sigma_v$, kN/m^2	55.0	54.3	52.4	45.5	40.9	34.8	28.8	18.5	7.1	1.3

At z = 10 m, 2z/B = 4

x, m	0	0.5	1	2	2.5	3.125	3.75	5	7.5	12.5
2x/B	0	0.2	0.4	0.8	1	1.25	1.5	2	3	5
I_3	0.306	0.304	0.301	0.285	0.275	0.259	0.242	0.205	0.134	0.051
$\Delta\sigma_v$, kN/m^2	30.6	30.4	30.1	28.5	27.5	25.9	24.2	20.5	13.4	5.1

Note: I_3 is from Table 8.5; $\Delta\sigma_v = q \times I_3$.

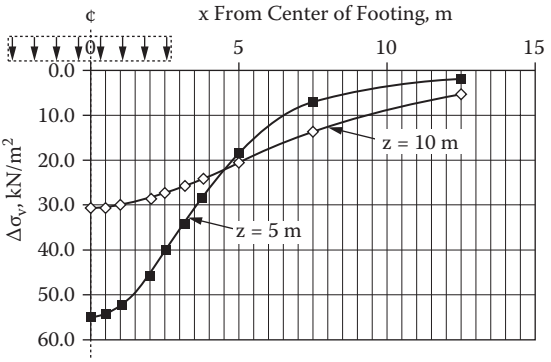

FIGURE 8.9 Solution for Exercise 8.3.

Solution:

at z = 5 m, 2z/B = 2 × 5/5 = 2.

at z = 10 m, 2z/B = 2 × 10/5 = 4

For the above 2z/B values, I_3 values were read from Table 8.5 and $\Delta\sigma_v$ values were computed in Table 8.6 for various x values. The result are plotted in Figure 8.9 for a half space (x>0 region).

8.6 VERTICAL STRESS INCREMENT UNDER A CIRCULAR FOOTING

A popular footing shape is circular one, and Boussinesq's solution is integrated for a uniformly loaded circular area as seen in Figure 8.10. Equation 8.8 is the solution for $\Delta\sigma_v$ directly under the center of circular footing.

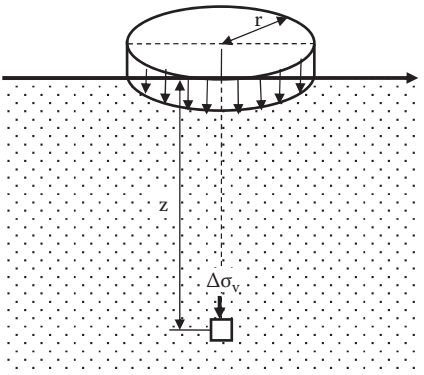

FIGURE 8.10 $\Delta\sigma_v$ under the center of circular footing.

TABLE 8.7
Influence Factor I_4 by Equation 8.9 (Circular Load)

z/r	I_4	z/r	I_4
0	1.000	1.2	0.547
0.1	0.999	1.4	0.461
0.2	0.992	1.6	0.390
0.3	0.976	1.8	0.332
0.4	0.949	2	0.284
0.5	0.911	2.5	0.200
0.6	0.864	3	0.146
0.7	0.811	3.5	0.111
0.8	0.756	4	0.087
0.9	0.701	4.5	0.070
1	0.646	5	0.057

$$\Delta\sigma_v = q\left[1 - \frac{1}{\left[\left(r/z\right)^2 + 1\right]^{3/2}}\right] = q\, I_4 \tag{8.8}$$

$$I_4 = 1 - \frac{1}{\left[\left(r/z\right)^2 + 1\right]^{3/2}} \tag{8.9}$$

I_4 values are tabulated in Table 8.7 and plotted in Figure 8.11 as a function of z/r.

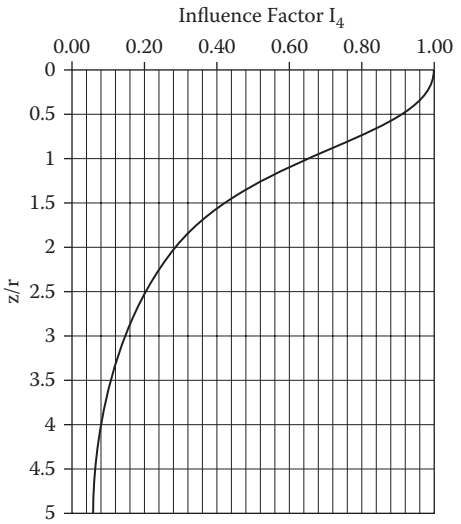

FIGURE 8.11 Influence factor I_4.

8.7 VERTICAL STRESS INCREMENT UNDER AN EMBANKMENT LOAD

Another frequently encountered loading pattern is due to embankments. Figure 8.12 shows a half section of embankment load. The integrated solution is given by:

$$\Delta\sigma_v = \frac{q}{\pi}\left[\frac{B_1 + B_2}{B_1}(\alpha_1 + \alpha_2) - \frac{B_2}{B_1}\alpha_2\right] = q\, I_5 \tag{8.10}$$

$$I_5 = \frac{1}{\pi}\left[\frac{B_1 + B_2}{B_1}(\alpha_1 + \alpha_2) - \frac{B_2}{B_1}\alpha_2\right] \tag{8.11}$$

$$\alpha_1 = \tan^{-1}\left(\frac{B_1 + B_2}{z}\right) - \tan^{-1}\left(\frac{B_2}{z}\right) \tag{8.12}$$

$$\alpha_2 = \tan^{-1}\left(\frac{B_2}{z}\right) \tag{8.13}$$

Table 8.8 shows influence factor I_5 as function of B_1/z and B_2/z and Figure 8.13 plots the results. This is a convenient solution to obtain the stress increment under embankments by using a superposition of solutions as demonstrated in Exercise 8.4. Since the Boussinesq's solution is for an elastic media, the **principle of superposition** of several independent solutions is perfectly legitimate.

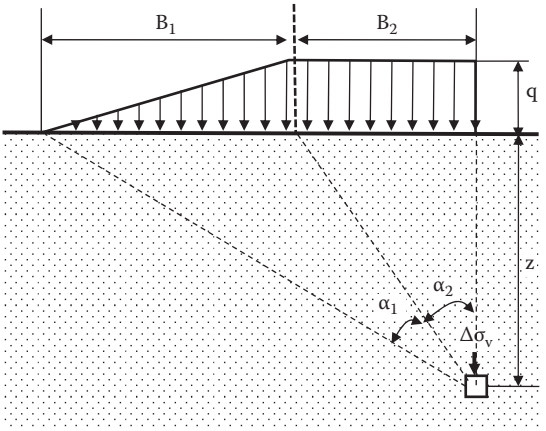

FIGURE 8.12 Vertical stress increment under a half embankment load.

TABLE 8.8
Influence Factor I_5 by Equation 8.11 (Half Embankment Load)

	B_1/z														
B_2/z	**0.01**	**0.02**	**0.04**	**0.06**	**0.1**	**0.2**	**0.4**	**0.6**	**0.8**	**1**	**2**	**4**	**6**	**8**	**10**
0	0.003	0.006	0.013	0.019	0.032	0.063	0.121	0.172	0.215	0.250	0.352	0.422	0.447	0.460	0.468
0.1	0.066	0.069	0.076	0.082	0.094	0.123	0.176	0.221	0.258	0.288	0.375	0.434	0.455	0.466	0.473
0.2	0.127	0.130	0.136	0.141	0.153	0.179	0.227	0.265	0.297	0.322	0.394	0.444	0.462	0.471	0.477
0.3	0.183	0.186	0.191	0.196	0.206	0.230	0.271	0.303	0.330	0.351	0.411	0.452	0.468	0.476	0.480
0.4	0.233	0.235	0.240	0.245	0.253	0.274	0.308	0.336	0.358	0.375	0.425	0.459	0.472	0.479	0.483
0.5	0.277	0.279	0.283	0.287	0.294	0.311	0.340	0.363	0.381	0.395	0.437	0.466	0.477	0.482	0.486
0.6	0.314	0.316	0.319	0.322	0.329	0.343	0.367	0.386	0.400	0.412	0.446	0.471	0.480	0.485	0.488
0.7	0.345	0.347	0.349	0.352	0.357	0.369	0.389	0.404	0.416	0.426	0.454	0.475	0.483	0.487	0.489
0.8	0.371	0.372	0.375	0.377	0.381	0.391	0.407	0.419	0.429	0.437	0.461	0.478	0.485	0.489	0.491
0.9	0.392	0.393	0.395	0.397	0.401	0.408	0.422	0.432	0.440	0.447	0.467	0.481	0.487	0.490	0.492
1	0.410	0.411	0.412	0.414	0.416	0.423	0.434	0.442	0.449	0.455	0.471	0.484	0.489	0.491	0.493
1.2	0.436	0.436	0.437	0.438	0.440	0.445	0.452	0.458	0.463	0.466	0.478	0.488	0.491	0.493	0.495
1.4	0.453	0.454	0.454	0.455	0.456	0.459	0.464	0.469	0.472	0.475	0.483	0.490	0.493	0.495	0.496
1.6	0.465	0.466	0.466	0.467	0.467	0.470	0.473	0.476	0.478	0.480	0.487	0.492	0.495	0.496	0.497
1.8	0.474	0.474	0.474	0.475	0.475	0.477	0.479	0.481	0.483	0.485	0.489	0.494	0.496	0.497	0.497
2	0.480	0.480	0.480	0.480	0.481	0.482	0.484	0.485	0.487	0.488	0.491	0.495	0.496	0.497	0.498
3	0.493	0.493	0.493	0.493	0.493	0.494	0.494	0.494	0.495	0.495	0.496	0.498	0.498	0.499	0.499
5	0.498	0.498	0.498	0.498	0.498	0.498	0.498	0.498	0.499	0.499	0.499	0.499	0.499	0.499	0.499

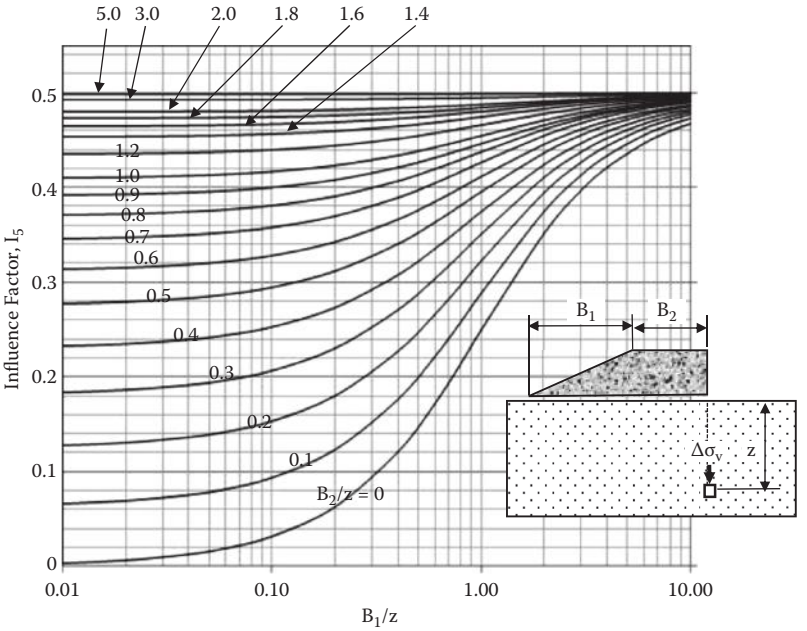

FIGURE 8.13 Influence factor I_5.

Exercise 8.4

An embankment as seen in Figure 8.14 is constructed. Determine $\Delta\sigma_v$ at z = 12 m below the ground surface: (a) directly below the centerline of the embankment, and (b) directly under the toe of the embankment. Use the total unit weight of embankment as $\gamma_t = 19.5$ kN/m^3.

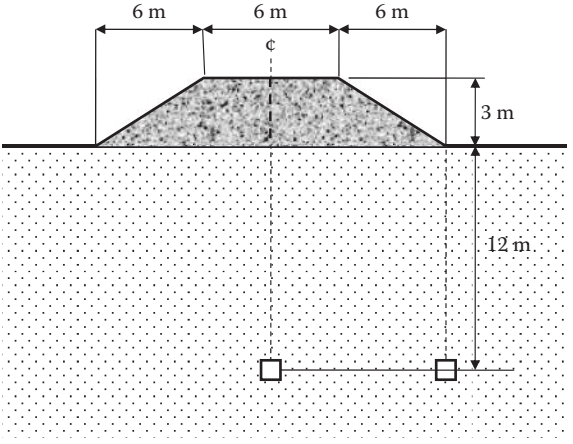

FIGURE 8.14 Exercise 8.4 problem.

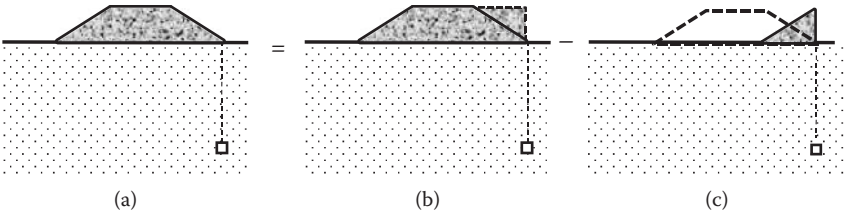

FIGURE 8.15 Superposition to solve Exercise 8.4 (2).

Solution:

$$q = \gamma_t H = 19.5 \times 3 = 58.5 \text{ kN/m}^2.$$

(a) Under the center, the solution is obtained by a superposition of two equal half embankments. For each half embankment,
$B_1 = 6$ m and $B_2 = 3$ m
$B_1/z = 6/12 = 0.5$, $B_2/z = 3/12 = 0.25$
From Figure 8.13, $I_5 = 0.268$ is read.
From Equation 8.10,

$$\Delta\sigma_v = 2 \times q \times I_5 = 2 \times 58.5 \times 0.268 = \mathbf{31.36\ kN/m^2} \leftarrow$$

(b) Under the toe of the embankment, the following superposition is made. That is, (a) = (b) – (c) in Figure 8.15.
For Figure 8.15 (b), $B_1 = 6$ m, $B_2 = 12$ m
$B_1/z = 6/12 = 0.5$, $B_2/z = 12/12 = 1.0$
From Table 8.8, $I_5 = 0.438$ is obtained.
For Figure 8.15 (c), $B_1 = 6$ m, $B_2 = 0$ m
$B_1/z = 6/12 = 0.5$, $B_2/z = 0/12 = 0$
From Figure 8.13, $I_5 = 0.148$ is read.
From Equation 8.10 and superposition of two figures (i.e., (b) – (c)),

$$\Delta\sigma_v = q \times (I_5\ (b) - I_5\ (c)) = 58.5 \times (0.438 - 0.148) = \mathbf{16.97\ kN/m^2} \leftarrow$$

8.8 VERTICAL STRESS INCREMENT UNDER CORNER OF RECTANGULAR FOOTING

Newmark (1935) integrated Boussinesq's equation over a rectangular loading area (Figure 8.16), and the solution under a corner of the footing is given by:

$$\Delta\sigma_v = q\, I_6 \tag{8.14}$$

$$I_6 = \frac{1}{4\pi}\left[\frac{2mn\sqrt{m^2+n^2+1}}{m^2+n^2+m^2n^2+1} \bullet \frac{m^2+n^2+2}{m^2+n^2+1} + \tan^{-1}\left(\frac{2mn\sqrt{m^2+n^2+1}}{m^2+n^2-m^2n^2+1}\right)\right] \tag{8.15}$$

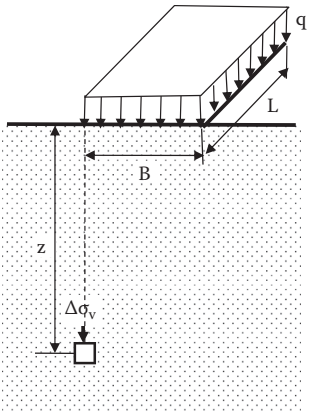

FIGURE 8.16 $\Delta\sigma_v$ under the corner of rectangular footing.

where m = B/z and n = L/z.

Note that when $\tan^{-1}$ (**) term in Equation 8.15 becomes negative, π shall be added to that term to obtain the correct I_6 values.

B and L (or m and n) are exchangeable parameters so that B or L could be assigned for either side of a footing. Table 8.9 and Figure 8.17 show I_6 values as function of m and n.

The solution in Equation 8.14 is the one under a corner of rectangular footing. However, the solution can be used to compute $\Delta\sigma_v$ under any point of rectangular footing using the **principle of superposition**. Figure 8.18 shows $\Delta\sigma_v$ computations under various points of footings and real loaded footing areas are shown with darker color and imaginary footing sections are drawn with dotted lines. Case (a) is under a corner of a footing, Case (b) is under a midpoint of footing, and Case (c) and Case (d) are under outsides of footing. By bringing the point of computation to a corner of footing, including imaginary sections, the following procedures are used.

Case (a): Loaded area = I, Equation 8.14 is directly used.

Case (b): Loaded areas = I + II + II + IV,

$$\Delta\sigma_v\,(I + II + III + IV) = \Delta\sigma_v\,(I) + \Delta\sigma_v\,(II) + \Delta\sigma_v\,(III) + \Delta\sigma_v\,(IV)$$

Case (c): Loaded areas = I + II,

$$\Delta\sigma_v\,(I + II) = \Delta\sigma_v\,(I + III) + \Delta\sigma_v\,(II + IV) - \Delta\sigma_v\,(III) - \Delta\sigma_v\,(IV)$$

Case (d): Loaded areas = I,

$$\Delta\sigma_v\,(I) = \Delta\sigma_v\,(I + II + III + IV) - \Delta\sigma_v\,(II + IV) - \Delta\sigma_v\,(III + IV) + \Delta\sigma_v\,(IV)$$

In the above expression, for example, $\Delta\sigma_v$ (I + II) means the stress increment computation due to the combined footing area I and II. In this manner, all computation points are located at the corners of combined or single footings, and Equation 8.14

TABLE. 8.9
Influence Factor I_6 by Equation 8.15 (Under Corner of Rectangular Footing)

	m													
n	**0.1**	**0.2**	**0.3**	**0.4**	**0.5**	**0.6**	**0.7**	**0.8**	**0.9**	**1**	**1.5**	**2**	**5**	**10**
0.1	0.005	0.009	0.013	0.017	0.020	0.022	0.024	0.026	0.027	0.028	0.030	0.031	0.032	0.032
0.2	0.009	0.018	0.026	0.033	0.039	0.043	0.047	0.050	0.053	0.055	0.059	0.061	0.062	0.062
0.3	0.013	0.026	0.037	0.047	0.056	0.063	0.069	0.073	0.077	0.079	0.086	0.089	0.090	0.090
0.4	0.017	0.033	0.047	0.060	0.071	0.080	0.087	0.093	0.098	0.101	0.110	0.113	0.115	0.115
0.5	0.020	0.039	0.056	0.071	0.084	0.095	0.103	0.110	0.116	0.120	0.131	0.135	0.137	0.137
0.6	0.022	0.043	0.063	0.080	0.095	0.107	0.117	0.125	0.131	0.136	0.149	0.153	0.156	0.156
0.7	0.024	0.047	0.069	0.087	0.103	0.117	0.128	0.137	0.144	0.149	0.164	0.169	0.172	0.172
0.8	0.026	0.050	0.073	0.093	0.110	0.125	0.137	0.146	0.154	0.160	0.176	0.181	0.185	0.185
0.9	0.027	0.053	0.077	0.098	0.116	0.131	0.144	0.154	0.162	0.168	0.186	0.192	0.196	0.196
1	0.028	0.055	0.079	0.101	0.120	0.136	0.149	0.160	0.168	0.175	0.194	0.200	0.204	0.205
1.5	0.030	0.059	0.086	0.110	0.131	0.149	0.164	0.176	0.186	0.194	0.216	0.224	0.230	0.230
2	0.031	0.061	0.089	0.113	0.135	0.153	0.169	0.181	0.192	0.200	0.224	0.232	0.240	0.240
5	0.032	0.062	0.090	0.115	0.137	0.156	0.172	0.185	0.196	0.204	0.230	0.240	0.249	0.249
10	0.032	0.062	0.090	0.115	0.137	0.156	0.172	0.185	0.196	0.205	0.230	0.240	0.249	0.250

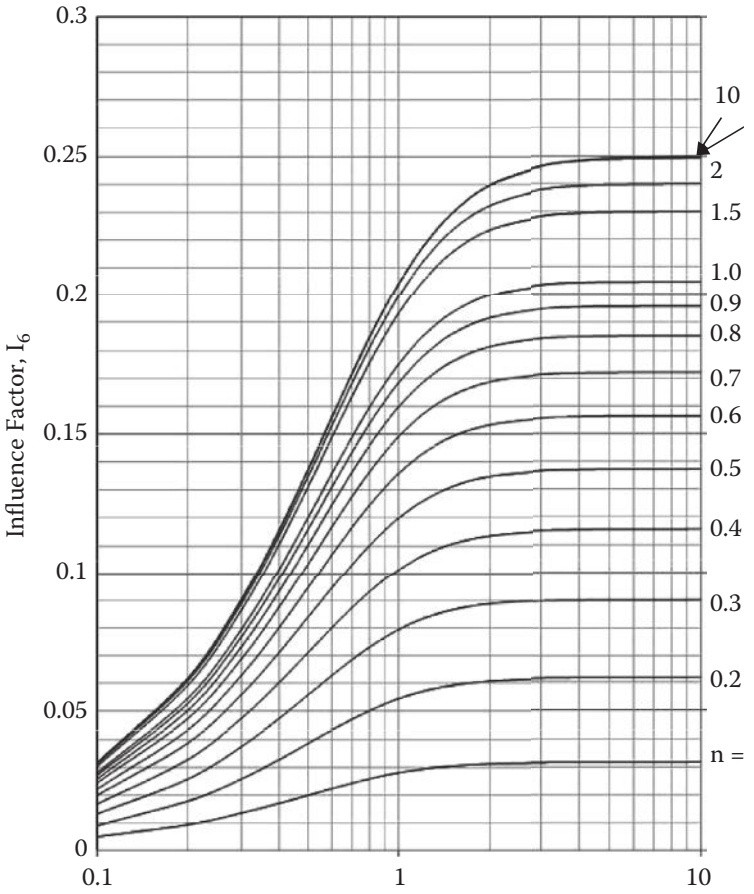

FIGURE 8.17 Influence factor $I_{6.}$

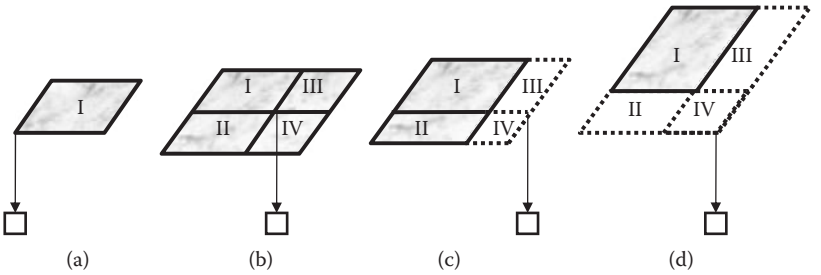

FIGURE 8.18 $\Delta\sigma_v$ computations under various points of footings.

is applicable. In Case (d), the footing IV is included in the footings (II + IV) and (III + IV) and subtracted twice. Thus, $\Delta\sigma_v$ (IV) is added once. Note that for each real or imaginary footing, B and L values are different, and different I_6 values shall be obtained for all those footings.

Exercise 8.5

A loaded footing ABCD with q = 200 kN/m^2 on the ground is shown in Figure 8.19. Compute $\Delta\sigma_v$ under Points E, F, B and G at depth 5 m.

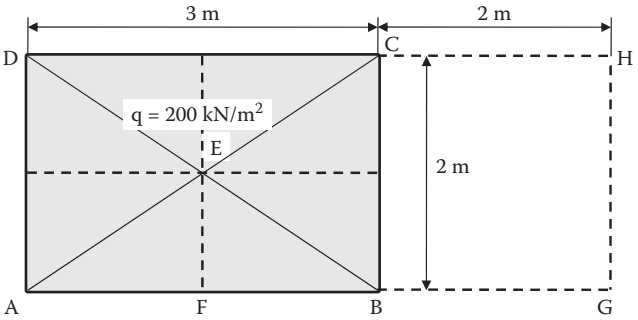

FIGURE 8.19 Exercise 8.5 problem.

Solution:

1. At Point E, there are four equal footings for which Point E corners.
   B = 1.5 m and L = 1 m, thus m = B/z = 1.5/5 = 0.3 and n = L/z = 1/5 = 0.2,
   From Figure 8.16, I_6 = 0.026
   From Equation 8.14, $\Delta\sigma_v = 4 \times q\, I_6 = 4 \times 200 \times 0.026 =$ **20.8 kN/m^2** ←

2. At Point F, there are two equal footings for which Point F corners.
   B = 1.5 m and L = 2 m, thus m = B/z = 1.5/5 = 0.3 and n = L/z = 2/5 = 0.4,
   From Figure 8.16, I_6 = 0.047
   From Equation 8.14, $\Delta\sigma_v = 2 \times q\, I_6 = 2 \times 200 \times 0.047 =$ **18.8 kN/m^2** ←

3. At Point B, Point B is directly under a corner of footing.
   B = 3 m and L = 2 m, thus m = B/z = 3/5 = 0.6 and n = L/z = 2/5 = 0.4,
   From Figure 8.16, I_6 = 0.080
   From Equation 8.14, $\Delta\sigma_v = q\, I_6 = 200 \times 0.08 =$ **16.0 kN/m^2** ←

4. At Point G, there are two imaginary footings (AGHD and BGHC), at both of which Point G corners.
   For AGHD, B = 5 m and L = 2 m, thus m = B/z = 5/5 = 1.0 and
   n = L/z = 2/5 = 0.4,

From Figure 8.16, $I_6 = 0.101$
For BGHC, B = 2 m and L = 2 m, thus m = B/z = 2/5 = 0.4 and n = L/z = 2/5 = 0.4,
From Figure 8.16, I_6=0.060
From Equation 8.14, $\Delta\sigma_v$ (ABCD) = $\Delta\sigma_v$ (AGHD) − $\Delta\sigma_v$ (BGHC) = q Σ I_6
= 200 × (0.101 − 0.060) = **8.2 kN/m²** ←

8.9 VERTICAL STRESS INCREMENT UNDER IRREGULARLY SHAPED FOOTING

Newmark (1942) developed an innovative chart to compute vertical stress increment due to any irregularly shaped footing on the ground. The chart is called the **Newmark's influence chart**.

Based on integration of Boussinesq's point load equation (Equation 8.2), special co-centered circles are constructed as illustrated in Figure 8.20 so that when segments in the circles, which are bordered by two adjacent circles (i.e., A_1, A_2, A_3 …,), are loaded with a same uniform pressure q on the ground, the vertical stress increments $\Delta\sigma_v$ at a depth z under the center of the circles are the same. In other words, all the segmented areas have the same level of influence to induce the vertical stress under the center point in soil mass.

The co-centered circles are further divided equally in their radial direction. Figure 8.21 shows an influence chart, in which above constructed circles are equally divided into 20 (18° each). All the elements in the chart, when equally loaded, induce

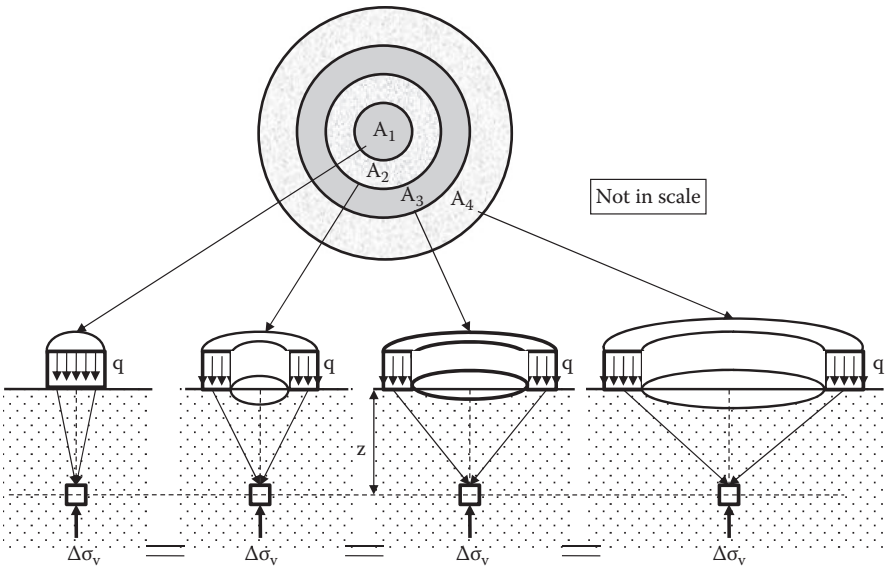

FIGURE 8.20 Construction of Newmark's influence chart.

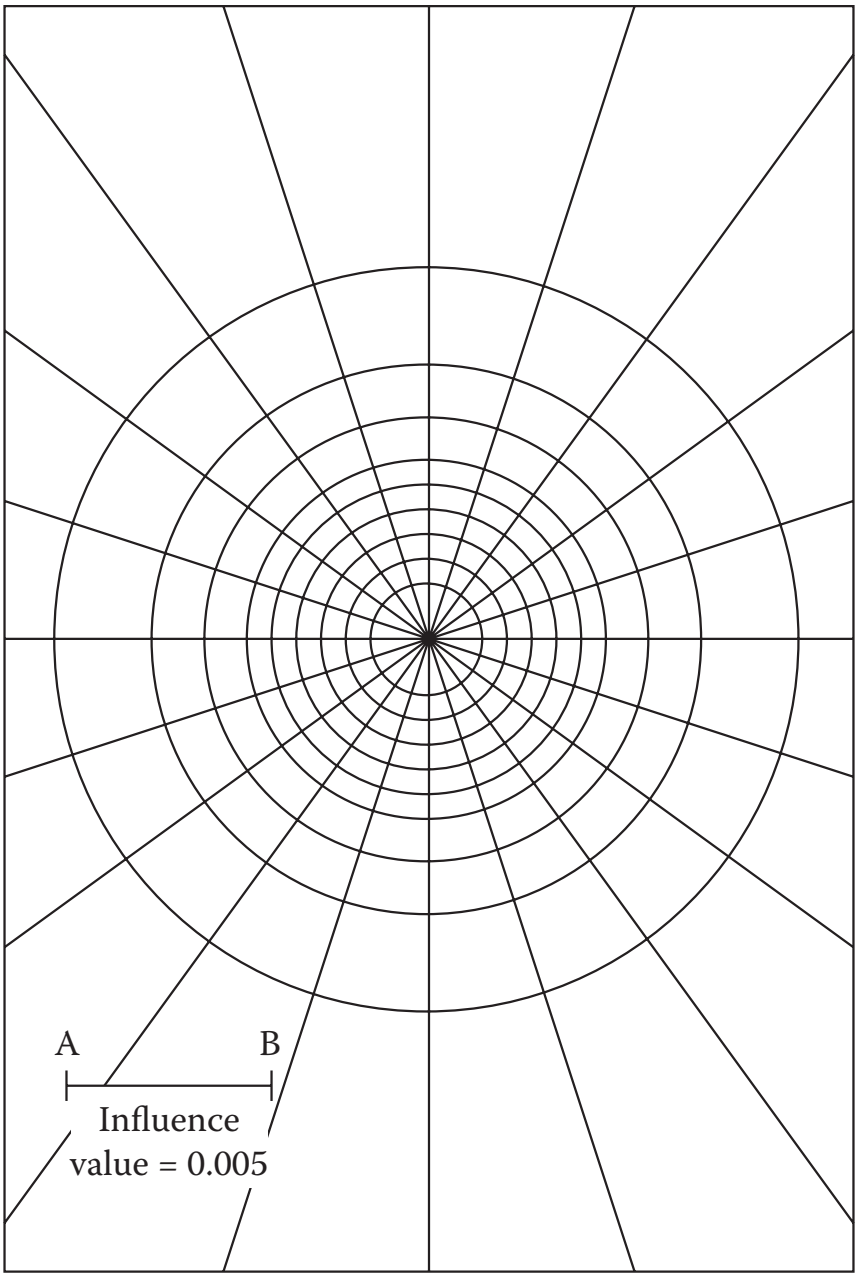

FIGURE 8.21 Influence chart. (After Newmark, N. M. [1942].)

the same vertical stress increments under the center of the circles. It can be seen that elements have smaller areas near the center and have larger areas far from the center.

An influence chart shall have its own influence value (0.005 in Figure 8.21) and fixed scale (AB in Figure 8.21), which are based on the way the chart is constructed using Equation 8.2. Therefore, the values and the scale may be different for different charts.

The following is the procedure on how to obtain a $\Delta\sigma_v$ value for an irregularly shaped footing with a uniform load on the ground by using an influence chart:

1. Determine the depth z at which $\Delta\sigma_v$ is calculated.
2. Determine the point under which $\Delta\sigma_v$ is calculated.
3. Draw the shape of footing on the chart ***with a scale of z equal to the fixed scale AB, and bring the point of stress computation (Step (2) above) to the center of the chart***.
4. Count the number of elements, which are covered by the drawn footing shape. The number of fully covered elements, N_{full}, and the number of partially covered elements, $N_{partial}$, are counted and the number of full equivalent elements N can be calculated as $N_{full} + \frac{1}{2}N_{partial}$.
5. Vertical stress increment $\Delta\sigma_v$ is then computed by

$$\Delta\sigma_v = q\ N\ (I.V.) \tag{8.16}$$

where

q: load intensity on the footing
N: Number of full equivalent elements, which are covered by the footing
I.V.: **Influence value** of the chart

Exercise 8.6

A footing shape is shown in Figure 8.22 and a uniform load q = 200 kN/m^2 is loaded on the footing. Compute $\Delta\sigma_v$ under Point A at depth z = 20 m.

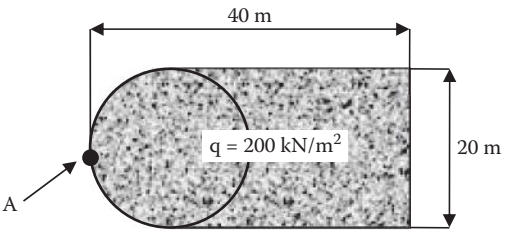

FIGURE 8.22 Uniformly loaded footing for Exercise 8.6.

Solution:

On an influence chart, the given footing shape is drawn with AB = z = 20 m and with Point A at the center of the chart as in Figure 8.23.

$N_{full} = 32$, and $N_{partial} = 22$ are obtained from Figure 8.23.
$N = N_{full} + \frac{1}{2}N_{partial} = 32 + \frac{1}{2}(22) = 43$
From Equation 8.16,
$\Delta\sigma_v = q\,N\,(I.V.) = 200 \times 43 \times 0.005 =$ **43 kN/m²** ←

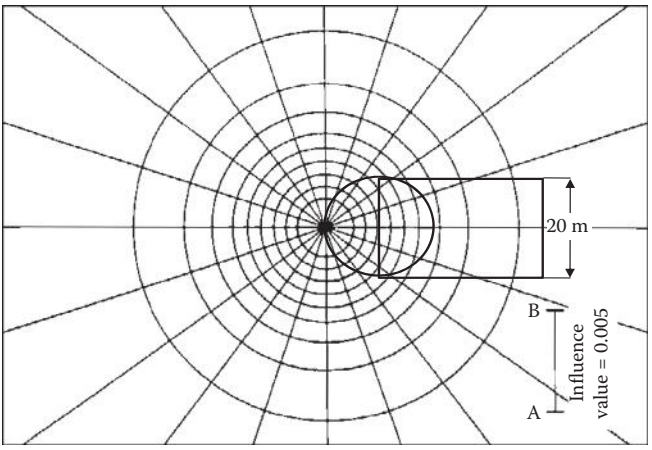

FIGURE 8.23 Solution for Exercise 8.6.

8.10 SUMMARY

The calculation of the incremental stresses $\Delta\sigma_v$ described in this chapter is the one to use for determining the future settlement of soil masses. Chapter 9 fully utilizes the equations of this chapter. Note that the solutions presented in this chapter are mostly based on the Boussinesq's elastic solution. Since it is the elastic solution, the **principle of superposition** is valid and thus any combination of the solutions is possible for rather complicated loading patterns on the ground surface.

REFERENCES

Boussinesq, J. (1885), Application des Potentiels á L'Étude de L'Équilibre et due Mouvement des Solides Élastiques, Gauthier-Villars, Paris.

Newmark, N. M. (1935), Simplified Computation of Vertical Pressures in Elastic Foundations, Circular 24, University of Illinois Engineering Experiment Station.

Newmark, N. M. (1942), Influence Chart for Computation of Stresses in Elastic Soil, Bulletin No. 338, University of Illinois Engineering Experiment Station.

Problems

8.1. A 10 kN point load is applied at the center of 1.5 m × 2 m square footing on the ground surface. By using the 2:1 slope method, compute the vertical stress increments under the footing at z = 0 to 10 m with 2 m depth intervals. Plot the results with the depth z.

8.2. 100 kN and 120 kN point loads are applied on the ground surface as seen in the figure. Compute the vertical stress increment under Point A down to the depth z = 20 m. Plot the results with the depth z.

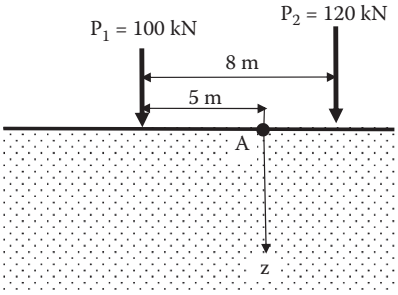

8.3. 50 kN, 100 kN and 150 kN point loads are applied at Points A, B, and C , respectively, on the ground surface as seen in the figure. Compute the vertical stress increment under Point D down to the depth z = 20 m. Plot the results with the depth z.

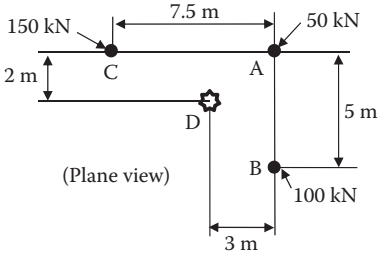

8.4. 50 kN/m and 100 kN/m vertical line loads are applied on the ground surface as shown in the figure. Compute the vertical stress increment under Point A to z = 30 m. Plot the results with the depth z.

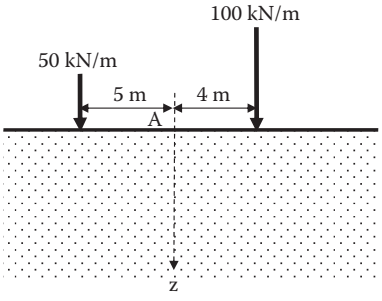

8.5. 100 kN point load and 40 kN/m line load are applied on the ground surface as shown. Compute the variation of the vertical stress increment at the depth z = 5m directly underneath Line AB. Plot the results from Points A to B.

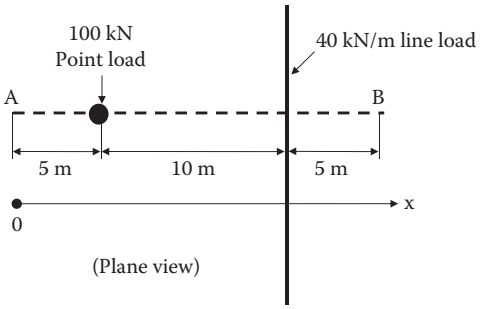

8.6. A 50 kN/m^2 strip load is applied on the ground surface over a 4 m wide strip footing. Compute the variations of the vertical stress increment under the center of the footing. Compute down to z = 20 m and plot the results.

8.7. For Problem 8.6, compute $\Delta\sigma_v$ under the corner of the footing.

8.8. A circular (0.8 m diameter) footing with q = 50 kN/m^2 is placed on the ground surface. Compute and plot the distribution of the vertical stress increment under the center of the footing down to the depth z = 10 m.

8.9. A 100 kN column load is applied on the ground surface. Compute and plot the distributions of the vertical stress increment under the center of the footing with the depth to z = 10 m in the following cases:
(a) 100 kN is applied as a point load.
(b) 100 kN is applied on 2.0 m × 2.0 m square footing (use 2:1 slope method).
(c) 100 kN is applied on 2.257-m-diameter circular footing.
Note that the stress intensity at the footing level for (b) and (c) are the same.

8.10. An embankment shown in the figure is constructed. Compute and plot the distributions of the vertical stress increment, (a) under the center, and (b) under the toe of the embankment down to the depth z =10 m.

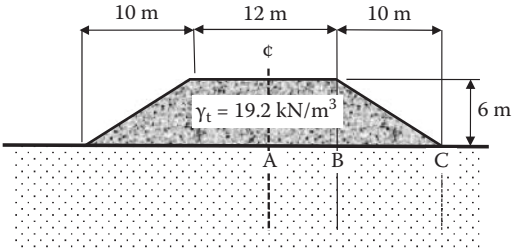

8.11. For the same embankment as in Problem 8.10, compute the vertical stress increment under Points A, B, and C at z = 10 m and plot the results with the horizontal distance from the center of the embankment.

8.12. A rectangular footing is uniformly loaded with q = 75 kN/m^2 as shown in the figure. Compute the vertical stress increments under Points A, B, and C at z = 5 m.

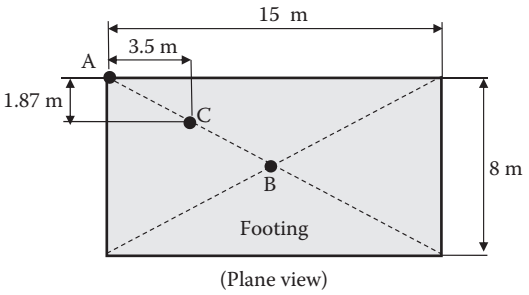

8.13. A footing is uniformly loaded with q = 100 kN/m^2 as shown in the figure. Compute the vertical stress increments under Points A, B, and C at z = 10 m.

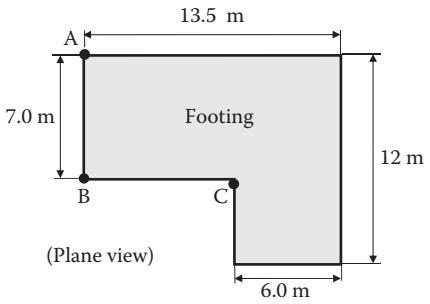

8.14. A circular (1.0 m diameter) footing with q = 80 kN/m^2 is placed on the ground surface. Compute the vertical stress increment under the edge (perimeter) of the footing at the depth z = 1 m. Use Newmark's influence chart.

8.15. An irregular-shaped footing shown in the figure is loaded with 80 kN/m^2 uniform load on the ground. Compute the vertical stress increment under Point A at the depth z = 5 m.

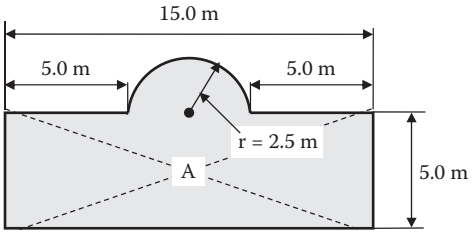

8.16. An irregular-shaped footing shown in the figure is loaded with 60 kN/m^2 uniform load on the ground. Compute the vertical stress increment under Point A at the depth z = 4 m.

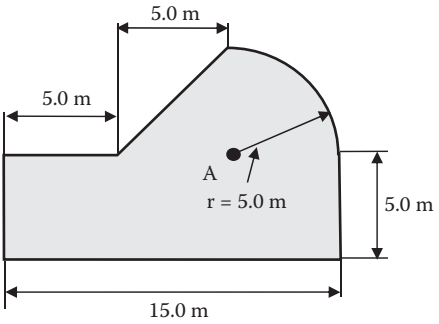

9 Settlements

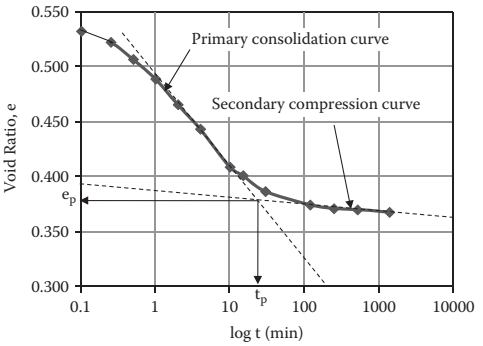

9.1 INTRODUCTION

Soils, in general, are stable if the stress level is maintained or water content remains constant. However, when stresses applied in soil mass are changed, it deforms and causes settlement or swelling in some instances. A major source of stress change is due to the footing load on the ground; Chapter 8 discussed how to estimate those stress increases in various types of foundation loads. Soil behaves, in some degree, as an elastic material and, at the same time, as a plastic material. Thus, upon the increase in stresses, response is elastic and plastic. The elastic response occurs instantaneously, but the plastic response is a time-dependent phenomenon. The former is more dominated in granular soils, and the latter is more in cohesive soils. Instantaneous elastic settlement is termed as **immediate settlement** S_i, and the time-dependent settlements are due to **consolidation** phenomena. The consolidation is also categorized into **primary consolidation** S_c and **secondary compression** S_s as will be discussed later in this chapter. Thus, the **total settlement** S_t due to increased stresses is obtained as a summation of those (that is, $S_t = S_i + S_c + S_s$).

9.2 ELASTIC SETTLEMENTS

For an idealized circular footing on an idealized uniform elastic infinitive half-space soil mass as seen in Figure 9.1, an elastic solution for the surface settlement (***Schleicher 1926***) is given by:

$$S_i = C_d B \left(\frac{1-\mu^2}{E_s} \right) \Delta\sigma \tag{9.1}$$

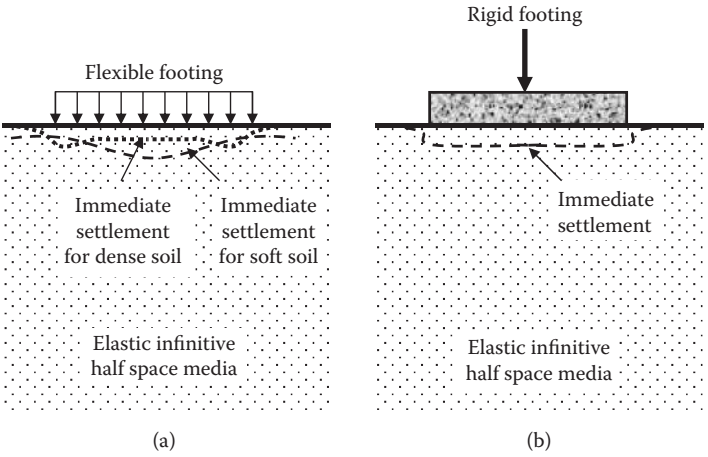

FIGURE 9.1 Flexible and rigid footings on elastic half-space media.

Where B is the footing diameter, μ is the **Poisson's ratio** of soil, E_s is the **modulus of elasticity** of soil, and $\Delta\sigma$ is the applied uniform (or average in case of rigid footing) stress on the footing. C_d is the modification factor to count other shape (rectangular with B × L dimension) of the footing, rigidity of footing, and location of settlement computation, as summarized in Table 9.1.

TABLE 9.1
Modification Factor C_d in Equation 9.2

		Flexible Footing		Rigid Footing
Shape of Footing	**L/B**	**at Center**	**at Corner**	
Circular	—	1.00	0.64	0.79
Rectangular	1 (square)	1.12	0.56	0.99
	1.5	1.36	0.67	1.07
	2	1.52	0.76	1.21
	3	1.78	0.88	1.42
	5	2.10	1.05	1.70
	10	2.53	1.26	2.10
	20	2.99	1.49	2.46
	50	3.57	1.8	3.0
	100	4.00	2	3.43

Source: After Winterkorn, H. F. and Fang, H-Y (1975). *Foundation Engineering Handbook*, Van Nostrand Reinhold, New York.

TABLE 9.2
Ranges of Poisson's Ratios of Soils

Soil Type	Poisson's Ratio, μ
Most clay soils	0.4–0.5
Saturated clay soils	0.45–0.50
Cohesionless—medium and dense	0.3–0.4
Cohesionless—loose to medium	0.2–0.35

Source: After Bowles, J. E. (1996). *Foundation Analysis and Design* (5th ed.), McGraw-Hill, New York.

The ranges of Poisson's ratios and modulus of elasticity of soils are given in Table 9.2, and Table 9.3, respectively.

TABLE 9.3
Ranges of Modulus of Elasticity of Soils

Soil		Modulus of Elasticity, MPa
Clay	Very soft	2–15
	Soft	5–25
	Medium	15–50
	Hard	50–100
	Sandy	25–250
Glacial till	Loose	10–150
	Dense	150–720
	Very dense	500–1440
Loess		15–60
Sand	Silty	5–20
	Loose	10–25
	Dense	50–81
Sand and gravel	Loose	50–150
	Dense	100–200
Shale		150–5000
Silt		2–20

Source: After Bowles, J. E. (1996). *Foundation Analysis and Design* (5th ed.), McGraw-Hill, New York.

Exercise 9.1

A 2 m × 4 m rectangular footing carries 200 kN/m^2 of surface load. Soil underneath the footing is medium-dense sand. Estimate the immediate settlement under the center of the footing in cases of, (a) flexible footing, and (b) rigid footing.

Solution:

From Table 9.2 and Table 9.3, choose μ = 0.3 and E = 40 MPa for medium-dense sandy soil. From Table 9.1, for L/B = 2.0, C_d = 1.52 for case (a), and C_d = 1.21 for case (b). From Equation 9.1,

(a) flexible footing $S_i = 1.52 \times 2 \times \left(\frac{1 - 0.3^2}{40000} \right) \times 200 = 0.0138\,\text{m} = \mathbf{13.8\,mm}$

(b) rigid footing $S_i = 1.21 \times 2 \times \left(\frac{1 - 0.3^2}{40000} \right) \times 200 = 0.0110\,\text{m} = \mathbf{11.0\,mm}$

The solutions make sense that a rigid footing gave a smaller settlement than for a flexible footing under the same footing load.

Equation 9.1 is the solution for footings on the ground surface. In many cases, footings are embedded in a certain depth from the ground surface and, thus, Equation 9.1 would give a rather conservative solution for such cases. Also, an infinitively deep half-space elastic media is an idealized situation. In reality, there would be a hard layer at a certain depth, which would reduce the immediate settlement. Readers are referred to extended solutions (***Janbu et al. 1956,*** **and** ***Mayne and Poulos 1999***) for problems in such cases.

As can be seen in Equation 9.1, the amount of settlement is largely influenced by properties of soils μ and E_s. In particular, the estimation of E_s is not an easy task for a given soil and thus computed settlement shall be treated as a rough estimate unless E_s is properly assessed by proper laboratory tests or field methods. Fortunately, immediate settlement occurs during or right after the construction, and thus, contractors can do proper corrective measures at the construction site if needed.

9.3 PRIMARY CONSOLIDATION SETTLEMENT

Upon increase in stresses in an element, a time-delayed deformation and then settlement occurs for saturated cohesive soils due to its plastic behavior. When additional boundary stresses are applied to an element, it tends to be compressed. However, due to low permeability of the clay, water cannot escape from the element at once, but eventually water goes out and the volume of the element decreases. This is a time-delay process of volume decrease (settlement) and is classified as a **primary consolidation** process.

9.4 ONE-DIMENSIONAL PRIMARY CONSOLIDATION MODEL

Terzaghi (1925) developed a model that explains well the primary consolidation process as seen in Figure 9.2. The model consists of a water-filled cylinder with a piston, which is supported by a spring. In the piston, there is a small hole to allow drainage. There is also a standpipe to monitor the water pressure inside of the cylinder.

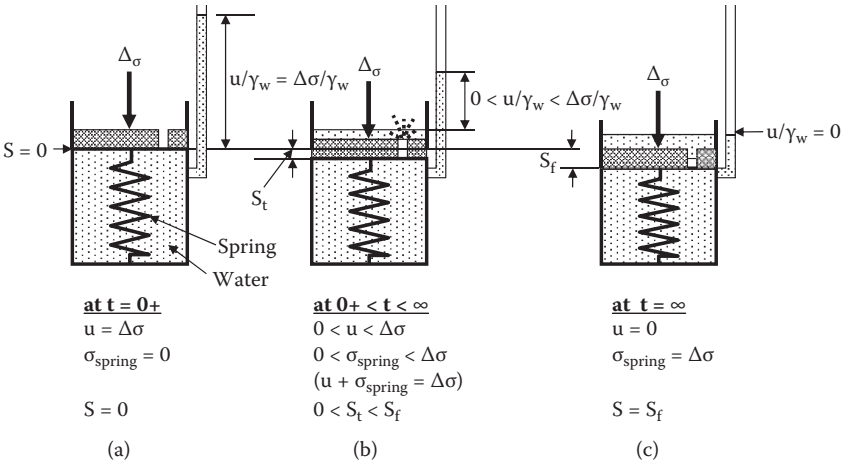

FIGURE 9.2 Terzaghi's one-dimensional primary consolidation model.

In the model, stress increment $\Delta\sigma$ is applied on top of the piston at time 0+. At time 0+, there is no settlement since there is no time for water to escape from the small hole. If there is no settlement (S = 0), stress in the spring σ_{spring} is zero. And thus applied stress $\Delta\sigma$ is totally carried by the water pressure ($u = \Delta\sigma$) as seen in Figure 9.2a. When time is allowed for some water to drain from the hole in the piston, the piston moves down and settlement starts; at the same time, applied stress $\Delta\sigma$ is transferred more to the spring σ_{spring} from the water pressure u as seen in Figure 9.2b. When a sufficient time is allowed for water to completely drain in Figure 9.2c (at the infinitive time in the theory), all water is drained (u = 0) and the final consolidation settlement is attained ($S = S_f$). At this stage all external pressure $\Delta\sigma$ is carried by the stress in the spring ($\sigma_{spring} = \Delta\sigma$).

Note that this is exactly the same model as the one used in the effective stress discussion in Chapter 7. The soil's skeleton is modeled by the spring, and the effective stress σ' is represented by σ_{spring}. The model clearly demonstrates that the time delayed volume change and thus ***the settlement occurs due to the escape of water from the element*** and ***the stress transfer from the total water pressure at t = 0+ to the total effective stress at t = ∞ during the consolidation process***.

9.5 TERZAGHI'S CONSOLIDATION THEORY

Terzaghi developed a theory for the above mentioned consolidation model. It assumes that:

1. The specimen is fully saturated.
2. Water and solid components are incompressible.
3. Darcy's law is strictly applied.
4. Flow of water is one dimensional.

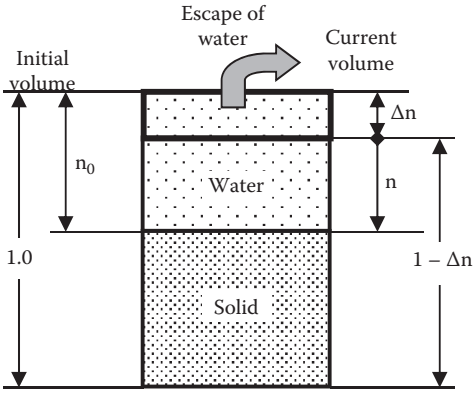

FIGURE 9.3 Three-phase model for consolidation process.

Note that those assumptions are nearly all valid for one-dimensional consolidation for fully saturated soils. Figure 9.3 shows a three-phase diagram of a fully saturated soil. In the model, the original total volume is 1.0, and the original volume of void (water) is initial porosity, n_o. During the consolidation process, when the effective stress increased from initial σ'_0 to the current σ', water is squeezed out at the amount of Δn, and the current volume of void becomes n as seen. Thus,

$$\Delta n = n_o - n = m_v \Delta\sigma' = m_v(\sigma' - \sigma'_o) \tag{9.2}$$

where $\Delta\sigma'$ is the effective stress change, and m_v is defined as the **coefficient of volume change**, which is a parameter to connect the effective stress change to the volume change. By taking the first derivative of Equation 9.3 with respect to time t,

$$\frac{\partial \Delta n}{\partial t} = \frac{\partial n_o}{\partial t} - \frac{\partial n}{\partial t} = 0 - \frac{\partial n}{\partial t} = m_v\left(\frac{\partial \sigma'}{\partial t} - \frac{\partial \sigma'_o}{\partial t}\right) = m_v\left(\frac{\partial \sigma'}{\partial t}\right) - 0 \tag{9.3}$$

Then,

$$\frac{\partial n}{\partial t} = -m_v \frac{\partial \sigma'}{\partial t} \tag{9.4}$$

Figure 9.4 shows a square tube element with $1 \times 1 \times dz$ dimensions. Water flows toward upper z direction, and the inflow water velocity v and the outflow velocity $v + (\partial v/\partial z)dz$ are shown. q_{in} and q_{out} are the inflow water rate and the outflow flow rate, respectively. If q_{in} and q_{out} are the same, there is no volume change. When q_{out} is

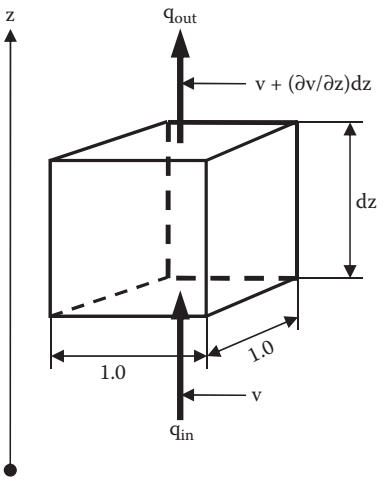

FIGURE 9.4 Vertical water flow through a square tube ($1 \times 1 \times dz$).

larger than q_{in}, the volume of the tube decreases, resulting in settlement. By knowing that $q_{out} - q_{in}$ is the volume change per unit time for $1 \times 1 \times dz$ total volume, and $\partial n/\partial t$ in Equation 9.4 is also the volume change per unit time for 1.0 total volume, the following equation is obtained:

$$q_{out} - q_{in} = (v_{out} - v_{in})A = (v_{out} - v_{in}) \cdot 1 \cdot 1 = \left(v + \frac{\partial v}{\partial z} dz \right) - v$$

$$= \frac{\partial v}{\partial z} dz = -\frac{\partial n}{\partial t} dz = m_v \frac{\partial \sigma'}{\partial t} dz \tag{9.5}$$

where A is the cross-sectional area for water flow (i.e., 1×1). In Equation 9.5, note that the positive value of $(q_{out} - q_{in})$ is the volume decrease and the positive value of $-(-\partial n/\partial t)dz$ is also volume decrease. From Equation 9.5, Equation 9.6 is obtained.

$$\frac{\partial v}{\partial z} = m_v \frac{\partial \sigma'}{\partial t} \tag{9.6}$$

Now, in Chapter 7, the effective stress is defined as $\sigma' = \sigma - u$ and taking the first derivative with respect to time t,

$$\frac{\partial \sigma'}{\partial t} = \frac{\partial \sigma}{\partial t} - \frac{\partial u}{\partial t} = 0 - \frac{\partial u}{\partial t} = -\frac{\partial u}{\partial t} \tag{9.7}$$

where $\partial\sigma/\partial t = 0$ since the applied total stress σ is constant during consolidation process and thus,

$$\frac{\partial \sigma'}{\partial t} = -\frac{\partial u}{\partial t} \tag{9.8}$$

Here, Darcy's law for water flow (Chapter 6) is introduced.

$$v = k \cdot i = k\frac{-\partial h_p}{\partial z} = k\frac{-\partial\left(\frac{u}{\gamma_w}\right)}{\partial z} = -\frac{k}{\gamma_w}\frac{\partial u}{\partial z} \tag{9.9}$$

where k is the coefficient of permeability, and i is the hydraulic gradient. ∂h_p is the pressure head difference, and is negative for positive water flow velocity v in Figure 9.4. From Equation 9.9,

$$\frac{\partial v}{\partial z} = -\frac{k}{\gamma_w}\frac{\partial^2 u}{\partial z^2} \tag{9.10}$$

By equating Equation 9.6 and Equation 9.10, and substituting Equation 9.8,

$$\frac{\partial u}{\partial t} = \frac{k}{m_v \gamma_w}\frac{\partial^2 u}{\partial z^2} = C_v \frac{\partial^2 u}{\partial z^2} \tag{9.11}$$

where

$$C_v = \frac{k}{m_v \gamma_w} \tag{9.12}$$

Equation 9.11 is called the **consolidation equation**. Cv is the **coefficient of consolidation** with a unit of length^2/time (m^2/sec, or ft^2/sec, etc.) and is a key material parameter in consolidation theory.

Equation 9.11 expresses the change of pore water pressure (u) relative to time (t) and space (z) domains, and takes a popular form of partial differential equations. The equation is in the same form of the thermal diffusion equation. To solve the second order of partial differential equations, four boundary (or initial) conditions are required. Figure 9.5a plots the pore water pressure u with depth z as a faction of time t. The top and bottom layers are assigned as drainage layers like sand or gravel, and the clay layer (2H thickness) is sandwiched between them. Excess pore water pressure can only be drained through the drainage layers, and thus, at the mid-depth H, the highest pore water pressure remains for $0<t<\infty$ as seen. The initial and boundary conditions for this case are

1. u (at any z, t = 0) = $\Delta\sigma$
2. u (at any z, t = ∞) = 0

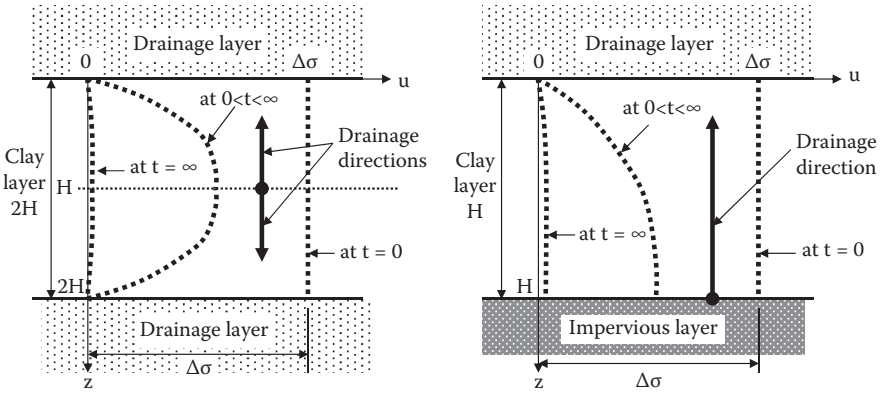

FIGURE 9.5 Initial and boundary conditions for the consolidation equation.

3. u (z = 0, at any t) = 0
4. u (z = 2H, at any t) = 0

The above conditions can also be applied to Figure 9.5b, where the bottom layer is impervious, so that water drainage occurs only at the top boundary. In this case, the clay thickness is treated as H and then it becomes mathematically equivalent to Figure 9.5a condition. Note that the drawing of the upper half (down to z = H) of Figure 9.5a is same as the entire drawing (down to z = H) of Figure 9.5b.

Pore water pressure u is assigned to have the following form:

$$u(z,t) = Z(z) \bullet T(t) \tag{9.13}$$

where Z(z) and T(t) are independent functions of z and t, respectively. By using the initial and boundary conditions and substituting Equation 9.13 into the consolidation equation, Equation 9.11, the following solution is obtained:

$$u(z,t) = \frac{4}{\pi}\Delta\sigma \sum_{N=0}^{\infty}\left[\frac{1}{2N+1}\sin\frac{(2N+1)\pi z}{2H} \bullet e^{-\frac{(2N+1)^2\pi^2 C_v}{4H^2}t}\right] \tag{9.14}$$

By substituting N = 0 to several higher values, the solution converges and the numerical solution is obtained for given z and t. To make an operation much simpler, **time factor** T_v is introduced as

$$T_v = \frac{C_v t}{H^2} \qquad \left[\ 0\ \right] \tag{9.15}$$

This is a nondimensional variable to express the time relative to material parameter C_v and drainage distance H. In this equation, H shall be taken as the longest distance to the drainage layer. When T_v is substituted into Equation 9.14, it becomes

$$u(z,t) = \frac{4}{\pi}\Delta\sigma \sum_{N=0}^{\infty}\left[\frac{1}{2N+1}\sin\frac{(2N+1)\pi z}{2H} \cdot e^{-\frac{(2N+1)^2\pi^2}{4}T_v}\right]$$

$$= f\left(\Delta\sigma, \frac{z}{2H}, T_v\right) \tag{9.16}$$

In this equation form, the pore water pressure u is expressed as a function of three independent parameters, $\Delta\sigma$, z/2H, and T_v.

By referring to the three-phase diagram of Figure 9.3 and using Equation 9.2, the final consolidation settlement S_f (at $t = \infty$) for a clay layer of thickness H can be obtained as

$$S_f = \Delta n_f \cdot H = m_v \Delta\sigma'_f H = m_v \Delta\sigma H \tag{9.17}$$

In the above expression, subscript "f" stands for "final." Meanwhile, the settlement S_t at any arbitrary time, t, is obtained from an integration of settlement $\Delta n \times dz$ for a small clay thickness dz over total clay layer thickness H as seen in Figure 9.6 and thus:

$$S_t = \int_0^H \Delta n \cdot dz = \int_0^H m_v \Delta\sigma' dz = m_v \int_0^H (\Delta\sigma - u)\, dz = m_v \Delta\sigma H - m_v \int_0^H u dz \tag{9.18}$$

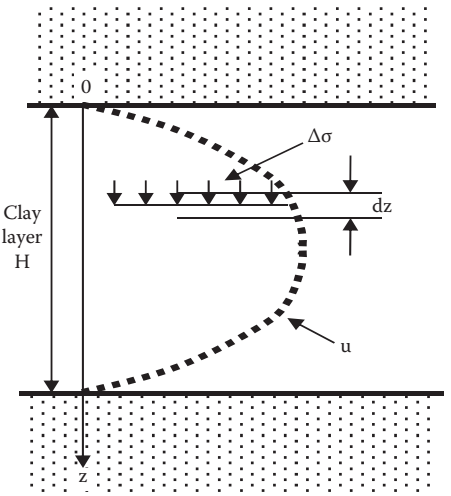

FIGURE 9.6 Settlement computation model.

where $\Delta\sigma$ is the increased stress at depth z. Since u is given in Equation 9.16, Equation 9.18 becomes

$$S_t = m_v \Delta\sigma H \left[1 - \frac{8}{\pi^2} \sum_{N=0}^{\infty} \left(\frac{1}{2N+1} \cdot e^{-\frac{(2N+1)^2 \pi^2}{4} T_v} \right) \right] \tag{9.19}$$

Now, the **degree of consolidation** U is defied as the percentage of settlement at an arbitrary time t to its final settlement at t = ∞, and it is computed from Equation 9.17 and Equation 9.19 as

$$U = \frac{S_t}{S_f} = \left[1 - \frac{8}{\pi^2} \sum_{N=0}^{\infty} \left(\frac{1}{2N+1} \cdot e^{-\frac{(2N+1)^2 \pi^2}{4} T_v} \right) \right] = f(T_v) \tag{9.20}$$

As seen in Equation 9.20, the degree of consolidation U is only a function of time factor T_v. There are unique relationships between U and T_v, and those are shown in Table 9.4 and plotted in Figure 9.7.

TABLE 9.4
Relationships between U and T_v

U (%)	T_v	U (%)	T_v
0	0	3.751	0.001
5	0.00196	5.665	0.0025
10	0.00785	7.980	0.005
15	0.0177	9.772	0.0075
20	0.0314	11.28	0.01
25	0.0491	17.84	0.025
30	0.0707	25.23	0.05
35	0.0962	30.90	0.075
40	0.126	35.68	0.1
45	0.159	56.22	0.25
50	**0.197**	76.40	0.5
55	0.239	87.26	0.75
60	0.286	93.13	1
65	0.340	99.83	2.5
70	0.403	100	5
75	0.477	100	7.5
80	0.567	100	9.5
85	0.684		
90	**0.848**		
95	1.129		
100	∞		

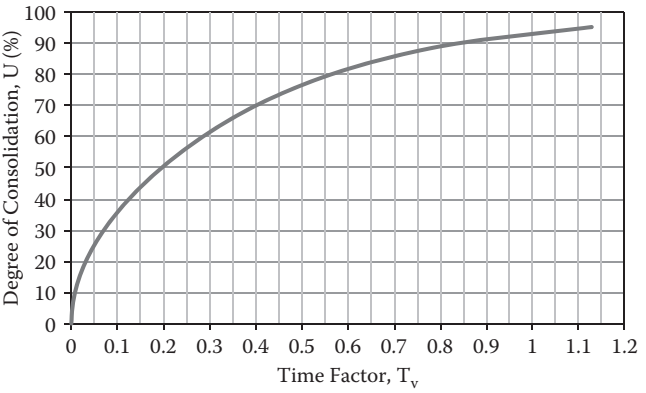

FIGURE 9.7 U versus T_v relationship.

On the first two columns of Table 9.4, $T_{50} = 0.197$ and $T_{90} = 0.848$ are often used to evaluate the midterm (50%) consolidation and near final (90%) consolidation, respectively. Also note that it takes the infinitive time to accomplish 100% consolidation from the theory, although practically it reaches to 100.000% when T_v is 5.0 and above.

Exercise 9.2

In a laboratory consolidation test, 12.7 mm (½ in.)-thick clay specimen was tested with top and bottom drained condition, and 90% consolidation was accomplished in 15.8 minutes (t_{90} = 15.8 min). In the field, the same clay material with the thickness of 6.5 m is sandwiched by top sand and bottom gravel layers for drainage. How long does the field clay take to accomplish 50% and 90% consolidation, respectively?

Solution:

In the laboratory test, top and bottom are drainage layers so that the clay thickness 12.7 mm = 2H and T_{90} = 0.848 from Table 9.4. Inserting those values in Equation 9.15,

$$C_v = \frac{H^2}{t_{90}} T_{90} = \frac{\left(\frac{12.7}{2}\right)^2}{15.8} 0.848 = 2.164 \ \text{mm}^2/\text{min}$$

From the field drainage condition, 2H = 6.5 m. Also T_{50} = 0.197 from Table 9.4. Utilizing Equation 9.15, 50% consolidation time, t_{50}, is

$$t_{50} = \frac{H^2}{C_v} T_{50} = \frac{\left(\frac{6.5 \times 1000}{2}\right)^2}{2.164} 0.197 = 9.615 \times 10^5 \ \text{min} = \mathbf{667.7\ days} \ \leftarrow$$

Similarly, for 90% consolidation time t_{90},

$$t_{90} = \frac{H^2}{C_v} T_{90} = \frac{\left(\frac{6.5 \times 1000}{2}\right)^2}{2.164} 0.848 = 41.39 \times 10^5 \text{ min} = 2874 \text{ days} = \mathbf{7.87 \text{ years}} \leftarrow$$

Or from Equation 9.15, and by using a common C_v value,

$$C_v = \frac{H^2}{t_{50}} T_{50} = \frac{H^2}{t_{90}} T_{90}, \text{ then, } t_{90} = \frac{T_{90}}{T_{50}} t_{50} = \frac{0.848}{0.197} \times 667.7 = 4.305 \times 667.7$$

$$= 2874 \text{ days} = \mathbf{7.87 \text{ years}} \leftarrow$$

Exercise 9.2 demonstrates the usefulness of a nondimensional time factor T_v. Equation 9.15 was used first to determine C_v value from the laboratory experiment, and then the same equation was used to determine the real time of consolidation in the field. It is most important to realize that ***H in Equation 9.15 is half the thickness of clay layer for double drainage, or full thickness for single layer drainage***. If H is taken as the full thickness (i.e., H = 6.5 m) in Exercise 9.2 by mistake, the result would be four times different from the correct one.

Exercise 9.3

A clay layer has a thickness of 4.5 m. After 6 months, it settled to 30% of the total settlement and 50 mm of the settlement was observed. For a similar clay layer and loading condition, if the thickness of clay is 20 m, how much settlement occurs at the end of 3 years? Assume that the top of the clay layer is a drainage layer and the bottom is an impervious layer for both 4.5 m and 20-m-thick clay layers.

Solution:

For the 4.5-m-thick clay, since 30% settlement is 50 mm, the final settlement will be

$$S_{f,\ 4.5m} = 50/0.30 = 166.7 \text{ mm}$$

H = 4.5 m since the top is only drainage layer in this case and thus,

$$C_v = \frac{H^2}{t_{30}} T_{30} = \frac{(4.5)^2}{6} 0.0707 = 0.239 \text{ m}^2/\text{month}$$

For the 20-m-thick clay, the final settlement $S_{f,20m}$ is proportional to the one for 4.5 m clay, thus

$$S_{f,\ 20m} = 166.7 \times (20/4.5) = 740 \text{ mm.} \leftarrow$$

At the end of 3 years,

$$T_v = \frac{C_v t}{H^2} = \frac{0.239 \times (3 \times 12)}{20^2} = 0.0215$$

From the right two columns of Table 9.4, corresponding to $T_v = 0.0215$, U = 16.3% was obtained by a linear interpolation of data points. Thus, 20 m-thick clay settles at the end of 3 years in the amount of

$$S_{3\ yrs,\ 20m} = S_{f,\ 20m} \times U_{3\ yrs} = 740 \times 0.163 = \textbf{120.6 mm.} \leftarrow$$

In Exercise 9.3, the degree of saturation U was found from the T_v value, and this is another example of the versatility of T_v equation (Equation 9.16).

9.6 LABORATORY CONSOLIDATION TEST

Small-scale laboratory consolidation tests are performed for clay specimens to determine several key consolidation parameters, including the coefficient of consolidation C_v value. An undisturbed thin-wall tube specimen is obtained from the field, where consolidation settlement is anticipated due to future footing load. The specimen is carefully trimmed to fit inside of a rigid consolidation ring as seen in Figure 9.8. A typical dimension of the ring is 63.5 mm (2.5 in.) diameter and 12.7 mm (½ in.) high. The consolidation ring filled with the specimen is placed inside of the consolidation device, and the upper porous stone and a loading cap are placed on top of the specimen. The device is normally filled with water to avoid drying out of the specimen during the test. The whole device is set up on a rigid platform. Consolidation load is applied and the vertical deformation is monitored with a dial gauge. In this system, soil deforms only in a vertical direction due to the escape of water during consolidation process.

The first consolidation stress σ (load divided by specimen area) is applied at time zero and the vertical deformation dial (δ_v) is continuously read at t = 0, 0.1, 0.25, 0.5, 1, 2, 4, 8, 15, 30 minutes, and 1, 2, 4, 8, and 24 hours. Thus, one consolidation stress application takes a whole day. At the end of 24 hours (not necessarily exactly

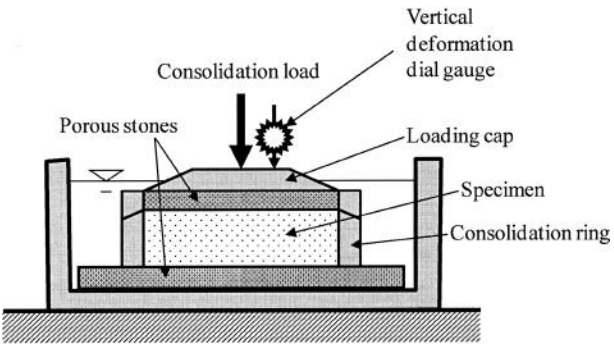

FIGURE 9.8 Consolidation test setup.

24 hours, but elapsed time shall be recorded), consolidation stress σ is normally doubled, and δ_v at the similar time intervals are recorded. Then σ is doubled again for the third consolidation stress. The preceding process is repeated with typical σ values of 25, 50, 100, 200, 400, 800, and 1600 kPa until the design maximum consolidation stress value is attained. This increasing stress process is called the **loading process** of consolidation, which takes about 1 week.

At the end of the test with the maximum consolidation stress, an **unloading process** is performed. The σ value is deduced to 1600, 400, 100, 25 kPa, or such. During this process, rebound on specimen occurs and only the final dial gauge readings are recorded at several hours after each unloading process. Thus, the whole unloading process takes about a day. After the unloading process, wet and dry weights and water content of the specimen are measured by weighing and drying it in an oven overnight.

9.7 DETERMINATION OF C_V

From each consolidation stress, a set of data with δ_v and t is obtained. Table 9.5 shows a sample set of data obtained.

There are two practical methods available to determine the coefficient of consolidation C_v from laboratory consolidation tests: the **log t method** and $\sqrt{t}$ **method**.

9.7.1 Log t Method

The log t versus δ_v data from Table 9.5 is plotted in Figure 9.9. The middle section of data points shows a linear relation and a straight line is drawn as a **primary consolidation** curve. The later section of the curve also shows a linear relation, and the

TABLE 9.5
Sample Consolidation Test Data, δ_v and t (σ = 1566 kPa)

Elapsed Time, t (min)	Reading in Vertical Dial Gauge, δ_v (mm)	$\sqrt{t}$
0	17.74	0.00
0.1	17.56	0.32
0.25	17.47	0.50
0.5	17.33	0.71
1	17.17	1.00
2	16.96	1.41
4	16.76	2.00
10	16.45	3.16
15	16.38	3.87
30	16.25	5.48
120	16.14	10.95
250	16.11	15.81
520	16.10	22.80
1400	16.08	37.42

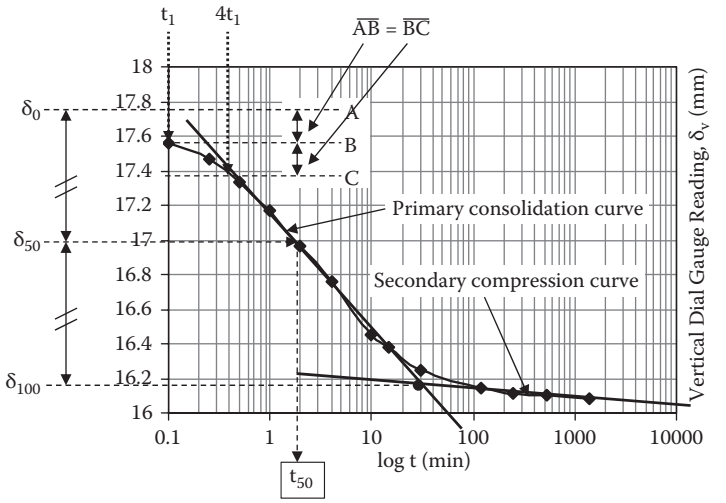

FIGURE 9.9 Log t method.

second straight line is drawn as the **secondary compression** curve. The intersection of the two straight lines is considered as the **end of the primary consolidation** and leveled as δ_{100} in the figure. The initial section of the data points is a curve that is assumed to be a parabolic. By this assumption, t_1 and $4t_1$ points are chosen on the curve as seen (in the example, $t_1 = 0.1$ min and $4\ t_1 = 0.4$ min). Corresponding δ_v values are identified as B and C levels in the figure, respectively. Since $t = 0.0$ cannot be plotted in the log scale, the initial vertical deformation δ_0 (Point A level) is then determined by taking $\overline{AB} = \overline{BC}$. Once δ_0 and δ_{100} are determined, the mid-point δ_{50} is obtained. Corresponding time is designated as t_{50} or the time to reach 50% primary consolidation. From Equation 9.15 for T_v, the coefficient of consolidation C_v is obtained as:

$$C_v = \frac{H^2}{t_{50}} T_{50} = \frac{H^2}{t_{50}} 0.196 \tag{9.21}$$

Note that H in Equation 9.21 shall be the longest drainage distance so that it shall be a half of the specimen thickness in common laboratory consolidation tests.

9.7.1 $\sqrt{t}$ METHOD

The same data in Table 9.5 are plotted with $\sqrt{t}$ versus δ_v in Figure 9.10.

In the figure, at the initial portion of the data, a linear relation is observed and a straight line is drawn. The intersection with $\sqrt{t} = 0$ axis is assigned as δ_0. Starting from the δ_0 point, the second straight line with the inverse slope of 1.15 times the first line is drawn as seen with a broken line. The interception of the second line with

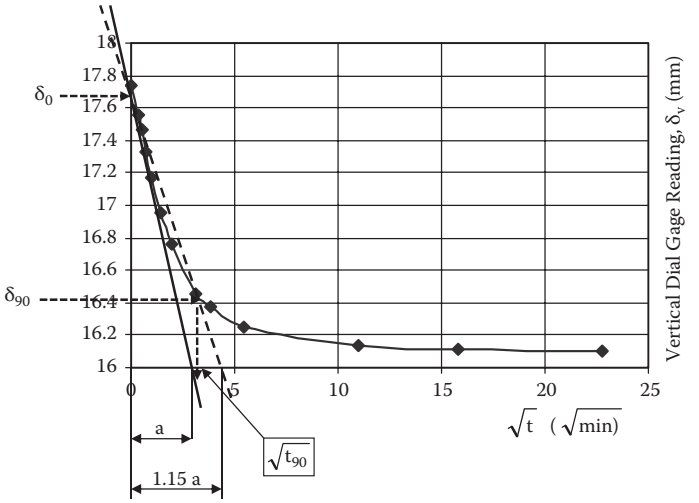

FIGURE 9.10 $\sqrt{t}$ method.

the data curve is assigned as 90% of primary consolidation point. The corresponding time is read as $\sqrt{t_{90}}$ and thus t_{90} value is obtained. From Equation 9.15, Cv value is computed as

$$C_v = \frac{H^2}{t_{90}} T_{90} = \frac{H^2}{t_{90}} 0.848 \tag{9.22}$$

In both methods, the coefficient of consolidation C_v values are determined with various consolidation stresses, since δ_v and t relations are obtained for each consolidation stress. Those values might be different when the consolidation stress is varied, or those are nearly the same. Engineers have to make a decision on the selection of C_v values for design based on the analyzed data. The selection of those two methods depends very much on a preference of the engineers. As a common rule, log t method (Equation 9.21) could be better used for evaluating the earlier stage of consolidation process since it uses 50% consolidation time, while $\sqrt{t}$ method (Equation 9.22) could be better suited for the final stage consolidation estimation because it uses 90% consolidation.

9.8 e-LOG σ CURVE

First of all, note that in traditional consolidation theory and practice, "**e-log p curve**" has been used as common terminology, where p donates the stress symbol. However, throughout this book, σ is used as the symbol for stress. Therefore, "**e-log σ curve**" replaces the old term "e-log p curve" throughout.

Laboratory data are analyzed for the final settlements achieved under given consolidation stresses σ at the end of 24 hours of consolidations. An example data is analyzed in Table 9.6.

TABLE 9.6
Example of e-log σ Curve Analysis

(a) Specimen Information

Description of Soil:	**Silty organic clay**	**Specimen diameter D**	**76.04 mm**
Location:	Craney Island, Virginia	**Initial specimen height H_o**	19.06 mm
Water contents:			
at beginning of test (whole specimen)		42.3 %	
at beginning of test (auxiliary specimen)		42.4 %	
at end of test (whole specimen)		31.3 %	
Weight of dry specimen, W_s	109.68 gf	**Solid height, H_s**	8.98 mm

(b) e-log σ Computation

A	B	C	D	E	F
Consolidation Stress, σ, kPa	**Final Vertical Dial Reading, δ, mm**	**Change in Specimen Height, Δδ, mm**	**Final Specimen Height, H, mm**	**Height of Void, H_v, mm**	**Final Void Ratio, e**
0.00	22.86	0	19.06	10.08	1.122
14.21	22.71	0.15	18.91	9.93	1.106
28.53	22.34	0.37	18.54	9.56	1.064
53.84	21.76	0.58	17.96	8.98	0.999
107.69	20.82	0.93	17.02	8.04	0.895
215.31	19.41	1.41	15.61	6.63	0.738
430.69	17.74	1.67	13.94	4.96	0.553
861.39	16.08	1.66	12.28	3.30	0.368
430.69	16.17	–0.09	12.37	3.39	0.377
107.69	16.42	–0.25	12.62	3.64	0.405
53.81	16.65	–0.23	12.85	3.87	0.431
28.52	16.82	–0.17	13.02	4.04	0.450

Note: Height of solid $H_s = W_s/(\gamma_{wat} G_s A_{Specimen}) = W_s/(\gamma_{wat} G_s \pi D^2/4)$
column A: Applied consolidation stress.
column B: Final vertical dial reading at the end of each stress σ_i.
column C: $\Delta\delta_i = \delta_{i-1} - \delta_i$ (positive number for loading and negative number for unloading).
column D: $H_i = H_{i-1} - \Delta\delta_i$.
column E: $H_{v,i} = H_i - H_s$.
Column F: $e_i = H_{v,i} / H_s$.

In the table, δ values in column B are the final vertical dial gauge readings under corresponding consolidation stresses σ, and the rest can be readily computed using the spreadsheet format shown.

Exercise 9.4

Based on a three-phase diagram, find the solid height H_s of the example data in Table 9.6 for this fully saturated clay. Specific gravity G_s was found to be 2.69.

Solution:

For the three-phase diagram in Figure 2.4, W_s = 109.68 gf, G_s = 2.69 and thus, Equation 2.13 gives:

$$V_s = \frac{W_s}{G_s \gamma_w} = \frac{109.68 \text{ gf} \times g}{2.69 \times 9.81 \text{ kN/m}^3} = \frac{0.10968 \text{ kgf} \times 9.81 \text{ m/sec}^2}{2.69 \times 9.81 \times 10^3 \text{ N/m}^3}$$

$$= 4.077 \times 10^{-5} \text{ m}^3$$

Since $V_s = H_s$ • (area of specimen) and the diameter of the specimen D = 76.04 mm,

$$H_s = \frac{V_s}{\pi\left(\frac{D}{2}\right)^2} = \frac{4.077 \times 10^{-5}}{\pi\left(\frac{76.04 \times 10^{-3}}{2}\right)^2} = 0.00898 \text{ m} = \mathbf{8.98 \text{ mm}}$$

Now, from Table 9.6, relationships between consolidation stress σ (in log scale) and final void ratio e are plotted in Figure 9.11. This curve is called the **e-log σ curve** and is a key relationship to determine final consolidation settlement. The loading curve (decreasing e with increase in σ) and unloading curve (increasing e with decease in σ) are seen in the figure. In the loading section, a linear relation is observed at higher stress level and a straight line is drawn as **virgin compression curve**. The virgin curve is the e and σ relations for naturally deposited soils on the bottom of lakes (or rivers), which are fully consolidated under their own gravity. The slope of the virgin curve is read as **compression index** C_c, and is given by

$$C_c = \frac{-(e - e_i)}{\log\sigma - \log\sigma_i} = \frac{-(e - e_i)}{\log\frac{\sigma}{\sigma_i}}, \quad \text{thus}, \Delta e = e_i - e = C_c \log\frac{\sigma}{\sigma_i} \tag{9.23}$$

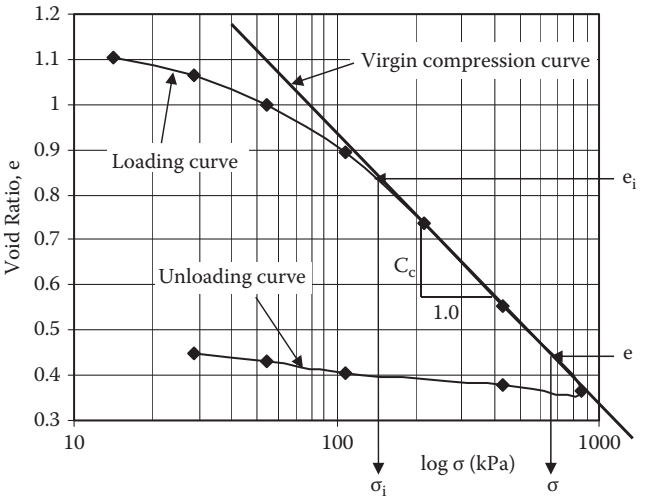

FIGURE 9.11 e-log σ curve.

where (e_i, σ_i) and (e, σ) are arbitrary points on the virgin curve as seen. Equation 9.23 is used to estimate consolidation settlement for soils, which follow only the virgin curve relation. Table 9.7 shows typical values of C_c for various soil types.

Skempton (1944) proposed the following equation to calculate C_c:

$$C_c' = 0.007\ (LL\text{-}10) \quad \text{for remolded clays} \tag{9.24}$$

TABLE 9.7
Typical Values of Compression Index C_c

			C_c	
Soil	**Liquid Limit**	**Plastic Limit**	**Undisturbed**	**Remolded**
Boston blue clay	41	20	0.35	0.21
Chicago clay	58	21	0.42	0.22
Louisiana clay	74	26	0.33	0.29
New Orleans clay	79	26	0.29	0.26
Fort Union clay	89	20	0.26	
Mississippi loess	23–43	17–29	0.09–0.23	
Delaware organic silty clay	84	46	0.95	
Indiana silty clay	36	20	0.21	0.12
Marine sediment, B.C. Canada	130	74	2.3	

Source: Winterkorn, H. F. and Fang, H-Y (1975). *Foundation Engineering Handbook*, Van Nostrand Reinhold, New York.

Terzaghi and Peck (1967) proposed the follow equation for low- to medium-sensitive undisturbed clays:

$$C_c \approx 1.3\, C_c' = 0.009\,(LL\text{-}10) \quad \text{for undisturbed clays} \tag{9.25}$$

The above equations are used only as guidance to evaluate approximate consolidation settlement initially. More accurate value shall be determined from the laboratory consolidation tests.

9.9 NORMALLY CONSOLIDATED AND OVERCONSOLIDATED SOILS

Any specimen that will be tested comes from a certain depth at the site; thus it has been subjected to a prior effective overburden stress and that stress has been relaxed during the sampling process. Therefore, it makes the laboratory e-log σ curve different from the virgin curve. At the beginning of loading curve, compression rate (reduction in e) is much smaller than the one of the virgin curve and the curve merges to the virgin curve at a higher σ value. ***The stress at the turning point on the e-log σ curve is the stress at which soil has previously experienced the historical maximum consolidation in the field***. This stress is called **preconsolidation stress**.

Casagrande (1936) developed an empirical method to determine preconsolidation stress σ_c for a given e-log σ curve. Referring to Figure 9.12, the maximum curvature (or minimum radius) point M is first identified on the curve. Staring from M, the tangential line MT to e-log σ curve and the horizontal line MH are drawn. Lines

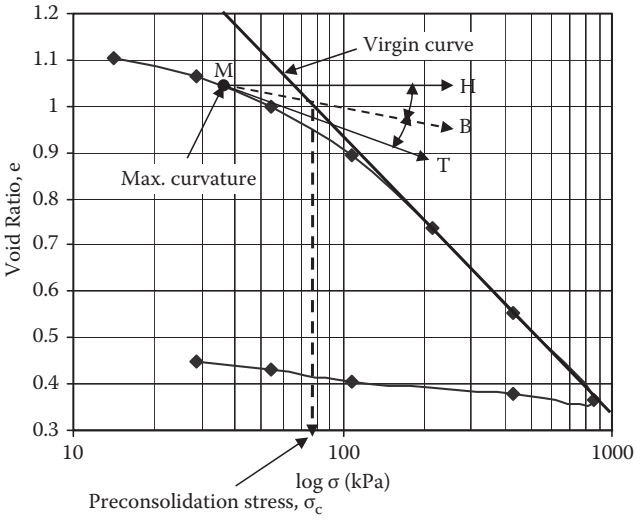

FIGURE 9.12 Casagrande's preconsolidation stress determination.

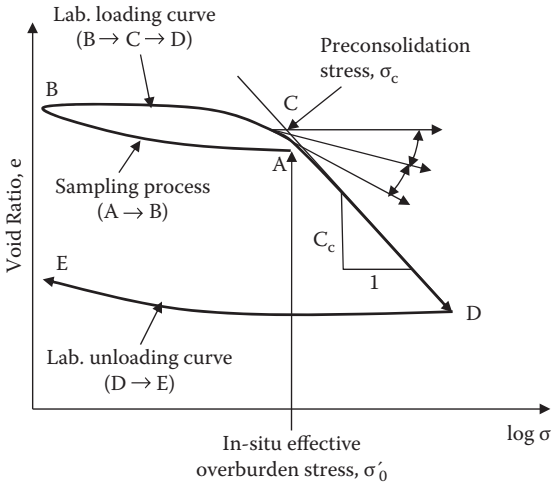

FIGURE 9.13 e-log σ curve for normally consolidated soils.

MT and MH are bisected by MB. The stress at the intersection of MB and the virgin curve is defined as preconsolidation stress σ_c as seen.

When preconsolidation stress is found to be the same as the current effective overburden stress σ'_0 at the site from which the sample is obtained, the soil is called **normally consolidated**. Referring to Figure 9.13, a soil has been consolidated at the site under its own weight till sampling takes place (Point A). During the sampling process (A to B), the in situ stress (at A) is reduced to nearly zero (at B) and reloaded in the laboratory consolidation process (B, C to D). The loading path B to C is a reloading process and thus the slope is rather small. After passing the preconsolidation stress point C, soil enters to a new stress territory and the slope becomes steeper (to the value of C_c). After the maximum stress point D in the laboratory, unloading process (D to E) takes place and its slope is similar to the one of A to B curve.

On many occasions, however, the in situ effective overburden stress σ'_0 is found to be smaller than laboratory obtained preconsolidation stress σ_c as seen in Figure 9.14. The site might have been subjected to the stress higher than σ'_0 during its geological history. This soil is called **overconsolidated soil**. The e-log σ curve starts from Point O with the consolidation stress with $\sigma'_{0,max}$ (historical maximum effective overburden stress) and a portion of the stress has been reduced to Point A (current σ'_0). Note that its historical maximum stress cannot be seen visually at the present time. Similarly, the sampling process follows A to B and the laboratory loading process goes from B, C, and D. Preconsolidation stress found on laboratory e-log σ curve at Point C is similar to the value of the historical maximum effective overburden stress $\sigma'_{0,max}$. The removal of consolidation stress from $\sigma'_{0,max}$ to σ'_0 are due to meltdown of glacial ice, excavation, erosion of top soils, permanent rise of ground water table, etc. In particular, past glacial ice load, which covered over the North American continent resulted in heavily overconsolidated soils in the region.

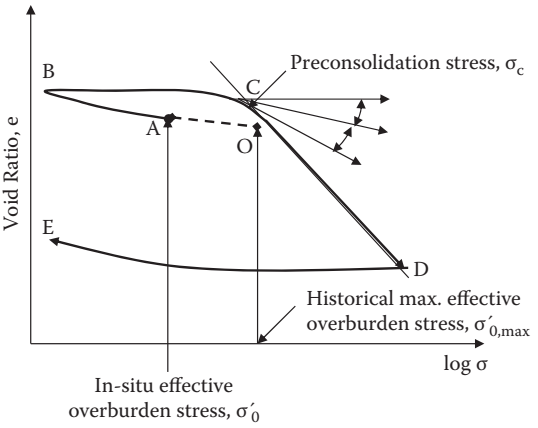

FIGURE 9.14 e-log σ curve for overconsolidated soils.

Overconsolidation ratio (OCR) is defined as

$$\text{OCR} = \frac{\text{historical max imum effective overburden stress}}{\text{current effective overburden stress}} = \frac{\sigma'_{0,\max}}{\sigma'_0} \tag{9.26}$$

The OCR value for normally consolidated soils is 1.0, and it is higher than 1.0 for overconsolidated soils.

Exercise 9.5

In a northern city in the United States, the area had been covered with 100-m-thick ice load in an early historical time. Some soil in the city is obtained from 10 m deep below the ground surface. The water table was near the ground surface. Estimate the value of OCR for this soil specimen. Assume that the area had not been subjected to any major erosion or excavation.

Solution:

Assume that soil's unit weight is 19 kN/m^3, and ice's unit weight is the same as that of water (9.81 kN/m^3) and thus

$\sigma'_{0,max} = 9.81 \times 100 + (19 - 9.81) \times 10 = 981 + 91.9 = 1073$ kPa

$\sigma'_0 = (19 - 9.81) \times 10 = 91.9$ kPa,

thus, OCR = $\sigma'_{0,max}/\sigma'_0 = 1073/91.9 =$ **11.7** ←

Like the example in Exercise 9.5, many soils in the northern regions of the United States and Canada are heavily overconsolidated due to the historical glacial ice load. This created unique soil properties. For example, **glacial till** is a highly compacted

mixture of gravel, sand, silt, and clay (glacier carried and deposited materials) and has an excellent bearing capacity for foundations. However, since the lateral stress has not been relaxed as much as the vertical stress, upon the release of ice load, there are rather high lateral stress trapped in the soil elements. It creates rather high lateral stress against earth structures. Also, when the area is excavated or slopes are cut, relaxation in the lateral stress causes gradual increase of the volume (swelling), and thus, the water migrates into the soil elements to make weaker soil zones, which may possibly lead to gradual failure (**creep failure**) of the slope.

Normally consolidated and overconsolidated soils show quite different behaviors in many aspects, such as the shear strength, settlement, swell, lateral earth pressure, etc., and thus, identification of σ_c relative to σ'_0 is an important practice during the consolidation data analyses.

9.10 FINAL CONSOLIDATION SETTLEMENT FOR THIN CLAY LAYER

Assume that a relatively thin clay layer with total thickness of H is subjected to an incremental stress $\Delta\sigma$ due to a new footing, and its initial vertical effective stress is σ'_0 at its mid-depth as seen in Figure 9.15. Final primary consolidation settlement can be computed as follow.

9.10.1 Normally Consolidated Soils

As shown in Figure 9.16, σ'_0 and $\sigma'_0 + \Delta\sigma$ are on the virgin curve, and its slope is C_c. In this case, Equation 9.24 is used to calculate Δe as

$$\Delta e = e_i - e = C_c \log \frac{\sigma'_0 + \Delta\sigma}{\sigma'_0} \tag{9.27}$$

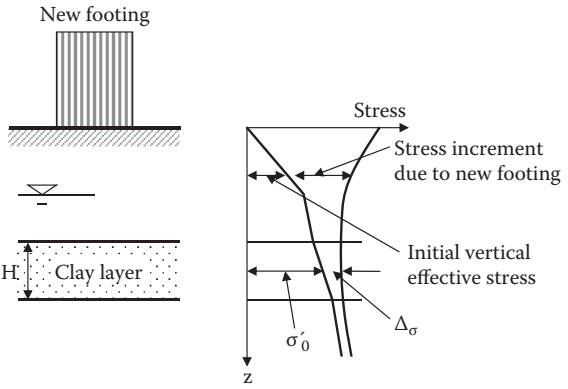

FIGURE 9.15 Consolidation settlement computation for a thin single layer.

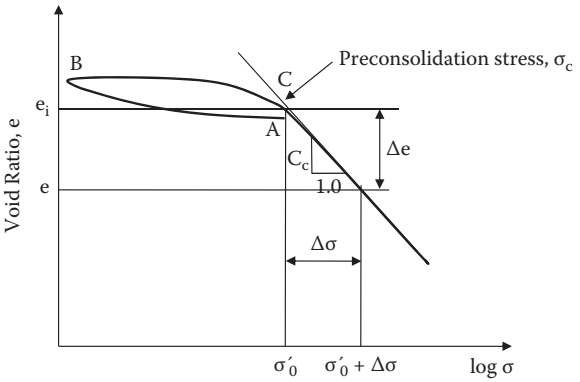

FIGURE 9.16 Settlement computation for normally consolidated soils.

The void ratio change Δe occurs to the total initial height $(1 + e_0)$. Thus, proportionally, the final settlement S_f to the total initial clay thickness H is

$$\frac{\Delta e}{1+e_0} = \frac{S_f}{H}, \quad \text{thus, } S_f = \frac{H}{1+e_0}\Delta e = \frac{H}{1+e_0} C_c \log \frac{\sigma'_0 + \Delta\sigma}{\sigma'_0} \tag{9.28}$$

Or Δe value can be directly read from e-log σ curve, and it is applied into the first term of Equation 9.28 to obtain final total consolidation settlement S_f.

9.10.2 Overconsolidated Soils

For this type of soils, σ'_0 and $\sigma'_0 + \Delta\sigma$ are not necessarily on the virgin curve as seen in Figure 9.17, and thus, the constant C_c value with Equation 9.28 cannot be used

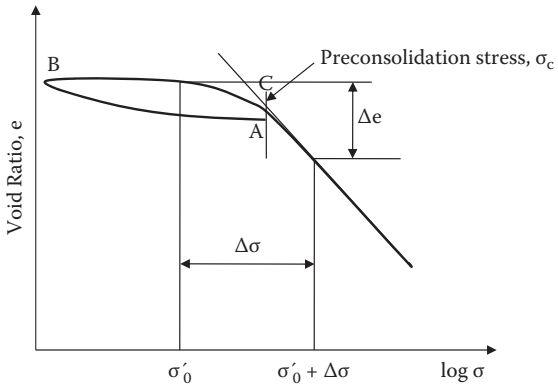

FIGURE 9.17 Settlement computation for overconsolidated soils.

for the settlement computation. In this case, Δe value are directly read from e-log σ curve and substituted into the first term of Equation 9.28

$$S_f = \frac{H}{1+e_0}\Delta e \tag{9.29}$$

It shall be noted that ***for the amount of settlement computation*** in Equation 9.28 and Equation 9.29, ***"H" is always the total thickness of clay layer regardless of top and bottom drainage conditions***, which was a key factor in choosing H or 2H in T_v equation (Equation 9.15).

Exercise 9.6

A 3-m-thick clay layer is sandwiched between dry sand on the top and saturated gravel on the bottom as seen in Figure 9.18. Soil properties are given in the figure. On top of the sand layer is applied 1000 kN of a point load. Estimate final consolidation settlement of the clay layer directly under the loading point. Handle the clay layer as a single layer; it is normally consolidated without remolding.

Solution:

Initial effective vertical stress at the midpoint (depth at 5.5 m) of the clay layer is
$\sigma'_o = 18.0 \times 4 + (19.0\text{-}9.81) \times 1.5 = 85.79$ kPa
Incremental stress $\Delta\sigma$ at z = 5.5 m is obtained from Boussinesq's point load equation (Equation 8.2) under the center (r = 0):

$$\Delta\sigma = \frac{3}{2\pi} \bullet \frac{P}{z^2} = \frac{3}{2\pi} \bullet \frac{1000}{5.5^2} = 15.78\,\text{kPa}$$

From Equation 9.25, $C_c = 0.009(LL\text{-}10) = 0.009 \times (34\text{-}10) = 0.216$ for undisturbed soil.

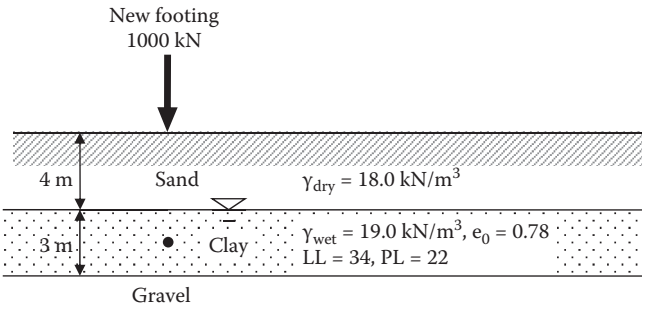

FIGURE 9.18 Exercise 9.6 problem.

By substituting the above values into Equation 9.28 for this normally consolidated clay,

$$S_f = \frac{H}{1+e_0} C_c \log \frac{\sigma'_0 + \Delta\sigma}{\sigma'_0} = \frac{3}{1+0.78} 0.216 \bullet \log \frac{85.79+15.78}{85.79} = \mathbf{0.0267\ m} \leftarrow$$

9.11 CONSOLIDATION SETTLEMENT FOR MULTILAYERS OR A THICK CLAY LAYER

When clay layers are thick or consist of several different clay layers, one-step computation by Equations 9.28 and 9.29 is not suitable, since σ'_o and $\Delta\sigma$ are not considered to be constant values throughout the depth of the clay layers, as seen in Figure 9.19. In this case, the whole clay layer is divided into several sublayers as seen in the figure. Final settlement $S_{f,i}$ for each sublayer is computed from the methods described in Section 9.10, using H_i, $\sigma'_{o,i}$ and $\Delta\sigma_i$ values, which can be obtained at the midpoints of each sub-layer i. The final total settlement S_f is the summation of $S_{f,i}$.

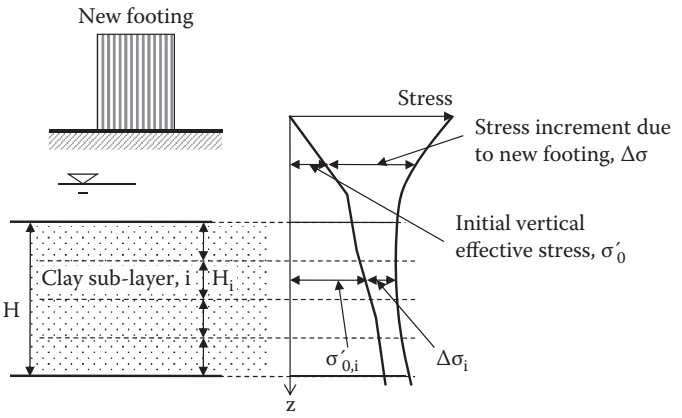

FIGURE 9.19 Consolidation settlement computation for multilayers or a thick layer.

Exercise 9.7

A 20-m-thick uniform clay layer as shown in Figure 9.20 is anticipated to settle after a new footing is placed on the site. Distributions of computed initial vertical effective stress σ'_0 and incremental stress $\Delta\sigma$ due to the new footing under the center of the footing are plotted also in the figure. The e-log σ curve is obtained from laboratory consolidation test for a clay sample at the site in Figure 9.21.

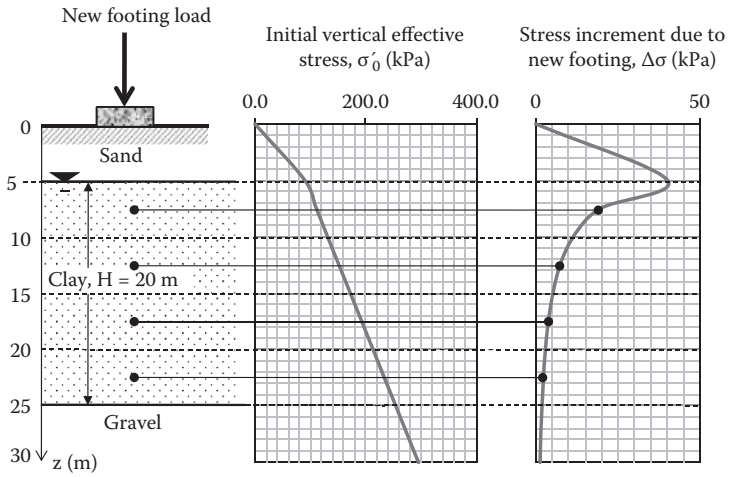

FIGURE 9.20 Exercise 9.7 problem.

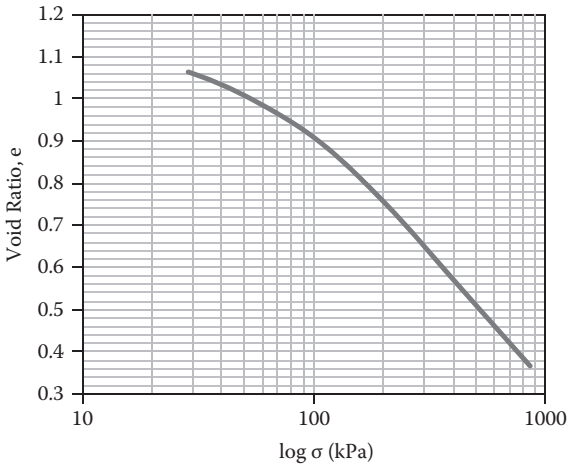

FIGURE 9.21 e-log σ curve for Exercise 9.7.

Compute total final consolidation settlement of the clay layer under the center of the footing.

Solution:

200 m-thick clay layer is divided into four equal sublayers and σ'_0 and incremental stress $\Delta\sigma$ for each sublayer are read at the midpoints in Figure 9.20. Corresponding e_0 to σ'_0 and e_f to $\sigma'_0 + \Delta\sigma$ of each sublayer are read from Figure 9.22 (enlarged

version of Figure 9.21). Note that in Figure 9.22 only $\sigma'_0 + \Delta\sigma$ and e_f lines for the first sublayer are shown. The results are summarized in Table 9.8, where Equation 9.29 was used to compute $S_{f,i}$.
Thus, estimated total final settlement of the 20 m-thick clay layer is 0.273 m. ←

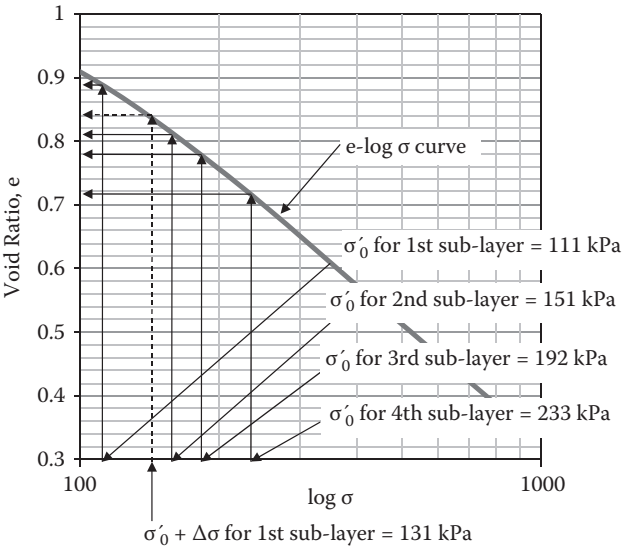

FIGURE 9.22 Enlarged curve of Figure 9.21.

TABLE 9.8
Settlement Computation for Thick or Multiclay Layers

Sub-Layer, i	H (m)	$\sigma'_{o,i}$ (kPa)	$\Delta\sigma_i$ (kPa)	$\sigma'_{o,i} + \Delta\sigma_i$ (kPa)	$e_{0,i}$	$e_{f,i}$	Δe_i	$S_{f,i}$ (m)
1	5	111	20	131	0.89	0.84	0.05	0.132
2	5	151	7	158	0.81	0.79	0.02	0.055
3	5	192	4	196	0.78	0.76	0.02	0.056
4	5	233	2.5	235.5	0.69	0.68	0.01	0.030
Σ	**20**	—	—	—	—	—	—	**0.273**

Table 9.8 is based on utilization of the e-log σ curve to obtain Δe_i. If clays are normally consolidated, $S_{f,i}$ can be calculated from Equation 9.28. In such cases, C_c values for all sublayers shall be assigned if those vary with several different clay layers. Selection of sublayer thickness depends on the engineer's judgment by allowing rather small variation of σ'_0 and $\Delta\sigma$ within sublayers.

9.12 SUMMARY OF PRIMARY CONSOLIDATION COMPUTATIONS

As discussed so far, in primary consolidation theory and practice, there are two different computations: (1) amount of final consolidation settlement, and (2) time to reach a certain percentage of the consolidation. It is very practical and less confusing to separate consolidation problems into two categories: (1) ***how much***, and (2) ***how soon*** (rate problem). By doing so, the selection of key consolidation equations, and the handling of the clay layer thickness (H or 2H) become easier. The following summarized these two different procedures.

9.12.1 "How Much" Problem

Depending on normally consolidated or overconsolidated, Equation 9.28 or Equation 9.29 are used, respectively.

$$S_f = \frac{H}{1+e_0}\Delta e = \frac{H}{1+e_0} C_c \log \frac{\sigma'_0 + \Delta\sigma}{\sigma'_0} \quad \text{for normally consolidated soils} \tag{9.28}$$

or

$$S_f = \frac{H}{1+e_0}\Delta e \quad \text{for overconsolidated soils} \tag{9.29}$$

In Equation 9.28 for normally consolidated soils, Δe can be read directly from the e-log σ curve, which consists of only the virgin curve, or it is obtained from computed C_c, σ'_0, and $\Delta\sigma$ values. Meanwhile, in Equation 9.29 for overconsolidated soils, only the e-log σ curve is available to compute the final settlement. ***In both cases, H is the full thickness of clay layer regardless of top and bottom drainage conditions***.

9.12.2 "How Soon" Problem (Rate Problem)

This problem always utilizes the relationship between the time factor T_v (Equation 9.15) and the degree of consolidation U (Table 9.4).

$$T_v = \frac{C_v t}{H^2} \tag{9.15}$$

In this case, H is the longest drainage distance, and thus, ***if only one boundary layer is pervious and the other is impervious, H in Equation 9.15 is the full clay layer thickness. On the other hand, if both the top and bottom layers are pervious, H in Equation 9.16 is half the clay layer thickness***.

9.13 SECONDARY COMPRESSION

In Terzaghi's consolidation theory discussed so far, when generated pore water pressure is fully dissipated, it is the end of consolidation and that part of consolidation is called the **primary consolidation**. In the theory, it takes infinitive time, but practically, it will be completed in a certain finite time as observed as δ_{100} in Figure 9.9. After the primary consolidation is over, soil continues to compress with a slower rate as seen as the secondary compression curve in Figure 9.23 (replot of Figure 9.9 in terms of void ratio e and log t). **Secondary compression** is not due to dissipation of pore water pressure, but rather due to slow rearrangement of fine particles and even other reasons.

The amount of secondary compression is sometimes very significant since it continues for a long time. The slope of the secondary compression curve in e versus log t is taken as C_α and defined as **secondary compression index** in Figure 9.23. Thus, from the figure,

$$C_\alpha = \frac{\Delta e}{\log t - \log t_p} = \frac{\Delta e}{\log \dfrac{t}{t_p}}, \quad \text{thus} \quad \Delta e = C_\alpha \log \frac{t}{t_p} \tag{9.30}$$

where t is any arbitrary time and t_p is the time at the end of primary consolidation; e_p is also defined as the void ratio at the end of primary consolidation in Figure 9.23. By using a similarity law of settlement Δe to the total height $1 + e_p$ and the secondary compression settlement S_s to the total clay layer thickness H,

$$\frac{\Delta e}{1+e_p} = \frac{S_s}{H}, \quad \text{thus}, S_s = \frac{\Delta e}{1+e_p} H = \frac{H}{1+e_p} C_\alpha \log \frac{t}{t_p} = C'_\alpha H \log \frac{t}{t_p} \tag{9.31}$$

where C'_α is $C_\alpha/(1 + e_p)$ and is called **modified secondary compression index**. Once C_α or C'_α is determined from laboratory e-log t curve, Equation 9.31 is rewritten to Equation 9.32 to take any arbitrary time interval t_1 to t_2 ($t_1 < t_2$). Note that t_1 shall be larger than t_p.

$$S_s = \frac{H}{1+e_p} C_\alpha \log \frac{t_2}{t_1} = C'_\alpha H \cdot \log \frac{t_2}{t_1} \tag{9.32}$$

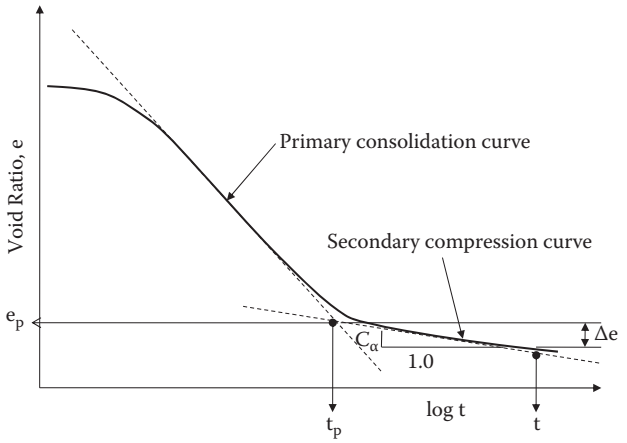

FIGURE 9.23 Secondary compression curve.

Equation 9.33 is used to estimate S_s for any time interval t_1 to t_2 during the secondary compression process.

C_α or C'_α value can be obtained from laboratory consolidation tests. Also, it was found empirically that the ratio of C_α to the compression index C_c is rather constant for a given group of materials. For inorganic clays and silts, the ratio (C_α/C_c) is about 0.04 ± 0.01, and the ratio for organic clays and silts is about 0.05 ± 0.01 for most of natural soils (***Terzaghi et al. 1996***).

Exercise 9.8

For the same problem as in Exercise 9.6 (Figure 9.18), estimate the secondary compression settlement S_s from the year 20 to the year 40. The e-log t curve at a similar stress condition to the insitu value is given in Figure 9.24.

Solution:

From Figure 9.24, the secondary compression index C_α is read as the slope of the secondary compression curve.

$$C_\alpha = \frac{-(e_2 - e_1)}{\log t_2 - \log t_1} = \frac{-(0.365 - 0.395)}{\log \dfrac{10000}{0.1}} = 0.006$$

and $e_p = 0.378$ from the figure. By substituting those values with $t_1 = 20$ and $t_2 = 40$ years into Equation 9.32,

$$S_s = \frac{H}{1+e_p} C_\alpha \log \frac{t_2}{t_1} = \frac{3}{1+0.378} 0.006 \log \frac{40}{20} = 0.00393 \text{ m} \leftarrow$$

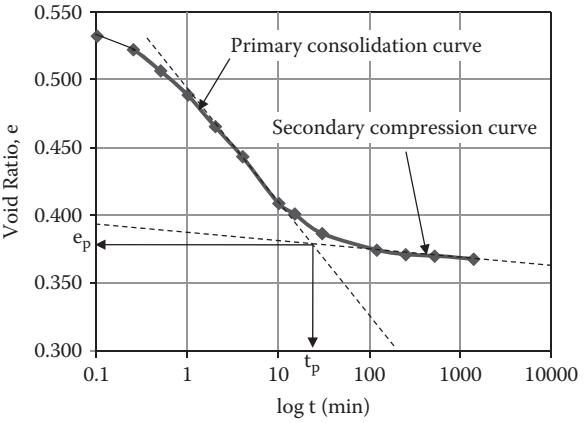

FIGURE 9.24 Exercise 9.8 (e-log t curve).

In Exercise 9.6, primary consolidation settlement was 0.0267 m, and thus, the above obtained secondary compression settlement for a period of 20 years adds an additional 14.7 % settlement, and it cannot be simply neglected.

9.14 ALLOWABLE SETTLEMENT

Theoretically speaking, if a building settles evenly, it would not cause any damages to the structure. However, in practice, most foundations settle unevenly (**differential settlement**) due to uneven load distributions and nonuniform subsurface soil conditions. If differential settlement occurs, walls may crack, doors and windows may jam, and tall structures may tilt and tumble. In other occasions, for example, if a paved parking lot settles with a certain amount (**total settlement**), it would create problems for accesses to the roads and buildings. Accordingly, the total and the differential settlements are to be controlled during and after construction. **Allowable settlements** are specified by design engineers based on the safety and the functionality of buildings and earth structures. Table 9.9 gives a guidance of those various allowable settlements based on both theory and observations of structures that have suffered damage.

TABLE 9.9
A Guidance for Allowable Settlement

Type of Movement	Limiting Factor	Maximum Settlement
Total settlement	Drainage and access	150–600 mm
	Probability of differential settlement	
	Masonry walls	25–50 mm
	Framed buildings	50–100 mm
Tilting	Tower, stacks	0.004B
	Rolling of trucks, stacking of good	0.01S
	Crane rails	0.003S
Differential	Brick walls in buildings	0.0005S–0.002S
	Reinforced-concrete building frame	0.003S
	Steel building frame, continuous	0.002S
	Steel frame, simple	0.005S
Maximum permissible settlement	Front slab, 100 mm thick	0.02S

Note: B = footing base width; S = column spacing.

Source: After ***Sowers, G. F. (1979)****. Introductory Soil Mechanics and Foundations: Geotechnical Engineering*, 4th Ed., MacMillan, New York.

9.15 GROUND IMPROVING TECHNIQUES AGAINST CONSOLIDATION SETTLEMENT

When the estimated settlement exceeds the allowable settlement, some remedial measures are necessary. Depending on the in situ situations, several options are available.

1. Replace the whole compressible soils with less compressible soils if the thickness of the soils is rather thin and if it is economically feasible.
2. Changing the soil property into less compressible one by **chemical grouting, cement grouting,** or **lime mixing**.
3. Reinforce soft ground by utilizing **geosynthetics** materials.
4. Accelerate consolidation time prior to major structural construction by means of **vertical drain** (**paper drain, wick drain,** or **sand drain**) techniques.
5. **Preload** the area and induce consolidation prior to construction.
6. **Vacuum** is applied in the soft clay to induce negative pore water, and thus it increases the effective stress. The increased effective stress works as a preloading as in (5) above.

Detailed procedures of the above techniques can be found in other literatures such as ***Hausmann (1990)*** for ground modification, ***Koerner (2005)*** for geosynthetics reinforcement, etc.

The techniques mentioned in the items (4), (5), and (6) above are addressed in the following based on consolidation concept learned in this chapter.

9.15.1 Vertical Drain (Paper Drain, Wick Drain, and Sand Drain) Techniques

The time factor equation (Equation 9.16) is rewritten as

$$t = \frac{H^2}{C_v} T_v \tag{9.33}$$

Equation 9.33 implies that consolidation time t is proportional to H^2, where H is the longest drainage distance. The techniques call to shorten H in the field with inserted vertical drainage materials.

The drainage materials may be paper, wick, or sand columns. The technique was first developed in the 1960s by using long strips of colligated cardboards (paper), which were inserted into soft ground. As seen in Figure 9.25, stripes of vertical drains are arranged so that the drainage distance H_d is much shorter than the original drainage distance H/2 without vertical drain installation. For example, if H_d to H/2 ratio becomes 1/5, the consolidation time reduces to 1/25, according to Equation 9.33. Presently, the wick drain replaced the paper drain in most applications. The wick is made of synthetic materials. It consists of a long core material in the center with

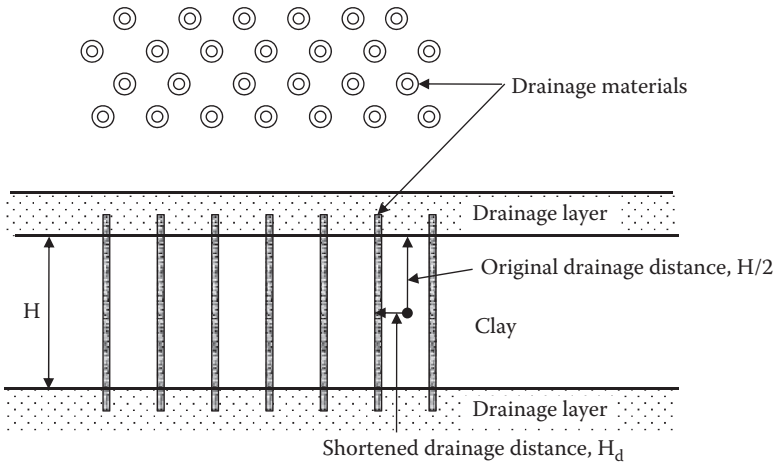

FIGURE 9.25 Principle of vertical drain (paper, wick, and sand drain) techniques.

drain ribs in the longitudinal direction and geofabric filter material around it, as seen in Figure 9.26.

A sand drain works with the same principle. Bore holes are drilled through soft soil layers and sand is filled in the holes to make sand columns. At the **Kansai International Airport** project (first phase) in Japan (see photos on the cover page and in Figure 1.4), 1,000,000 sand columns were installed in order to stabilize 20-m-thick soft soils under water to construct 511 ha of a man-made island. The sand columns had 400 mm diameter and were placed with 2.5-m pitches.

9.15.2 Preloading Technique

In the **preloading technique**, dirt (mostly soil) of a few meters high is placed to cover the future building site. It is left for several months to a year. The dirt is then removed and buildings are constructed on the site.

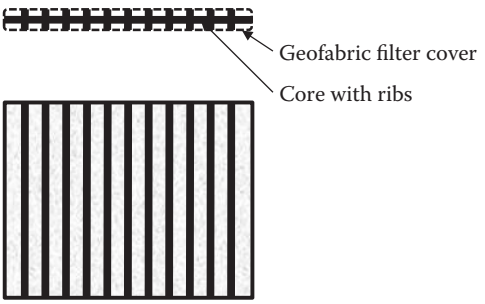

FIGURE 9.26 Wick drain.

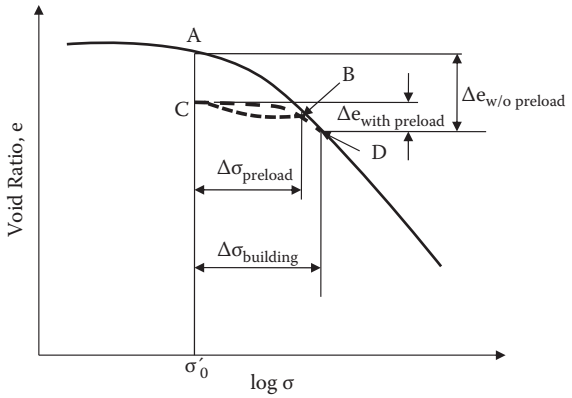

FIGURE 9.27 Principle of preloading technique.

This technique reduces future consolidation settlement. The entire processes of the loading and unloading of dirt and the building construction are plotted in an e-log σ diagram as seen in Figure 9.27. Point A is the starting point at the site before construction. During the preloading process of the dirt with $\Delta\sigma_{preload}$, it moves from Point A to B. During removal of the dirt, it moves back to Point C. During the building construction process with $\Delta\sigma_{building}$, it moves back again from Point C to D. When the resulting changes in void ratio are compared in the cases of with-preloading ($\Delta e_{with\ preload}$) and without-preloading ($\Delta e_{w/o\ preload}$), it is clear from the figure that $\Delta e_{with\ preload}$ is much smaller than $\Delta e_{w/o\ preload}$. Thus, consolidation settlement during building construction will be considerably reduced.

This cost-effective technique is often used for rather small-scale projects (office building or shopping mall construction) for which there are some flexibilities in the construction schedule, since the preloading process requires some extra time to achieve. Also, preloading technique is used together with vertical drain methods to reduce both the consolidation time as well as the amount of consolidation settlement.

9.15.3 Vacuum Consolidation Technique

Recently, a new technique called **vacuum consolidation** has been developed. This induces a vacuum in the soft clay soil through pipes in a sealed environment by impermeable membranes. Typically, 80 kPa (–78% of the atmospheric pressure) or greater vacuum (negative pore water pressure) can be applied by this method. Because of induced vacuum pressure in the soil mass, the atmospheric pressure works the same way as in the preloading technique through the impermeable membrane on top of the ground. An 80-kPa vacuum pressure is equivalent to about 4.0 m height of soil load in the preloading technique. Readers are referred to other references on the topics (e.g., ***Carter et al., 2005; Chu and Yan, 2005***).

9.16 SUMMARY

Settlements, in particular, consolidation settlements, are a major soil mechanics problem as shown in Chapter 1 (examples are Pisa's tower and Kansai International Airport). The theory and practice were fully presented in this chapter. Normally consolidated versus overconsolidated soils are quite different in their behaviors and thus differences shall be clearly recognized. The way to handle the thickness of clay layer H or 2H were clearly distinguished in this chapter (Section 9.12) by taking always H for "how much" problems and H or 2H for "how soon" problems.

REFERENCES

Bowles, J. E. (1996), *Foundation Analysis and Design*, 5th ed., McGraw-Hill, New York.

Carter, J. P., Chai, J. C., and Hayashi, S. (2005), Ground deformation induced by vacuum consolidation, *Journal of Geotechnical and Geoenvironmental Engineering*, ASCE, Vol. 131, No. 12, pp. 187–192.

Casagrande, A. (1936), Determination of the preconsolidation load and its practical significance, *Proceedings, 1st International Conference on Soil Mechanics and Foundation Engineering*, Cambridge, MA, Vol. 3, 60–64.

Chu, J. and Yan, S. W. (2005), Estimation of degree of consolidation for vacuum preloading projects, *International Journal of Geomechanics*, Vol. 5, No. 2, pp. 187–192.

Hausmann, M. R. (1990), *Engineering Principles of Ground Modification*, McGraw-Hill, New York.

Janbu, N., Bjerrum, L., and Kjaernsli, B. (1956), *Norwegian Geotechnical Institute Publication*, No. 16.

Koerner, R. M. (2005), *Designing with Geosynthetics*, 5th ed., Pearson/Prentice Hall.

Mayne, P. W. and Poulos, H. G. (1999), Approximate displacement influence factors for elastic shallow foundations, *Journal of Geotechnical and Environmental Engineering*, ASCE, Vol. 125, No. 6, 453–460.

Schleicher, F. (1926), Zur Theorie Des Baugrundes, *Der Bauingenieur*, No. 48, 49.

Skempton, A. W. (1944), Notes on the compressibility of clays, *Quarterly Journal of the Geological Society of London*, Vol. 100, 119–135.

Sowers, G. F. (1979), *Introductory Soil Mechanics and Foundations: Geotechnical Engineering*, 4th ed., Macmillan, New York.

Terzaghi, K. (1925), *Erdbaumechanik*, Franz Deuticke.

Terzaghi, K. and Peck, R. B. (1967), *Soil Mechanics in Engineering Practice*, 2nd Edition, John Wiley & Sons, New York.

Terzaghi, K., Peck, R. B., and Mesri, G. (1996), *Soil Mechanics in Engineering Practice*, 3rd ed., John Wiley & Sons, New York.

Winterkorn, H. F. and Fang, H.-Y. (1975), *Foundation Engineering Handbook*, Van Nostrand Reinhold, New York.

Problems

9.1 A circular footing (2.0 m diameter) with $q = 200\ kN/m^2$ is placed on a hard clay soil layer. Estimate the immediate settlement in the following cases.
- (a) Under the center of flexible footing
- (b) Under the corner of flexible footing
- (c) Under a rigid footing

9.2 1 m × 1 m rectangular footing with q = 200 kN/m² is placed on a medium-dense sandy soil layer. Estimate the immediate settlement in the following cases.
(a) Under the center of flexible footing
(b) Under the corner of flexible footing
(c) Under a rigid footing

9.3 Terzaghi's consolidation theory assumes (1) specimen is fully saturated, (2) water and solid components are incompressible, (3) Darcy's law is strictly applied, and (4) the flow of water is one dimensional. What will be the most critical shortcomings on those assumptions when the theory is applied to real field conditions?

9.4 A clay specimen was tested in the laboratory consolidation device, which had 12.7 mm (½ inch) thick and the top and the bottom boundaries were drained. A 50% consolidation time on the specimen was obtained as 28.4 minutes. Determine the following:
(a) Time for 50% consolidation in the field with this soil with a 2.5 m thickness where only the top layer is drained.
(b) Time for 90% consolidation in the field with this soil with a 2.5 m thickness where only the top layer is drained.
(c) For the same field condition above, at the end of 1 year after the placement of load, how much primary consolidation settlement occurs relative to its final amount of the settlement?
(d) The same question in (c), but at the end of 5 years.

9.5 A clay specimen was tested in the laboratory consolidation device, which was 25.4 mm (1 inch) thick and only the top boundary was drained. There was 90% consolidation time on the specimen obtained as 2.2 hours. Determine the following:
(a) Time for 50% consolidation in the field with this soil with 9.6 m thickness where both top and bottom layers are drained.
(b) Time for 90% consolidation in the field with this soil with 9.6 m thickness where both top and bottom layers are drained.
(c) For the same field condition above, at end of 1 year after the placement of load, how much primary consolidation settlement occurs relative to its final amount of the settlement?
(d) The same question as in (c), but at the end of 5 years.

9.6 In the field with a 5.5-m-thick clay layer with a top and bottom drained condition, a field preloading test was performed. From the observed settlement curve, 20% consolidation has been achieved in 2.5 month. A nearby site with the similar soil has a 7.0-m-thick clay layer. Estimate
(a) Time for 50% consolidation of 7.0-m-thick clay layer
(b) Time for 90% consolidation of 7.0-m-thick clay layer

9.7 A set of vertical deformation and time relation is obtained below from a consolidation test, in which the thickness of the specimen = 12.7 mm with top and bottom drained. Determine
(a) t_{50} and C_v by the log t method
(b) t_{90} and C_v by the $\sqrt{t}$ method

Time Min.	Vertical Deformation Dial Reading mm
0	8.54
0.1	8.29
0.25	8.12
0.5	7.92
1	7.56
2	7.12
4	6.78
10	6.63
15	6.59
30	6.52
120	6.44
245	6.42
620	6.38
1420	6.34

9.8 A set of vertical deformation and time relation is obtained below from a consolidation test, in which the thickness of the specimen = 12.7 mm with top and bottom drained. Determine

(a) t_{50} and C_v by the log t method

(b) t_{90} and C_v by the $\sqrt{t}$ method

Time Min.	Vertical Deformation Dial Reading mm
0	7.83
0.1	7.71
0.25	7.52
0.5	7.28
1	6.91
2	6.52
4	6.32
10	6.23
15	6.21
30	6.16
114	6.11
236	6.06
652	6.03
1530	5.98

9.9 A laboratory consolidation test is performed and the following data are obtained:

Consolidation Stress kPa	Final Vertical Deformation Dial Reading mm
0	17.53
25	17.42
50	17.22
100	16.97
200	16.38
400	14.76
800	11.38
400	11.46
100	11.92
50	12.25
25	12.53

Given conditions:

Specimen diameter = 76.0 mm
Initial specimen height = 25.4 mm
Weight of dry specimen = 192.5 gf
$G_s = 2.70$

(a) Compute and plot e-log σ relation.
(b) Determine preconsolidation stress by Casagrande's method.
(c) Compute the compression index C_c.
(d) Is this soil normally consolidated or overconsolidated if the specimen's current effective overburden stress is 150 kPa?

9.10 A laboratory consolidation test is performed and the following data are obtained:

Consolidation Stress kPa	Final Vertical Deformation Dial Reading mm
0	14.02
25	13.94
50	13.78
100	13.47
200	12.70
400	11.18
800	9.10
400	9.32
100	9.60
50	9.79
25	10.02

Given conditions:

Specimen diameter = 76.0 mm
Initial specimen height = 12.7 mm
Weight of dry specimen = 50.6 gf
$G_s = 2.70$

(a) Compute and plot e-log σ relation.
(b) Determine preconsolidation stress by Casagrande's method.
(c) Compute the compression index C_c.
(d) Is this soil normally consolidated or overconsolidated if the specimen's current effective overburden stress is 150 kPa?

9.11 The soil profile is shown in the figure below. A new footing will be placed on the ground and the average vertical stress increment at the midpoint of the clay layer due to the new footing will be $\Delta\sigma_v = 25.5$ kPa. Estimate the final primary consolidation settlement of the clay layer. Assume that the clay is normally consolidated.

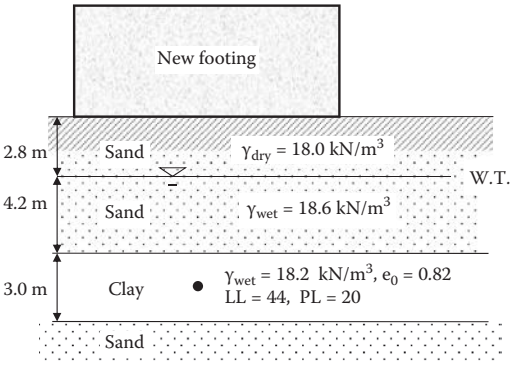

9.12 In Problem 9.11, what will be the amount of the secondary compression for 10 years after the end of primary consolidation? Assume that the primary consolidation will end at 4.5 year and the void ratio at the end of primary $e_p = 0.78$.

9.13 For the same soil profile and the loading condition as in Problem 9.11, a consolidation test is performed for a specimen from the clay layer. The e-log σ curve is obtained below. Estimate the final primary consolidation settlement of the clay layer.

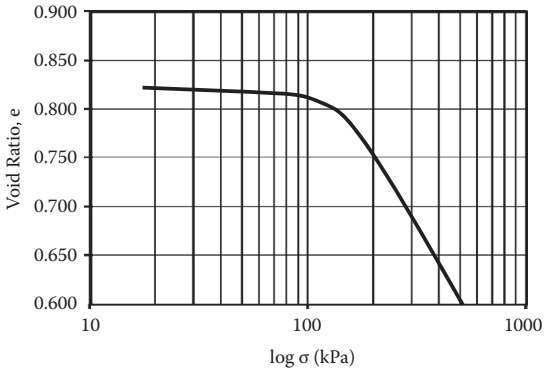

9.14 The soil profile for a future building construction site is shown below. The proposed footing is a 6.0 m diameter circular one with q = 200 kN/m^2

as shown. Estimate the final primary consolidation settlement of the 5 m thick normally consolidated clay layer.

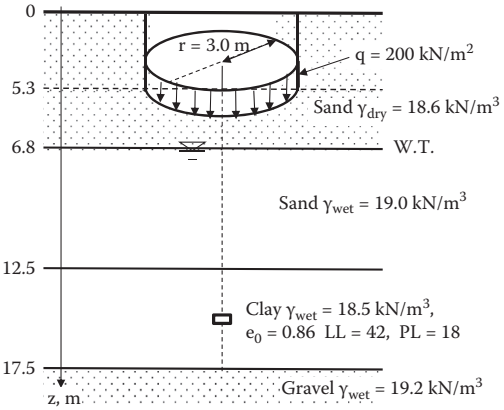

9.15 In Problem 9.14, estimate the amount of the secondary compression for a period of 10 years after the end of the primary consolidation. Assume that the primary consolidation will end at 10.2 year and the void ratio at the end of primary $e_p = 0.77$.

9.16 The soil profile and the loading condition are given in the figure. Total new footing stress including the foundation at z = 2m is 400 kN/m^2. The soil profile has a rather thick clay layer (15 m) so that the layer shall be divided into several sublayers to adequately estimate the consolidation settlement. Divide it into three sublayers and compute the primary consolidation settlement at the midpoint of each layer, and then make a summation for the total final settlement. Assume that the clay is normally consolidated and use Newmark's rectangular footing solution for the stress increment computation.

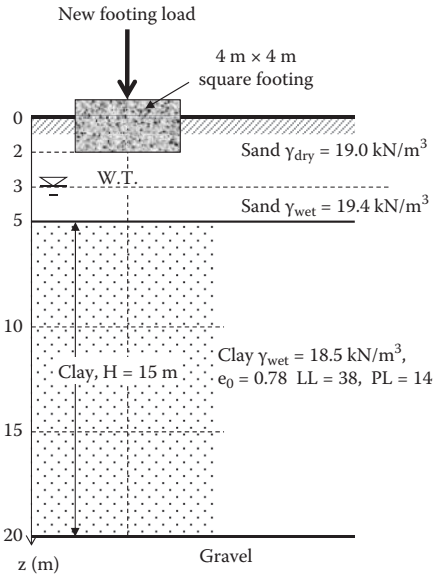

9.17 For the same soil profile and the loading condition as in Problem 9.16, the e-log σ curve of the clay specimen is obtained by the laboratory test below. The figure on the right is an enlarged version of the left in regular σ scale. Compute the final primary consolidation settlement of this clay by dividing it into three sublayers as in Problem 9.16.

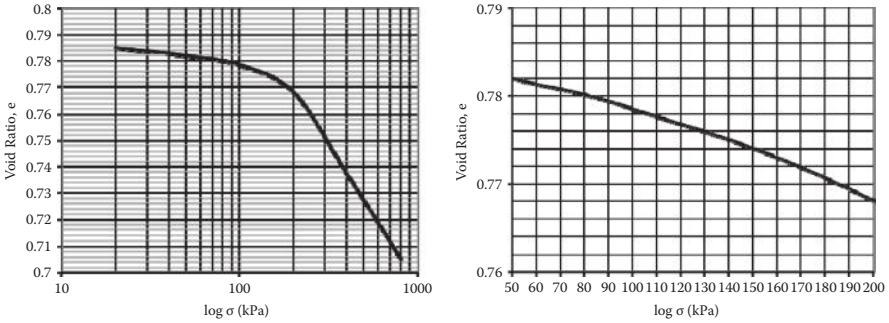

9.18 How can the vertical drains reduce consolidation time?

9.19 How can the preloading method reduce the amount of consolidation settlement?

9.20 Discuss about the applicability of the preloading technique to (a) a normally consolidated clay layer, and (b) to an overconsolidated clay layer.

10 Mohr's Circle in Soil Mechanics

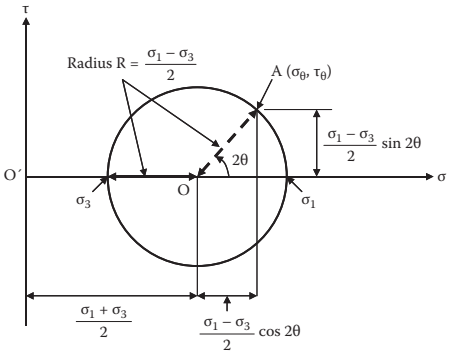

10.1 INTRODUCTION

Mohr's circle may have been already studied in most students' curriculum in their early solid mechanics or strength of materials classes. In this chapter, in order to apply it conveniently to soil mechanics problems, the sign conventions are clearly defined and the use of the **pole (origin of planes)** is emphasized. Mohr's circle becomes a very powerful tool to study the failure mechanism of soils and the lateral earth pressure theory, as will be seen in Chapters 11 and 12.

10.2 CONCEPT OF MOHR'S CIRCLE

In the late 1800s, ***Mohr (1887)*** presented a graphic solution to determine stresses at a mass. When an external load is applied, an infinitesimal element will be subjected to the boundary stresses as seen in Figure 10.1. The magnitudes of the developed stresses can only be defined when the direction of the plane, which passes through the element, is known. On a plane at the element, there is **normal stress**, which acts perpendicular (normal) to the plane, and **shear stress**, which acts on the plane in parallel to the face direction. In Figure 10.1, normal stress σ_θ and shear stress τ_θ are shown on the θ-plane, which inclines at +θ (counterclockwise) angle from the horizontal plane. The magnitudes of σ_θ and τ_θ do change when the θ angle changes. Mohr's circle is a technique to graphically determine the values of σ_θ and τ_θ values

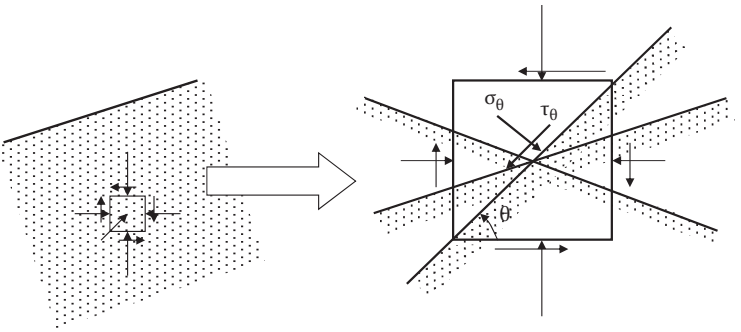

FIGURE 10.1 Mohr's circle concept.

on a given plane with inclination θ angle. Note that Mohr's stress solution is applied only to the two-dimensional (plane strain) problems.

10.3 STRESS TRANSFORMATION

Figure 10.2a shows an infinitesimal element, which is subjected to boundary normal stress σ_x and shear stress τ_{xy} on x-plane and σ_y and τ_{yx} on y-plane. These stresses maintain a static equilibrium; τ_{xy} is the shear stress applied on x-plane in y-direction and τ_{yx} is the one on y-plane in x-direction. We call τ_{xy} and τ_{yx} **conjugated shear stresses** and $|\tau_{xy}| = |\tau_{yx}|$, maintaining the moment equilibrium of the element. Note that the x-plane is the one where x value is constant (not the direction of x-axis) and thus ***the normal stress σ_x is applied normal to x-plane. The direction of x-plane and the direction of σ_x stress are not the same and they are rather perpendicular to each other***. The same principle also applies to y-plane and σ_y. Also, ***compressive normal stress is assigned positive*** in soil mechanics problems in contrary to the other disciplines.

Figure 10.2b shows a triangular element ABE with all the boundary stresses on it. Assign AE distance as unity. ***All normal and shear stresses are assumed to have***

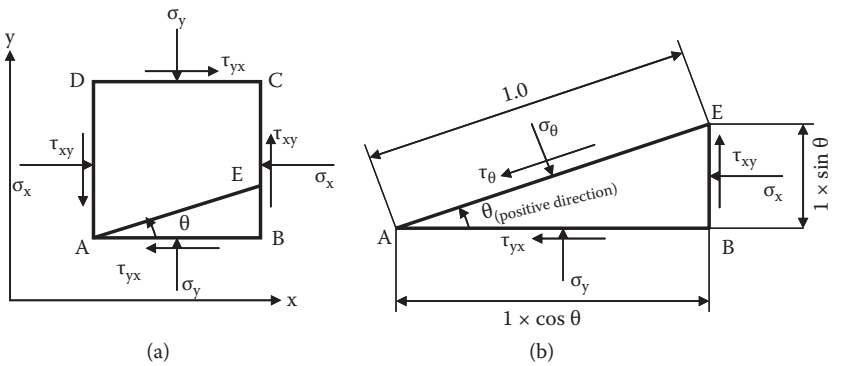

FIGURE 10.2 Stresses on an infinitesimal element.

positive values in the assigned directions in the figure. Applying horizontal and vertical force equilibriums to stresses on the element ABE:

$$\Sigma V = \sigma_y \cos\theta + \tau_{xy} \sin\theta - \sigma_\theta \cos\theta - \tau_\theta \sin\theta = 0 \tag{10.1}$$

$$\Sigma H = (-\tau_{yx}) \cos\theta - \sigma_x \sin\theta + \sigma_\theta \sin\theta - \tau_\theta \sin\theta = 0 \tag{10.2}$$

And by knowing that $\tau_{xy} = \tau_{yx}$, σ_θ and τ_θ are solved as

$$\sigma_\theta = \frac{\sigma_y + \sigma_x}{2} + \frac{\sigma_y - \sigma_x}{2} \cos 2\theta + \tau_{xy} \sin 2\theta \tag{10.3}$$

$$\tau_\theta = \frac{\sigma_y - \sigma_x}{2} \sin 2\theta - \tau_{xy} \cos 2\theta \tag{10.4}$$

By changing θ values, a combination of σ_θ and τ_θ values on any arbitrary θ plane can be obtained from Equation 10.3 and Equation 10.4.

When $d\sigma_\theta/d\theta = 0$ is applied to Equation 10.3 to find the θ value for the maximum or the minimum normal stress, or $\tau_\theta = 0$ is applied to Equation 10.4 to seek the θ value for zero shear stress, the following equation emerges:

$$\tan 2\theta = \frac{2\tau_{xy}}{\sigma_y - \sigma_x} \tag{10.5}$$

and $\tan 2\theta$ takes a certain value for given τ_{xy}, σ_y, and σ_x . This implies that the maximum or the minimum normal stress, and the zero shear stress appear on the same θ value (θ plane); the condition repeats in every 90 degrees from the nature of $\tan 2\theta$. This condition is assigned as the **principal stress condition**. The maximum normal stress with the zero shear stress is called the **major principal stress** σ_1, while the minimum normal stress with the zero shear stress is called the **minor principal stress** σ_3 (note that $\sigma_3 < \sigma_1$). These principal stresses act on the **major** and the **minor principal stress planes** and intersect each other with 90^o as seen in Figure 10.3.

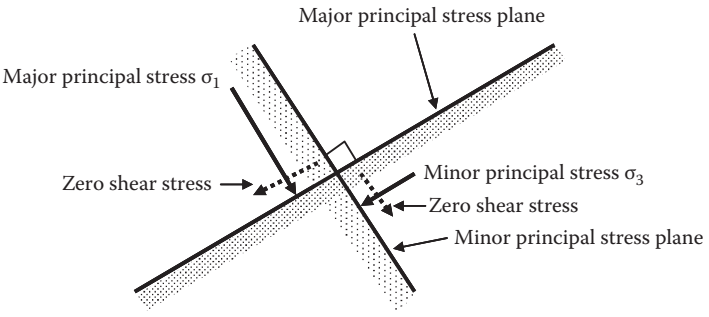

FIGURE 10.3 Major and minor principal stresses and corresponding planes.

By substituting Equation 10.5 into Equation 10.3 and Equation 10.4, Equation 10.6 and Equation 10.7 are obtained.

$$\sigma_\theta = \frac{\sigma_x + \sigma_y}{2} \pm \sqrt{\left(\frac{\sigma_x - \sigma_y}{2}\right)^2 + \tau_{xy}^2} \tag{10.6}$$

$$\tau_\theta = 0 \tag{10.7}$$

In Equation 10.6, the larger σ_θ value is assigned as σ_1 and the smaller one as σ_3, and the following major and minor principal stresses are obtained:

$$\sigma_1 = \frac{\sigma_x + \sigma_y}{2} + \sqrt{\left(\frac{\sigma_x - \sigma_y}{2}\right)^2 + \tau_{xy}^2} \tag{10.8}$$

$$\sigma_3 = \frac{\sigma_x + \sigma_y}{2} - \sqrt{\left(\frac{\sigma_x - \sigma_y}{2}\right)^2 + \tau_{xy}^2} \tag{10.9}$$

In Figure 10.2, when y-plane coincides with the major principal stress plane and x-plane is the minor principal stress plane, $\sigma_y = \sigma_1$, $\sigma_x = \sigma_3$, and $\tau_{xy} = \tau_{yx} = 0$; Equations 10.3 and Equation 10.4 yields to

$$\sigma_\theta = \frac{\sigma_1 + \sigma_3}{2} + \frac{\sigma_1 - \sigma_3}{2}\cos 2\theta \tag{10.10}$$

$$\tau_\theta = \frac{\sigma_1 - \sigma_3}{2}\sin 2\theta \tag{10.11}$$

Exercise 10.1

Boundary stresses σ_x and τ_{xy} on the x-plane and σ_y and τ_{yx} on the y-plane are given in Figure 10.4. Using analytical equations, compute σ_θ and τ_θ on the θ-plane, which inclines 20° clockwise from y-plane (horizontal plane).

Solution:

Comparing sign conventions in Figure 10.2 and Figure 10.4, assign σ_x = 50 kPa, σ_y = 25 kPa, τ_{xy} = –12.5 kPa and θ =–20°. Note that the directions of τ_{xy} and θ are

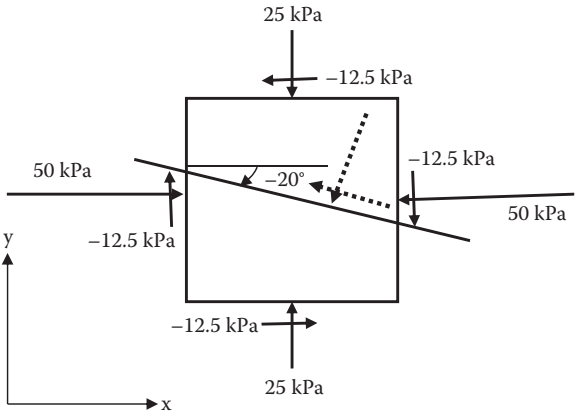

FIGURE 10.4 Exercise 10.1 problem.

opposite in between two figures and thus those are assigned as negative values. Appling the preceding values to Equation 10.3 and Equation 10.4,

$$\sigma_\theta = \frac{25+50}{2} + \frac{25-50}{2}\cos 2(-20°) + (-12.5)\sin 2(-20°) = 35.95\,\text{kPa}$$

$$\tau_\theta = \frac{25-50}{2}\sin 2(-20^o) - (-12.5)\cos 2(-20^o) = 17.60\,\text{kPa}$$

The directions of these solutions are drawn in Figure 10.4 with dotted lines. Note that both are positive numbers so that the directions of those stresses are the same as the ones in Figure 10.2.

As seen in Exercise 10.1, for analytical solutions, signs of the stresses and the plane direction shall match the ones in the figure (Figure 10.2) for which analytical equations (Equation 10.3 and Equation 10.4) are derived. In particular, positive or negative value of shear stress τ and plane direction angle (θ) shall not be mistaken.

10.4 MOHR'S CIRCLE CONSTRUCTION

The expressions of Equation 10.8 and Equation 10.9 suggest the construction of Mohr's circle as shown in Figure 10.5. In Mohr's circle, the normal stress is plotted in the horizontal axis and the shear stress in the vertical axis. And thus, a stress combination of σ and τ on a plane appears as a point on the drawing. The circle is a trace of those stress combinations on any arbitrary planes of an infinitesimal element. In Figure 10.5, X and Y points on the circle correspond to the stress combinations on x-plane and y-plane, respectively. Since $|\tau_{xy}| = |\tau_{yx}|$, a connected line between X and Y passes the center of the circle O. σ_1 and σ_3 are located on the normal stress σ axis,

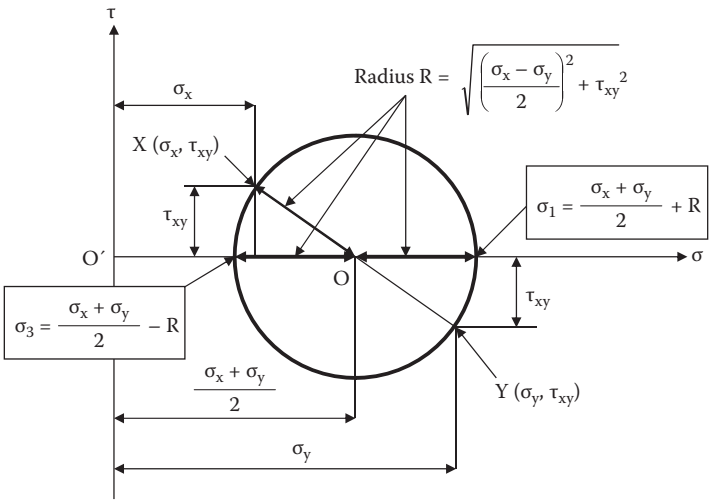

FIGURE 10.5 Mohr's circle construction (1).

where shear stresses τ are zero. From the geometry of the circle, Equation 10.8 and Equation 10.9 are readily identified.

When σ_1 and σ_3 are known values, Equation 10.10 and Equation 10.11 make Mohr's presentation much easier as seen in Figure 10.6; σ_1 and σ_3 are first plotted on the σ axis and a circle is drawn to pass through those points as the maximum and the minimum points. From the center of the circle, a radial line OA with angle 2θ is drawn counterclockwise from the σ_1 stress point. The values of σ and τ at Point A

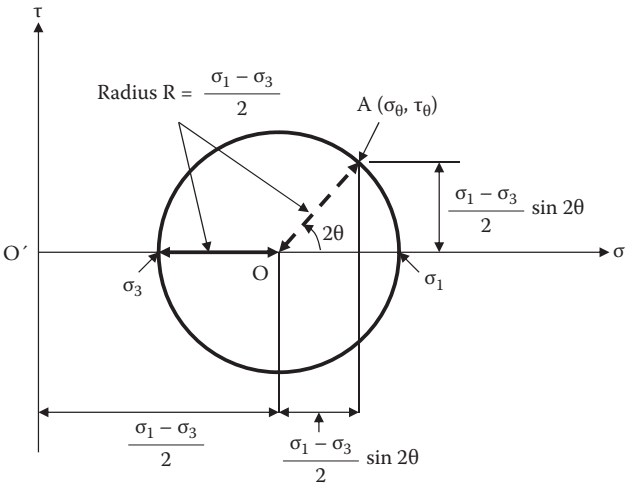

FIGURE 10.6 Mohr's circle construction (2).

give the stresses σ_θ and τ_θ on A plane (θ is the angle from the major principal stress plane counterclockwise). Equation 10.10 and Equation 10.11 can be easily obtained from the drawn geometry. The angle θ is arbitrary so that any stress combinations on any θ planes can be readily read on the circle. It shall be noted that the real angle θ between two planes appeared as 2θ on Mohr's circle in the same direction (either counterclockwise or clockwise). The above relationship (θ angle in real planes and 2θ angle in Mohr's circle in the same direction) is not limited to the σ_1 plane to an arbitrary plane θ as seen in Figure 10.6, but it is also applicable to any two arbitrary planes.

Exercise 10.2

Major and minor principal stresses are given as $\sigma_1 = 120$ kPa and $\sigma_3 = 50$ kPa as shown in Figure 10.7a. Determine the normal stress and shear stress on the plane, which inclined 45° counterclockwise from the horizontal.

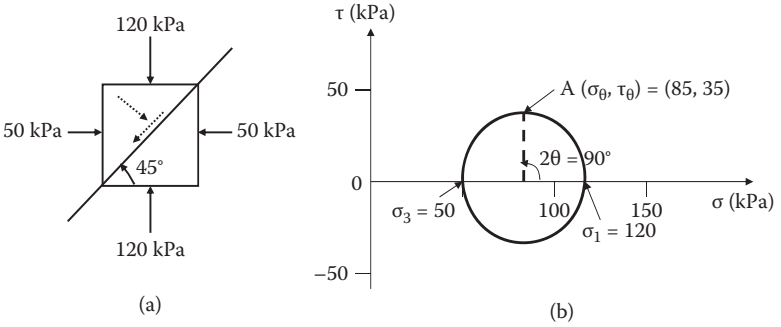

FIGURE 10.7 Exercise 10.2 problem and solution.

Solution:

On Mohr's circle, $\sigma_1 = 120$ kPa and $\sigma_3 = 50$ kPa are located on σ axis, and a circle is drawn to pass through those two points as seen in Figure 10.7b. $2\theta = 90°$ line is drawn counterclockwise from σ_1 stress point since the horizontal plane is σ_1 plane in the problem. Read the values of σ and τ at Point A, which gives $\sigma_{45} = 85$ kPa and $\tau_{45} = 35$ kPa. Both are positive values and those stress directions are shown in Figure 10.7a with dotted lines.

In all Mohr's circle problems, such as in Exercise 10.2, it is to be noted that the horizontal axis and the vertical axis shall be drawn with the same scales. Otherwise, a circle would no longer be a circle, and would be, rather, an oval shape, invalidating the graphic solution. Also drawing of a clear and large circle is essential to get accurate solutions. If circles are properly and carefully drawn, solution up to three digits accuracy could be possible.

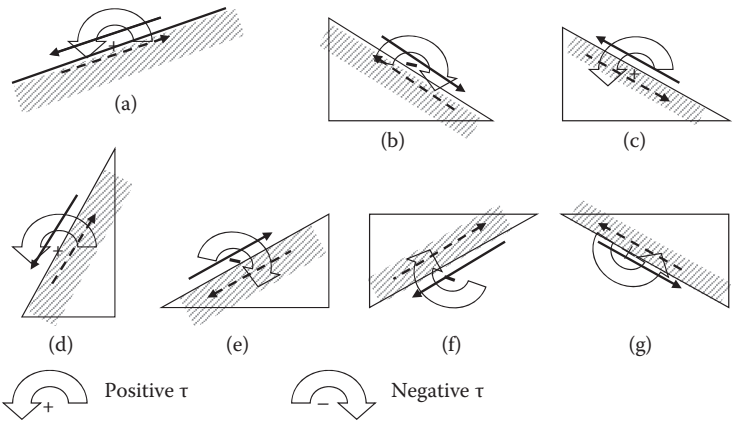

FIGURE 10.8 Sign convention of shear stresses.

10.5 SIGN CONVENTION OF SHEAR STRESS

In the discussions so far, it was clearly mentioned that (1) ***compressive normal stress is considered as positive,*** and (2) ***counterclockwise plane direction*** θ ***is treated as positive***. However, sign of shear stress has not been clearly defined. For example, in Figure 10.4, shear stress 12.5 kPa on the lower surface of the rectangle was treated as −12.5 kPa in order to adhere to the shear stress direction in Figure 10.2. Is the shear stress 12.5 kPa on the upper surface of the element negative, too, even if the directions are opposite to each other? The answer is that both are negative. Why is that so? It is crucial to clearly define the direction of shear stress in Mohr's circle. ***The sign convention of the shear stress is just a promise to make, but it must be adhered to its definition throughout the discussion***.

The authors recommend these to be defined as follows. As shown in Figure 10.8a, a real shear stress is applied on the surface of a body (downward and toward left). Draw an imaginary coupling shear stress with the same magnitude but in the opposite direction inside the body surface (shown in a dotted line). This pair of shear stresses makes a moment rotation. The direction of the moment is counterclockwise in the figure or it could be clockwise in other occasions. ***If the moment is counterclockwise, define it as positive shear stress. If the moment is clockwise, define it as negative shear stress***. Figure 10.8b–g shows several examples of the direction of moments. With the above definition, clearly shear stresses in (a), (c), (d), and (g) are positive and those in (b), (e), and (f) are negative.

Therefore, in Figure 10.4, shear stresses 12.5 kPa on the upper and lower surfaces make both counterclockwise rotation of the moment, and thus, they are positive shear stresses in this definition. On the other hand, on the right and the left surfaces of the element, both the moments are in clockwise directions, and thus, they are negative shear stresses. ***In Mohr's circles the upper domain ($\tau > 0$) is always for positive shear stresses, and the lower domain ($\tau < 0$) is for negative shear stresses***. These rules shall not be violated for correct utilization of Mohr's circle.

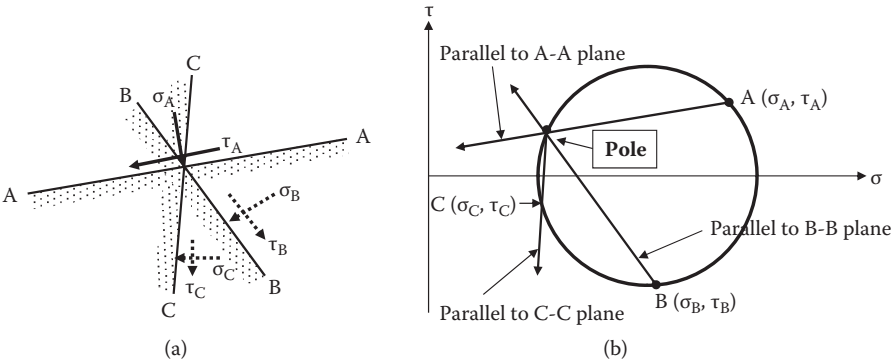

FIGURE 10.9 Determination of the pole.

10.6 POLE (ORIGIN OF PLANES) OF MOHR'S CIRCLE

The concept of the **pole** (or **origin of planes**) is a very powerful tool to solve many soil mechanics problems. In particular, it is conveniently utilized in describing the shear failure mechanism (Chapter 11) and the lateral earth pressure theory (Chapter 12).

In Figure 10.9a, known stresses σ_A and τ_A on a known A-A plane are drawn, and assume that Mohr's circle of this element is also known. Corresponding σ_A and τ_A is plotted as point "A" in the Mohr's circle in Figure 10.9b. Starting from the stress point A (σ_A, τ_A) on the circle, draw a parallel line to the direction of A-A plane, on which stresses (σ_A, τ_A) act. Find the intersection of the line on the circle. That is the "**pole**."

This is a unique point on the circle. If a line starts from any arbitrary stress point (i.e., B (σ_B, τ_B) in Figure 10.9b), the parallel line to B-B plane also passes through the pole. After the pole is found on Mohr's circle, starting from the pole, draw a parallel line to any particular plane (i.e., C-C plane in Figure 10.9a), and find the intersection C on Mohr's circle. Stresses (σ_C, τ_C) at Point C are the stresses that act on the C-C plane.

Exercise 10.3

Figure 10.10a shows the major and minor principal stress planes and an arbitrary A-A plane. Figure 10.10b shows corresponding Mohr's circle. The pole is determined first and then stresses on A-A plane are obtained at Point A by drawing parallel lines according to the pole method. In Mohr's circle's theory, the angle $AO\sigma_1$ in Figure 10.10c shall be 2θ. Prove it.

Solution:

Connect $A\sigma_3$, $A\sigma_1$ and $P\sigma_3$ in Figure 10.10c:

From the drawing, $\angle P'P\sigma_1 = \theta$.

From the trigonometry, $\angle A\sigma_1 P = \angle A\sigma_3 P = \alpha$ and $\angle P\sigma_3\sigma_1 = \angle PA\sigma_1 = \beta$

On the triangle $A\sigma_1 P$, $(\angle PA\sigma_1) + (\angle A\sigma_1 P) = \beta + \alpha = \angle P'P\sigma_1 = \theta$.

Therefore, $\theta = \beta + \alpha = \angle A\sigma_3\sigma_1$

On the cord $A\sigma_1$ of the circle, $\angle AO\sigma_1 = 2 \times (\angle A\sigma_3\sigma_1) = 2(\beta + \alpha) = 2\theta$

Thus, $\angle AO\sigma_1 = 2\theta$ has been proven.

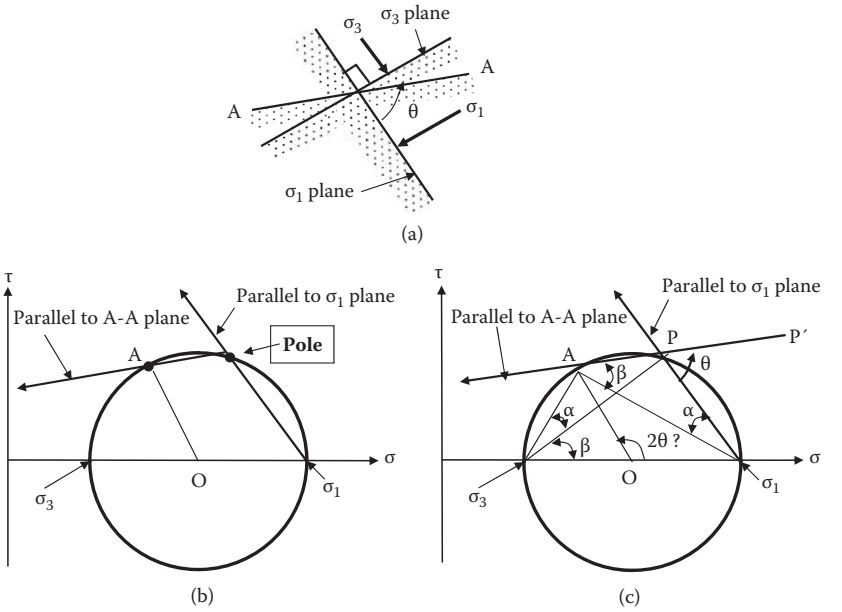

FIGURE 10.10 Exercise 10.3 (proof of the pole method).

Exercise 10.3 proves that the pole and then the stress point A determined by simple parallel drawing to its plane direction, indeed, is the same as the stresses on plane A found by θ (in real plane angle) and 2θ (in Mohr's circle) relation in Mohr's analytical method.

Thus, once the pole is found on Mohr's circle, stress combination (σ and τ) on any known plane can be found, simply by drawing a line starting from the pole parallel to the plane direction and by finding its intersection on the circle.

Exercise 10.4

Figure 10.11a shows a stress condition on an element, which is the same as Exercise 10.2, but the whole picture is rotated by 30° counterclockwise. By using the pole, determine stresses on the plane with 45° counterclockwise inclined from the major principal stress plane.

Solution:

First Mohr's circle is drawn with σ_1 = 120 kPa and σ_3 = 50 kPa in Figure 10.11b. Draw a line starting from σ_1 parallel to the σ_1 plane direction and find the pole at its intersection on Mohr's circle. Once the pole is found, start from the pole, and draw a line parallel to a 45° direction and then find the intersection on the circle

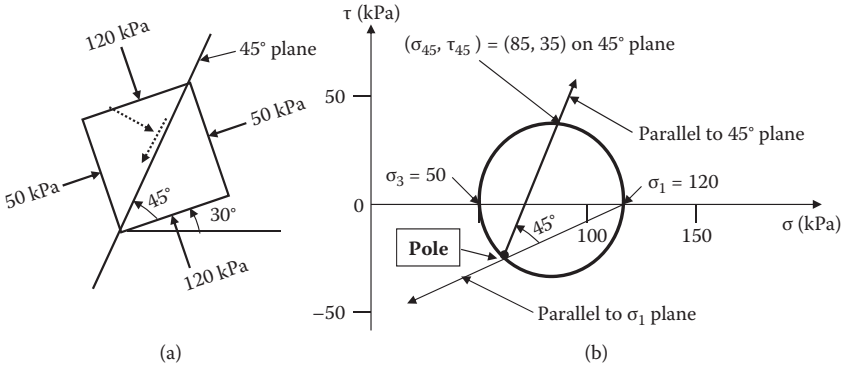

FIGURE 10.11 Exercise 10.4 problem and solution.

as the stress point on the 45° plane as seen. If the values are carefully read, σ_{45} = 85 kPa and τ_{45} = 35 kPa are obtained, which are the same solution as in Example 10.2. Rotation of the entire system did not change any stress values since relative plane directions were kept the same in those two exercises.

Exercise 10.5

Stresses on two perpendicular planes are given in Figure 10.12a, which is the same as Exercise 10.1. Using the pole's concept, find the stresses on a –20° plane and the directions of major and minor principal stress planes.

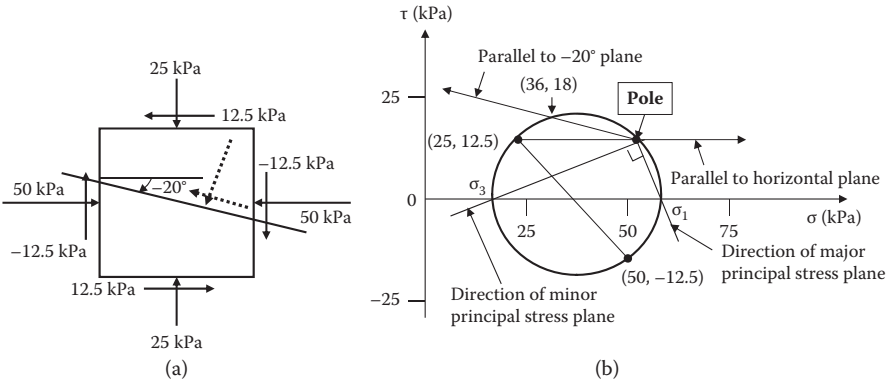

FIGURE 10.12 Exercise 10.5 problem and solution.

Solution:

First Mohr's circle is drawn in Figure 10.12b. Note that due to shear stress sign convention, the shear stresses on the vertical surfaces are assigned as negative (moment rotation is clockwise). Starting from (25, 12.5) on the mohr's diagram,

a horizontal line is drawn since the stresses (25, 12.5) act on the horizontal plane. Its Mohr's circle intersection is the pole. Starting from the pole, –20° line is drawn and the intersection on the circle finds stresses (36, 18), which give nearly the same result as in Exercise 10.1. Next connect the pole and σ_1 and σ_3 on the σ axis, which give the directions of the major and the minor principal stress planes, respectively, as seen in Figure 10.12b. As can be seen, those two principale stresses intercept each other at 90°.

The Mohr's circle concept so far is applied for infinitesimal square elements. However, it can be also applied to triangle elements as seen in the following exercise.

Exercise 10.6

In Figure 10.13a, stresses on Planes A and B are given. Determine normal and shear stresses on Plane C by using the pole.

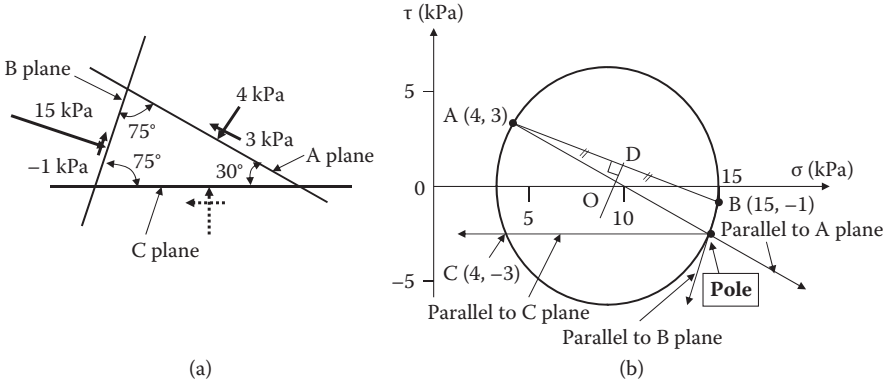

FIGURE 10.13 Exercise 10.6 problem and solution.

Solution:

In Figure 10.13b, draw stress points A and B on σ and τ domain. Note that the signs of shear stresses are already identified in Figure 10.13a according to the sign conventions of this chapter. Connect A and B and identify the mid-point D. From Point D, draw a normal line to find the center O of Mohr's circle on the σ axis. Draw a circle with the center O and passing the stress points A and B. Once Mohr's circle is determined, starting from A, draw a line parallel to A plane direction to find the pole as the intersection on the circle. If it starts from Point B, a line parallel to Plane B also passes the pole as shown in Figure 10.13b. Staring from the pole, draw the parallel line to C plane to find stresses on C plane at its intersection on the circle. It can be read as (4, –3) and the directions of these stresses are drawn in Figure 10.13a with dotted lines.

10.7 SUMMARY OF USAGE OF MOHR'S CIRCLE AND POLE

Graphical solution of Mohr's circle and the usage of the pole are summarized below:

1. Correctly identify the sign (positive or negative) of normal stresses and shear stresses according to Section 10. 5.
2. Draw a Mohr's circle either by known σ_1 and σ_3 as demonstrated in Exercises 10.2 and 10.4, or by two known stress points as in Exercises 10.5 and 10.6.
3. Draw a line from a known stress point in Mohr's circle parallel to the plane on which those stresses act. Find the intersection on the circle as the pole.
4. To find stresses (σ, τ) on any other plane, draw a straight line from the pole parallel to a desired plane and find the intersection on the circle, at which (σ, τ) can be read as the stresses on that particular plane.
5. To find the direction of the plane for a particular stress point on Mohr's circle, connect the pole and that stress point on the circle with a straight line, which yields the direction of the plane.

10.8 EXAMPLES OF USAGE OF MOHR'S CIRCLE AND POLE IN SOIL MECHANICS

Two important examples of utilization of the pole are given below, although these will be presented again in Chapters 11 and 12 in details.

10.8.1 Shear Failure Direction on Soil Specimen

As seen in Figure 10.14a, a cylindrical specimen is subjected to axial and lateral stresses σ_1 and σ_3. Stress σ_1 is increased until failure while σ_3 is kept constant. During

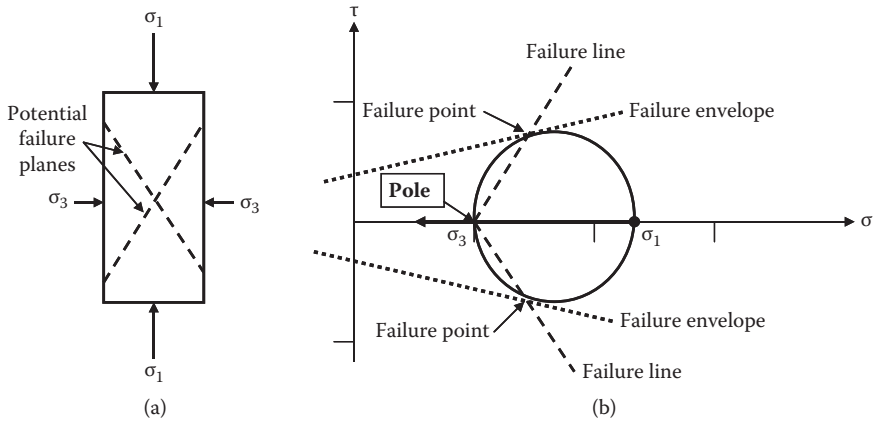

FIGURE 10.14 Directions of shear failure in triaxial compression test.

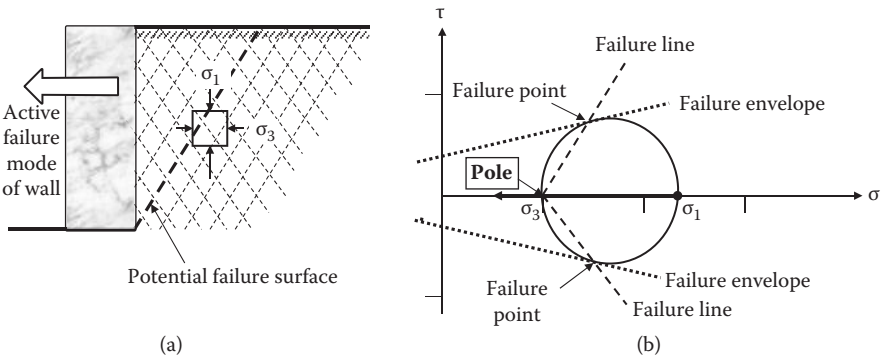

FIGURE 10.15 Failure zone in Rankine's active earth pressure theory.

that process, Mohr's circle increases in its diameter until it touches the failure envelopes as seen in Figure 10.14b. The circle in Figure 10.14b defines the stress condition at failure and failure points are identified on the circle.

First determine the pole. Staring from $\sigma_1$point and draw a parallel line to σ_1 plane, which is horizontal in this case. The intersection on the circle is the pole, which happens to be at σ_3. Starting from the pole, connect to the failure points on the circle. Those two lines are the directions of potential failure surfaces on the specimen as drawn in Figure 10.14a.

10.8.2 Failure Zone in Rankine's Lateral Earth Pressure Theory

Figure 10.15a shows a potential retaining wall failure when the wall may move in leftward direction (**active failure**). By knowing that $\sigma_1 > \sigma_3$, Mohr's circle is constructed, and the pole is identified in Figure 10.15b. Similar to the previous example for shear testing, potential failure lines are drawn by connecting the pole and the failure stress points in the circle. A group of failure lines are drawn in the backfill section of the wall, although the actual failure surface is the one with bold broken line. Those lines are parallel to the failure line directions in Figure 10.15b. The potential failure zone with a group of failure lines is called the **active failure zone** in **Rankin's theory** (Chapter 12).

10.9 SUMMARY

Mohr's circle is a very convenient tool in soil mechanics applications. However, clear definitions of sign conventions of shear stresses and normal stresses are necessary. In particular, the sign convention of shear stresses is critical for a proper usage of the concept. In this chapter, after defining the conventions clearly, the concept of the pole was introduced. Powerful applications of Mohr's circle with the concept of pole were demonstrated via shear failure surface determination during the shear test, and Rankine's lateral earth pressure theory. Those two topics are covered later in the book in detail (Chapters 11 and 12).

REFERENCE

Mohr, O. (1887), Über die Bestimmung und die graphische Darstellung von Trägheitsmomenten ebener Flächen, *Civilingenieur*, columns 43–68.

Problems

10.1 A soil element is subjected to the boundary stresses shown in the figure below. Determine analytically (not graphically) the normal stress σ_θ and the shear stress τ_θ on the θ-plane as identified. Note that only the magnitudes of the shear stress are shown in the figure. Their correct signs shall be determined according to the sign convention of Figure 10.2 for the analytical equations.

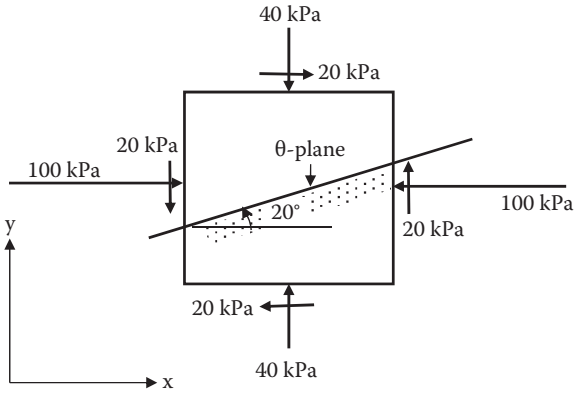

10.2 A soil element is subjected to the boundary stresses shown in the figure below. Determine analytically (not graphically) the normal stress σ_θ and the shear stress τ_θ on the θ-plane as identified. Note that only the magnitudes of the shear stress are shown in the figure. Their correct signs shall be determined according to the sign convention of Figure 10.2 for the analytical equations.

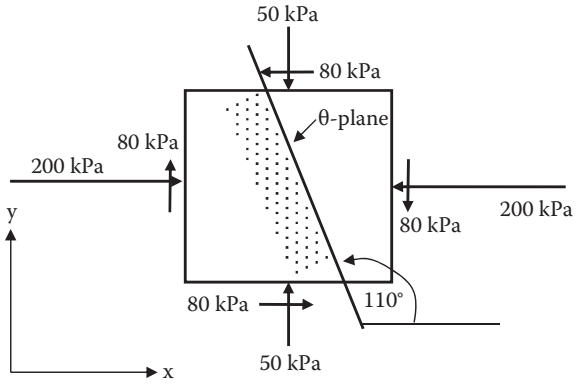

10.3 A soil element is subjected to the boundary stresses shown in the figure below. Determine analytically (not graphically) the normal stress σ_θ and the shear stress τ_θ on the θ-plane as identified. Note that only the magnitudes of the shear stress are shown in the figure. Their correct signs shall be determined according to the sign convention of Fig. 10.2 for the analytical equations.

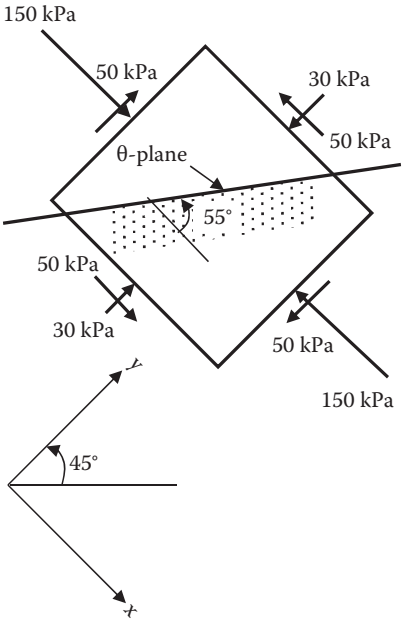

10.4 A soil element is subjected to the boundary stresses shown in the figure below. Determine analytically (not graphically) the normal stress σ_θ and the shear stress τ_θ on the θ-plane as identified. Note that only the magnitudes of the shear stress are shown in the figure. Their correct signs shall be determined according to the sign convention of Figure 10.2 for the analytical equations.

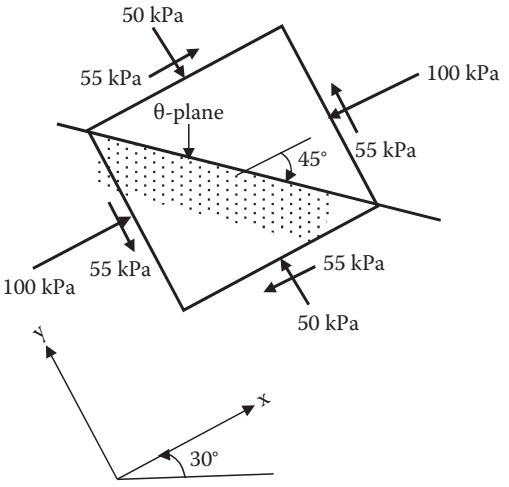

10.5 Identify the sign (positive or negative) of the shear stresses shown in the figure, according to the definition made in this book.

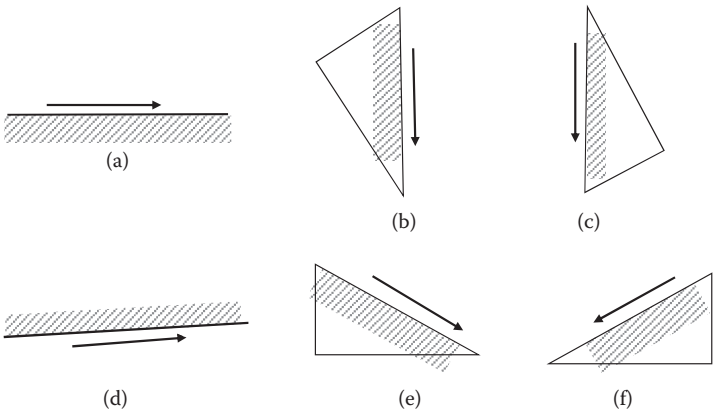

10.6. For the figure in Problem 10.1, solve it graphically by using Mohr's circle with the following steps
(a) Draw Mohr's circle.
(b) Identify the pole.
(c) Identify the stress point of the θ-plane.
(d) Read σ_θ and τ_θ values from the graph.
(e) Show the directions of those stresses on the surface of the θ-plane.

10.7 For the figure in Problem.10.2, solve it graphically by using Mohr's circle with the following steps
(a) Draw Mohr's circle.
(b) Identify the pole.
(c) Identify the stress point of the θ-plane.
(d) Read σ_θ and τ_θ values from the graph.
(e) Show the directions of those stresses on the surface of the θ-plane.

10.8 For the figure in Problem10.3, solve it graphically by using Mohr's circle with the following steps
(a) Draw Mohr's circle.
(b) Identify the pole.
(c) Identify the stress point of the θ-plane.
(d) Read σ_θ and τ_θ values from the graph.
(e) Show the directions of those stresses on the surface of the θ-plane.

10.9 For the figure in Problem10.4, solve it graphically by using Mohr's circle with the following steps
(a) Draw Mohr's circle.
(b) Identify the pole.
(c) Identify the stress point of the θ-plane.
(d) Read σ_θ and τ_θ values from the graph.
(e) Show the directions of those stresses on the surface of the θ-plane.

10.10 A triangular soil element is subjected to the boundary stresses as shown. Determine the normal stress σ_c and the shear stress τ_c on the C-plane as identified.

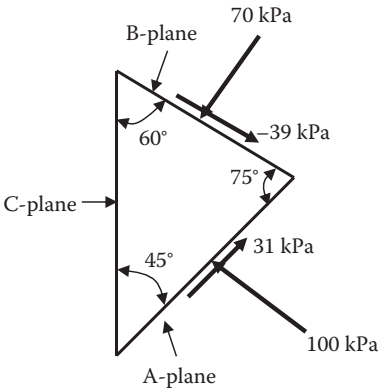

10.11. A triangular soil element is subjected to the boundary stresses as shown. Determine the normal stress σ_c and the shear stress τ_c on the C-plane as identified.

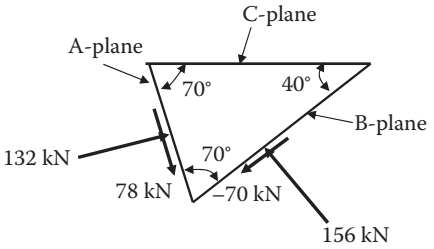

10.12. For a soil element shown in the figure, determine

(a) The magnitudes of the minor and the major principal stresses σ_1 and σ_3.

(b) Identify the directions of those planes in (a) above.

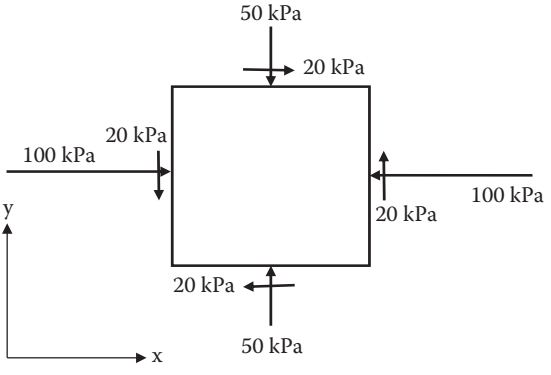

10.13. For a soil element shown in the figure, determine

(a) The magnitudes of the maximum and the minimum shear stresses τ_{max} and τ_{min} on Mohr's circle.

(b) Identify the directions of those planes in (a) above.

(c) What is the angle between those two planes in (b) above?

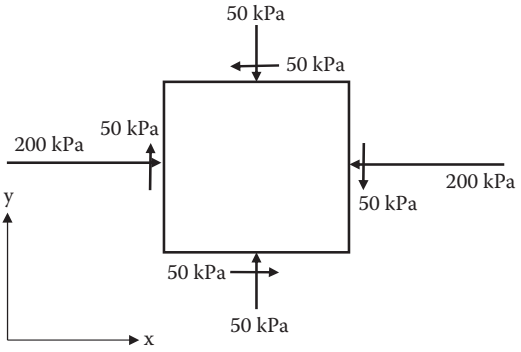

11 Shear Strength of Soils

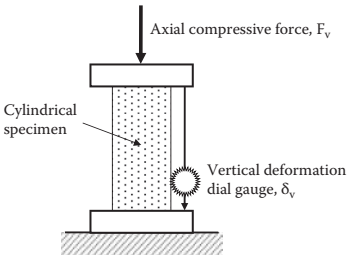

11.1 INTRODUCTION

The strength of soil is a key design parameter in designing building foundations, embankments, retaining structures, and other earth structures. In shallow foundation design, the capacity of the foundation to support footing load is given by the soil's **bearing capacity** (Chapter 13), which is a function of its strength parameters. **Lateral earth pressure** theories (Chapter 12) at ultimate stages (that is, active or passive failure stages) use the strength parameters of the soil. **Slope stability analysis** also requires the strength of the soil as a resisting force against sliding along a potential sliding surface. In this chapter, soil strength is defined and laboratory and field determination techniques on the shear strength parameters are presented. Proper interpretation of those parameters and the application to field problems are presented and critically reviewed.

11.2 FAILURE CRITERIA

Soil strength may be attributed to two distinctly different mechanisms of materials: one is its **frictional resistance** and the other is **cohesive resistance** along the shearing zone. As seen in Figure 11.1, shearing of a soil assemblage in (a), which is subjected to normal stress and shear stress, is modeled with a block on a solid plate with a rough surface as seen in (b). In the model, shear stress τ is resisted by frictional mechanism and cohesive resistance between the interface of the block and the solid plate. Frictional resistance $\tau_{friction}$ follows Coulomb's friction law ($\tau_{friction} = \sigma \tan\varphi$), where σ is the normal stress and φ is called the **angle of internal friction** of soil. The angle φ can be interpreted as the friction angle between facing soil elements along the shear surface. Cohesion resistance c is called **cohesion** of soil. In the block model, it could be simulated by heavy grease coated between the block and the plate, and thus, it is independent of the applied normal stress σ. In soils, normal

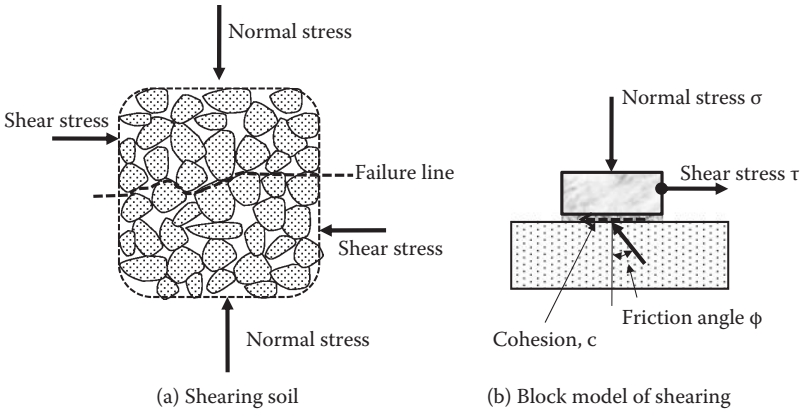

FIGURE 11.1 Shearing in soil mass.

stress independent cohesion comes from particle-to-particle close-range interactive forces as studied in Chapter 3, and it is a material property of fine particles (clays or cohesive soils).

Accordingly, the total shear stress at failure τ_f is expressed as

$$\tau_f = c + \sigma \tan\varphi \tag{11.1}$$

Equation 11.1 is a linear relationship between σ and τ and plotted as a straight line in Figure 11.2a. The line defined by Equation 11.1 is called the **failure envelope**, which implies that if any stress combination of σ and τ on any arbitrary plane (as shown in Figure 11.2b) plots below the failure envelope line, there is no failure. On the other hand, if stress combination of σ and τ goes above the envelope, the failure occurs on that plane. In practice, combinations of σ and τ cannot go beyond the envelope, and thus, the envelope defines the upper limit of stress combination on any plane of an element. Figure 11.2 also plots a mirror image of the failure envelope in the negative domain of the shear stress with a dotted line, since the negative shear stress merely

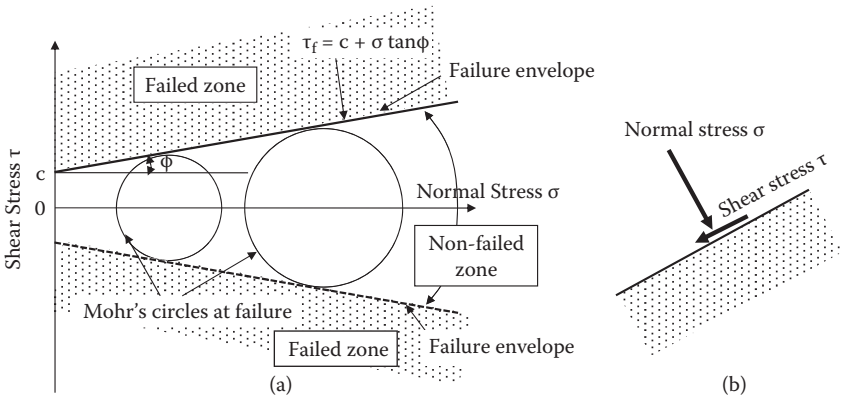

FIGURE 11.2 Failure criteria.

changes its direction, and thus those two failure envelopes define the safe limits of stress combination of σ and τ. In the figure, two Mohr's circles at failure are drawn, which make tangent at the failure envelopes as seen. In other words, Mohr's circles cannot cross the failure envelopes.

Equation 11.1 is called the **Mohr–Coulomb failure criteria**, which is attributed from Coulomb's contribution on frictional law and linear representation of its relation and Mohr's contribution on defining failure with a unique combination of normal stress σ and shear stress τ.

Figure 11.2 also suggests that importance of shear stress rather than normal stress on failure of soils. As an example, imagine a soil element in a deep earth such as in a deep salt mine (e.g., 1000 m deep). The vertical normal stress of the dry soil element at 1000 m deep is very high ($\sigma_v = \gamma_{soil} \bullet z \approx 20.0 \times 1000 = 20{,}000$ kPa). How can that soil element survive under such high normal stress? At that element, lateral normal stress σ_h is about a half of σ_v (see K_0 discussion in Chapter 12) and thus $\sigma_h \approx 10{,}000$ kPa. A Mohr's circle is drawn in Figure 11.3 for this soil element. Even though the circle has large σ values, it is still below the failure envelope, and thus it is safe in any plane directions. Increasing normal stress is not a critical factor for failure as seen in the above example. However, if shear stress τ is increased, it will easily touch the failure envelope, and thus, shear stress is critically important on the failure of soils. This is the reason why soil strength is often referred to as **shear strength**.

Terzaghi (1925) modified the Mohr–Coulomb equation to include his **effective stress concept** as

$$\tau_f = c' + \sigma' \tan\varphi' = c' + (\sigma - u) \tan\varphi' \tag{11.2}$$

where all strength parameters c' and φ' are expressed in terms of the effective normal stress σ' $(= \sigma - u)$. His concept is that soil strength is controlled by the effective stress (stresses in the soil's skeleton) rather than the total stress. It is found to govern the failure mechanism of soils, which is examined in detail later in this chapter.

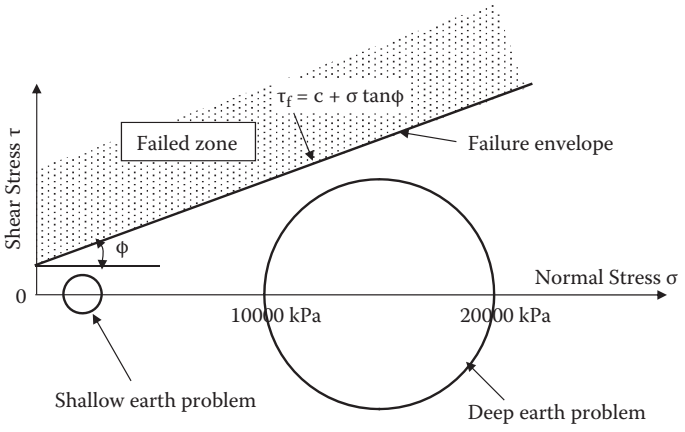

FIGURE 11.3 Deep earth and high normal stress problem.

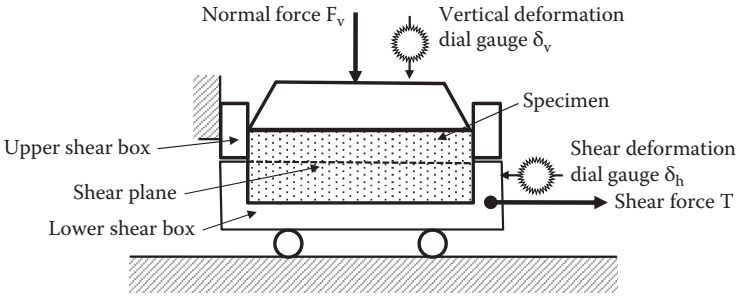

FIGURE 11.4 Direct shear test setup.

There are many different soil testing devices to determine c and φ or c′ and φ′ in the laboratory as well as in the field. Commonly used shear testing devices and their interpretation of results are discussed in the following sections.

11.3 DIRECT SHEAR TEST

This is the oldest and simplest device to determine soil strength parameters. As seen in Figure 11.4, it consists of upper and lower shear boxes, and a soil specimen is placed inside the box. Vertical normal force F_v and hence the normal stress σ (=F_v/specimen area) is applied and kept constant. In most devices, the upper box is fixed, and the lower box is movable on low friction rollers at the base. Also special care is made to minimize friction at contacting surfaces between the upper and the lower shear boxes such as with low friction Teflon push bolts, etc. The lower box is pulled or pushed to apply shear force T, and hence, the shear stress τ (=T/specimen area) is induced along the middle of the specimen.

In this device, shear failure surface is forced to develop in near horizontal direction. Measurements during the test are constant σ, and changes in τ, vertical deformation δ_v, and horizontal shear deformation δ_h. The change in δ_v measurement is directly proportional to the volume change of the specimen ΔV (= $\Delta\delta_v$ • specimen area) since the cross-sectional area of the specimen remains the same. Thus, under a given normal stress σ, τ versus $\Delta\delta_h$ and ΔV versus $\Delta\delta_h$ are plotted as seen in Figure 11.5.

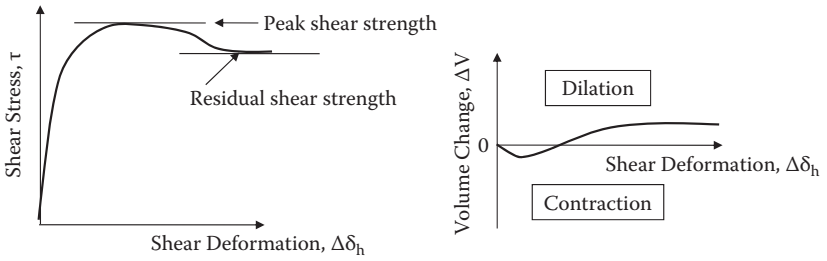

FIGURE 11.5 Direct shear test result.

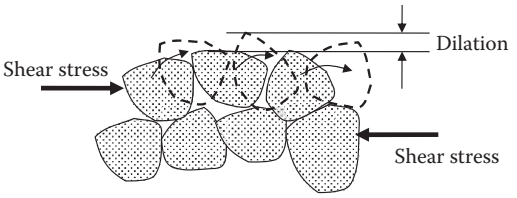

FIGURE 11.6 Dilatancy model.

Figure 11.5a defines the **peak shear strength** and the **residual shear strength**. The former is generally used as the shear strength of the soil τ_f. The latter is the strength after a large deformation, and it may be used to evaluate the stability of earth structures when large deformation is allowed beyond its peak strength.

Soil may contract or dilate during shearing as seen in Figure 11.5b, mostly depending on its initial density. It is interesting to notice that soil is a very unique material, which increases its volume upon application of shear stress (**dilatancy**), in particular, for dense sands and heavily overconsolidated clays. It is because densely packed grains or particles have to move or roll over neighboring grains to change their relative positions during shearing as seen in Figure 11.6.

For a given soil with a similar density, several direct shear tests are conducted under different normal stresses. Peak shear strength values τ_f are measured for each test. Then σ and τ_f relations are plotted as in Figure 11.7. A linear line relation is obtained through the data points and the intersection on τ_f axis gives the cohesion component c; the slope of the line makes the internal friction angle φ. For different soils and different densities, lines are different so that different c and φ values are obtained.

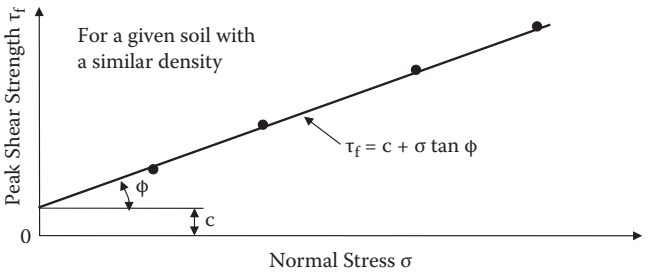

FIGURE 11.7 Determination of φ and c from direct shear tests.

11.4 UNCONFINED COMPRESSION TEST

This rather simple test is used for cohesive specimens only, which can stand alone without any lateral confinement of the specimen during the test. As seen in Figure 11.8, a specimen is trimmed to have a cylindrical shape and placed on a loading platform. The specimen height to diameter ratio shall be at least 2.0 or more to avoid the end boundary effect during the shear. Axial compressive force F_v is gradually increased until failure with a measurement of axial deformation δ_v.

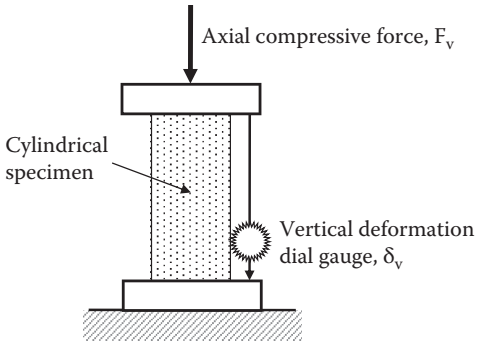

FIGURE 11.8 Unconfined compression test setup.

In general, the test is completed within 10 to 20 minutes so that during this process the water content of the specimen remains nearly constant. Pore water pressure may build up inside the specimen, but it will not have enough time to dissipate during a short period of shearing time. This process is called **undrained shear test** and discussed later in this chapter.

Axial normal stress σ_v (F_v/specimen area) and axial strain ε_v ($\Delta\delta_v$/initial specimen height) is plotted in Figure 11.9. Two curves for typical soils are seen: (a) heavily overconsolidated or dense soils with a clear peak value, and (b) for normally consolidated or loose soils without a clear peak value. The peak σ_v values or σ_v values at a certain defined failure strain ε_v, e.g. at ε_v = 10% or 15% strain, etc., are taken as **unconfined compression strength** q_u. In this experiment, q_u is the major principal stress at failure. Lateral normal stress is the minor principal stress and is zero with no lateral confinement (unconfined). Accordingly, Mohr's circle is drawn as in Figure 11.10. A horizontal failure envelope ($\varphi = 0$) is drawn to contact the failure Mohr's circle. Thus, the maximum shear stress at failure C_u is equal to

$$C_u = q_u/2 \tag{11.3}$$

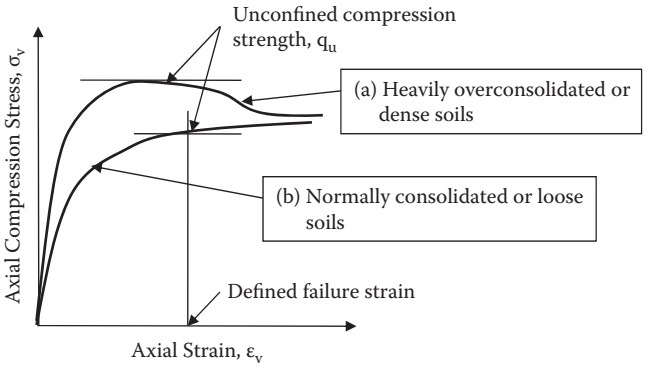

FIGURE 11.9 Unconfined compression test result.

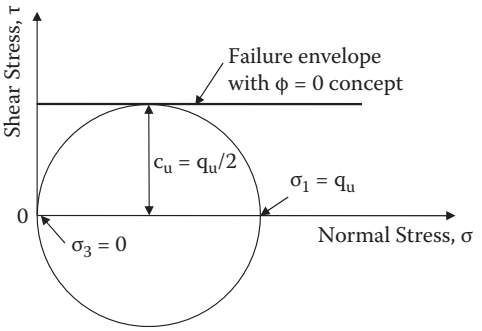

FIGURE 11.10 Determination of C_u from unconfined compression test.

In Figure 11.10, a horizontal failure envelope is drawn and is called as $\varphi = 0$ **concept** in determining shear strength of cohesive soils It will be discussed later in the section of **unconsolidated undrained test**.

11.5 TRIAXIAL COMPRESSION TEST

11.5.1 General Concept and Test Setup

A triaxial compression test device is routinely used to determine the shear strength of soils for more general stresses and drainage conditions. It applies three principal stresses, σ_1, σ_2, and σ_3, to a cylindrical specimen and the intermediate principal stress σ_2 is equal to the minor principal stress σ_3 as seen in Figure 11.11. The axial stress is increased until failure, while the lateral confining pressure is kept constant during the shear. Thus, the axial stress is the major principal stress σ_1 and the lateral confining pressure is the minor principal stress σ_3. Note that since σ_2 is always equal to σ_3, and thus, this is not tri(three)-axial test equipment in the true sense of the term.

A specimen is enclosed in a thin rubber membrane (typically 8–15 μm thick) and placed on a loading platform. Figure 11.12 shows the schematic setup of a typical triaxial compression test device. In this system, the lateral confining pressure is applied through a thin rubber membrane to the specimen via chamber pressure. During the test, the confining pressure, in general, is kept constant and the axial compressive

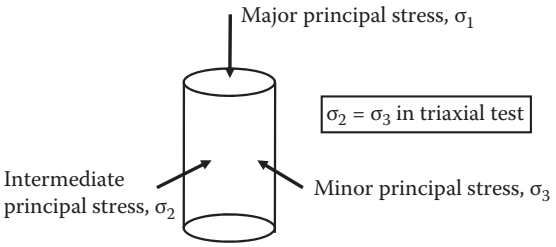

FIGURE 11.11 Triaxial stresses on a cylindrical specimen.

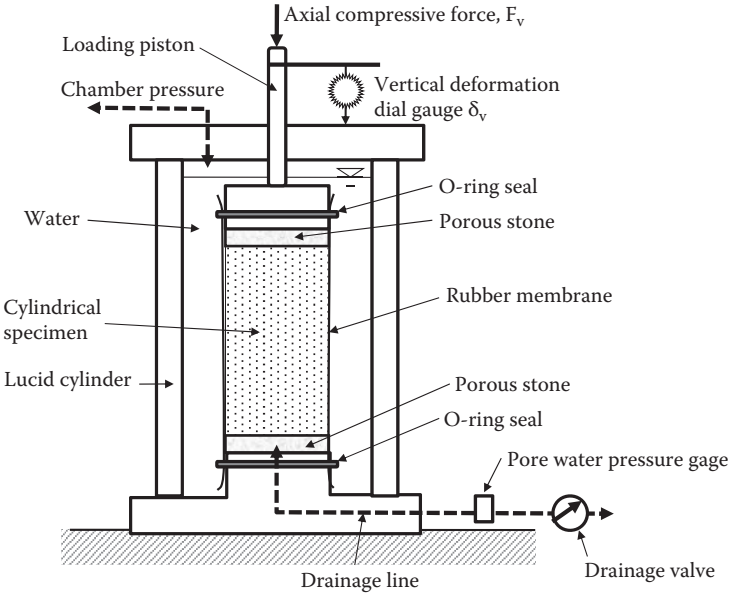

FIGURE 11.12 A typical triaxial test setup.

force F_v is increased to failure. The vertical deformation δ_v is measured to compute the axial strain.

For a free body diagram of the upper section of soil specimen as seen in Figure 11.13, the vertical force equilibrium is established by neglecting weight of soil, loading cap, and loading piston as follow:

$$F_v + \sigma_3 \bullet A_s = \sigma_1 \bullet A_s, \text{ and thus, } F_v/A_s = \sigma_1 - \sigma_3 \tag{11.4}$$

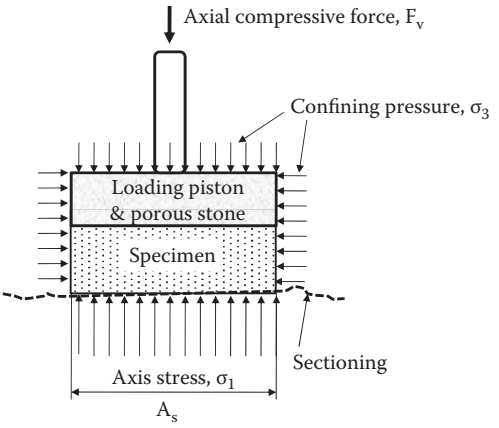

FIGURE 11.13 Free body diagram of triaxial specimen.

where F_v is the applied vertical force on the top of the piston and A_s is the specimen's cross-sectional area. $\sigma_1 - \sigma_3$ is called the **deviatoric stress,** and it is increased from zero to failure stress during the shear test.

In a typical triaxial test, the confining stress σ_3 is kept constant and the vertical force F_v is increased until failure. The deviatric stress $\sigma_1 - \sigma_3$ ($=F_v/A_s$) and the vertical strain ε_1 ($=\delta_v/L_o$) is monitored, where δ_v is the measured vertical deformation increment and L_o is the initial specimen height.

Exercise 11.1 demonstrates how to utilize triaxial test data to obtain shear strength parameters c and φ in general sense.

Exercise 11.1

Triaxial test data with three different confining pressures for a similar soil are shown in Figure 11.14. The deviatric stress $(\sigma_1 - \sigma_3)$ is plotted with the vertical strain ε_1 and the failure strengths $(\sigma_1 - \sigma_3)_f$ are identified for those tests. After drawing Mohr's circles at failure for three specimens, determine cohesion component c and the angle of internal friction φ of this soil.

Solution:

From the data,
For Specimen 1

$\sigma_3 = 80$ kPa

$(\sigma_1 - \sigma_3)_f = 174$ kPa and thus,

$\sigma_{1f} = (\sigma_1 - \sigma_3)_f + \sigma_3 = 174 + 80 = 254$ kPa.

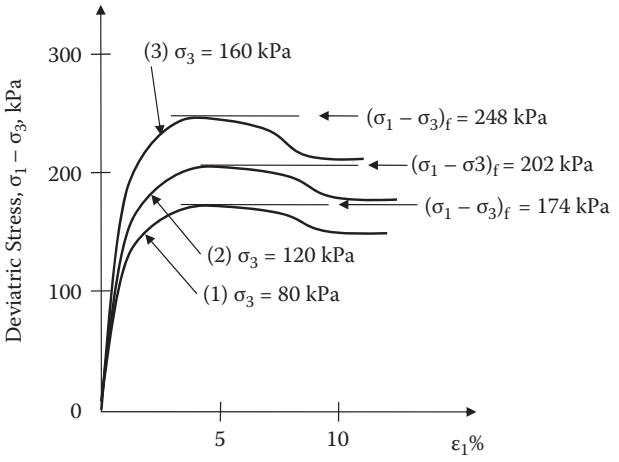

FIGURE 11.14 Exercise 11.1 problem (results from triaxial tests).

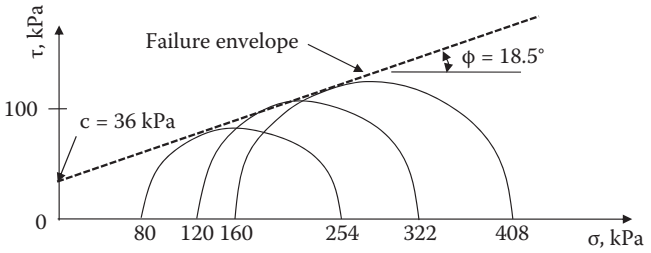

FIGURE 11.15 Exercise 11.1 (determination of φ and c).

For Specimen 2

$\sigma_3 = 120$ kPa

$(\sigma_1 - \sigma_3)_f = 202$ kPa and thus,

$\sigma_{1f} = (\sigma_1 - \sigma_3)_f + \sigma_3 = 202 + 120 = 322$ kPa.

and

For Specimen 3

$\sigma_3 = 160$ kPa

$(\sigma_1 - \sigma_3)_f = 248$ kPa and thus,

$\sigma_{1f} = (\sigma_1 - \sigma_3)_f + \sigma_3 = 248 + 160 = 408$ kPa.

Based on the above σ_{1f} and σ_3 values, Mohr's circles at failure are constructed in Figure 11.15. A failure envelope is also drawn by just touching those Mohr's circles at failure, and the cohesion c and the angle of internal friction φ are read as **36 kPa** and **18.5°**, respectively, as seen.

Real practice of triaxial test requires more detailed techniques on how the specimen is prepared and how it is sheared in terms of pore water pressure dissipation during the shear. In this respect, the drainage line and the drainage valve in Figure 11.12 play significant roles. As seen in the figure, the drainage line is connected from the inside of the specimen through the porous stone. During the preshearing process, the drainage value is kept open to allow the dissipation of induced pore water pressure for a **consolidated test** or kept closed for an **unconsolidated test**. During the shear, the drainage valve could be either closed for an **undrained test** or opened for a **drained test**. When the valve is closed, the pore water pressure gauge monitors the pore water pressure buildup inside the specimen.

11.5.2 Initial Consolidation Process and Drainage Condition during Shear

In the following discussions, it is assumed that soils are fully saturated. A triaxial specimen is, in general, brought to the laboratory in a thin wall tube. It is then

extruded, and trimmed into a cylindrical specimen with approximately 2 to 1 sample height to diameter ratio. The specimen is then placed in the device, and the confining pressure through the membrane is increased to a certain value. At this stage, if the drainage valve is open, the specimen will be compressed by the confining pressure, and the water in pore space of the specimen will be squeezed out through the drainage line and consolidation process will take place. When the specimen is left for several hours to an overnight, primary consolidation will be completed under an applied confining pressure. The process is called a **consolidated test** for sample preparation process. When the previously described consolidation process is not allowed, by keeping the drainage valve closed, or by not allowing sufficient time for consolidation, the test is called an **unconsolidated test**.

During the shear, the drainage line could be kept open for a **drained test** or closed for an **undrained test**. Note that drained test cannot be simply accomplished by opening the drainage valve. It is rather accomplished by allowing generated pore water pressure be fully dissipated during the process of shear, and thus a drained test takes, in general, a long time (slow shearing) for cohesive soils such as a few days to a week or more. On the other hand, an undrained test does not require a long shearing time as in a drained test, and it could be completed in an hour or so (quick shearing). In general, undrained tests are accompanied with pore water pressure measurement.

Thus, types of triaxial tests are any combination of **preshear** conditions (either consolidated or unconsolidated) and **drainage conditions during shear** (either drained or undrained). Four combinations are possible, but the three listed below are practically used:

Consolidated Drained Test (CD Test, S Test)
Consolidated undrained test (CU test, Q_c test) with/without pore water pressure measurement.
Unconsolidated Undrained Test (UU Test, Q_u Test)

In the previous list, "S test" stands for "slow test" since the drainage process during the shear takes a long time, and "Q test" stands for "quick test" since an undrained test could be finished in a short time. Note that S and Q designations only will be applicable for cohesive soils. For granular soils (sands and gravels), both drained and undrained tests do not require a large amount of time due to the high permeability of the materials.

11.5.3 Consolidated Drained (CD) Triaxial Test

First, the specimen is fully consolidated and then it is sheared slowly to allow the generated pore water pressure to be fully dissipated. It requires at least one day for the consolidation process and several days for conducting drained shear. First, a clay specimen is prepared with enough water to have the water content above its liquid limit, and then the consolidated drained test is performed. For nearly zero consolidation pressure, the strength of specimen is nearly equal to zero since the specimen's

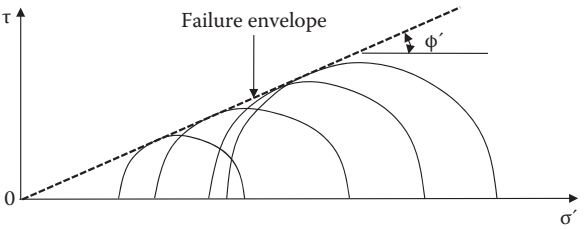

FIGURE 11.16 Failure envelope from CD test for normally consolidated soils.

initial water content was above the liquid limit. With a small consolidation pressure, the specimen gains some strength due to the consolidation process. During the shear it also gains some more strength due to the drainage of water. With higher consolidation pressure, it gains more strength due to its higher reduction in water content through the consolidation and drained shear processes. Accordingly, nearly proportional sizes of failure Mohr's circles to their consolidation pressures are drawn to define the failure envelope of the soil as seen in Figure 11.16.

The preceding specimens started from a very high water content (above their liquid limit) and gradually gained strength due to consolidation in a process similar to the natural forming of soil deposits under bottoms of lakes or rivers. These are called **normally consolidated soils** as discussed in the consolidation section of Chapter 9. Accordingly, consolidated drained strength of normally consolidated soils is expressed as

$$\tau_f = \sigma' \tan \varphi' \tag{11.5}$$

This is the same equation as in Equation 11.2 (Terzaghi's effective stress equation) with $c' = 0$. During the drained test, pore water pressure is zero, and thus, the applied total stress is also the effective stress. ***Note that zero cohesion component c′ in this case does not necessarily mean that soil is resisted purely by friction. In fact, shear resistance of clays is mostly contributed from cohesive resistance, but its expression merely implies that when consolidation pressure is zero, then there will be no strength.*** This discussion suggests that failure criteria in Equation 11.1 and Equation 11.2 shall be considered as just expressions to determine failure shear strength τ_f, and that ***the strength parameters (c, φ, and c′, φ′) are not the cohesion and friction of the materials in true sense, but rather the cohesive and frictional components in those expressions***.

A soil specimen that was brought from the field has been subjected to at least in situ effective overburden stress or even higher effective stress during its historical time as discussed as normal or overconsolidated soils in Chapter 9. Thus, when the soil is sheared in a consolidated drained test, it has some amount of shear strength due to its preconsolidation stress even for small laboratory consolidation stress. When the consolidation stress in the test is less than the preconsolidation stress, the specimen is overconsolidated. Figure 11.17 plots Mohr's circles at failure for overconsolidated specimens. The failure envelope has the form of Equation 11.2 with cohesion component c′ and frictional component φ′.

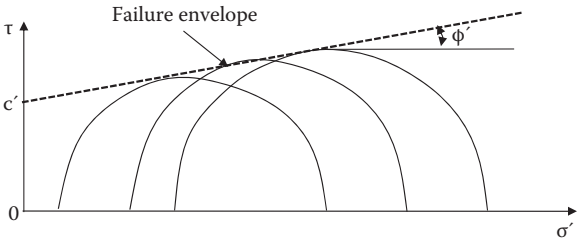

FIGURE 11.17 Failure envelope from CD test for overconsolidated soils.

When the consolidation stress exceeds its preconsolidation stress, then the shear strength will follow the failure envelope observed in Figure 11.16 or Equation 11.5. Accordingly, the entire failure envelope from the consolidated drained test consists of two straight lines as shown in Figure 11.18: Curve (a) or Equation 11.2 for the consolidation stress up to its preconsolidation stress, and Curve (b) or Equation 11.5 for the consolidation stress above the preconsolidation stress. A bi-linear failure envelope is analogical to the bi-linear e-log σ curve of the consolidation test as seen in Figure 11.19. Below and above the preconsolidation stress, the rates of soils′ volume change and shear strength are quite different.

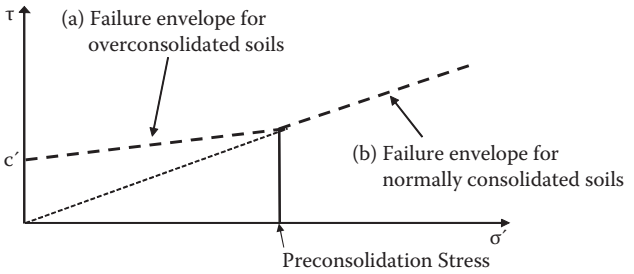

FIGURE 11.18 Failure envelope from CD test for full range of consolidation stresses.

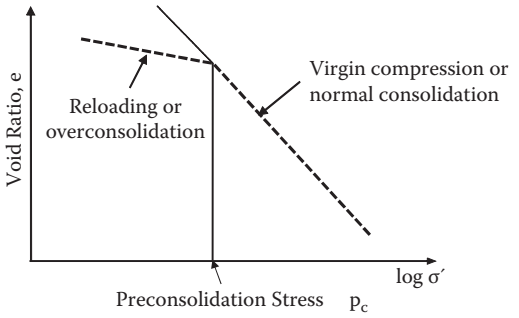

FIGURE 11.19 e-log σ′ curve from consolidation test.

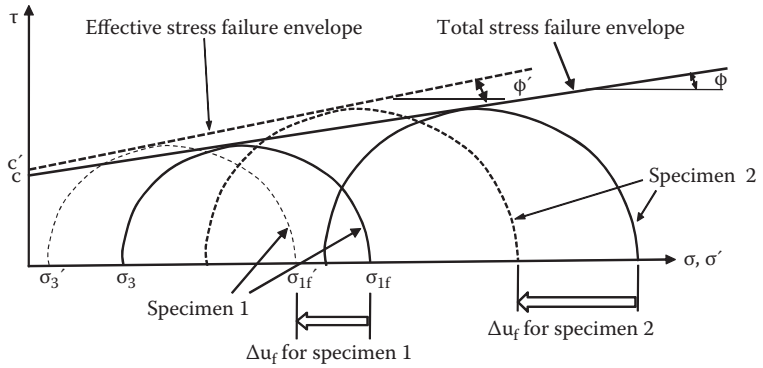

FIGURE 11.20 Total stress and effective stress analyses from CU test.

11.5.4 Consolidated Undrained (CU) Triaxial Test with Pore Water Pressure Measurement

This is the most widely used triaxial shear test in practice. The specimen is first fully consolidated in the triaxial cell. Then the drainage valve is closed and sheared by increasing the deviatric stress $\sigma_1 - \sigma_3$ to failure while σ_3 is kept constant. At the same time, pore water pressure Δu is measured during shearing process. Measurements during the test are $\sigma_1 - \sigma_3$, and Δu with the vertical strain ε_1.

By obtaining σ_3, σ_{1f}, and Δu_f at the failure for a given specimen, the total principal stresses (σ_3, σ_{1f}) as well as the effective principal stresses ($\sigma_3' = \sigma_3 - \Delta u_f$, $\sigma_{1f}' = \sigma_{1f} - \Delta u_f$) are calculated and Mohr's circles at failure are drawn both in the total stress and in the effective stress. These circles are shown in Figure 11.20, where solid lines are in the total stress and dotted lines are in the effective stress. The diameters of Mohr's circles are the same for both total stress and effective stress, but the latter circle is shifted toward left with an amount of Δu_f for a positive pore water pressure at failure.

Similarly, another set of failure Mohr's circles are drawn for differently consolidated Specimen 2. The failure envelopes, which are tangent to those circles, are then drawn to determine the total stress strength parameters c and φ as well as the effective stress parameters c′ and φ′ as seen. To obtain these strength parameters, at least two CU tests with different consolidation stresses are needed as in Figure 11.20. In practice, however, three or more CU tests with different consolidation stresses for similar specimens are performed to determine reliable c, φ, c′, and φ′ values.

Exercise 11.2

Consolidated undrained triaxial tests for two similar specimens with different consolidation stresses were performed and the data in Figure 11.21 is obtained, which includes pore water pressure measurements. Plot Mohr's circles at failure for two specimens in both the total stress and in the effective stress and determine the shear strength parameters c and φ from the total stress failure envelope and c′ and φ′ from the effective stress failure envelope.

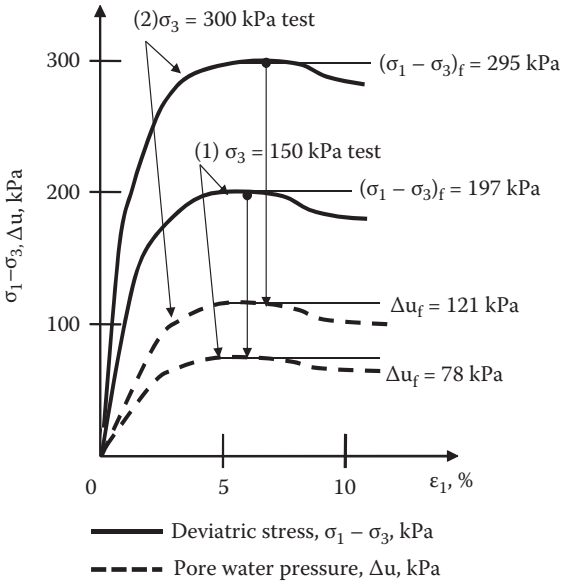

FIGURE 11.21 Exercise 11.2 problem (results from CU tests).

Solution:

From the data plot,
For Specimen 1,

$$\sigma_3 = 150 \text{ kPa}$$

$$(\sigma_1 - \sigma_3)_f = 197 \text{ kPa}$$

$$\Delta u_f = +78 \text{ k Pa}$$

and thus,

$$\sigma_{1f} = (\sigma_1 - \sigma_3)_f + \sigma_3 = 197 + 150 = 347 \text{ kPa}.$$

Effective stresses are:

$$\sigma_3' = \sigma_3 - \Delta u_f = 150 - 78 = 72 \text{ kPa}$$

$$\sigma_{1f}' = \sigma_{1f} - \Delta u_f = 347 - 78 = 269 \text{ kPa}$$

For Specimen 2,

$$\sigma_3 = 300 \text{ kPa}$$

$$(\sigma_1 - \sigma_3)_f = 295 \text{ kPa}$$

$$\Delta u_f = 121 \text{ k Pa}$$

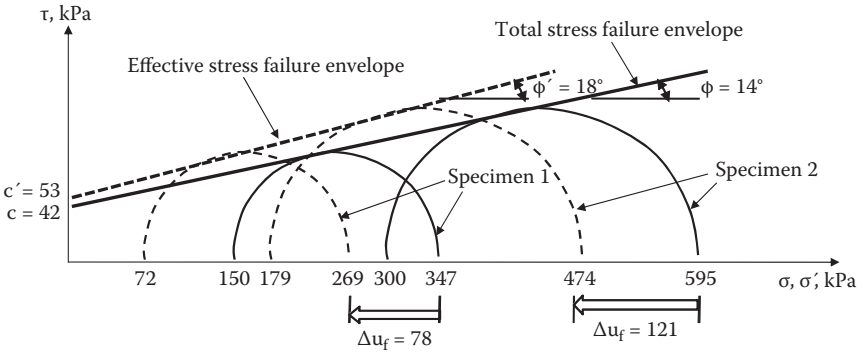

FIGURE 11.22 Exercise 11.2 (determination of c, φ and c′, φ′).

and thus,

$$\sigma_{1f} = (\sigma_1 - \sigma_3)_f + \sigma_3 = 295 + 300 = 595 \text{ kPa}$$

Effective stresses are

$$\sigma_3' = \sigma_3 - \Delta u_f = 300 - 121 = 179 \text{ kPa}$$

$$\sigma_{1f}' = \sigma_{1f} - \Delta u_f = 595 - 121 = 474 \text{ kPa}$$

From those values, Mohr's circles at the failure are drawn in Figure 11.22. The total stress failure envelope is drawn to touch the total stress Mohr's circles (solid lines) and the effective stress failure envelope is drawn to touch the failure circles in effective stresses (doted lines). Accordingly, c = 42 kPa, φ = 14° for the total stress, and c′=53 kPa , φ′ = 18° for the effective stress are read from the plot.

From the consolidated undrained (CU) test with pore water pressure measurement, similar bi-linear failure envelopes are obtained independently for the total stress (solid line) and for the effective stress (dotted line) as seen in Figure 11.23.

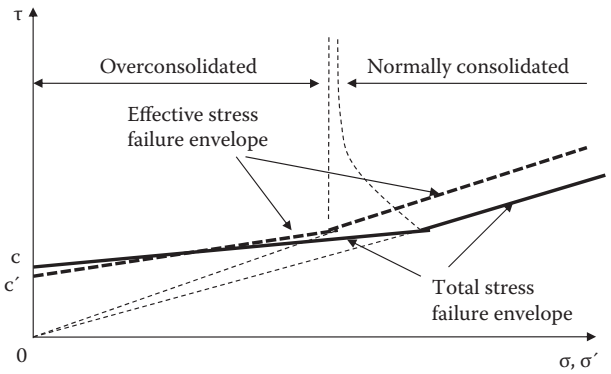

FIGURE 11.23 Failure envelopes from CU test for full range of consolidation stresses.

It shall be noted in Figure 11.23 that the breaking points of the two bi-linear failure envelopes that separate the normally consolidated and the overconsolidated specimens could not be at the same normal stress since the Mohr failure circle for the effective stress moves towards left from the Mohr failure circle for the total stress with the same diameter when positive pore water pressure is generated. Also, it can be seen that for a small consolidation stress region, where the overconsolidation ratio (OCR) is high, there could be negative pore water pressure buildup at failure, and thus the Mohr failure circle for the effective stress could be drawn to the right side of the Mohr failure circle for the total stress. This could result in overlapping of the failure envelopes at a low consolidation stress, as seen.

11.5.5 Effective Stress Parameters from CU and CD Tests

The CU test result provides c' and φ' values, in addition to c and φ, when analyzed in the effective stress using measured pore water pressure. These c' and φ' parameters have the same meanings of c' and φ' obtained from the consolidated drained (CD) shear test, since CD test data is always analyzed in the effective stress (=total stress) with zero pore water pressure. In fact, ***Rendulic (1936)*** had shown experimentally that ***the effective stress failure envelope is unique regardless of testing methods (drained or undrained)***. The above fact enables engineers to save testing time by running rather quick CU test and obtaining drained parameters c' and φ' by doing the effective stress analysis, instead of running a slow CD test. In another words, ***the effective stress analysis of CU test result can be substituted for a CD test***.

Another important conclusion on the shear strength is that ***the unique effective failure envelope is the one to govern the failure mechanism of soils***. For example, when the undrained total stress strength is known, the amount of pore water pressure generation can be estimated with the knowledge of the uniqueness of the effective failure envelope, as demonstrated in Exercise 11.3.

Exercise 11.3

For a normally consolidated specimen, it was found that $\varphi = 16°$ and $\varphi' = 28°$. If a similar specimen is sheared with $\sigma_3 = 120$ kPa in CU test with pore water pressure measurement, estimate the deviatric stress $(\sigma_1 - \sigma_3)_f$ and pore water pressure Δu_f at failure.

Solution:

1. Since the specimen is normally consolidated, draw total and effective stress failure envelopes from the origin (c = 0) with $\varphi = 16^o$ and $\varphi' = 28^o$, respectively, as seen in Figure 11.24.
2. Draw the total stress failure Mohr's circle with $\sigma_3 = 120$ kPa, which touches the total stress failure envelope and read $\sigma_{1f} = 205$ kPa on the graph. And thus the deviatric stress at failure $\mathbf{(\sigma_1 - \sigma_3)_f} = 205 - 120 = \mathbf{85\ kPa}$ (diameter of the Mohr's circle).←

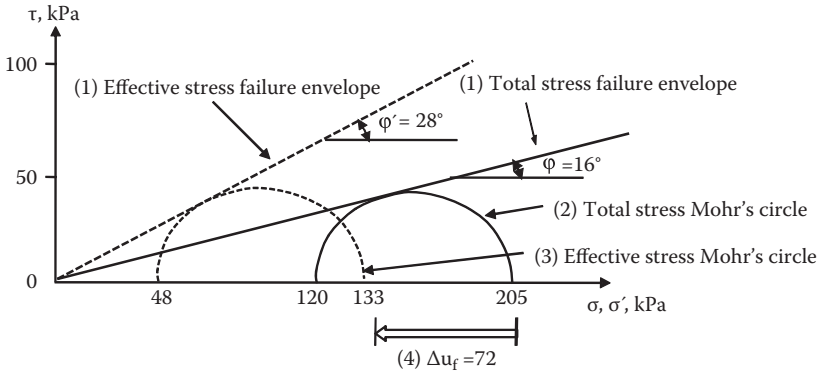

FIGURE 11.24 Exercise 11.3 solution.

3. With the same diameter with the above circle, draw the effective stress failure Mohr's circle, which contacts at the effective stress failure envelope and read $\sigma_3' = 48$ kPa and $\sigma_{1f}' = 133$ kPa on the graph.
4. Pore water pressure generation at the failure is the amount of horizontal shift on two Mohr's circles and thus $\Delta u_f = 205 - 133 =$ **72 kPa** as seen in the graph.

In Exercise 11.3, since the effective stress failure envelope is unique, the amount of pore water pressure generation (shift of failure Mohr's circle to left) is governed by the effective stress failure envelope.

11.5.6 Unconsolidated Undrained (UU) Test

The simplest triaxial compression test would be an **unconsolidated undrained (UU) test**. During sample preparation time, the specimen is not allowed any consolidation process. Shortly after placing the specimen in the chamber, the confining stress is applied through the specimen membrane and sheared under undrained condition; that is, the drainage valve is kept closed, and it is sheared in a short time. Since during the sample preparation and shearing processes, there will be no escape of the pore water from the specimen, and thus, no change in the water content of the specimen will take place. Therefore, the anticipated soil strengths are the same for any confining stress. Figure 11.25 shows Mohr's circles at failure for similar fully saturated

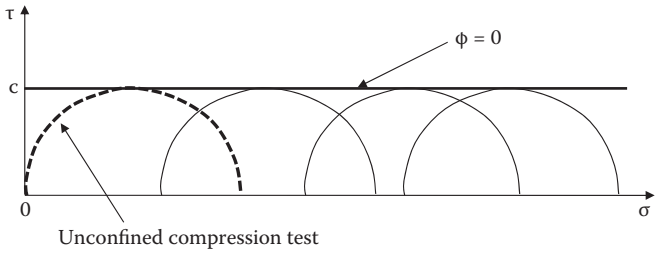

FIGURE 11.25 UU test results and $\varphi = 0$ concept.

specimens under different confining stresses from the UU test. The diameters of Mohr's circles at failure are the same and the drawn failure envelope is horizontal, which implies $\varphi = 0$ (**$\varphi = 0$ concept**).

When the $\varphi = 0$ concept is adapted, there will be no need to run several UU tests to determine c value. In Figure 11.25, Mohr's circle at failure from unconfined compression test ($\sigma_3 = 0$) is seen as a special case of UU test. If an unconfined compression test is run properly, then the cohesion component c is determined by drawing a horizontal line to make a tangent with Mohr's circle at failure as seen in Figure 11.10. In that case, UU tests with several confining stresses will no longer be needed.

11.6 OTHER SHEAR TEST DEVICES

There are many other laboratory as well as in situ shear devices to determine soil's strength parameters. They could include true triaxial device, plane strain triaxial device, torsional shear device, simple shear device, ring shear device, etc. They are mostly used as research tools and not routinely used by practicing engineers. The readers can refer to related literatures on those. In this section, popularly used small shear devices (vane shear device, tor-vane shear device, and pocket penetrometer) are introduced.

11.6.1 Vane Shear Device

For the **vane shear device**, a rigid cross-shaped vane such as seen in Figure 11.26 is often used in the field as well as in the laboratory. A vane is inserted into the soil. In the field, it is generally installed to the tip of the boring rod. The shaft is twisted, and

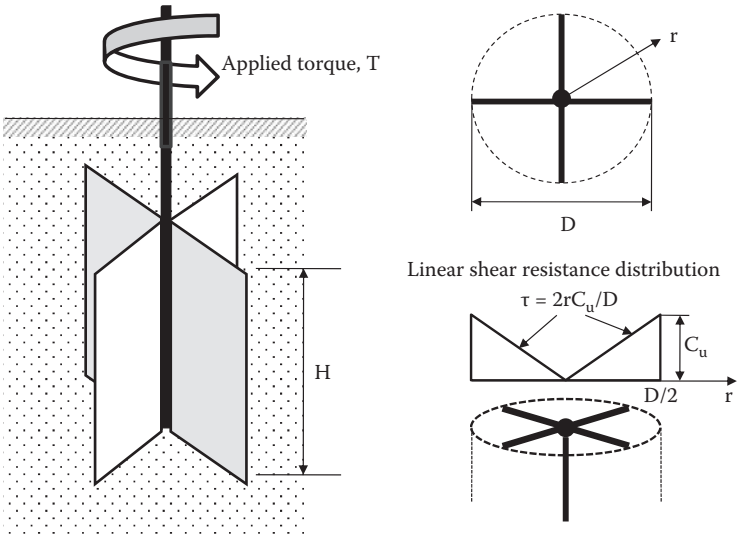

FIGURE 11.26 Vane shear test device.

applied torque T is measured at failure. Shear resistance comes from the perimeter area, and the top and the bottom surfaces of the vane. Upon the application of the torque T along the perimeter, full resistance C_u will be developed, where C_u is the same as the undrained shear strength.

On the top and the bottom shear surfaces of the vane, shear resistance could be the maximum value of C_u at r = D/2, and is zero at the center of the torque, since there is no rotation there. If the distribution of the shear resistance on the top and the bottom shear surfaces is assumed as a linearly increasing function with the radius r, $\tau = C_u \bullet r/(D/2)$ as seen in Figure 11.26, the measured maximum torque T_f is related to the maximum shear resistance C_u by integrating local torque τ x r over the top and the bottom shear surfaces, and the perimeter area:

$$T_f = \pi C_u \left[\frac{D^3}{8} + \frac{D^2}{2} H \right] \tag{11.6}$$

From Equation 11.6, the undrained shear strength C_u can be obtained. Field vane shear test is generally considered to be very useful and a reliable tool, since the stress conditions are at in situ and samples are less disturbed in comparison with laboratory specimens. Also, it is rather economical to perform. Note that the vane shear test is conducted within a short period of time, and thus, it can be categorized as an unconsolidated undrained (UU) test.

11.6.2 Tor-Vane Shear Test

Figure 11.27 shows a schematic drawing of a hand-twisting **tor-vane shear device**. Similar to the vane shear test, rigid fins are inserted into the surface of soil and twisted until failure. The measured torque is converted into the shear resistance near the surface of soil specimen. This is mostly used in the laboratory to provide supplementary shear strength information or for quality control of sampled specimens. The nature of shear strength obtained from this test is similar to the one of UU test.

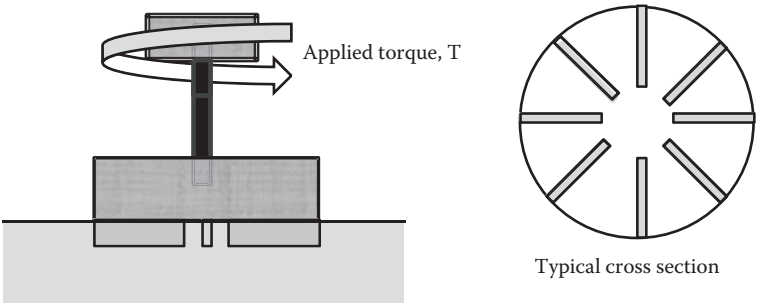

FIGURE 11.27 Tor-vane shear test device.

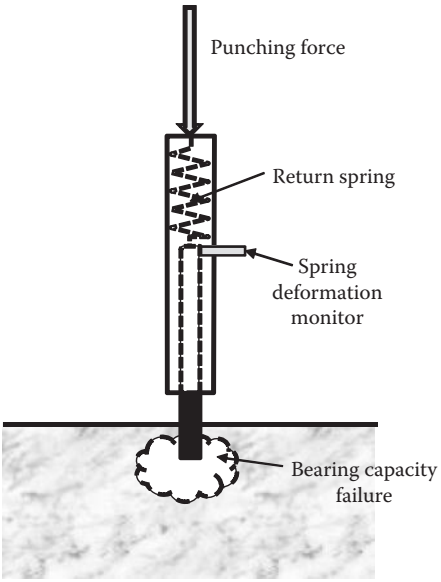

FIGURE 11.28 Pocket penetrometer.

11.6.3 Pocket Penetrometer

The **pocket penetrometer** is a punching probe as seen in Figure 11.28. The device is pushed by hand into the soil until failure. The maximum deformation of the spring is monitored to identify the punching force. The failure punching force is an indication of the soil's **bearing capacity** (Chapter 13) and is calibrated to UU shear strength. The device is mostly used in the laboratory to provide supplementary shear strength information or to check the quality of specimens.

Note that the vane shear, the tor-vane shear, and the pocket penetrometer test are all equivalent to the UU test, since no consolidation takes place and shearing time is very quick. Thus, results obtained from those tests are compared with the shear strength C_u ($=q_u/2$) obtained from unconfined compression test or UU test.

11.7 SUMMARY OF STRENGTH PARAMETERS FOR SATURATED CLAYS

As discussed in the previous sections, shear strength parameters c and φ, and c′, and φ′ depend on types of shear test (UU, CD, or CU test) and consolidation history (normally consolidated or overconsolidated). They are summarized below.

11.7.1 UU Test

The $\varphi = 0$ concept is applicable and thus φ is always zero. UU strength C_u is conveniently expressed as C_u/σ_{vo}', where σ_{vo}' is the effective overburden stress. Several empirical correlations are available:

By ***Skempton and Henkel (1953)*** for normally consolidated clays

$$C_u/\sigma_{vo}' = 0.11 + 0.037\ PI \tag{11.7}$$

By ***Bjerrum and Simons (1960)*** for normally consolidated clays

$$C_u/\sigma_{vo}' = 0.045\ (PI)^{0.5} \quad \text{for PI} > 50\% \tag{11.8}$$

$$C_u/\sigma_{vo}' = 0.018\ (LI)^{0.5} \quad \text{for LI} > 50\% \tag{11.9}$$

In these equations, a plasticity index (PI) and liquidity index (LI) are expressed in percentages. Note that the C_u/σ_{vo}' values obtained from these equations shall be considered as approximate ones.

11.7.2 CD Test and CU Test (Effective Stress)

For normally consolidated clays, $c' = 0$ and φ' is in a range of 20°–42° ***(Bowles 1996)***. For overconsolidated clays, there are various combinations of non-zero c' and φ' values.

11.7.3 CU Test (Total Stress)

For normally consolidated clays, $c = 0$ and φ is non-zero values. For overconsolidated clays, there are various combinations of non-zero c and φ values.

Table 11.1 summarizes shear strength parameters from different types of shear test.

TABLE 11.1
Shear Strength Parameters from Different Shear Test

Shear Strength Parameters	Types of Shear Test
c and φ	CU test (total stress analysis)
c' and φ'	CD test, CU test (effective stress analysis)
C_u ($=q_u/2$) ($\varphi = 0$ concept)	Unconfined compression, UU, vane shear, tor-vane shear, pocket penetrometer

11.8 APPLICATIONS OF STRENGTH PARAMETERS FROM CD, CU, AND UU TESTS TO IN SITU CASES

Now a big question arises: ***How to utilize those different strength parameters in various field problems***? Simple answers to the above question are:

1. Observe field phenomenon carefully in terms of preshearing condition (consolidated or unconsolidated) and shearing mode of anticipated failure (quick or slow failure).
2. Based on the observation above, use appropriate soil strength parameters, which match the anticipated field phenomena.

The following typical cases are discussed as practical problems that are usually encountered in the field.

11.8.1 Construction of Embankment on Soft Clay Soil at Once (UU Case)

Figure 11.29 shows a case in which an embankment is constructed on soft foundation clay in a rather short period of time, for example, in few days, a week, or so. In this case, there will not be enough time for the foundation clay to be consolidated. If the soil fails, the failure will occur suddenly, and thus, it will be the undrained condition. Shear strength C_u shall be the one from unconfined compression strength or its equivalent for stability analysis along the potential failure surface.

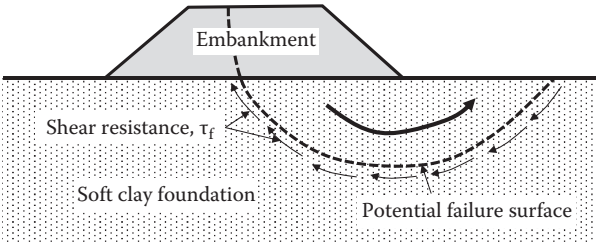

FIGURE 11.29 Quick construction of embankment on soft clay.

11.8.2 Foundation Design for Rapidly Constructed Structures

If super structures are constructed in a rather short period of time, its foundation shall be designed based on UU soil parameters, since there will be a very little consolidation time and failure mode will be rather sudden if it fails as shown in Figure 11.30.

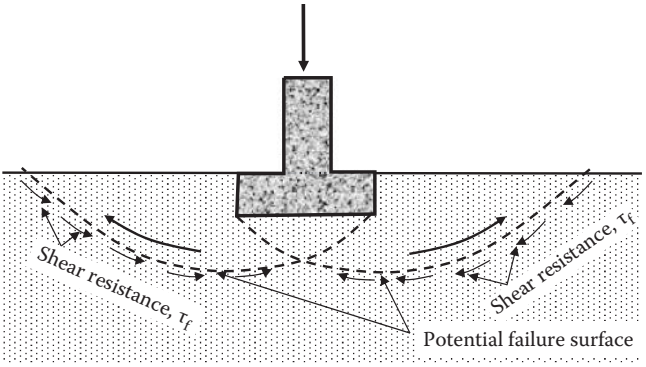

FIGURE 11.30 Construction of a footing in a short period of time.

11.8.3 Staged Construction of Embankment on Soft Clay (CU Case)

When an embankment cannot be constructed at once due to rather low shear strength of the foundation clay, **staged construction** will be the choice. As seen

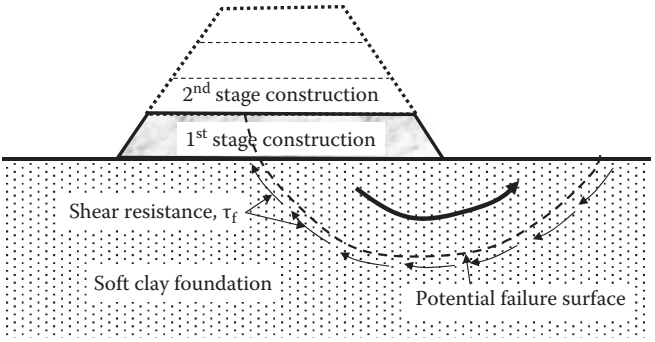

FIGURE 11.31 Staged construction of embankment on soft clay.

in Figure 11.31, the first stage embankment is placed on the ground. Since the load increment is small, the original foundation clay could have enough strength to carry its weight. At this stage stability analysis shall be carried out by using shear strength from UU test. Then the first stage load is left there for a while, for example, for a month or more. During that period, the consolidation process begins and the foundation clay will gain some strength. When the gained strength will be enough to carry the second stage load, a new load is applied and it is left for another period for further consolidation. The process is repeated until the final height of the embankment is attained. In this case, total stress soil parameters by CU test are the strength parameters for each stage of construction. Strength gain occurs during consolidation process, but anticipated failure will be sudden if it fails (undrained).

11.8.4 Stability of Cut Slope (CD Case)

Figure 11.32 shows a vertical cut made in a clayey soil. Due to the cohesion component, it is possible to do a vertical cut safely to a certain depth (Chapter 12). Assume that the **cut slope** is stable at time of the excavation. Near the cut section, soil is subjected to stress decrease, and it is a reversed phenomenon of consolidation. Stress relaxation will promote gradual swelling of the soil and it starts to attract pore water to the zone. When the water content increases, the soil's strength decreases. Initially stable slope will gradually increase the danger of sliding with time due to the above phenomenon. The failure mode may be progressive and slow due to gradual increase in the water

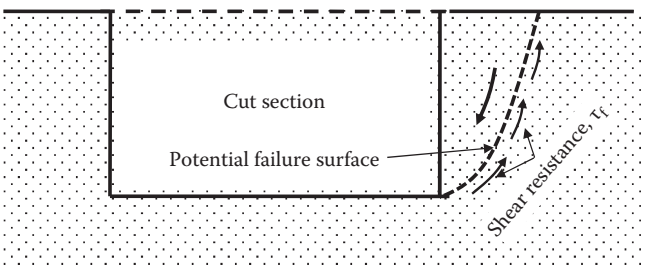

FIGURE 11.32 Cut-slope and potential slope failure.

content of soils along the potential failure surface. Thus, CD strength parameters will be the proper ones to be used in such cases. However, it shall be noted that if the anticipated failure mode is sudden in the above case, CU parameters shall be used.

As observed in above cases, the selection of CD, CU, and UU parameters depends on the preshearing condition (consolidated or unconsolidated) and the shearing process (slow failure or sudden failure). In particular, the evaluation of failure mode is very significant. Most failure modes would be sudden if the soil does not have enough shear strength, and slow failure would occur in very limited cases such as possible progressive failure in the cut-and-creep type of failure mode. It shall be noted that, though UU or equivalent tests are rather simple ones, there are many applications of the UU case as seen in above examples.

11.9 STRENGTH PARAMETERS FOR GRANULAR SOILS

Granular soils (sand and gravel, and maybe some silt) have very little inter-particle interactive forces due to rather larger particle sizes (Chapter 3). Therefore, the most of their shear resistance comes from a frictional component. Thus, c can be assumed to be zero for granular soils. In addition, these soils have a rather high permeability so that the pore water pressure will normally dissipate very quickly in most applications. Accordingly, for both wet and dry granular soils, Equation 11.10 is used without the c component.

$$\tau_f = \sigma \tan\varphi \tag{11.10}$$

The failure envelope starts at the origin of the σ-τ diagraph with φ angle inclination, and the angle of internal friction φ is the sole parameter to determine the shear strength. The φ values are influenced by soil's various properties such as density or void ratio, gradation (uniform or well graded), angularity (rounded or angular), grain surface roughness, etc. Among those, density (or void ratio) would most significantly influence the φ values of granular materials. The typical values of φ are given in Table 11.2.

TABLE 11.2
Typical Ranges of Angle of Internal Friction φ for Sandy Soils

Type of Soil	Density	Peak φ Value	Residual φ Value
Sand, rounded	Loose	28° to 30°	
	Medium	30° to 35°	26° to 30°
	Dense	35° to 38°	
Sand, angular	Loose	30° to 35°	
	Medium	35° to 40°	30° to 35°
	Dense	40° to 45°	
Sandy gravel		34° to 48°	33° to 36°

Source: After Murthy, V. N. S. (2003). *Geotechnical Engineering*, Marcel Dekker, New York.

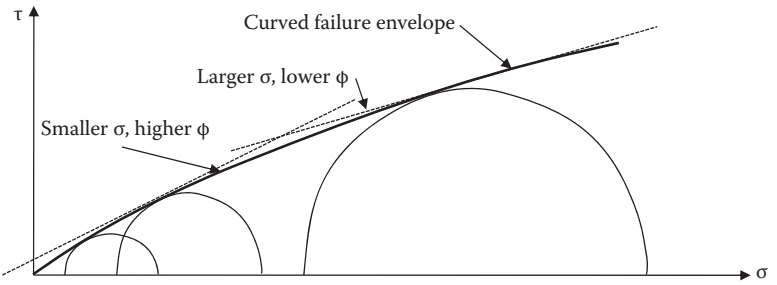

FIGURE 11.33 Curved failure envelope for granular soils.

A straight line failure envelope or a constant φ angle for a given soil with a given density is generally assumed for granular soils as discussed. However, in reality, it was empirically observed that the failure envelope for granular soils is slightly curved as seen in Figure 11.33. It implies that a slightly higher φ angle is at a lower confining stress and a lower φ angle is at a higher stress. The importance of the above fact is addressed by a nonconservative application of small-scale model test data in the evaluation of in situ earth structure behavior. In a small scale model test, the stress level, which mostly comes from the gravitational force of soils, is small, and thus, the failure phenomenon is controlled by a rather high φ value, while in an in situ earth structure, the stress level is high, which provides a lower φ value.

The geotechnical **centrifuge model test** is meant to overcome the previously mentioned shortcomings of the small scale model test. For example, if an 0.5-m-high model earth dam is subjected to 20 *g* of the centrifugal gravity on a rotating platform, its stress level in the model increases to the level of a 10 m (0.5 m × 20) high earth dam, and thus, similar φ values would be utilized in both the 0.5-m-high model under 20 *g* centrifugal force and the 10-m-high prototype under 1 *g* condition. Readers are referred to other references (e.g., ***Taylor 1995***) for details of geotechnical centrifuge testing.

11.10 DIRECTION OF FAILURE PLANES IN SHEARED SPECIMEN

Mohr's circle and the concept of the **pole** can be effectively utilized in order to evaluate the direction of anticipated (or observed) failure planes on a sheared specimen. A specimen is sheared under triaxial condition (σ_1 on horizontal plane and σ_3 on vertical plane) as seen in Figure 11.34a and the effective stresses σ_1' and σ_3' with measured pore water pressure u are calculated. First, assume that the soil strength is defined by c′ and φ′ in general, and a Mohr's circle at failure is drawn in Figure 11.34b. To find the pole, by referring to Section 10.7, draw a line from a known stress point σ_1' on Mohr's circle parallel to the plane (horizontal) on which these stresses act. Find the intersection on the circle as the pole. The pole is at the same point as σ_3' in the figure. Alternatively, draw a line from a known stress point σ_3' on Mohr's circle parallel to the plane (vertical) on which these stresses act. Find the intersection on the circle as the pole. The pole is also at σ_3' point.

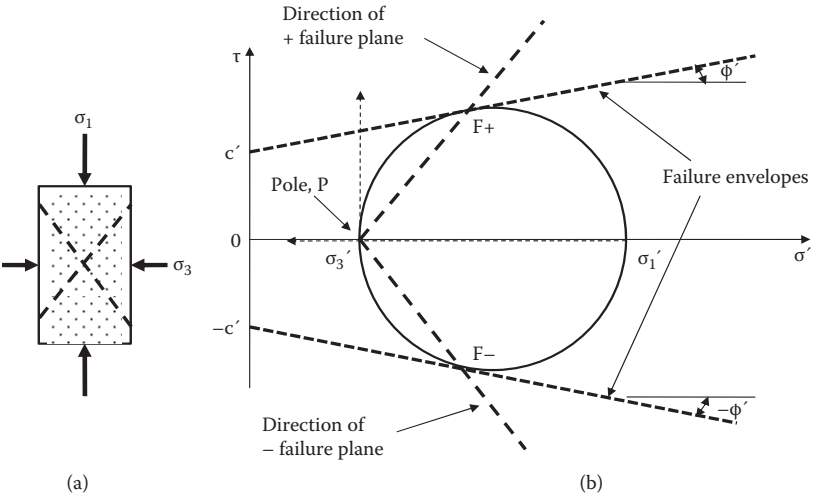

FIGURE 11.34 Directions of failure planes in triaxial specimen.

Next, to know the direction of a stress point on Mohr's circle, connect a line from the pole to that stress point on the circle. That is the direction of the plane on which these stresses (σ', τ) act. In this case, points F+ and F– are the stress points for the failure planes and thus PF+ and PF– are the directions of potential failure planes on the specimen as seen in Figure 11.34b. Many failure lines, which are parallel to PF+ and PF–, are possible, but a few failure lines could be observed in real soil specimens.

As seen in a similar figure in Figure 11.35, the angle of the failure plane direction ψ is analytically related to φ' values as follows:

For a triangle O′F σ_3', since O′F = O′σ_3', $\angle$ O′σ_3'F= $\angle$ O′F σ_3' = ψ

Based on the triangle O″O′F, $\angle$ FO′σ_1'= 90° + φ' = 2ψ, and thus the direction of failure plane from the horizontal $\psi = 45° + \varphi'/2$ (11.11)

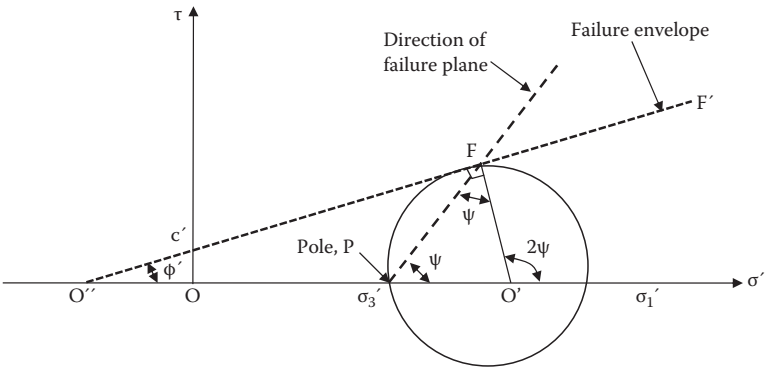

FIGURE 11.35 Analytical solution of failure plane direction.

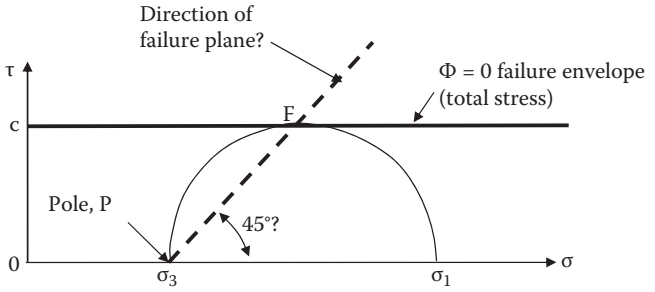

FIGURE 11.36 Questionable failure plane direction based on total stress Mohr's circle.

Note that the above discussion of the failure plane direction shall be applied only to the effective stress failure envelope, since the failure of soils is determined when Mohr's circle of failure in the effective stress just touches the unique effective stress failure envelope as discussed earlier in this chapter. For example, if this is applied to tests with a $\varphi = 0$ failure envelope (UU test, or unconfined compression test), the failure plane direction shall be 45° from the horizontal as seen in Figure 11.36. As a matter of fact, it is not true. Soil will fail along a plane with $45° + \varphi'/2$ from the horizontal, instead. A mistake was made here because the $\varphi = 0$ failure envelope is not in the effective stress mode; it is rather in the total stress mode.

Exercise 11.4

A drained triaxial compression test for a normally consolidated clay specimen was conducted with $\sigma_3' = 100$ kPa. After the test, the failure planes on the specimen were observed. The failure plane angle was measured as 55° inclined from the horizontal. Determine (a) the effective angle of internal friction φ' (b) σ_1' at failure.

Solution:

(a) $\psi = 55°$ and thus $\varphi' = \mathbf{20}°$ from Equation 11.11. ←

(b) In Figure 11.37, the failure envelope is drawn with 20° from the origin (normally consolidated).

A failure Mohr's circle with $\sigma_3' = 100$ kPa is searched by trial and error, which just touches the failure envelope.
Read σ_{1f}' value on the σ' axis as **204 kPa** ←

Or, analytically, applying sine law to the triangle OO′F;
$\sin\varphi' = O'F/OO' = [(\sigma_{1f}' - \sigma_3')/2]/[(\sigma_{1f}' + \sigma_3')/2] = (\sigma_{1f}' - 100)/(\sigma_{1f}' + 100) = \sin 20°$
then, $\sigma'_{1f} = \mathbf{204.0\ kPa}$ is obtained. ←

In the figure, failure plane direction $\sigma_3'F$ is also graphically seen.

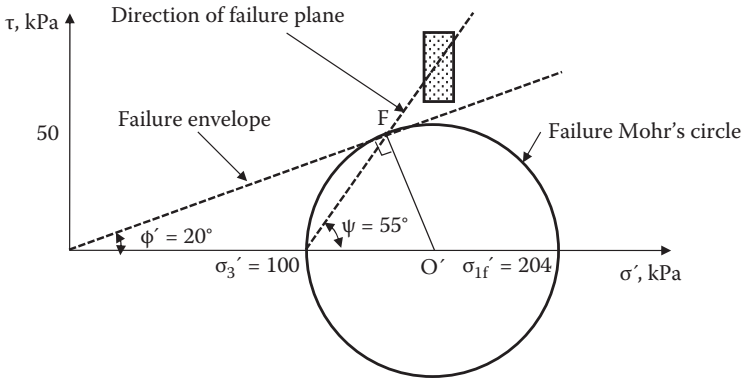

FIGURE 11.37 Exercise 11.4 solution.

11.11 SUMMARY

Shear strength determination is another important practice in many soil mechanics problems (foundation design, slope stability, retaining wall design, etc.). There are several shear testing procedures available and different shear strength parameters are obtained from those tests. Detailed of these were presented in this chapter. It is most important for engineers to understand which ones are the proper shear strength parameters for a given problem. They all depend on the anticipated field conditions in terms of preshearing condition (i.e., consolidated or unconsolidated) and shear failing mode (drained or undrained). They were discussed and summarized in detail in Sections 11.7 and 11.8. In Section 11.10, the concept of the pole of Mohr's circle (Chapter 10) was effectively utilized in the determination of the directions of the failure planes during shear.

REFERENCES

Bjerrum, L. and Simons, N. E. (1960), Comparison of shear strength characteristics of normally consolidated clays, *Proceedings of Research Conference on Shear Strength of Cohesive Soils*, ASCS, pp. 711–726.

Bowles, J. E. (1996), *Foundation Analysis and Design*, 5th ed., McGraw-Hill, New York.

Murthy, V. N. S. (2003), *Geotechnical Engineering*, Marcel Dekker, New York.

Rendulic, L. (1936), Relation between void ratio and effective principal stresses for a remolded silty clay, *Proceedings of the 1st International Conference on Soil Mechanics and Foundation Engineering*, Vol. III, pp. 48–53.

Skempton, A. W. and Henkel, D. J. (1953), The Post-Glacial Clays of the Thames Estuary at Tillbury and Shellhaven, *Proceedings of the 3rd International Conference on Soil Mechanics and Foundation Engineering*, Zurich, Vol. I, pp. 302–308.

Taylor, R. N. (editor) (1995), *Geotechnical Centrifuge Technology*, Blackie Academic and Professional. Glasgow.

Terzaghi, K. (1925), *Erdbaumechanik*, Franz Deuticke.

Problems

11.1 Why doesn't the high water pressure crush a soil element at a deep ocean bottom?

11.2 Why doesn't the soil's high overburden stress crush a soil element under a deep soil deposit?

11.3 Four direct shear tests were performed in a 10 cm × 10 cm square shear box for soil specimens with a similar density and the following data were obtained. Determine the angle of internal friction φ and the cohesion component c of the soil.

Applied Vertical Force F_v, Newton	Measured Peak Shear Force F_h, Newton
200	272
400	324
1000	487
1500	632

11.4 For a dry sandy soil, a direct shear test was performed. Its vertical normal force was 10 kg (mass) and the measured shear force was 6.34 kg (mass). The specimen was prepared in a circular shear box with 10 cm in diameter.
(a) Determine the angle of internal friction φ of the soil.
(b) When the normal stress of 150 kPa is applied, what will be the failure shear stress of this soil?

11.5 For normally consolidated clay specimens, drained direct shear tests were conducted and the following data were obtained. Determine the drained angle of internal friction φ′ of the clay.

Applied Normal Stress, kPa	Measured Peak Shear Stress, kPa
150	22.4
300	44.6
400	59.8
500	71.6

11.6 For clay specimens, drained direct shear tests were conducted and the following data were obtained. Determine the drained angle of internal friction φ′ and the cohesion component c′ of the clay.

Applied Normal Stress, kPa	Measured Peak Shear Stress, kPa
100	66.2
200	87.2
300	105.1
400	116.4

11.7 An unconfined compression test was performed on a clayey specimen with 7.0 cm in diameter and 15.0 cm in height and the following data was obtained. Plot the stress and strain curve and determine the unconfined compression strength q_u and the cohesion C_u of the soil.

Vertical Deformation δ_v, mm	Measured Axial Force F_v, kgf
0	0
0.5	2.8
1.0	5.5
1.5	8.4
2.0	10.9
2.5	13.6
3.0	16.2
3.5	18.6
4.0	21.4
4.5	24.1
5.0	26.8
5.5	29.4
6.0	30.1
6.5	30.1
7.0	29.8
7.5	28.9
8.0	28.9

11.8 Consolidated drained triaxial tests were conducted for three similar specimens with different chamber pressures and the failure deviatoric stresses were measured as below.

(a) Determine the angle of internal friction φ' and the cohesion component c' of the soil.

(b) Is this soil normally consolidated or overconsolidated?

Test	Chamber Pressure σ_3, kPa	Measured Deviatoric Stress at Failure, $(\sigma_1 - \sigma_3)_f$, kPa
I	50	92
II	100	127
III	150	166

11.9 A consolidated drained triaxial test was conducted for a normally consolidated clay. Its consolidation pressure was 80 kPa and the deviatoric stress at failure was 135 kPa. Determine the effective angle of internal friction φ' of the soil.

11.10 The effective angle of internal friction φ' was found to be 26° for a normally consolidated soil. If the soil is tested in consolidated drained triaxial test under $\sigma_3 = 60$ kPa, what would be the failure deviatoric stress $\sigma_1 - \sigma_3$ stress?

11.11 For a soil, the effective angle of internal friction φ' was found to be 14° and the cohesion component c' was 46 kPa. The soil was tested in consolidated drained triaxial condition when the failure stress $(\sigma_1 - \sigma_{3)}$ was found to be 132 kPa. What was the confining pressure σ_3 for this test?

11.12 For the triaxial test in Problem 11.11,
(a) Estimate the potential failure planes in the specimen relative to the major principal stress plane.
(b) What are the normal stress σ_f and the stress τ_f on the failure plane in (b) above?

11.13 Two similar specimens from the same site were tested under consolidated undrained triaxial condition with pore water pressure measurements. The results are summarized below.

Specimen	Chamber pressure, kPa	Measured deviatoric stress at failure, kPa	Pore water pressure at failure, kPa
I	50	181	23
II	100	218	19

(a) Plot the Mohr's circles at failure in both the total stress and in the effective stress.
(b) Determine the strength parameters φ and c in the total stress and φ' and c' in the effective stress.

11.14 If the specimen in Problem 11.13 is tested under the chamber pressure $\sigma_3 = 85$ kPa,
(a) What will be the failure axial stress σ_1?
(b) What will be the pore water pressure at failure?

11.15 Two similar specimens from the same site were tested under consolidated undrained triaxial condition with pore water pressure measurements. The results are summarized below.

Specimen	Chamber Pressure, kPa	Measured Deviatoric Stress at Failure, kPa	Pore Water Pressure at Failure, kPa
I	25	83	7.5
II	50	109	15

(a) Plot the Mohr's circle at failure in both the total stress and in the effective stress.
(b) Determine the strength parameters φ and c in the total stress and φ' and c' in the effective stress.

11.16 If the specimen in Problem 11.15 is tested under the chamber pressure $\sigma_3 = 60$ kPa,
(a) What will be the failure axial stress σ_1?
(b) What will be the pore water pressure at failure?

11.17 A cohesive soil was tested in consolidated undrained triaxial test with pore water pressure measurement and $\varphi = 24°$ and $c = 26$ kPa in the total stress and $\varphi' = 27°$ and $c' = 30$ kPa are obtained. If the similar specimen is tested under $\sigma_3 = 45$ kPa,
(a) What will be the failure deviatoric stress?
(b) What will be the pore water pressure at failure?

11.18 A consolidated undrained test was conducted on a clay specimen. The consolidation and chamber pressure was 50 kPa and the failure σ_1 was 86.2 kPa. If the similar specimen, which is first, consolidated under 50 kPa consolidation pressure and then it is tested in an unconfined compression device, what will be the unconfined compression strength q_u?

11.19 A normally consolidated clay had $\varphi' = 25°$. When the same specimen is tested in an unconfined compression device and obtained the unconfined compression strength $q_u = 85$ kPa. How much pore water pressure is generated in this unconfined compression specimen at the failure?

11.20 A consolidated clay had $\varphi' = 12°$ and $c' = 30$ kPa. When the same specimen is tested in an unconfined compression device and the unconfined compression strength $q_u = 90$ kPa is obtained. How much pore water pressure is generated in this unconfined compression specimen at the failure?

11.21 In a vane shear test with D = 50 mm and H = 100 mm as in Figure 11.26, the measured torque at failure was 1.26 kg (mass)-m. What is the shear strength of the soil? The vane was inserted deep into the soil.

12 Lateral Earth Pressure

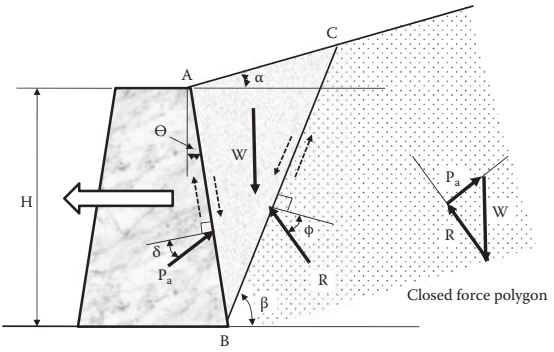

12.1 INTRODUCTION

When engineers face the designing of earth-retaining structures, bridge abutments, basement structures, sheet piles, support for excavated trenches, etc., a proper estimation of lateral earth pressure against those structures becomes most critical. This chapter first presents the classic lateral earth pressure theories by Coulomb and by Rankine, which still serve as the fundamentals on this subject. How to utilize those theories in practice is discussed thereafter.

12.2 AT-REST, ACTIVE, AND PASSIVE PRESSURES

Figure 12.1 shows a vertical underground wall in a soil mass. The amount of lateral earth pressure against the wall depends on how the wall moves relative to the soil mass. If the wall does not move at all, then the same lateral pressure is anticipated on the left face and on the right face of the wall. However, when the wall is moved toward right, the wall is pushed against the soil mass and thus higher lateral pressure is developed on the right face of the wall. On the other hand, on the left face of the wall the lateral pressure is reduced since the wall moves away from the soil.

It is convenient to express the lateral earth pressure σ_h as the ratio to its vertical stress σ_v:

$$\sigma_h = K\sigma_v \tag{12.1}$$

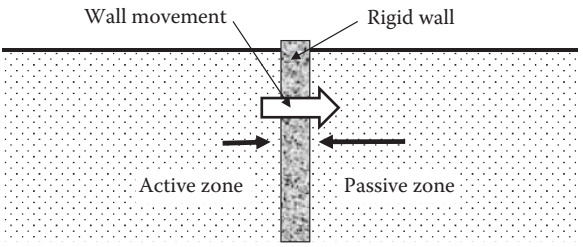

FIGURE 12.1 Lateral earth pressure against an underground wall.

where K is the **coefficient of lateral earth pressure** and it changes, depending on the wall movement relative to soil mass. Figure 12.2 plots the change of K with the amount of wall movement.

When the wall is moved toward the right, K increases and reaches to the maximum value K_p with a sufficient wall movement. At that stage, soil mass on the right side of the wall fails. The lateral earth pressure at this critical stage, is called **passive earth pressure**, and K_p is called the **coefficient of passive earth pressure**. On the left side of the soil mass, K value decreases and approaches to the minimum value K_a. That critical stage is called **active earth pressure**, and K_a is called the **coefficient of active earth pressure**. With zero wall movement, K value is K_0, which is called the **coefficient of lateral earth pressure at rest**. As shown in Figure 12.2, the following relationship can be observed:

$$K_p > K_0 > K_a \tag{12.2}$$

Note that to achieve either passive or active critical stages, it requires a sufficient amount of wall movement. Passive stage requires a larger wall movement than the active stage. Typical wall movement (δ) to the wall height (H) ratio to achieve those

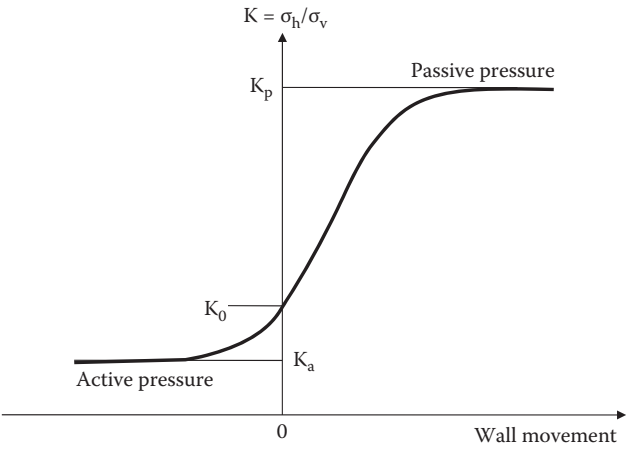

FIGURE 12.2 Coefficient of lateral earth pressure K versus wall movement.

critical stages is approximately 0.01 for the passive case and 0.001 for the active case in loose sandy soil mass.

12.3 AT-REST EARTH PRESSURE

At-rest pressure is the lateral earth pressure when there is no wall movement at all. For example, a rigid basement wall may be subject to this where the stability of the building is not a concern. As can be seen in Figure 12.2, the coefficient of lateral earth pressure K changes sharply around the zero wall deformation (i.e., $K = K_0$). It implies that K_0 measurement is very sensitive to a small wall movement.

There are several solutions to determine K_0.

12.3.1 Elastic Solution

This is based on an assumption that soil is an elastic media. This is a reasonable assumption since there is no wall movement at all in this situation.

$$K_0 = \frac{\mu}{1-\mu} \tag{12.3}$$

where μ is the soil's **Poisson's ratio**. Typical values of μ were given in Table 9.2. If $\mu = 0.3$ is taken for sands, K_0 is 0.43, and if $\mu = 0.4$ is taken for clays, K_0 is 0.67.

12.3.2 Empirical Formulae

Jaky (1944) developed an empirical formula for normally compacted sandy soils:

$$K_0 = 1 - \sin\varphi' \tag{12.4}$$

where φ′ is the drained angle of internal friction of soils. Jaky's formula is widely used for its simplicity as well as its validity for loose sandy soils.

However, when it is **overcompacted** for sandy soils and overconsolidated for clays, the K_0 value increases. Based on 170 different soils in literatures, ***Mayne and Kulhawy (1982)*** reported that the following single equation covers for both granular as well as cohesive soils with normally consolidated or overconsolidated cases:

$$K_0 = (1 - \sin\varphi')\ (OCR)^{\sin\varphi'} \tag{12.5}$$

where φ′ is the drained angle of internal friction, and OCR is the **overconsolidation ratio** (=maximum historical effective overburden stress/current effective overburden stress as defined in Equation 9.26). In case of sandy soils, it shall be interpreted as the **overcompaction ratio**, which bears the same definition of Equation 9.26 (Chapter 9).

Once the K_0 value is found, the at-rest lateral earth pressure σ_h' against the wall is calculated by

$$\sigma_h' = K_0\,\sigma_v' = K_0\,((\Sigma\gamma_i z_i + \Sigma\gamma_j' z_j) \tag{12.6}$$

In Equation 12.6, γ_i and γ_j' are the total and the buoyant unit weights of the soil, respectively; γ_i shall be used for soil above the water table, and γ_j' shall be used for soil below the water table as exercised in Equation 7.5. Note that when the wall is located under water table, a hydrostatic water pressure u is also applied against the wall in addition to the lateral earth pressure.

Exercise 12.1

A stable underground wall is subjected to at-rest lateral pressure and water pressure. Total depth of the underground wall is 10 m and the water table is at 5 m below the ground surface.

(a) Plot the at-rest lateral earth and water pressure distributions against the wall.
(b) Calculate the resultant force against the wall and its point of application. The soil's γ_t is 19.5 kN/m^3, and φ' is 38° for this normally compacted sandy soil.

Solutions:

(a) This is normally compacted sandy soil, thus, use Jaky's formula (Equation 12.4) for K_0 determination. $K_0 = 1 - \sin\varphi' = 1 - \sin 38° = 0.384$
at z = 5 m, $\sigma_h' = K_0\,\sigma_v = K_0\,\gamma z = 0.384 \times 19.5 \times 5 = 37.44$ kN/m^2
at z = 10 m, $\sigma_h' = K_0\,\sigma_v' = K_0\,(\gamma z_i + \gamma' z_j) = 0.384 \times [19.5 \times 5 + (19.5 - 9.81) \times 5] = 56.04$ kN/m^2, and $u = \gamma_w\, z_w = 9.81 \times 5 = 49.05$ kN/m^2

The distributions are plotted in Figure 12.3.

(b) Resultant force P = ½37.44 × 5 + ½(37.44 + 56.04) × 5+½49.05 × 5 = 93.6 + 233.7 + 122.63 = 449.93 kN/m ←
Moment about the base, M = 93.6 × 6.67 + ½37.44 × 5 × 3.33 + ½56.04 × 5 × 1.67 + 122.63 × 1.67 = 1374.76 kN/m-m
Point of application = M/P = 1374.76/449.93 = **3.06 m from the base**. ←

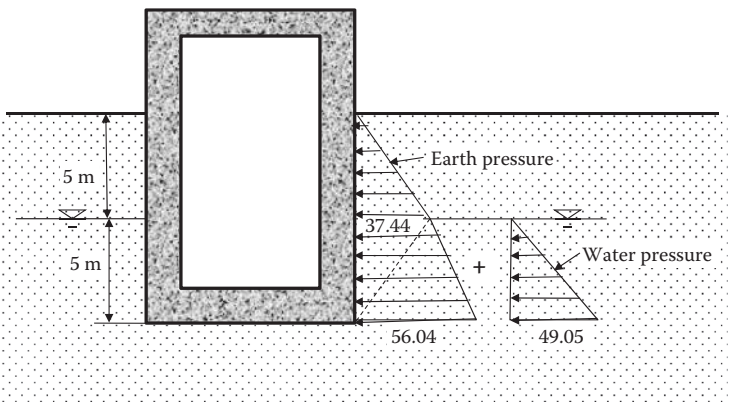

FIGURE 12.3 Lateral earth and water pressure distributions against basement wall.

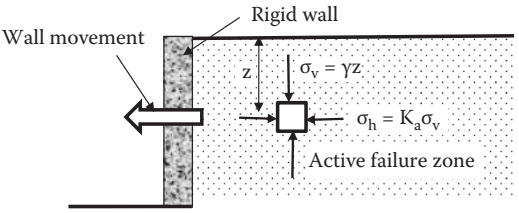

FIGURE 12.4 Rankine's active earth pressure development.

12.4 RANKINE'S LATERAL EARTH PRESSURE THEORY

Scottish engineer and physicist ***Rankine (1857)*** developed a lateral earth pressure theory behind yielded walls. He assumed that soil mass behind the wall enters into plastic equilibrium condition (failure) when a sufficient wall boundary is moved away from the backfill (active case) or toward the backfill (passive case).

12.4.1 Active Case

A rigid wall supports the horizontal backfill as seen in Figure 12.4. When the wall is moved toward left with a sufficient amount to create failure of backfill soil, all soil elements in the backfill enter into the plastic equilibrium conditions (failure). Since there is no shear stresses on the vertical and the horizontal planes under the horizontal backfill surface, σ_v (=γz) and σ_h at an element at depth z are the principal stresses, and the horizontal stress σ_h is the active lateral earth pressure at this plastic equilibrium condition. In the active case, σ_v is larger than σ_h and thus $\sigma_1 = \sigma_v$ and $\sigma_3 = \sigma_a$. Those are computed from:

$$\sigma_v = \gamma z = \sigma_1 \tag{12.7}$$

$$\sigma_h = \sigma_{h,a} = K_a\sigma_v = K_a\gamma z = \sigma_3 \tag{12.8}$$

Equation 12.7 and Equation 12.8 can be plotted in Mohr's circle at failure as discussed in Chapter 10. Figure 12.5 plots the above situation. In the figure, the pole

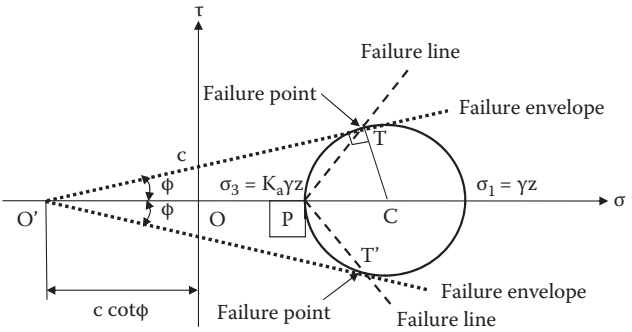

FIGURE 12.5 Mohr's circles at active failures of soil mass.

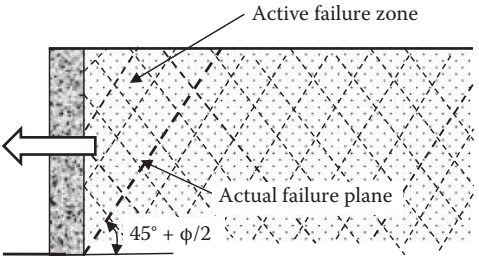

FIGURE 12.6 Potential active failure lines in soil mass.

of the Mohr's circle is determined by drawing a horizontal line from the σ_1 stress point and finding the intersection on the circle as Point P. The failure envelope ($\tau = c + \tan\varphi$) touches the circle at Point T, which is the failure point on the Mohr's circle. The direction of the failure plane is obtained by connecting the pole P and the failure point T. Thus, the line P-T is the direction of the failure plane in the soil mass, and the line P-T' on the negative shear stress domain of the figure is also the direction of the failure planes.

A group of lines that are all parallel to those two failure lines are drawn in the active zone of the soil mass as in Figure 12.6. The actual failure plane is the one to start from the base of the wall as plotted with a dark broken line. The zone between the wall face and the actual failure plane are the active failure zone, in which all elements are in plastic equilibrium conditions.

The angle of the active failure plane in the backfill soil is calculated from the geometry of Figure 12.5. The failure plane angle is identified as $\angle$TPC. For the right triangle TO′C, $\angle TC\sigma_1 = 90° + \varphi = 2 \times \angle$TPC, and thus;

$$\angle \text{TPC} = 45° + \varphi/2 \tag{12.9}$$

The magnitude of active lateral earth pressure $\sigma_{h,a}$ can also be calculated from the geometry in Figure 12.5. For the right triangle TO′C,

$$\sin\varphi = \frac{\text{TC}}{\text{O}'\text{C}} = \frac{\dfrac{\sigma_1 - \sigma_3}{2}}{\dfrac{\sigma_1 + \sigma_3}{2} + c\cot\varphi} \tag{12.10}$$

By solving the above equation for σ_3, and knowing that $\sigma_1 = \gamma z$ and $\sigma_3 = \sigma_{h,a}$, then,

$$\sigma_3 = \sigma_{h,a} = \gamma z \frac{1 - \sin\varphi}{1 + \sin\varphi} - 2c\frac{\cos\varphi}{1 + \sin\varphi} = \gamma z \tan^2\left(45^o - \frac{\varphi}{2}\right) - 2c\tan\left(45^o - \frac{\varphi}{2}\right) \tag{12.11}$$

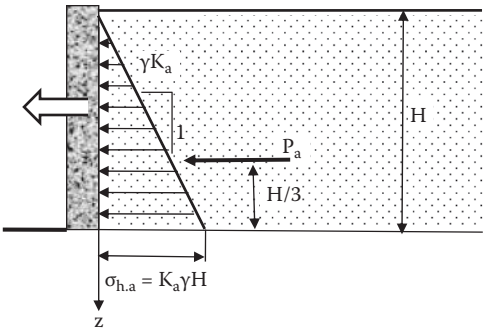

FIGURE 12.7 Rankine's active earth pressure distribution (c = 0).

c = 0 case (granular soils)
Equation 12.11 becomes

$$\sigma_{h,a} = \gamma z \tan^2\left(45^o - \frac{\varphi}{2}\right) = \gamma z K_a \tag{12.12}$$

where

$$K_a = \tan^2\left(45^o - \frac{\varphi}{2}\right) \tag{12.13}$$

The Rankine's active lateral earth pressure $\sigma_{h,a}$ acts normal to the vertical wall and increases linearly with the depth z and with a slope of $1/\gamma K_a$ as seen in Figure 12.7. The resultant active thrust P_a is given by:

$$P_a = \frac{1}{2} K_a \gamma H^2 \tag{12.14}$$

and P_a is applied at ⅓H point from the base of the wall.

c ≠ 0 case (c and φ materials)

Equation 12.11 indicates a linear increase of $\sigma_{h.a}$ with increasing depth z. However, there exits a non-zero negative value at the ground surface (z = 0), and thus, a negative pressure zone (tension zone) near the ground surface. The distribution of $\sigma_{h.a}$ is plotted in Figure 12.8.

The tension zone depth z_0 can be obtained by equating Equation 12.11 to zero:

$$z_0 = \frac{2c}{\gamma \tan\left(45^o - \frac{\varphi}{2}\right)} \tag{12.15}$$

Since the interface between the wall and the soil cannot sustain tension in most cases, the lateral stress at the tension zone is taken as zero, and thus, a linear pressure

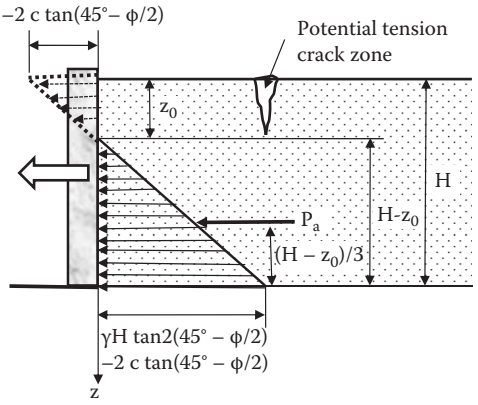

FIGURE 12.8 Rankine's active earth pressure distribution ($c \neq 0$).

distribution starts at z_0 to the wall height H as seen. The zone from $z = 0$ to z_0 makes potentially tension cracks in the ground and is called **tension crack zone**. The total active thrust P_a can be calculated from a triangle distribution as

$$P_a = \frac{1}{2}\left[\gamma H \tan^2\left(45^o - \frac{\varphi}{2}\right) - 2c\tan\left(45^o - \frac{\varphi}{2}\right)\right] \cdot \left[H - \frac{2c}{\gamma \tan\left(45^o - \frac{\varphi}{2}\right)}\right] \quad (12.16)$$

The point of application is at $(H - z_o)/3$ from the base of the wall.

12.4.2 Passive Case

When the boundary is moved against the soil mass as seen in Figure 12.9, a higher lateral pressure is developed, and the ultimate equilibrium (failure) stage is the passive earth pressure case. In this case, the lateral stress is larger than the vertical stress and thus:

$$\sigma_v = \gamma z = \sigma_3 \quad (12.17)$$

$$\sigma_h = \sigma_{h,p} = K_p \sigma_v = K_p \gamma z = \sigma_1 \quad (12.18)$$

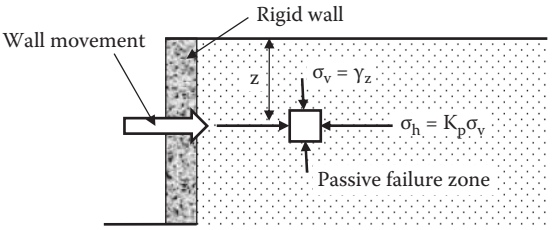

FIGURE 12.9 Rankine's passive earth pressure development.

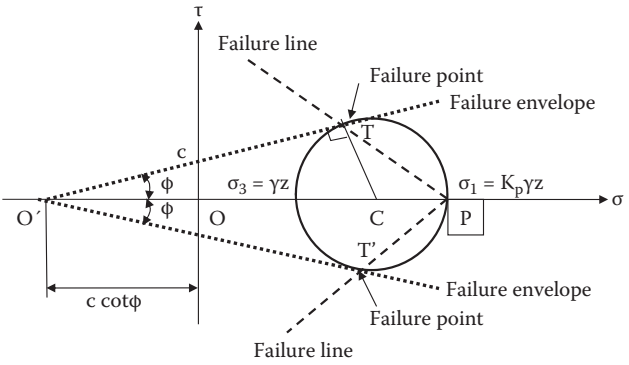

FIGURE 12.10 Mohr's circles at passive failures of soil mass.

Mohr's circle at failure is drawn in Figure 12.10 for the above passive stress condition. Note that the pole is not at the same point as in the active case (Figure 12.5) since the direction of σ_1 plane is the vertical plane in the passive case.

The directions of passive failure lines in Figure 12.10 make a group of potential passive failure lines behind the wall as seen in Figure 12.11, and the actual passive failure plane is shown with a dark broken line. Note that the passive failure zone behind the wall is much larger than the one in the active failure zone (Figure 12.6).

The direction of the failure plane is calculated by applying a trigonometry on the right triangle TO′C in Figure 12.10 as:

$\angle TC\sigma_3 = 180° - \angle TC\sigma_1 = 180° - (90° + \varphi) = 90° - \varphi = 2 \bullet \angle T\sigma_1 C$, and thus:

$$\angle T\sigma_1 C = 45° - \varphi/2 \tag{12.19}$$

By applying the trigonometry rule for the right triangle TO′C,

$$\sin\varphi = \frac{TC}{O'C} = \frac{\frac{\sigma_1 - \sigma_3}{2}}{\frac{\sigma_1 + \sigma_3}{2} + c\cot\varphi} \tag{12.20}$$

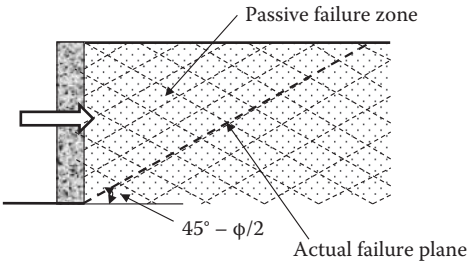

FIGURE 12.11 Potential passive failure lines in soil mass.

By solving the above equation for σ_1, and knowing that $\sigma_3 = \gamma z$ and $\sigma_1 = \sigma_{h,p}$, then,

$$\sigma_1 = \sigma_{h,p} = \gamma z \frac{1+\sin\varphi}{1-\sin\varphi} + 2c\frac{\cos\varphi}{1-\sin\varphi} = \gamma z \tan^2\left(45^o + \frac{\varphi}{2}\right) + 2c\tan\left(45^o + \frac{\varphi}{2}\right) \tag{12.21}$$

c = 0 case (granular soils)
Equation 12.21 becomes:

$$\sigma_{h,p} = \gamma z \tan^2\left(45^o + \frac{\varphi}{2}\right) = \gamma z K_p \tag{12.22}$$

where

$$K_p = \tan^2\left(45^o + \frac{\varphi}{2}\right) \tag{12.23}$$

Note that from Equation 12.13 and Equation 12.23, ***$K_p = 1/K_a$ relationship is obtained for c = 0 case***.

The Rankine's passive lateral earth pressure $\sigma_{h,p}$ acts normal to the vertical wall and increases linearly with depth z with a slope of $1/\gamma K_p$ as seen in Figure 12.12. The resultant passive thrust P_p is given by:

$$P_p = \frac{1}{2} K_p \gamma H^2 \tag{12.24}$$

and P_p is applied at ⅓H from the base of the wall.

c ≠ 0 case (c and φ materials)
Equation 12.21 shows a linear increase of $\sigma_{h,p}$ with increasing depth z. In the passive case, there is a positive pressure at z = 0, and there is no tension crack zone as seen in the active case.

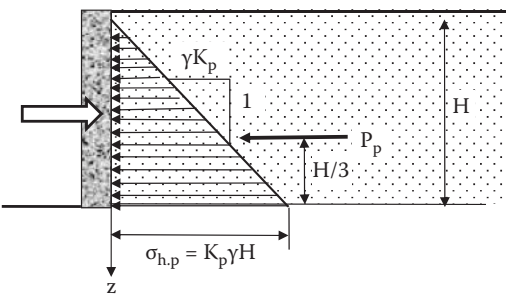

FIGURE 12.12 Rankine's passive earth pressure distribution (c = 0).

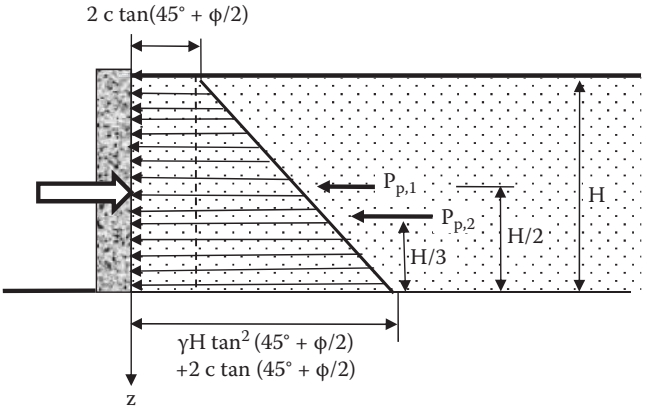

FIGURE 12.13 Rankin's passive earth pressure distribution ($c \neq 0$).

The resultant P_p can be calculated as summation of $P_{p,1}$ (rectangular distribution) and $P_{p,2}$ (triangular distribution) as seen in Figure 12.13:

$$P_{p,1} = 2\,c\,\tan\left(45^o + \frac{\varphi}{2}\right) \times H \tag{12.25}$$

$$P_{p,2} = \frac{1}{2}\gamma H^2 \tan^2\left(45^o + \frac{\varphi}{2}\right) \tag{12.26}$$

$P_{p,1}$ and $P_{p,2}$ are applied at ½H and ⅓H, respectively, from the base of the wall, and thus, the center of gravity computation technique is used to determine the point of application of the total passive thrust P_p ($=P_{p,1} + P_{p2}$).

12.4.3 Summary of Rankine's Pressure Distributions

In this section, Rankine's lateral pressure distributions against the vertical wall are summarized, which include the effect of a variety of water table elevations and multiple soil layers in the backfill. To make discussions more general, a single lateral earth pressure coefficient K is used, and thus, ***K is interpreted as any of K_a or K_p during this discussion***. This is also applicable to at-rest pressure distribution by assigning $K = K_0$.

Dry backfill and no water with c = 0

As seen in Figure 12.14, the lateral pressure distribution is triangular, and the point of the application of the total thrust is at one third from the base of the wall.

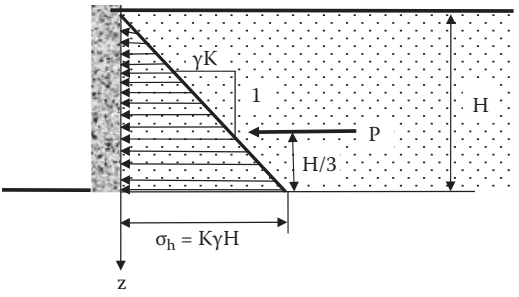

FIGURE 12.14 Lateral earth pressure distribution of dry backfill with c = 0.

Water table within backfill with c = 0

In this case, submerged unit weight shall be used for the earth pressure computation below the water table as seen in Figure 12.15. In addition, an equal amount of hydrostatic water pressures act from the both sides of the wall.

If the water table elevations in front of the wall and in the backfill are different, unequal hydrostatic water pressures shall be applied against the wall. It is a usual situation when tidal water fluctuates on the water front structures.

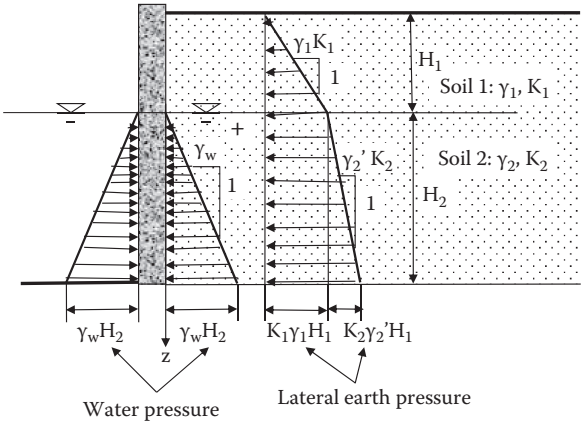

FIGURE 12.15 Lateral earth pressure distribution with water table with c = 0.

Multiple backfill soils with c = 0

In Figure 12.15 plot, a continuous lateral earth pressure distribution line was drawn for a case of $K_1 = K_2$ in order to avoid a confusion. If there are two different soil layers in the backfill and $K_1 \neq K_2$, the lateral pressure distribution could be discontinuous as seen in Figure 12.16.

There are two different pressures at the border point A, since K values are different depending on the side of soils (K_1 for Soil 1 layer and K_2 for Soil 2 layer) and thus:

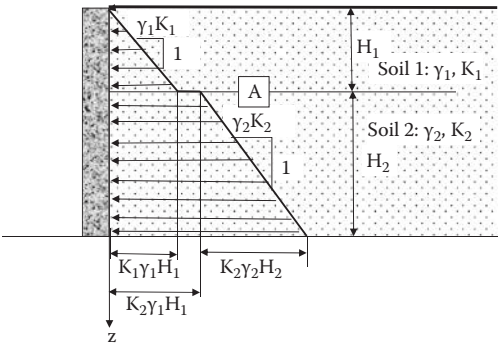

FIGURE 12.16 Lateral earth pressure distribution with two backfill soils with c = 0.

$$\sigma_{h,A} = K_1\gamma_1 H_1 \qquad \text{(just above Point A)} \tag{12.27}$$

$$\sigma_{h,A} = K_2\gamma_1 H_1 \qquad \text{(just below Point A)} \tag{12.28}$$

and at the base of the wall,

$$\sigma_{h,base} = K_2 (\gamma_1 H_1 + \gamma_2 H_2) \tag{12.29}$$

This concept can be easily applied for more layers and combinations with the water table elevation. Note that although this abrupt change in lateral pressure distribution is correct in theory, the real pressure distribution will change rather smoothly.

Multiple backfill soils with c ≠ 0

The same concept as the above can be applied. Since in c ≠ 0 case there would be a tension crack zone near the ground surface in active cases and it will not be in passive cases, Figure 12.17 plots patterns of pressure distributions for active and passive cases, separately.

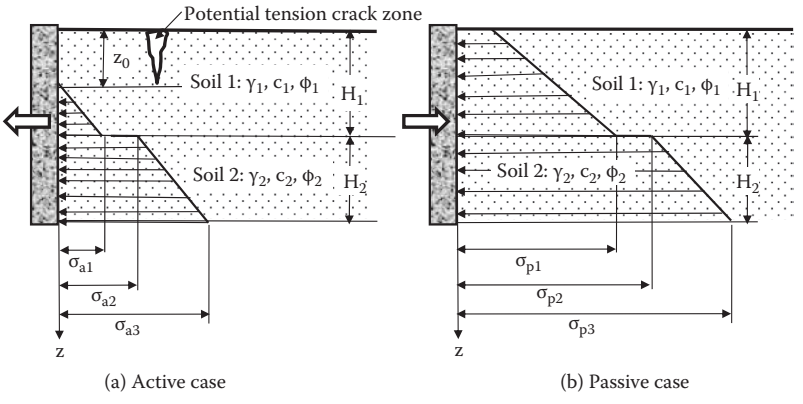

FIGURE 12.17 Lateral earth pressure distributions with two backfill soils with c ≠ 0.

Lateral pressure values at each level in Figure 12.17 can be calculated based on Equation 12.11 and Equation 12.21 and by applying soil properties for corresponding layers as below.
In active case

$$\sigma_{a1} = \gamma_1 H_1 \tan^2\left(45^o - \frac{\varphi_1}{2}\right) - 2c_1 \tan\left(45^o - \frac{\varphi_1}{2}\right) \tag{12.30}$$

$$\sigma_{a2} = \gamma_1 H_1 \tan^2\left(45^o - \frac{\varphi_2}{2}\right) - 2c_2 \tan\left(45^o - \frac{\varphi_2}{2}\right) \tag{12.31}$$

$$\sigma_{a3} = (\gamma_1 H_1 + \gamma_2 H_2)\tan^2\left(45^o - \frac{\varphi_2}{2}\right) - 2c_2 \tan\left(45^o - \frac{\varphi_2}{2}\right) \tag{12.32}$$

In a passive case

$$\sigma_{p1} = \gamma_1 H_1 \tan^2\left(45^o + \frac{\varphi_1}{2}\right) + 2c_1 \tan\left(45^o + \frac{\varphi_1}{2}\right) \tag{12.33}$$

$$\sigma_{p2} = \gamma_1 H_1 \tan^2\left(45^o + \frac{\varphi_2}{2}\right) + 2c_2 \tan\left(45^o + \frac{\varphi_2}{2}\right) \tag{12.34}$$

$$\sigma_{p3} = (\gamma_1 H_1 + \gamma_2 H_2)\tan^2\left(45^o + \frac{\varphi_2}{2}\right) + 2c_2 \tan\left(45^o + \frac{\varphi_2}{2}\right) \tag{12.35}$$

When utilizing Equation 12.30 through Equation 12.35, careful attention to φ_1, φ_2, c_1, and c_2 shall be made.

Exercise 12.2

Figure 12.18 shows a vertical retaining wall with a horizontal backfill, which may fail in active mode. Note that the water table elevations in front of the wall and at the back of the wall are different. (a) Compute and draw all lateral pressures act against the wall. (b) Compute the total thrust and its point of application.

Solution:

1. Tension crack depth $z_0 = 2c_1/[\gamma_1 \tan(45° - \varphi_1/2)]$
   $= 2 \times 10/[18.5 \times \tan(45° - 25°/2)] =$ **1.70 m**

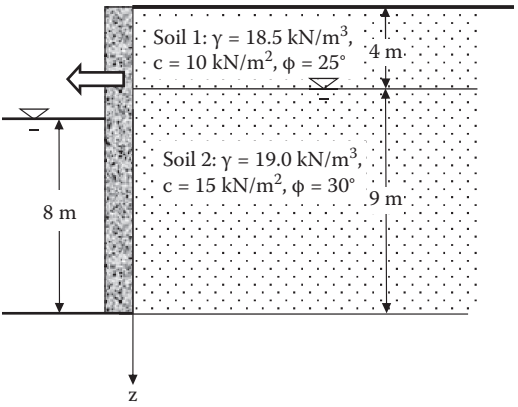

FIGURE 12.18 Exercise 12.2 problem.

Active earth pressures:

$\sigma_{a,\text{ at 4 m, soil 1}}$ = Equation 12.30 = $18.5 \times 4 \times \tan^2(45° - 25°/2) - 2 \times 10 \times \tan(45° - 25°/2)$

$= 30.03 - 12.74 =$ **17.29 kN/m²**

$\sigma_{a,\text{ at 4 m, soil 2}}$ = Equation 12.31 = $18.5 \times 4 \times \tan^2(45° - 30°/2) - 2 \times 15 \times \tan(45° - 30°/2)$

$= 24.67 - 17.32 =$ **7.35 kN/m²**

$\sigma_{a,\text{ at 13 m, soil 2}}$ = Equation 12.32 = $[18.5 \times 4 + (19.0 - 9.81) \times 9] \times \tan^2(45° - 30°/2)$

$- 2 \times 15 \times \tan(45° - 30°/2)$

$= 52.24 - 17.32 =$ **34.92 kN/m²**

Water pressures:

Water side: at z = 5m, u = 0 and at z = 13 m, u = $8 \times 9.81 =$ **78.48 kN/m²**

Backfill side: z = 4 m, u = 0, and at z = 13 m, u = $9 \times 9.81 =$ **88.29 kN/m²**

The above obtained pressure distributions are plotted in Figure 12.19.

(b) Total thrust and point of applications

$P_{a,\text{ soil 1}} = ½ \times 17.29 \times (4 - 1.7) =$ **19.88** kN/m² at $9 + (4 - 1.7)/3 =$ **9.77 m** from the base

$P_{a,\text{ soil 2}} = 7.35 \times 9 + ½ \times (34.92 - 7.35) \times 9 =$ **66.15** (applied at **4.5 m**) + **124.07** (at **3 m**)

$P_{w,\text{ backfill}} = ½ \times 88.29 \times 9 =$ **397.31** kN/m² at **3 m** from the base

$P_{w,\text{ front side}} = ½ \times 78.48 \times 8 =$ **313.92** kN/m² at **2.67 m** from the base (toward right)

Total thrust P = 19.88 + 66.15 + 124.07 + 397.31 − 313.92 = **293.49 kN/m** ←Point of application of P at z from the base of the walls = ∑(Moment)/P = (19.88 × 9.77 + 66.15 × 4.5 + 124.07 × 3 + 397.31× 3 − 313.92 × 2.67)/293.49 = **4.15 m** from the base of the wall. ←

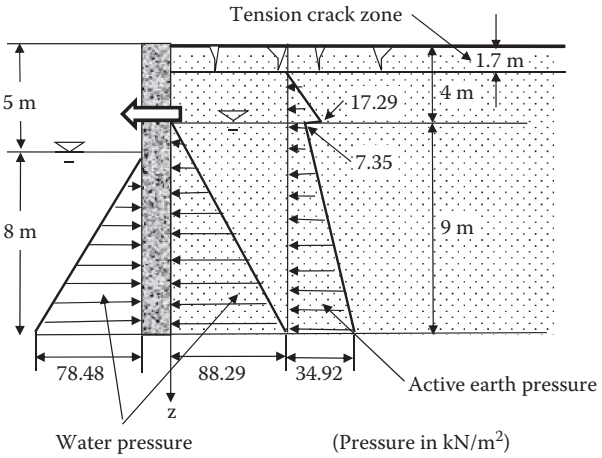

FIGURE 12.19 Active earth and water pressure distributions against the wall.

In this section Rankine's earth pressure theory for only level-ground backfill soil is covered. For Rankine's inclined backfill case, the readers are referred to other literatures (***Terzaghi 1943***, ***Mazindrani and Ganjali 1997***) for details.

12.5 COULOMB'S EARTH PRESSURE

French army engineer ***C. A. Coulomb (1776)*** derived formulae to evaluate the lateral earth pressures for sandy soils (c = 0 and φ materials) when the soil wedge behind the rigid wall just slides due to a sufficient wall movement. He established the force equilibrium on the sliding soil wedge and solved the reaction force from the wall as active or passive earth pressures.

12.5.1 Active Case

As seen in Figure 12.20, when a rigid wall moves toward left with a sufficient amount, a failing soil wedge ABC is formed, and Line AB and Line BC become failure surfaces. On the wedge, only three forces act: W (weight of the wedge), R (reaction force from soil mass), and P_a (reaction from the wall). Those forces keep an equilibrium condition and the force polygon will close as seen in the right side of the figure. In Figure 12.20, force R acts with φ angle normal to the slide line BC, along which shear failure of the soil takes place. P_a acts with δ angle inclined from the normal to the wall face; δ is the friction angle between the sliding soil and the wall, and is called the **wall friction angle**. Since W acts downward, all the directions of three forces and the magnitude of W are known, and thus, the magnitude of P_a is determined from a closed force polygon. P_a is the reaction from the wall face against the sliding wedge and it is, indeed, equal to the active earth thrust from the soil wedge against the wall at active stage by the force-reaction principle.

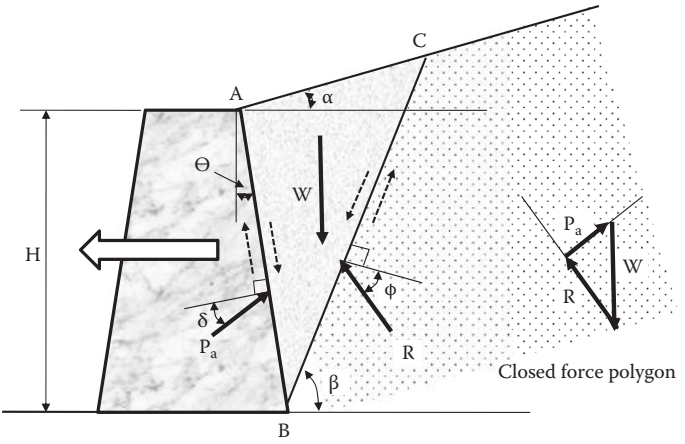

FIGURE 12.20 Coulomb's active earth pressure.

In the construction of Figure 12.20, however, the failure angle β is unknown and has to be assumed. Thus, for an assumed β angle, a P_a value is obtained. By trying several different β angles, P_a and β relations are obtained and plotted in Figure 12.21. The maximum value of trail P_a values is the active earth thrust by the Coulomb method.

Coulomb gave the analytical solution for the above active earth pressure P_a as:

$$P_a = \frac{1}{2}\gamma H^2 \frac{\cos^2(\varphi-\theta)}{\cos^2\theta\cos(\delta+\theta)\left[1+\sqrt{\dfrac{\sin(\delta+\varphi)\sin(\varphi-\alpha)}{\cos(\delta+\theta)\cos(\theta-\alpha)}}\right]^2} = \frac{1}{2}\gamma K_a H^2 \quad (12.36)$$

$$K_a = \frac{\cos^2(\varphi-\theta)}{\cos^2\theta\cos(\delta+\theta)\left[1+\sqrt{\dfrac{\sin(\delta+\varphi)\sin(\varphi-\alpha)}{\cos(\delta+\theta)\cos(\theta-\alpha)}}\right]^2} \quad (12.37)$$

where α and θ angles are defined in Figure 12.20. The value of the angle δ for ordinary concrete walls is generally taken as a value between δ = ½φ and ⅔φ.

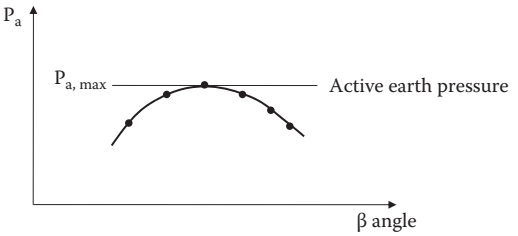

FIGURE 12.21 Active earth pressure determination by trails.

TABLE 12.1
Coulomb's K_a Values for $\theta = 0$ and $\alpha = 0$ with $\delta = \frac{1}{2}\varphi$ and $\frac{2}{3}\varphi$ by Equation 12.37

	K_a	
φ	$\delta = \frac{1}{2}\varphi$	$\delta = \frac{2}{3}\varphi$
26	0.353	0.347
28	0.326	0.321
30	0.301	0.297
32	0.278	0.275
34	0.256	0.254
36	0.236	0.235
38	0.217	0.217
40	0.199	0.200
42	0.183	0.184
44	0.167	0.167

Table 12.1 and Figure 12.22 show K_a values for vertical wall ($\theta = 0$) with horizontal backfill ($\alpha = 0$) with $\delta = \frac{1}{2}\varphi$ and $\frac{2}{3}\varphi$. From Figure 12.22, it can be seen that K_a deceases with increasing φ angle and the effect of the wall friction angle δ is small. Readers are encouraged to create their own spreadsheet to compute K_a values for other combinations of α, θ, φ, and δ values based on Equation 12.37.

It is noted that in Equation 12.37, when $\alpha = 0$ (horizontal backfill), $\theta = 0$ (vertical wall), and $\delta = 0$ (smooth wall) are chosen, Coulomb's K_a value becomes the same as the one by Rankine's formula (Equation 12.13).

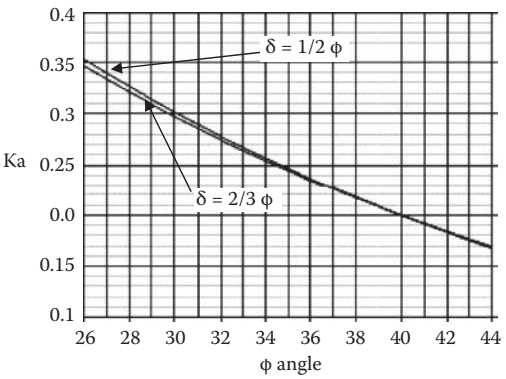

FIGURE 12.22 K_a with $\delta = \frac{1}{2}\varphi$ and $\frac{2}{3}\varphi$ ($\alpha = 0$ and $\theta = 0$).

12.5.2 Passive Case

The passive earth pressure theory by Coulomb similarly assumes that a solid wedge is formed behind a rigid wall, which is moved against the soil mass until failure as

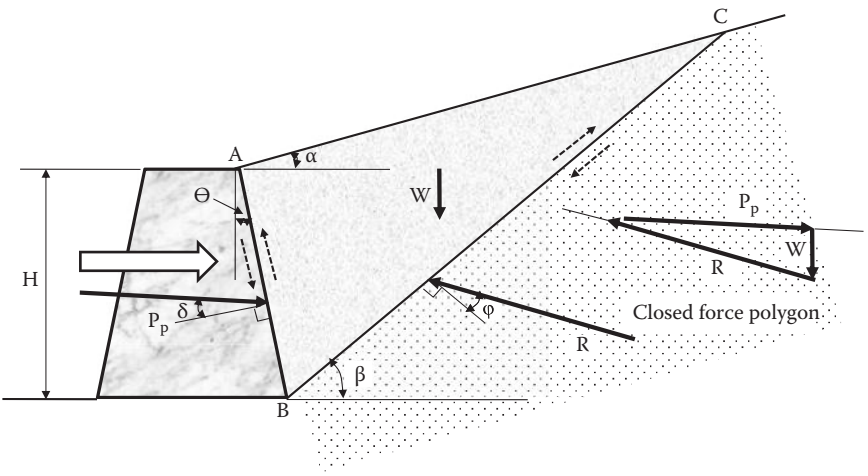

FIGURE 12.23 Coulomb's passive earth pressure.

seen in Figure 12.23. Note that in the passive case, the wedge is pushed up so that the reactions R and P_p act from opposite directions relative to the faces of the sliding wedge as compared with the active case in Figure 12.20. By assumed β angle, P_p is obtained from a closed force polygon. By trials for several β values, the minimum P_p is assigned as the passive earth thrust.

Analytical solution for Coulomb's passive earth pressure is given by:

$$P_p = \frac{1}{2}\gamma H^2 \frac{\cos^2(\varphi+\theta)}{\cos^2\theta\cos(\delta-\theta)\left[1-\sqrt{\frac{\sin(\delta+\varphi)\sin(\varphi+\alpha)}{\cos(\delta-\theta)\cos(\theta-\alpha)}}\right]^2} = \frac{1}{2}\gamma K_p H^2 \quad (12.38)$$

$$K_p = \frac{\cos^2(\varphi+\theta)}{\cos^2\theta\cos(\delta-\theta)\left[1-\sqrt{\frac{\sin(\delta+\varphi)\sin(\varphi+\alpha)}{\cos(\delta-\theta)\cos(\theta-\alpha)}}\right]^2} \quad (12.39)$$

Table 12.2 and Figure 12.24 show K_p values for a vertical wall (θ = 0) with horizontal backfill (α = 0) with δ = ½φ and ⅔φ. Much higher K_p values are obtained in comparison with K_a value and some differences between δ = ½φ and ⅔φ cases are observed. Again readers are encouraged to create own spreadsheet to obtain K_p values for other α, θ, δ, and φ values based on Equation 12.39.

It is noted again that for α = 0 (horizontal backfill), θ = 0 (vertical wall), and δ = 0 (smooth wall), Coulomb's K_p value by Equation 12.39 becomes the same as the one by Rankine's formula (Equation 12.23).

TABLE 12.2
Coulomb's K_p Values for $\theta = 0$, $\alpha = 0$ with $\delta = \frac{1}{2}\varphi$ and $\frac{2}{3}\varphi$ by Equation 12.39

	K_p	
φ	$\delta = \frac{1}{2}\varphi$	$\delta = \frac{2}{3}\varphi$
26	3.787	4.400
28	4.325	5.154
30	4.976	6.108
32	5.775	7.337
34	6.767	8.957
36	8.022	11.154
38	9.639	14.233
40	11.771	18.737
42	14.662	25.696
44	18.714	37.270

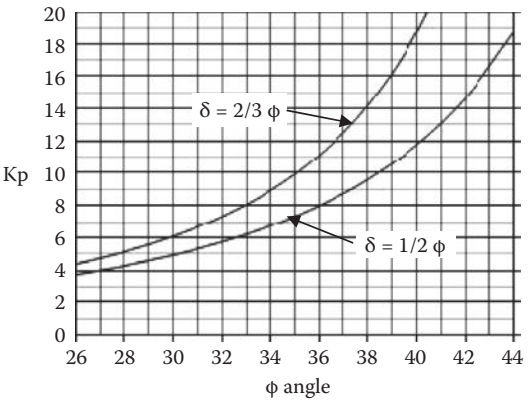

FIGURE 12.24 K_p with $\delta = \frac{1}{2}\varphi$ and $\frac{2}{3}\varphi$ ($\alpha = 0$ and $\theta = 0$).

12.5.3 Coulomb Lateral Pressure Distribution

In Coulomb's method, the total thrusts P_a and P_p are determined based on closed force polygons. Since the force diagram uses only $\sum V = 0$ and $\sum H = 0$ equilibriums (that is, $\sum M = 0$ is not used), the points of applications of P_a and P_p are not determined. Coulomb assumed that the distributions of the lateral pressures are triangular and thus P_a and P_p are applied at $\frac{1}{3}H$ from the base of the wall as seen in Figure 12.25.

The lateral pressure at the base of the wall $\sigma_{a,\,at\,base}$ and $\sigma_{p,\,at\,base}$ are assigned as:

$$\sigma_{a,\,at\,base} = \gamma H\, K_a \sin(90° - \theta) \tag{12.40}$$

$$\sigma_{p,\,at\,base} = \gamma H\, K_p \sin(90° - \theta) \tag{12.41}$$

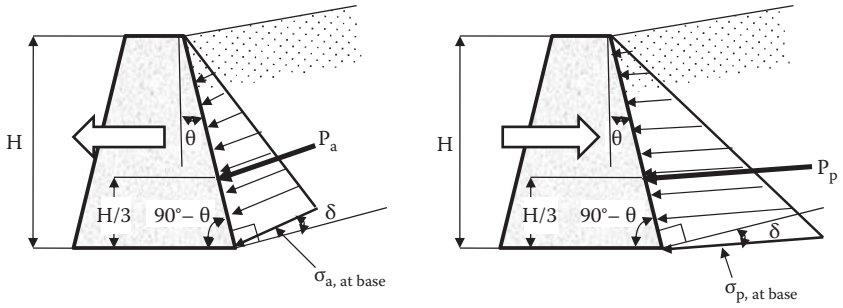

FIGURE 12.25 Coulomb's assumed lateral pressure distributions.

Then, P_a and P_p can be calculated by the area of pressure triangles:

$$P_a = \tfrac{1}{2}\,\sigma_{a,\ at\ base} \bullet (\text{face length of wall}) = \tfrac{1}{2}\,[\gamma H\, K_a \sin(90° - \theta)] \bullet [H/\sin(90° - \theta)] = \tfrac{1}{2}\gamma H^2 K_a$$

$$P_p = \tfrac{1}{2}\,\sigma_{p,\ at\ base} \bullet (\text{face length of wall}) = \tfrac{1}{2}\,[\gamma H\, K_p \sin(90° - \theta)] \bullet [H/\sin(90° - \theta)] = \tfrac{1}{2}\gamma H^2 K_p$$

By this way, above two equations become exactly same as in Equation 12.36 and Equation 12.38, respectively.

The points of applications of the thrusts P_a and P_p are at H/3 from the base of the wall. However, it shall be recognized that ***the application at H/3 is merely an assumption made by Coulomb***. As will be discussed later in this chapter this assumption is only applicable in a certain wall movement mode.

12.6 LATERAL EARTH PRESSURE DUE TO SURCHARGE LOAD

In many occasions, lateral earth pressures due to surcharge loads on backfill cannot be neglected. Those include due to traffic load, surface pavement, crane load, footing load, etc. Several examples of those cases are shown below.

12.6.1 Due to Infinitively Long Uniform Surcharge Load

When an infinitively long uniform surcharge load q_0 is placed on a level-ground backfill as seen in Figure 12.26, uniform lateral earth pressure is developed against the wall. The lateral pressure σ_h is:

$$\sigma_h = K\, q_0 \tag{12.42}$$

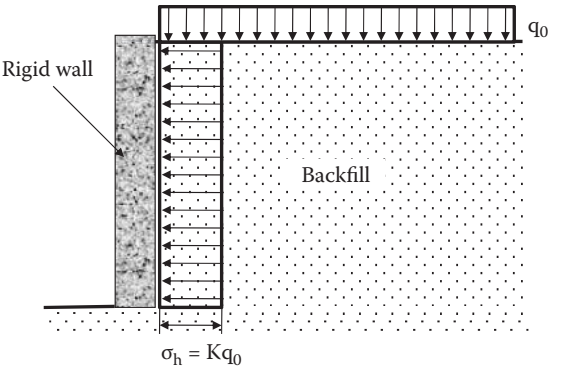

FIGURE 12.26 Lateral earth pressure due to uniform surcharge load.

where K could be any parameter of K_0, K_a, or K_p depending on the situation. This is an additional stress to the lateral stress due to the gravity of the backfill.

12.6.2 Due to Point Load (No Yielding Wall)

When a **point load** P is applied on the backfill as seen in Figure 12.27, the Boussinesq's solution can be utilized, by which the lateral stress σ_x in an elastic half space is provided. To obtain the lateral stress on a non-yielding wall, the Boussinesq's solution is

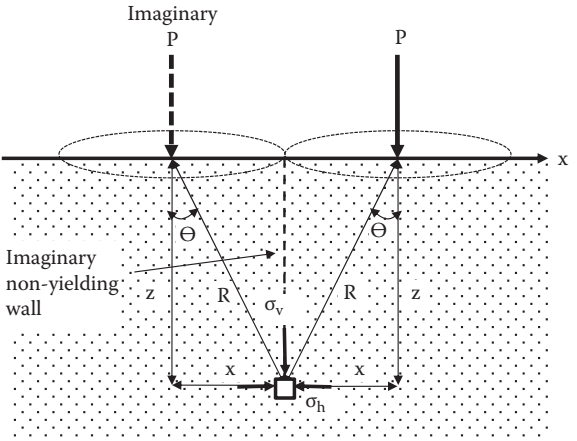

FIGURE 12.27 Boussinesq's lateral stress on nonyielding wall due to a point load.

doubled to account zero displacement of the wall by two symmetrical point loads as seen. Then, σ_h in this case yields:

$$\sigma_h = \frac{P}{\pi z^2}\left[\frac{3x^2z^3}{R^5} - \frac{(1-2\mu)z^2}{(R+z)R}\right] \qquad (\mu\text{: Poisson's ratio of soils}) \qquad (12.43)$$

12.6.3 Due to Line Load (No Yielding Wall)

Similarly, Boussinesq's line load solution is doubled to get lateral stress on a non-yielding vertical wall as (Figure 12.28):

$$\sigma_h = \frac{2q}{\pi}\frac{z}{x^2+z^2}\left[1-\cos(2\theta)\right] = \frac{2q}{\pi}\frac{\sin\theta\sin 2\theta}{R} \qquad (12.44)$$

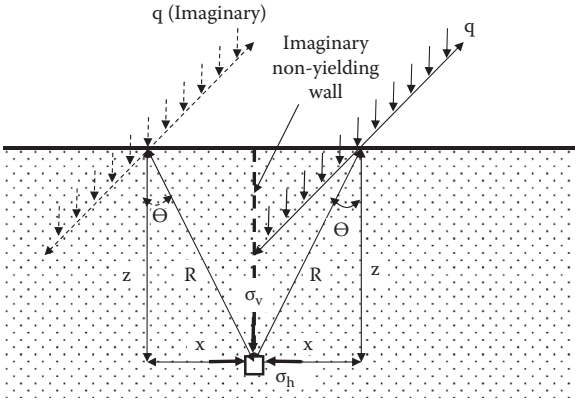

FIGURE 12.28 Boussinesq's lateral stress on nonyielding wall due to a line load.

Exercise 12.3

A line load q = 50 kN/m is applied at 1 m from the edge of the vertical wall. Compute the distribution of the lateral stress against the non-yielding wall down to z = 3 m.

Solution:

Equation 12.44 is utilized with q = 50 kN/m, x = 1 m and z = 0 to 3 m.

$R = (x^2 + z^2)^{0.5}$

$\theta = \tan^{-1}(x/z)$

A spreadsheet was created, and the result is plotted in Figure 12.29.

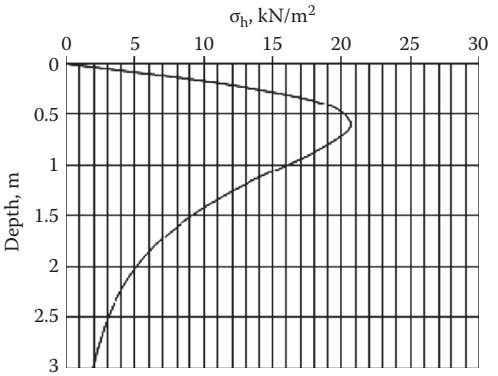

FIGURE 12.29 Lateral earth pressure against non-yielding wall due to line load.

12.6.4 Due to Strip Load (No Yielding Wall)

Similarly, Boussinesq's solution due to a strip load (Figure 12.30) is doubled to get lateral stress on a non-yielding wall as:

$$\sigma_h = \frac{2q}{\pi}\left[\beta - \sin\beta\,\cos(2\theta)\right] \tag{12.45}$$

where angles β and θ are defined in Figure 12.30.

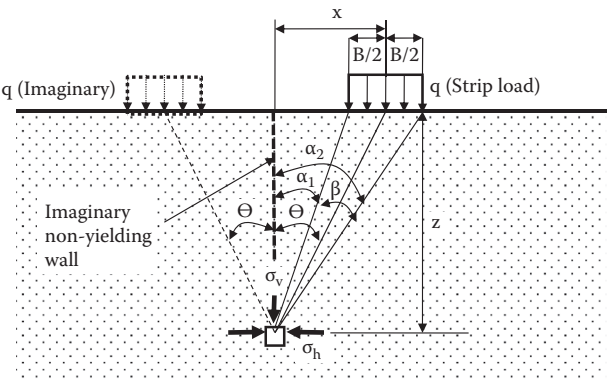

FIGURE 12.30 Boussinesq's lateral stress against nonyielding wall due to strip load.

Exercise 12.4

A 100 kN/m^2 strip load is applied with 1 m wide (B = 1 m) footing on top of backfill soil. The center of the footing is located at 3 m (x = 3m) from the edge of a vertical

TABLE 12.3
Solution to Exercise 12.4

z (m)	θ (radian)	β (radian)	σ_h (kN/m²)
0	0.0000	0.0000	0.00
1	1.2490	0.1022	11.70
2	0.9828	0.1556	13.70
3	0.7854	0.1674	10.66
4	0.6435	0.1602	7.36
5	0.5404	0.1471	4.97
6	0.4636	0.1333	*3.41*
7	0.4049	0.1206	2.40
8	0.3588	0.1095	1.73
9	0.3218	0.0999	1.28
10	0.2915	0.0917	0.97

wall. Compute and plot lateral stress distribution with depth down to 10 m for a non-yielding wall.

Solution:

From the geometry in Figure 12.30,

$\theta = \tan^{-1}(x/z)$

$\alpha_1 = \tan^{-1}[(x - B/2)/z]$

$\alpha_2 = \tan^{-1}[(x + B/2)/z]$

$\beta = \alpha_2 - \alpha_1$

$x = 3$ m, $B = 1$ m, and $q = 100$ kN/m².

Spreadsheet (Table 12.3) is constructed to compute σ_h values for $z = 0$ to 10 m by using Equation 12.45 and the above information. The results are plotted in Figure 12.31.

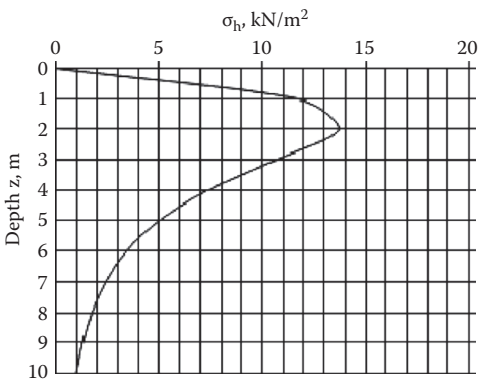

FIGURE 12.31 Lateral earth pressure against non-yielding wall due to strip load.

Note that the above Boussinesq's elastic solutions are used to estimate lateral earth pressures against vertical non-yielding walls (at-rest condition) due to various surcharge loads. However, its applicability to active and passive cases is questionable, since those conditions require sufficient wall displacements to cause failure in the backfill soils.

12.7 COULOMB, RANKINE, OR OTHER PRESSURES?

Two classic lateral earth pressure theories (Coulomb and Rankine) were presented at failed stage in backfill soils, and these two theories are still popular among practicing geotechnical engineers. Several questions may arise at this stage:

1. Is it engineer's preference to use either solution?
2. Are there any rules to select either solution?
3. Are there any limitations on those theories?

In order to answer the above questions, first, distinct differences between Coulomb theory and Rankine theory are listed below:

1. Rankine theory assumes that the entire backfill soils are in a state of plastic equilibrium (failure) as seen in Figure 12.6 and Figure 12.11, while Coulomb assumes that failure occurs only along failure surface in the backfill and along the wall face as seen in Figure 12.20 and Figure 12.23, and the inside of a failed wedge could be solid (nonfailed).
2. In Rankine theory, due to the plastic equilibrium of the entire soil elements, the distribution of the lateral pressure is a linearly increasing function (triangle distribution), while Coulomb's theory assumes its triangular distribution without any assurance.
3. Rankine pressure is applied normal to the boundary (wall) face, while Coulomb pressure is applied with δ angle (wall friction angle) inclined from the normal to the wall face.

Now consider typical earth pressure problems in Figure 12.32: (a) gravity retaining wall, (b) cantilever retaining wall, (c) basement wall, (d) geosynthetic reinforced earth, and (e) bridge abutment. Among those, obviously, Case (c) uses at-rest lateral earth pressure (K_0) since no movement of the basement wall of this stable structure is anticipated. Case (a) and Case (e) may be the Coulomb case since the back faces of the wall may become sliding planes. Meanwhile, Case (b) and Case (d) will be Rankine's case since the wall face will not be sliding surfaces. In Case (b) and Case (d), Rankine's lateral earth pressure is applied on imaginary vertical planes (shown with dotted lines).

Case (a) and Case (e) need further attention. Both could be a Coulomb's case. However, anticipated failure modes are different. In Case (a), the wall most likely fails by a rotation of the wall about the base of the wall, while Case (e) may be a failure mode of rotation about the top due to restriction of top movement due to the bridge structure.

Wall movement mode (rotation about top, rotation about base, and translational) makes pressure distribution different. Figure 12.33 demonstrates potential pressure distribution differences according to the different wall movement modes. In

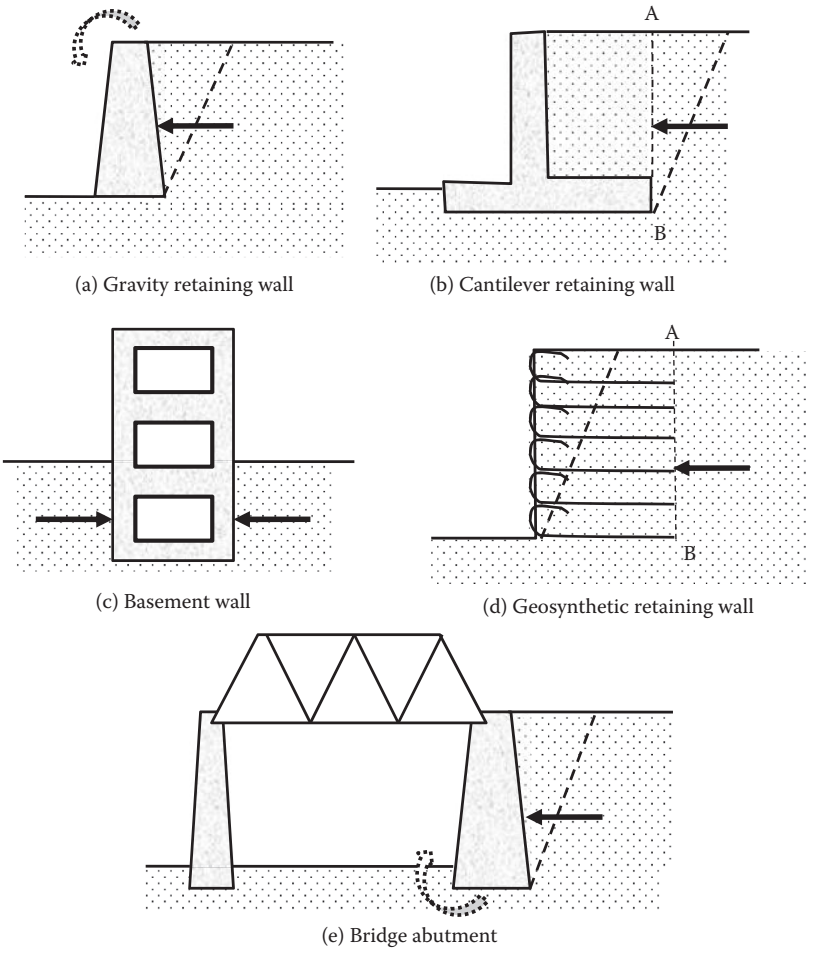

(a) Gravity retaining wall
(b) Cantilever retaining wall
(c) Basement wall
(d) Geosynthetic retaining wall
(e) Bridge abutment

FIGURE 12.32 Various lateral earth pressure problems.

Figure 12.33a, initial backfill soil elements are modeled with equal parallelograms. In figure (b), the wall is moved in a translational way. In this case, a solid soil wedge like the one observed in Coulomb's model would be formed in the backfill soil and the wall face becomes a sliding surface. Inside the wedge, initial parallelogram elements still maintain the original shapes. In figure (c), the wall is rotated about the base. Most likely all the backfill soil elements of the failed section deform to more skewed parallelograms as seen. This implies that the entire elements in the failed zone become plastic (failed) as in the case of Rankine theory. However, in figure (c), the back face of the wall may be a failure surface so that the Coulomb's solution with a triangle earth pressure distribution may be the most appropriate solution.

Based on the above observations of backfill soils, lateral earth pressure distributions are predicted in Figure 12.33 (d). At-rest pressure (K_0) from no wall movement

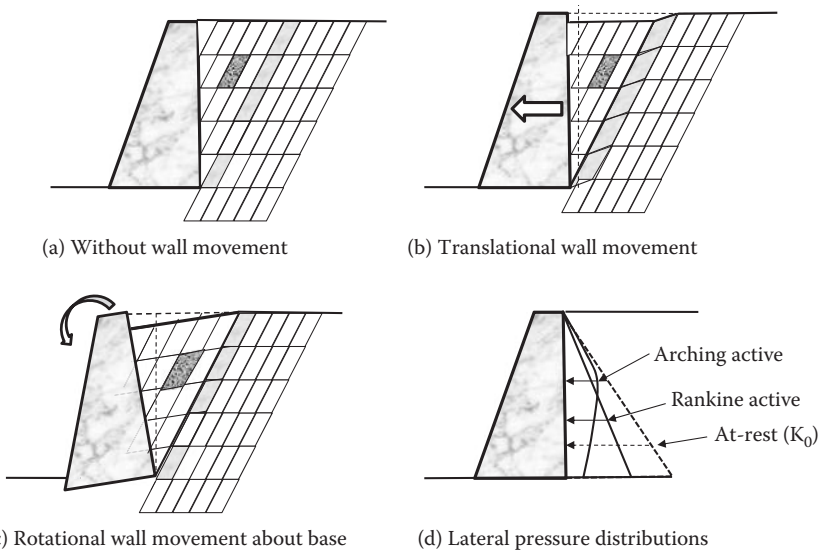

FIGURE 12.33 Different pressure distributions with different wall failure modes. (After Taylor, D. W. (1948). *Fundamentals of Soil Mechanics*, John Wiley & Sons, New York.)

(figure (a)) is seen with a dotted line. Since figure (c) is similar to the Rankine's pressure distribution, the pressure distribution will be triangular shape. figure (b) could be the Coulomb's condition since the solid failure wedge will be formed in the backfill. However, the distribution will be hardly triangular shaped as Coulomb assumed. In fact, those non-yielded soil elements, in particular, at the upper part of the wedge, form arches between the wall face and the failure plane in the backfill. **Arching stress** will be higher at the upper section of the backfill since more elements of soils are involved to form arches. Accordingly, the distribution will be the one shown as "arching active" in Figure 12.33d.

The above illustration suggests that Coulomb's triangular pressure distribution assumption is not always true, and thus, the point of application of the thrust could be different from ⅓H from the base of the wall. The readers can refer literatures (for example, ***Fang and Ishibashi 1985***) on the effect of wall movement modes on the lateral earth pressures.

12.8 SUMMARY

Estimation of lateral earth pressure is a very important practice in many foundation designs. Basic theories of Coulomb and Rankine were presented in this chapter, which are widely used by engineers at present. However, as demonstrated in Section 12.7, an adequate estimation of the lateral earth pressure is not as simple as it looks. Engineers shall be aware of those limitations and different assumptions behind those theories.

REFERENCES

Coulomb, C. A. (1776), Essai sur une Application des Règles des Maximus et Minimis à quelques Problèms de Statique Relatifs à l'Architecture (An attempt to apply the rules of maxima and minima to several problems of stability related to architecture). *Mémoires de l'Académie royale des Sciences,* Paris, Vol. 7, 343–382.

Fang, Y. S. and Ishibashi, I. (1986), Static Earth Pressures with Various Wall Movements, *Journal of Geotechnical Engineering,* ASCE, Vol. 112, No. 3, 317–333.

Jaky, J. (1944), The coefficient of Earth pressure at rest (in Hungarian), *Journal of Society of Hungarian Architects and Engineers*, 355–358.

Mayne, P. W. and Kulhawy, F. H. (1982), OCR relationships in soil, *Journal of Geotechnical Engineering*, ASCE, Vol. 108, No. GT6, 851–872.

Mazindrani, Z. H. and Ganjali, M. H. (1997), Lateral Earth pressure problem of cohesive backfill with inclined surface, *Journal of Geotechnical and Geoenvironmental Engineering*, ASCE, Vol. 123, No. 2, 110–112.

Rankine, W. J. M. (1857), On the stability of loose Earth, *Philosophical Transactions of Royal Society of London*, 147, Part 1, pp. 9–27.

Taylor, D. W. (1948), *Fundamentals of Soil Mechanics*, John Wiley & Sons, New York.

Terzaghi, K. (1943), *Theoretical Soil Mechanics*, John Wiley & Sons, New York.

Problems

12.1 through 12.4. Compute the lateral earth pressure at rest against the basement wall as seen in the figure.

(a) Plot the distribution of the earth pressure against the wall as well as the water pressure if any.

(b) Compute the total lateral thrust against the wall, including the water pressure if any.

(c) Compute the point of application of the total thrust against the wall.

			Soil 1			Soil 2		
	H_1	H_2	γ_1	φ_1	OCR_1	γ_2	φ_2	OCR_2
Problem	m	m	kN/m³	Degree		kN/m³	Degree	
12.1	6	0	18.5	35	1.0	—	—	—
12.2	6	0	18.5	35	2.0	—	—	—
12.3	2	4	18.5	35	1.0	19.0	40	1.0
12.4	2	4	18.5	35	4.0	19.0	40	2.0

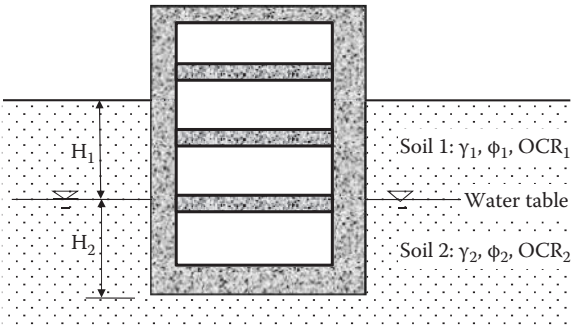

12.5 through 12.8. For a smooth rigid vertical wall with granular soil backfill as seen in the figure below, compute the Rankine's active lateral earth pressure against the wall (no need to compute the water pressure).

(a) Plot the distribution of the active earth pressure.
(b) Compute the total lateral earth thrust against the wall.
(c) Compute the point of application of the thrust.

			Soil 1		Soil 2		
	H_1	H_2	γ_1	φ_1	γ_2	φ_2	q_o
Problem	m	m	kN/m³	Degree	kN/m³	Degree	kPa
12.5	6	0	18.8	36	—	—	0
12.6	6	0	18.0	32	—	—	20
12.7	3	3	18.0	32	18.5	35	0
12.8	3	3	18.0	32	18.5	35	20

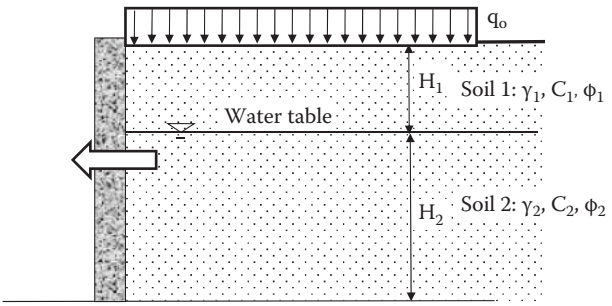

12.9 through 12.12. For a smooth rigid vertical wall with granular soil backfill as seen in the figure below, compute the Rankine's passive lateral earth pressure against the wall (no need to compute the water pressure).

(a) Plot the distribution of the active earth pressure.
(b) Compute the total lateral earth thrust against the wall.
(c) Compute the point of application of the thrust.

			Soil 1		Soil 2		
	H_1	H_2	γ_1	φ_1	γ_2	φ_2	q_o
Problem	m	m	kN/m³	Degree	kN/m³	Degree	kPa
12.9	6	0	18.8	36	—	—	0
12.10	6	0	18.0	32	—	—	20
12.11	3	3	18.0	32	18.5	35	0
12.12	3	3	18.0	32	18.5	35	20

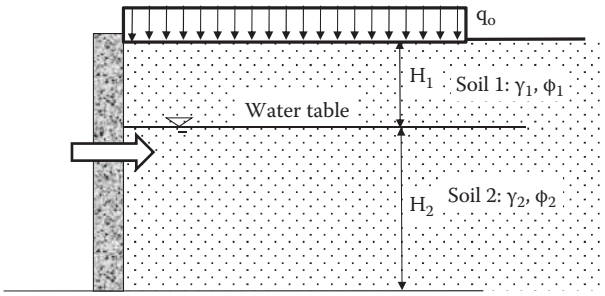

12.13 through 12.16. For a smooth rigid vertical wall with cohesive soil backfill as seen in the figure below, compute the Rankine's active lateral earth pressure against the wall (no need to compute the water pressure).

(a) Plot the distribution of the active earth pressure.
(b) Compute the total lateral earth thrust against the wall.
(c) Compute the point of application of the thrust.

			Soil 1			Soil 2			
Problem	H_1 m	H_2 m	γ_1 kN/m^3	c_1 kPa	φ_1 Degree	γ_2 kN/m^3	c_2 kPa	φ_2 Degree	q_o kPa
12.13	6	0	18.0	20.2	14	—	—	—	0
12.14	6	0	18.0	20.2	14	—	—	—	20
12.15	4	2	18.0	20.2	14	18.5	22.7	17	0
12.16	4	2	18.0	20.2	14	18.5	22.7	17	20

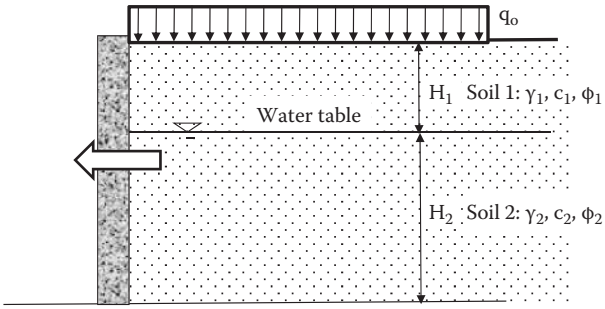

12.17 through 12.20. For a smooth rigid vertical wall with cohesive soil backfill as seen in the figure below, compute the Rankine's passive lateral earth pressure against the wall (no need to compute the water pressure).

(a) Plot the distribution of the passive earth pressure.
(b) Compute the total lateral earth thrust against the wall.
(c) Compute the point of application of the thrust.

			Soil 1			Soil 2			
Problem	H_1 m	H_2 m	γ_1 kN/m³	c_1 kPa	φ_1 Degree	γ_2 kN/m³	c_2 kPa	φ_2 Degree	q_o kPa
12.17	6	0	18.0	20.2	14	—	—	—	0
12.18	6	0	18.0	20.2	14	—	—	—	20
12.19	4	2	18.0	20.2	14	18.5	22.7	17	0
12.20	4	2	18.0	20.2	14	18.5	22.7	17	20

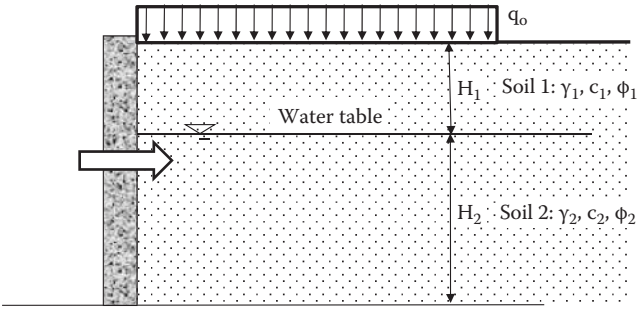

12.21 through 12.24. For a rigid retaining wall as seen below, compute Coulomb's active lateral earth thrust against the wall face AB and the point of application of the resultant force.

					Backfill Soil Property		
Problem	H m	Wall Friction Angle, δ, Degree	α Degree	θ Degree	γ, kN/m³	φ, Degree	c, kPa
12.21	4	20	0	0	19.2	40	0
12.22	4	17	0	0	18.5	34	0
12.23	4	20	0	20	19.2	40	0
12.24	4	20	10	20	19.2	40	0

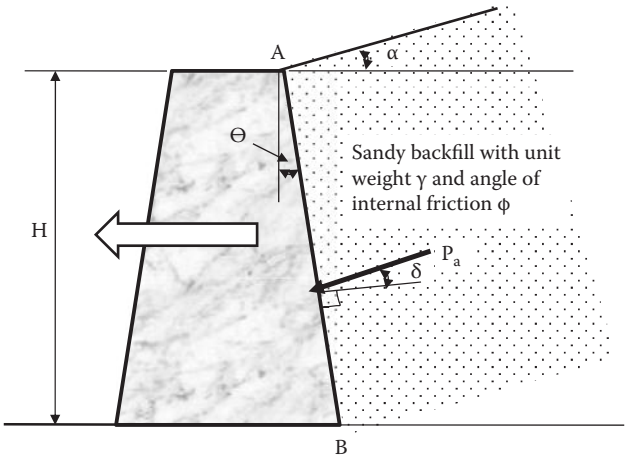

12.25 through 12.28. For a rigid retaining wall as seen below, compute Coulomb's passive lateral earth thrust against the wall face AB and the point of application of the resultant force.

Problem	H m	Wall Friction Angle, δ, Degree	α Degree	θ Degree	Backfill Soil Property		
					γ, kN/m³	φ, Degree	c, kPa
12.25	4	20	0	0	19.2	40	0
12.26	4	17	0	0	18.5	34	0
12.27	4	20	0	20	19.2	40	0
12.28	4	20	10	20	19.2	40	0

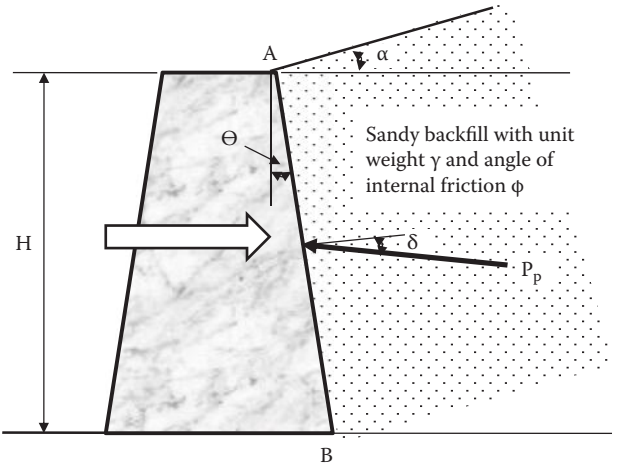

12.29. The figure below shows surcharge loads (a uniform surcharge load and two point loads) on the horizontal backfill. Compute and plot the induced lateral earth pressure distribution against the non-yielding vertical wall due to the combination of the surcharge loads. Compute it along the nearest wall face of the point loads.

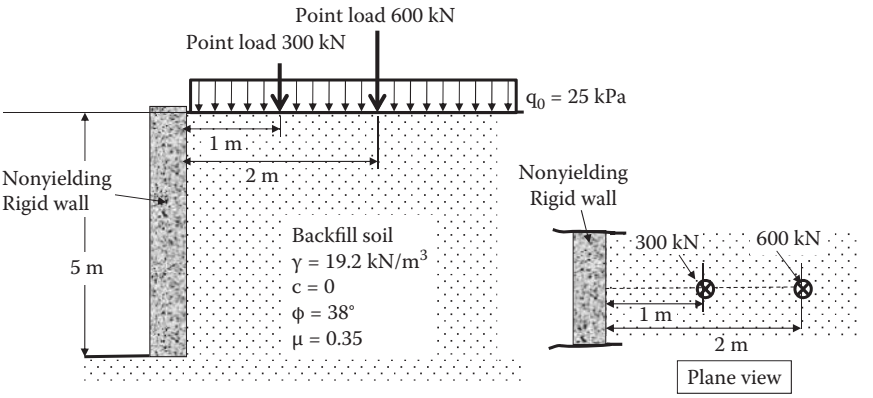

12.30. The figure below shows surcharge loads (a point load and a line load) on the horizontal backfill. Compute and plot the induced lateral earth pressure distribution against the nonyielding vertical wall due to the combination of the surcharge loads. Compute it along the nearest wall face of the point load.

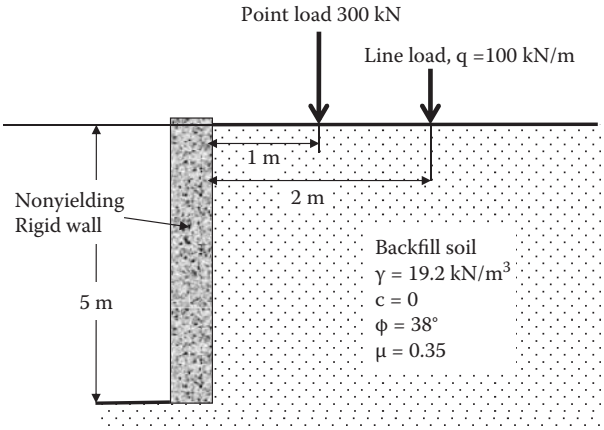

13 Bearing Capacity

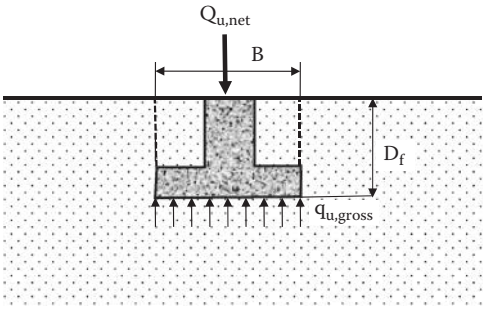

13.1 INTRODUCTION

Bearing capacity is the maximum pressure that the soil can support at foundation level without failure. This is a key design parameter for foundation design and also for design of retaining walls at the base level. This chapter deals with the basic theory and practice of this subject.

13.2 TERZAGHI'S BEARING CAPACITY THEORY

Terzaghi (1943) developed a bearing capacity solution for a continuous shallow foundation with a footing width B and an embedded depth D_f under a level ground as seen in Figure 13.1. He adapted the punching shear theory on metals of ***Prandtl (1920)*** to soils, including soil's gravitational force. He assumed that (1) soil shear strength is given by $\tau_f = c + \sigma_n \tan \varphi$, (2) footing depth D_f is replaced by a surcharge load ($q = \gamma D_f$), and (3) the footing base has a rough surface.

In the model, when the footing load increases, the footing base pushes the triangle zone I downward. Then zone I pushes zone II sideways, and zone II pushes zone III further. Zone I behaves as a rigid elastic body during the entire process. Zone III is the Rankine's passive earth pressure zone and zone II is a transitional zone. From the force equilibriums on those zones, Terzaghi obtained the following equation to determine the **ultimate bearing capacity** q_u as

$$q_u = cN_c + \gamma_1 D_f N_q + \tfrac{1}{2}\gamma_2 B N_\gamma \tag{13.1}$$

where, N_c, N_q, and N_γ are **bearing capacity factors** and functions of the effective angle of internal friction φ' of the soil. γ_1 is the unit weight of soil above the base of

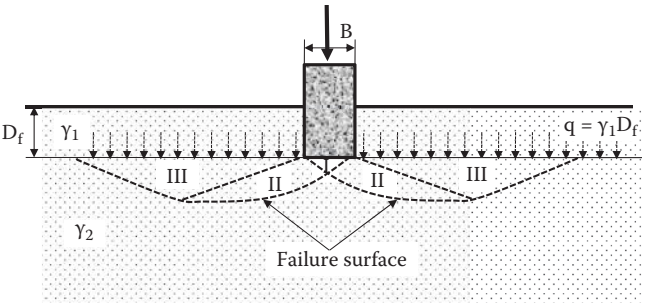

FIGURE 13.1 Terzaghi's bearing capacity model.

footing level and γ_2 is the unit weight of soil below the base level. The cN_c term is a contribution to the bearing capacity from the cohesion resistance along the failure surface, and it is zero for $c = 0$ materials (non-cohesive soils). The term $\gamma_1 D_f N_q$ is a contribution from the surcharge load $\gamma_1 D_f$ at the footing base level, and it is zero for foundations placed on the ground surface. The $\frac{1}{2}\gamma_2 B N_\gamma$ term is from the frictional resistance along the failure surface, and it is zero for $\varphi' = 0$ materials (cohesive soils).

It is interesting to note that in Equation 13.1 the unit of q_u is the stress unit such as kN/m^2. The bearing capacity q_u in the stress unit increases when the foundation width B increases by the contribution of the term $\frac{1}{2}\gamma_2 B N_\gamma$. This implies that in cases with $c = 0$ and $D_f = 0$ when the footing width B increases twice, the total footing load increases four times. It makes a sense since when B increases the shearing failure zone is enlarged and is extend to a deeper depth, and thus, the shear resisting surface increases more than in proportion to the increased footing width B.

Although Terzaghi gave original N_c, N_q, and N_γ equations, those are not shown here to avoid confusions since several major modifications were made since his original contribution. Those values are, instead, given in the following section.

13.3 GENERALIZED BEARING CAPACITY EQUATION

Terzaghi's bearing capacity equation is valid for limited cases: that is, (1) foundation is shallow, (2) two-dimensional strip footings, (3) no shearing resistance through the depth D_f zone, and (4) footing load is applied in vertical direction only. To extend the applicability of Equation 13.1 to more general situations, the following modified general bearing capacity is proposed by several researchers:

$$q_u = cN_c f_{cs} f_{cd} f_{ci} + \gamma_1 D_f N_q f_{qs} f_{qd} f_{qi} + \tfrac{1}{2}\gamma_2 B N_\gamma f_{\gamma s} f_{\gamma d} f_{\gamma i} \tag{13.2}$$

where

f_{cs}, f_{qs}, $f_{\gamma s}$: **shape factors** for different footing shapes other than strip footings
f_{cd}, f_{qd}, $f_{\gamma d}$: **depth factors** for deeper shallow foundations
f_{ci}, f_{qi}, $f_{\gamma i}$: **inclination factors** for various directions of footing load than the vertical load

Although several researchers (***De Beer 1970***, ***Hansen 1970***, ***Vesic 1973***, ***Hanna and Meyerhof 1981***, etc.) proposed modified bearing capacity factors, shape factors,

TABLE 13.1
Bearing Capacity Factors by Meyerhof

φ′	N_c	N_q	N_γ	φ′	N_c	N_q	N_γ
0	5.14	1.00	0.00	26	22.25	11.85	8.00
1	5.38	1.09	0.002	27	23.94	13.20	9.46
2	5.63	1.20	0.01	28	25.80	14.72	11.19
3	5.90	1.31	0.02	29	27.86	16.44	13.24
4	6.19	1.43	0.04	30	30.14	18.40	15.67
5	6.49	1.57	0.07	31	32.67	20.63	18.56
6	6.81	1.72	0.11	32	35.49	23.18	22.02
7	7.16	1.88	0.15	33	38.64	26.09	26.17
8	7.53	2.06	0.21	34	42.16	29.44	31.15
9	7.92	2.25	0.28	35	46.12	33.30	37.15
10	8.35	2.47	0.37	36	50.59	37.75	44.43
11	8.80	2.71	0.47	37	55.63	42.92	53.27
12	9.28	2.97	0.60	38	61.35	48.93	64.07
13	9.81	3.26	0.74	39	67.87	55.96	77.33
14	10.37	3.59	0.92	40	75.31	64.20	93.69
15	10.98	3.94	1.13	41	83.86	73.90	113.99
16	11.63	4.34	1.36	42	93.71	85.38	139.32
17	12.34	4.77	1.66	43	105.11	99.02	171.14
18	13.10	5.26	2.00	44	118.37	115.31	211.41
19	13.93	5.80	2.40	45	133.88	134.88	262.74
20	14.83	6.40	2.87	46	152.10	158.51	328.73
21	15.82	7.07	3.42	47	173.64	187.21	414.32
22	16.88	7.82	4.07	48	199.26	222.31	526.44
23	18.05	8.66	4.82	49	229.93	265.51	674.91
24	19.32	9.60	5.72	50	266.89	319.07	873.84
25	20.72	10.66	6.77				

Source: Meyerhof, G. G. (1963), *Canadian Geotechnical Journal*, Vol. 1, No. 1, 16–26.

depth factors, and inclination factors in Equation 13.2 based on experimental observations, the values of ***Meyerhof (1963)*** are presented here. Table 13.1 shows the bearing capacity factors N_c, N_q, and N_γ as functions of the effective angle of internal friction φ′, and Figure 13.2 plots those values.

Other modification factors by Meyerhof are summarized below.

Shape Factors F_{CS}, F_{QS}, $F_{\gamma S}$

For other than strip footings, such as rectangular, square, and circular footings, this modification is needed. For rectangular footings, B (width) and L (length) shall always be assigned as B ≤ L. For circular footings, B is the diameter of the footing and B = L is assigned.

$$\text{for } \varphi' = 0, \qquad f_{cs} = 1 + 0.2(B/L) \tag{13.3}$$

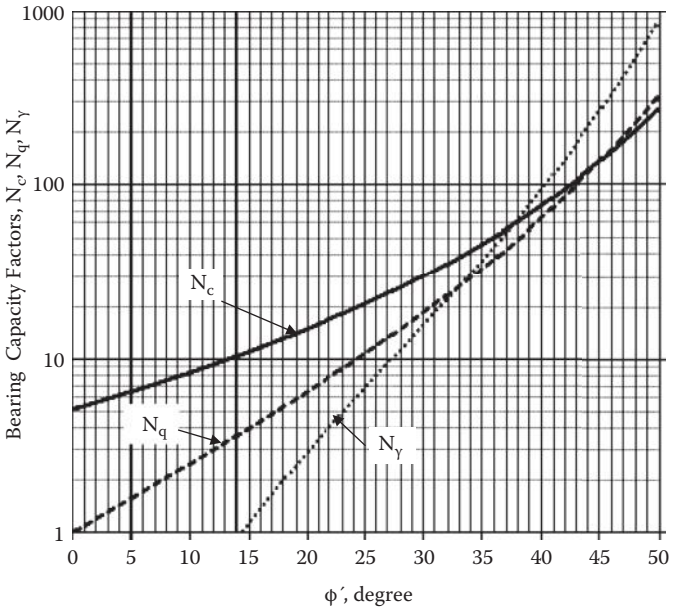

FIGURE 13.2 Bearing capacity factor N_c, N_q, and N_γ. (By Meyerhof, G. G. (1963), *Canadian Geotechnical Journal*, Vol. 1, No. 1, 16–26.)

$$f_{qs} = f_{\gamma s} = 1 \tag{13.4}$$

for $\varphi' \geq 10°$,

$$f_{cs} = 1 + 0.2(B/L)\tan^2(45° + \varphi'/2) \tag{13.5}$$

$$f_{qs} = f_{\gamma s} = 1 + 0.1(B/L)\tan^2(45° + \varphi'/2) \tag{13.6}$$

Depth Factors F_{cd}, F_{qd}, $F_{\gamma d}$

for $\varphi' = 0$,

$$f_{cd} = 1 + 0.2(D_f/B) \tag{13.7}$$

$$f_{qd} = f_{\gamma d} = 1 \tag{13.8}$$

for $\varphi' \geq 10°$,

$$f_{cd} = 1 + 0.2(D_f/B)\tan(45° + \varphi'/2) \tag{13.9}$$

$$f_{qd} = f_{\gamma d} = 1 + 0.1(D_f/B)\tan(45° + \varphi'/2) \tag{13.10}$$

Inclination Factors F_{ci}, F_{qi}, $F_{\gamma i}$

$$f_{ci} = f_{qi} = (1 - \beta/90°)^2 \tag{13.11}$$

$$f_{\gamma i} = (1 - \beta/\varphi')^2 \tag{13.12}$$

where β is the inclined angle of the footing load with respect to the vertical.

Note that all the modification factors approach to 1.0 for Terzaghi's original conditions (B/L = ∞, $D_f \approx 0$, and $\beta = 0°$) and Equation 13.1 can be used in that situation with the bearing capacity factors in Table 13.1.

Exercise 13.1

A strip footing with soil's parameters is shown in Figure 13.3. Determine the bearing capacity of this foundation soil.

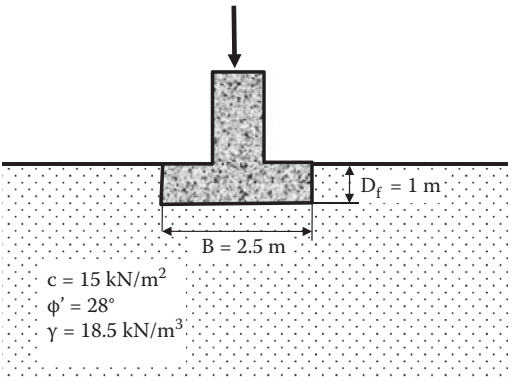

FIGURE 13.3 Footing for Exercise 13.1.

Solution:

For φ′ = 28°, from Table 13.1 or Figure 13.2, $N_c = 25.80$, $N_q = 14.72$, and $N_\gamma = 11.19$

Shape factors f_{cs}, f_{qs}, $f_{\gamma s}$:

This is a strip footing so that B/L = 0, then $f_{cs} = f_{qs} = f_{\gamma s} = 1$

Depth factors f_{cd}, f_{qd}, $f_{\gamma d}$:

for φ′ ≥ 10°, $f_{cd} = 1 + 0.2(D_f/B)\tan(45° + \varphi'/2) = 1 + 0.2(1/2.5)\tan(45° + 28°/2) = 1.133$

$f_{qd} = f_{\gamma d} = 1 + 0.1(D_f/B)\tan(45° + \varphi'/2) = 1 + 0.1(1/2.5)\tan(45° + 28°/2) = 1.067$

Inclination factors f_{ci}, f_{qi}, $f_{\gamma i}$:

Since β = 0, $f_{ci} = f_{qi} = f_{\gamma i} = 1.0$

From Equation 13.2, and $\gamma^1 = \gamma^2 = 18.5$ kN/m^3

$$q_u = cN_c f_{cs} f_{cd} f_{ci} + \gamma_1 D_f N_q f_{qs} f_{qd} f_{qi} + \tfrac{1}{2}\gamma_2 B N_\gamma f_{\gamma s} f_{\gamma d} f_{\gamma i}$$

$$= 15 \times 25.80 \times 1 \times 1.133 \times 1 + 18.5 \times 1 \times 14.72 \times 1 \times 1.067 \times 1 + \tfrac{1}{2} \times 18.5 \times 2.5 \times 11.19 \times 1 \times 1.067 \times 1$$

$$= 438.5 + 290.5 + 276.1 = \mathbf{1005.1\ kN/m^2} \leftarrow$$

Exercise 13.2

In Exercise 13.1, when **the footing width B is increased to 5.0 m**, what is the bearing capacity q_u?

Solution:

Depth factors f_{cd}, f_{qd}, $f_{\gamma d}$:

for $\varphi' \geq 10^o$, $f_{cd} = 1 + 0.2(D_f/B)\tan(45° + \varphi'/2) = 1 + 0.2(1/5.0)\tan(45° + 28°/2) = 1.067$

$f_{qd} = f_{\gamma d} = 1 + 0.1(D_f/B)\tan(45°+\varphi'/2) = 1 + 0.1(1/5.0)\tan(45° + 28°/2) = 1.033$

All other modification factors remain the same as in Exercise 13.1 and B = 5.0 m

$q_u = cN_c f_{cs} f_{cd} f_{ci} + \gamma_1 D_f N_q f_{qs} f_{qd} f_{qi} + \frac{1}{2}\gamma_2 B N_\gamma f_{\gamma s} f_{\gamma d} f_{\gamma i}$

$= 15 \times 25.80 \times 1 \times 1.067 \times 1 + 18.5 \times 1 \times 14.72 \times 1 \times 1.033 \times 1 + \frac{1}{2} \times 18.5 \times 5.0 \times 11.19 \times 1 \times 1.033\ 1$

$= 412.93 + 281.31 + 534.62 =$ **1228.9 kN/m²** (22.3% increase over Exercise 13.1) ←

Exercise 13.3

In Exercise 13.1 problem, if the footing is **a square footing with B = L = 2.5 m**, what is the bearing capacity q_u?

Solution:

Shape factors f_{cs}, f_{qs}, $f_{\gamma s}$ for B = L = 2.5 m :

For $\varphi' \geq 10°$, $f_{cs} = 1 + 0.2(B/L)\tan^2(45° + \varphi'/2) = 1 + 0.2(2.5/2.5)\tan^2(45° + 28°/2) = 1.55$

$f_{qs} = f_{\gamma s} = 1 + 0.1(B/L)\tan^2(45° + \varphi'/2) = 1 + 0.1(2.5/2.5)\tan^2(45° + 28°/2) = 1.28$

Depth factors and inclination factors remains the same as Exercise 13.1 and thus

$q_u = cN_c f_{cs} f_{cd} f_{ci} + \gamma_1 D_f N_q f_{qs} f_{qd} f_{qi} + \frac{1}{2}\gamma_2 B N_\gamma f_{\gamma s} f_{\gamma d} f_{\gamma i}$

$= 15 \times 25.80 \times 1.55 \times 1.133 \times 1 + 18.5 \times 1 \times 14.72 \times 1.28 \times 1.067 \times 1$

$+\frac{1}{2} \times 18.5 \times 2.5 \times 11.19 \times 1.28 \times 1.067 \times 1$

$= 679.6 + 371.9 + 353.4 =$ **1404.9 kN/m²** (39.8 % increase over Exercise 13.1) ←

Exercise 13.4

In Exercise 13.1, if **the footing load is inclined with 5° from the vertical**, what is the bearing capacity q_u?

Solution:

Inclination factors change from Exercise 13.1 with $\beta = 5^o$ and all others remain the same.

Inclination factors f_{ci}, f_{qi}, $f_{\gamma i}$:

$f_{ci} = f_{qi} = (1 - \beta^o/90^o)^2 = (1 - 5^o/90^o)^2 = 0.892$

$f_{\gamma i} = (1 - \beta/\varphi')^2 = (1 - 5^o/28^o)^2 = 0.675$

$q_u = cN_c f_{cs} f_{cd} f_{ci} + \gamma_1 D_f N_q f_{qs} f_{qd} f_{qi} + \frac{1}{2}\gamma_2 B N_\gamma f_{\gamma s} f_{\gamma d} f_{\gamma i}$

$= 15 \times 25.80 \times 1 \times 1.133 \times 0.892 + 18.5 \times 1 \times 14.72 \times 1 \times 1.067 \times 0.892$

$+ \frac{1}{2} \times 18.5 \times 2.5 \times 11.19 \times 1 \times 1.067 \times 0.675$

$= 391.1 + 259.2 + 186.4 =$ **836.7 kN/m²** (16.8 % reduction from Exercise 13.1) ←

From the above four exercises, the effect of the footing width, the footing shapes, and the inclination angle of footing load on the bearing capacity intensity q_u are clearly observed.

13.4 CORRECTION DUE TO WATER TABLE ELEVATION

One more influential parameter on the bearing capacity is the water table elevation relative to the footing depth. In the bearing capacity equations (Equation 13.1 and 13.2), the unit weights of soils γ_1 and γ_2 are included. Those are the ones for above the footing base level and below the base level, respectively. When soils are under the water table, the submerged unit weight γ_1' $(= \gamma_1 - \gamma_w)$ and γ_2' $(= \gamma_2 - \gamma_w)$ shall be used.

To accommodate these unit weight changes in the bearing capacity equations, Figure 13.4 is prepared. In the figure, Γ_1 and Γ_2 are assigned as general unit weights of soils above the footing base level and below the base level, respectively, and they are used in places of γ_1 and γ_2 in Equation 13.1 and Equation 13.2 when the ground water is encountered in the bearing capacity computation. Also z_w is defined as the ground. Water table elevation from the ground surface. It is assumed that when

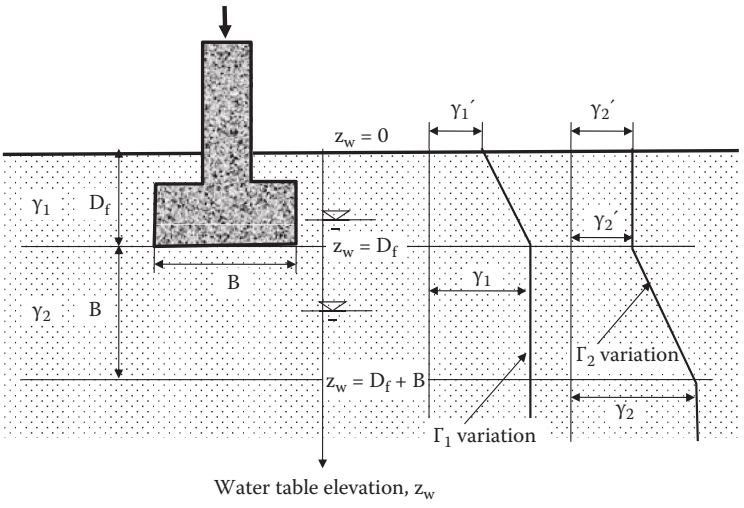

FIGURE 13.4 Effect of water table elevation on bearing capacity equations.

the water table is located beyond the depth B below the footing base level, there will be no effect by the water table at all on the bearing capacity. The depth B below the footing base is an approximated depth of anticipated bearing capacity failure. According to those observations and the assumption, following boundary values of general unit weights of soils, Γ_1 and Γ_2 can be defined:

Water table at $z_w = 0$ (on the top of ground surface)

$$\Gamma_1 = \gamma_1' \quad \text{and} \quad \Gamma_2 = \gamma_2'$$

Water table at $z_w = D_f$ (at the footing base level)

$$\Gamma_1 = \gamma_1 \quad \text{and} \quad \Gamma_2 = \gamma_2'$$

Water table at $z_w \geq D_f + B$ (beyond the depth B below the footing base)

$$\Gamma_1 = \gamma_1 \quad \text{and} \quad \Gamma_2 = \gamma_2$$

The variations of Γ_1 and Γ_2 are plotted in Figure 13.4 by approximating the changes between $z_w = 0$ to D_f for Γ_1, and between $z_w = D_f$ to $D_f + B$ for Γ_2 as linear lines. Accordingly, the following equations are obtained:

for $0 \leq z_w < D_f$

$$\Gamma_1 = \gamma_1 + \gamma_w (z_w/D_f - 1) \tag{13.13}$$

$$\Gamma_2 = \gamma_2' \tag{13.14}$$

for $D_f \leq z_w < D_f + B$

$$\Gamma_1 = \gamma_1 \tag{13.15}$$

$$\Gamma_2 = \gamma_2 + \gamma_w[z_w - (D_f + B)]/B \tag{13.16}$$

for $z_w \geq D_f + B$

$$\Gamma_1 = \gamma_1 \tag{13.17}$$

$$\Gamma_2 = \gamma_2 \tag{13.18}$$

Exercise 13.5

In Exercise 13.1, when ground water table is located, (a) at ground surface, and (b) at 2 m below the ground surface, compute the bearing capacity q_u for each case. Assume that the total unit weights of soils $\gamma_1 = \gamma_2 = 18.5$ kN/m^2 for both wet and dry conditions.

Solution:

(a) Water table elevation $z_w = 0$ m

$\Gamma_1 = \gamma_1 + \gamma_w (z_w/D_f - 1) = 18.5 + 9.81\ (0/1 - 1) = 18.5 - 9.81 = 8.69$ kN/m^3

$\Gamma_2 = \gamma_2' = 18.5 - 9.81 = 8.69$ kN/m^3

All other values remain the same as Exercise 13.1 and thus

$q_u = cN_c f_{cs} f_{cd} f_{ci} + \Gamma_1 D_f N_q f_{qs} f_{qd} f_{qi} + \frac{1}{2}\ \Gamma_2 B N_\gamma f_{\gamma s} f_{\gamma d} f_{\gamma i}$

$= 15 \times 25.80 \times 1 \times 1.133 \times 1 + 8.69 \times 1 \times 14.72 \times 1 \times 1.067 \times 1 + \frac{1}{2} \times 8.69 \times 2.5 \times 11.19 \times 1 \times 1.067 \times 1$

$= 438.5 + 136.5 + 129.7 =$ **704.7 kN/m**^{2} (29.9 % deduction from Exercise 13.1) ←

(b) Water table elevation $z_w = 2$ m ($D_f < z_w < D_f + B$)

$\Gamma_1 = \gamma_1 = 18.5$ kN/m^3

$\Gamma_2 = \gamma_2 + \gamma_w[z_w - (D_f + B)]/B = 18.5 + 9.81[2-(1 + 2.5)]/2.5 = 18.5 - 5.9 = 12.6$ kN/m^3

All other values remain the same as Exercise 13.1 and thus

$q_u = cN_c f_{cs} f_{cd} f_{ci} + \Gamma_1 D_f N_q f_{qs} f_{qd} f_{qi} + \frac{1}{2}\ \Gamma_2 B N_\gamma f_{\gamma s} f_{\gamma d} f_{\gamma i}$

$= 15 \times 25.80 \times 1 \times 1.133 \times 1 + 18.5 \times 1 \times 14.72 \times 1 \times 1.067 \times 1 + \frac{1}{2} \times 12.6 \times 2.5 \times 11.19 \times 1 \times 1.067 \times 1$

$= 438.5 + 290.6 + 188.1 =$ **917.2 kN/m**^{2} (8.7 % deduction from Exercise 13.1) ←

13.5 GROSS VERSUS NET BEARING CAPACITY

The bearing capacity q_u in the discussions so far is the ultimate **gross bearing capacity**, which is the ultimate stress value that the soil can carry at the base of the footing level, as seen in Figure 13.5. When the unit weight of concrete for the foundation is assumed to be the same as the unit weight of soils, the following vertical force equilibrium is obtained:

$$q_{u,gross} \bullet B = Q_{u,net} + \gamma_{soil} \bullet D_f \bullet B \tag{13.19}$$

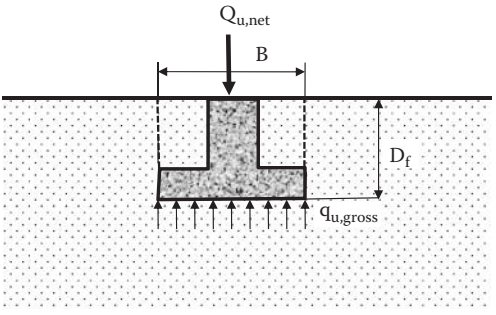

FIGURE 13.5 Gross and net bearing capacities.

And thus

$$q_{u,net} = Q_{u,net}/B = q_{u,gross} - \gamma_{soil} \bullet D_f \tag{13.20}$$

where $q_{u,net}$ is defined as the ultimate **net bearing capacity**, which is the maximum carrying stress level at the ground surface level. This implies that $Q_{u,net}$ (= $q_{u,net}$ • B) is the superstructure's total load, which the soil can support. Accordingly, Equation 13.1 and 13.2 can be rewritten in term of the net bearing capacity in Equation 13.21 and 13.22, respectively.

$$\begin{aligned} q_{u,net} &= q_u - \gamma_1 D_f = (cN_c + \gamma_1 D_f N_q + \tfrac{1}{2}\gamma_2 B N_\gamma) - \gamma_1 D_f \\ &= cN_c + \gamma_1 D_f (N_q - 1) + \tfrac{1}{2}\gamma_2 B N_\gamma \end{aligned} \tag{13.21}$$

$$\begin{aligned} q_{u,net} &= q_u - \gamma_1 D_f = (cN_c f_{cs} f_{cd} f_{ci} + \gamma_1 D_f N_q f_{qs} f_{qd} f_{qi} + \tfrac{1}{2}\gamma_2 B N_\gamma f_{\gamma s} f_{\gamma d} f_{\gamma i}) - \gamma_1 D_f \\ &= cN_c f_{cs} f_{cd} f_{ci} + \gamma_1 D_f (N_q f_{qs} f_{qd} f_{qi} - 1) + \tfrac{1}{2}\gamma_2 B N_\gamma f_{\gamma s} f_{\gamma d} f_{\gamma i} \end{aligned} \tag{13.22}$$

The gross and the net capacities shall not be mixed up. The net bearing capacity is the one used for designing superstructure above the foundation. The settlement of soils is caused due to increased stresses by new foundations, and thus, the net pressure is used for settlement analysis.

13.6 FACTOR OF SAFETY ON BEARING CAPACITY

Since the bearing capacity equations utilize many empirical factors as discussed, in addition to uncertainties on material properties, and spatial non-uniformity of soils, a proper value of **factor of safety** (FS) is needed to obtain the **design (allowable) bearing capacity**, q_d. There are several possible ways to apply factor of safety, among them (1) apply for $q_{u,gross}$ equations, (2) apply for material properties.

13.6.1 FS for Gross Bearing Capacity

The design bearing capacity is obtained by applying FS in the gross-bearing capacity equations (Equation 13.1 or Equation 13.2), and thus:

$$q_{d,gross} = q_{u,gross}/FS = (cN_c + \gamma_1 D_f N_q + \tfrac{1}{2}\gamma_2 B N_\gamma)/FS \tag{13.23}$$

$$q_{d,gross} = q_{u,gross}/FS = (cN_c f_{cs} f_{cd} f_{ci} + \gamma_1 D_f N_q f_{qs} f_{qd} f_{qi} + \tfrac{1}{2}\gamma_2 B N_\gamma f_{\gamma s} f_{\gamma d} f_{\gamma i})/FS \tag{13.24}$$

Then, the design net bearing capacity is obtained by subtracting $\gamma_1 D_f$ from $q_{d,gross}$ in Equation 13.23 or Equation 13.24 as:

$$q_{d,net} = q_{d,gross} - \gamma_1 D_f \tag{13.25}$$

Note that several literatures apply FS directly to $q_{u,net}$ in Equation 13.21 or Equation 13.22. However, it is more logical to apply FS to $q_{u,gross}$ first and then subtract $\gamma_1 D_f$ from it to obtain the design net value as in Equation 13.25, since $\gamma_1 D_f$ is a rather sure value so that there is no need to apply the same level of FS to it.

13.6.2 FS for Strength Parameters

Due to a certain degree of unreliability of soil shear strength parameters, the reduced design strength parameters are first obtained as:

$$c_d = c/FS \tag{13.26}$$

$$\varphi_d = \tan^{-1}(\tan\varphi/FS) \tag{13.27}$$

where c and φ are the measured cohesion and the angle of internal friction of soils and c_d and φ_d are design values of those. Then c_d and φ_d values are inserted into the net bearing capacity equations (Equation 13.21 or Equation 13.22) to obtain the design net bearing capacity value without further applying FS in the equations, or with a marginal FS value in the equations.

In either method, the determination of factor of safety is important, but it is not an easy task. It requires the best judgment of engineers based on wealth of experience on the subject matter.

13.7 SUMMARY

Knowing the bearing capacity is the first requirement for shallow foundation designs. In this chapter only the basic concept was presented. There are many alternative solutions and additional cases in this subject area. The readers shall refer to those detailed discussions in foundation engineering textbooks.

REFERENCES

De Beer, E. E. (1970), Experimental determination of the shape factors and bearing capacity factors of sand, *Geotechnique*, Vol. 20, No. 4, pp. 387–411.

Hanna, A. M. and Meyerhof, G. G. (1981), Experimental evaluation of bearing capacity of footings subjected to inclined loads, *Canadian Geotechnical Journal*, Vol. 18, No. 4, pp. 599–603.

Hansen, J. B. (1970), *A Revised and Extended Formula for Bearing Capacity*, Bulletin 28, Danish Geotechnical Institute, Copenhagen.

Meyerhof, G. G. (1963), Some recent research on the bearing capacity of foundations, *Canadian Geotechnical Journal*, Vol. 1, No. 1, 16–26.

Prandtl, L. (1920), Über die Härte plastischer Körper, Nachr. Kgl. Ges. Wiss. Göttingen, *Math. Phys*. Klasse.

Terzaghi, K. (1943), *Theoretical Soil Mechanics*, John Wiley & Sons, New York.

Vesic, A. S. (1973), Analysis of ultimate loads of shallow foundations, *Journal of the Soil Mechanics and Foundations Division*, ASCE, Vol. 99, No. SM1, pp. 45–73.

Problems

13.1. A rectangular footing (2.0 m × 3.0 m) is placed on a granular soil at 2 m below the ground surface as seen, determine
(a) Gross ultimate bearing capacity
(b) Net ultimate bearing capacity
(c) Net design bearing capacity with factor of safety = 2.5. Use Equation 13.25

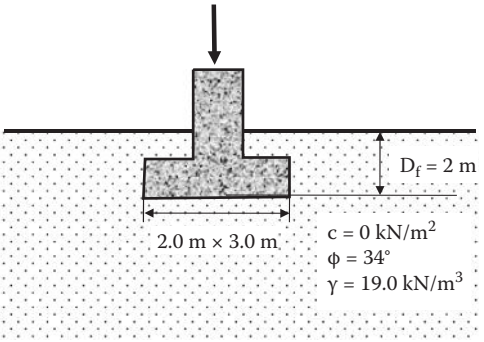

13.2. For Problem 13.1, the rectangular footing is replaced by a strip fooling with B = 2.0 m. The other conditions remain the same. Determine
(a) Gross ultimate bearing capacity.
(b) Net ultimate bearing capacity.
(c) Net design bearing capacity with factor of safety = 2.5. Use Equation 13.25.

13.3. In Problem 13.1, the load is inclined 5° from the vertical. The other conditions remain the same. Determine
(a) Gross ultimate bearing capacity.
(b) Net ultimate bearing capacity.
(c) Net design bearing capacity with factor of safety = 2.5. Use Equation 13.25.

13.4. For the same foundation as in Problem 13.1, when the ground water table is at the depth 3 m below the ground surface, determine
(a) Gross ultimate bearing capacity.
(b) Net ultimate bearing capacity.
(c) Net design bearing capacity with factor of safety = 2.5. Use Equation 13.25.

13.5. A rectangular footing (2.0 m × 3.0 m) is placed on a cohesive soil at 2 m below the ground surface as seen in this figure below. Determine
(a) Gross ultimate bearing capacity.
(b) Net ultimate bearing capacity.
(c) Net design bearing capacity with factor of safety = 3.0. Use Equation 13.25.

Assume that the soil properties above and the below the ground table are the same.

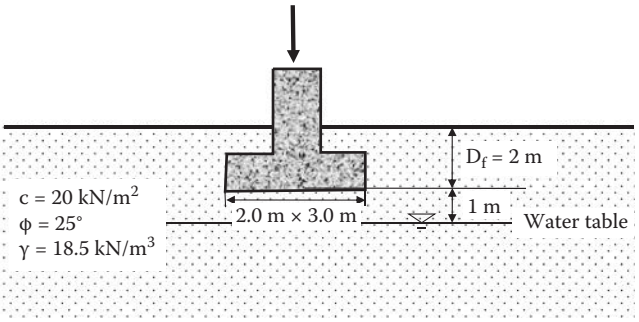

13.6. In Problem 13.5, the footing is replaced with a circular one with D = 1.392 m, which gives the same footing area as the 2.0 m × 3.0 m rectangular one in Problem 13.5. The other conditions remain the same. Determine
(a) Gross ultimate bearing capacity.
(b) Net ultimate bearing capacity.
(c) Net design bearing capacity with factor of safety = 3.0. Use Equation 13.25.

13.7. In Problem 13.5, the footing is replaced with a strip footing with B = 2.0 m. The other conditions remain the same. Determine
(a) Gross ultimate bearing capacity.
(b) Net ultimate bearing capacity.
(c) Net design bearing capacity with factor of safety = 3.0. Use Equation 13.25.

13.8 In Problem 13.5, the load is inclined 5° from the vertical. The other conditions remain the same. Determine
(a) Gross ultimate bearing capacity.
(b) Net ultimate bearing capacity.
(c) Net design bearing capacity with factor of safety = 3.0. Use Equation 13.25.

Numerical Answers to Selected Problems

2.3 (a) $\gamma_t = 11.01 kN/m^3$, (b) w = 426%
2.4 (a) $\gamma_t = 19.93$ kN/m^3, (b) S = 79.6%, (c) $\gamma_d = 17.33$ kN/m^3
2.5 (a) S = 59.4%, (b) $\gamma_d = 16.89$ kN/m^3, (c) $\gamma' = 9.19$ kN/m^3, $\gamma_t = 20.44$ kN/m^3
2.6 (a) $\gamma_t = 17.76$ kN/m^3, (b) $\gamma_t = 19.72$ kN/m^3, (c) $G_s = 2.68$
2.7 (a) S = 42.9%, (b) e = 0.538, (c) w = 10.7%, (d) $\gamma_t = 18.85$ kN/m^3
2.8 (a) W = 1850 kN, (b) n = 0.350, (c) W = 1795.5 kN

3.11 SL = 15.3%

5.1 $D_r = 67.2\%$
5.2 $\gamma_t = 18.96$ kN/m^3
5.4 (c) e = 0.426, S = 74.9%, (d) $\gamma_t = 20.50$ kN/m^3, (e) w = 8.3% to 14.8%
5.5 (c) e = 0.488, and S = 76.9 %, (d) $\gamma_t = 20.27$ kN/m^3, (e) w = 10.7% to 16.0%
5.8 (a) $V_{borrow} = 2763$ m^3, (b) $W_{borrow} = 53881$ kN
5.9 $\gamma_d = 16.23$ kN/m^3
5.10 (a) CBR = 10

6.1 (b) q = 4.52 m^3/day
6.2 (a) k = 0.04 cm/sec, (b) k = 0.0346 cm/sec, (c) k = 0.164 cm/sec
6.3 k = 0.0399 cm/sec
6.4 k = 0.0108 cm/sec
6.5 k = 0.000418 cm/sec
6.6 k = 0.000387 cm/sec
6.7 k = 0.000355 cm/sec
6.8 k = 0.000195 cm/sec
6.9 (b) q = 0.583 cm^3/sec/cm
6.10 (b) q = 0.443 cm^3/sec/cm
6.11 (b) q = 0.505 cm^3/sec/cm
6.12 (b) q = 0.401 cm^3/sec/cm
6.13 (b) $P_w = 798.2$ kN/m
6.14 (b) $P_w = 1182.5$ kN/m

7.5 $\sigma'_A = 81.9$ kPa, $\sigma'_B = 125.4$ kPa, $\sigma'_C = 167.8$ kPa, $\sigma'_D = 241.3$ kPa
7.6 $\sigma'_A = 180$ kPa, $\sigma'_B = 293.0$ kPa, $\sigma'_C = 338.9$ kPa
7.7 $\sigma'_A = 126.0$ kPa, $\sigma'_B = 177.5$ kPa, $\sigma'_C = 230.9$ kPa, $\sigma'_D = 296.6$ kPa
7.8 (a) $\Delta\sigma' = +62.1$ kPa increase
7.9 (a) $\Delta\sigma' = -71.2$ kPa decrease
7.10 (a) $h_{capillary} = 0.2$ to 1 m, (b) $h_{capillary} = 2$ to 10 m, (c) $h_{capillary} = 20$ to 100 m

7.13 (a) $u_{hydrostatic} = 3.92$ kPa, (b) $u_{seepage} = 1.96$ kPa, (c) $u_{total} = 5.88$ kPa, (d) $i_c = 0.886$, (e) FS = 1.33
7.14 $H_1 > 90.63$ cm
7.15 (a) FS = 4.75, (b) FS = 3.59
7.16 6.27 m
7.17 10.0 m
7.18 3.25 m
8.11 $\Delta\sigma_v(A) = 94.92$ kN/m^2, $\Delta\sigma_v(B) = 82.48$ kN/m^2, $\Delta\sigma_v(C) = 27.65$ kN/m^2
8.12 $\Delta\sigma_v(A) = 17.1$ kN/m^2, $\Delta\sigma_v(B) = 52.8$ kN/m^2, $\Delta\sigma_v(C) = 41.33$ kN/m^2
8.13 $\Delta\sigma_v(A) = 17.5$ kN, $\Delta\sigma_v(B) = 18.3$ kN/m^2, $\Delta\sigma_v(C) = 34.9$ kN/m^2
8.14 $\Delta\sigma_v = 14.8$ kN/m^2
8.15 $\Delta\sigma_v = 44.8$ kN/m^2
8.16 $\Delta\sigma_v = 44.6$ kN/m^2

9.1 (a) $S_i = 4.25$ mm, (b) $S_i = 2.72$ mm, (c) $S_i = 3.36$ mm
9.2 (a) $S_i = 4.08$ mm, (b) $S_i = 2.04$ mm, (c) $S_i = 3.60$ mm
9.4 (a) $t_{50} = 8.37$ years, (b) $t_{90} = 35.96$ years, (c) U ≈ 17%, U ≈ 38%
9.5 (a) $t_{50} = 2.08$ years, (b) $t_{90} = 8.97$ years, (c) U ≈ 36%, (d) U ≈ 76%
9.6 (a) $t_{50} = 2.2$ years, (b) $t_{90} = 9.1$ years
9.7 (a) $C_v = 7.9$ mm^2/min, (b) $C_v = 9.47$ mm^2/min
9.8 (a) $C_v = 43.2$ mm^2/min, (b) $C_v = 34.2$ mm^2/min
9.9 (c) $C_c = 1.24$
9.10 (c) $C_c = 0.696$
9.11 $S_f = 0.0498$ m
9.12 $S_s = 0.0105$ m
9.13 $S_f = 0.0248$ m
9.14 $S_f = 0.0404$ m
9.15 $S_s = 0.0096$ m
9.16 0.261 m
9.17 0.0353 m

10.1 $\sigma_\theta = 59.87$ kPa, $\tau_\theta = -34.6$ kPa
10.2 $\sigma_\theta = 233.9$ kPa, $\tau_\theta = -13.1$ kPa
10.3 $\sigma_\theta = 63.54$ kPa, $\tau_\theta = -73.48$ kPa
10.4 $\sigma_\theta = 20.0$ kPa, $\tau_\theta = 25.0$ kPa
10.6 (d) $\sigma_\theta = 59.9$ kPa, $\tau_\theta = -34.6$ kPa
10.7 (d) $\sigma_\theta = 239$ kPa $\tau_\theta = -13$ kPa
10.8 (d) $\sigma_\theta = 64$ kPa, $\tau_\theta = -73$ kPa
10.9 (d) $\sigma_\theta = 20$ kPa, $\tau_\theta = 25$ kPa
10.10 $\sigma_c = 43$ kPa, $\tau_c = 24$ kPa
10.11 $\sigma_c = 60$ kPa, $\tau_c = -50$ kPa
10.12 (a) $\sigma_1 = 107$ kPa, $\sigma_3 = 43$ kPa
10.13 (a) $\tau_{max} = +90$ kPa, $\tau_{min} = -90$ kPa

11.3 $\varphi = 15.3^o$ and c = 22 kPa
11.4 (a) $\varphi = 32.4^o$, (b) $\tau_N = 95.1$ kPa
11.5 $\varphi' = 8.3^o$

11.6 $c' = 44$ kPa, $\varphi' = 8.2^o$
11.7 $q_u = 77$ kPa
11.8 (a) $\varphi' = 15^o$, $c' = 21$ kPa
11.9 $\varphi\ ' = 27.2^o$
11.10 93.7 kPa
11.11 22.2 kPa
11.12 (b) $\sigma_f = 72.7$ kPa, $\tau_f = 64$ kPa
11.13 (b) $c = 58$ kPa and $\varphi = 14^o$, $c' = 63$ kPa and $\varphi' = 14.5^o$
11.14 (a) $\sigma_1 = 288$ kPa, (b) $u_f = 25$ kPa
11.15 (b) $c = 20$ kPa and $\varphi = 20.2^o$, $c' = 18$ kPa and $\varphi' = 24.2^o$
11.16 (a) $\sigma_1 = 181$ kPa, (b) $u_f = 13$ kPa
11.17 (a) $\sigma_1 - \sigma_3 = 143.5$ kPa, (b) $u_f = 18.5$ kPa
11.18 $q_u = 36.2$ kPa
11.19 $u_f = -58$ kPa (negative)
11.20 $u_f = -30$ kPa (negative)
11.21 $C_u = 27.97$ kPa

12.1 (b) P = 142.0 kN/m
12.2 (b) P = 211.1 kN/m
12.3 (b) Total P = 173.39 kN/m, (c) at 1.84 m from the base of the wall
12.4 (b) Total P = 236.96 kN/m, (c) at 2.06 m from the base of the wall
12.5 (b) Total P = 87.85 kN/m, (c) at 2.0 m from the base of the wall
12.6 (b) Total P = P_{soil}136.42 kN/m, (c) at 2.27 m from the base of the wall
12.7 (b) Total P = 79.39 kN/m, (c) at 2.22 m from the base of the wall
12.8 (b) Total P = 114.08 kN/m, (c) at 2.48 m from the base of the wall
12.9 (b) Total P = 1303.5 kN/m, (c) at 2.0 m from the base of the wall
12.10 (b) Total P = 1445.1 kN/m, (c) at 2.27 m from the base of the wall
12.11 (b) Total P = 1005.7 kN/m, (c) at 2.08 m from the base of the wall
12.12 (b) Total P = 1422.4 kN/m, (c) at 2.32 m from the base of the wall
12.13 (b) Total P = 53.73 kN/m, (c) at 1.042 m from the base of the wall
12.14 (b) Total P = 126.98 kN/m, (c) at 2.172 m from the base of the wall
12.15 (b) Total P = 28.155 kN/m, (c) at 1.228 m from the base of the wall
12.16 (b) Total P = 98.89 kN/m, (c) at 2.546 m from the base of the wall
12.17 (b) Total P = 841.1 kN/m, (c) at 2.37 m from the base of the wall
12.18 (b) Total P = 1037.6 kN/m, (c) at 2.49 m from the base of the wall
12.19 (b) Total P = 860.19 kN/m, (c) at 2.35 m from the base of the wall
12.20 (b) Total P = 1064.3 kN/m, (c) at 2.460 m from the base of the wall
12.21 $P_a = 30.56$ kN/m
12.22 $P_a = 37.89$ kN/m
12.23 $P_a = 56.83$ kN/m
12.24 $P_a = 64.97$ kN/m
12.25 $P_p = 1808$ kN/m
12.26 $P_p = 1002$ kN/m
12.27 $P_p = 819.8$ kN/m
12.28 $P_p = 1354$ kN/m

13.1 (a) $q_{u,gross} = 2512$ kN/m^2, (b) $q_{u,net} = 2474$ kN/m^2, (c) $q_{d,net} = 966.8$ kN/m^2
13.2 (a) $q_{u,gross} = 2032$ kN/m^2, (b) $q_{u,net} = 1994$ kN/m^2, (c) $q_{d,net} = 774.8$ kN/m^2
13.3 (a) $q_{u,gross} = 2021$ kN/m^2, (b) $q_{u,net} = 1983$ kN/m^2, (c) $q_{d,net} = 770.6$ kN/m^2
13.4 (a) $q_{u,gross} = 2288$ kN/m^2, (b) $q_{u,net} = 2250$ kN/m^2, (c) $q_{d,net} = 877.1$ kN/m^2
13.5 (a) $q_{u,gross} = 1379$ kN/m^2, (b) $q_{u,net} = 1342$ kN/m^2, (c) $q_{d,net} = 410.3$ kN/m^2
13.6 (a) $q_{u,gross} = 1598$ kN/m^2, (b) $q_{u,net} = 1561$ kN/m^2, (c) $q_{d,net} = 495.7$ kN/m^2
13.7 (a) $q_{u,gross} = 1198$ kN/m^2, (b) $q_{u,net} = 1161$ kN/m^2, (c) $q_{d,net} = 362.3$ kN/m^2
13.8 (a) $q_{u,gross} = 1199$ kN/m^2, (b) $q_{u,net} = 1162$ kN/m^2, (c) $q_{d,net} = 362.7$ kN/m^2

Unit Conversion Table

English (U.S.) to SI	SI to English (U.S.)
Length	
1 ft = 0.3048 m = 30.48 cm = 304.8 mm	1 m = 3.2808 ft = 39.37 in
1 in = 25.4 mm = 2.54 cm	1 cm = 0.3937 in = 3.2808×10^{-2} ft
	1 mm = 0.039 in
Area	
1 ft^2 = 0.0929 m^2 = 929 cm^2	1 m^2 = 10.764 ft^2 = 1550 in^2
= 9.29×10^4 mm^2	1 cm^2 = 0.155 in^2
1 in^2 = 6.452×10^{-4} m^2 = 6.452 cm^2	1 mm^2 = 0.00155 in^2
= 645.2 mm^2	
Volume	
1 ft^3 = 0.0283 m^3	1 m^3 = 35.32 ft^3
1 in^3 = 16.387 cm^3 = 16387 mm^3	1 cm^3 = 0.06102 in^3
1 U.S. gallon = 3785 cm^3 = 3.78 liters	1 liter = 0.264 U.S. gallons
Mass	
1 lbm = 0.4536 kg	1 kg = 2.2046 lbm
Density (mass)	
1 lbm/ft^3 = 16.02 kg/m^3	1 kg/m^3 = 0.0624 lbm/ft^3
Unit weight	
1 lbs/ft^3 (pcf) = 0.157 kN/m^3	1 kN/m^3 = 6.36 lbs/ft^3 (pcf)
1 lbs/in^3 (pci) = 271.4 kN/m^3	= 0.00636 kips/ft^3
Force	
1 lb = 4.448 N	1 N = 0.2248 lb
1 kips = 4.448 kN	1 kN = 0.2248 kips
1 British (short) ton = 8.896 kN	1 kN = 0.1124 British (short) ton

(*continued*)

English (U.S.) to SI	SI to English (U.S.)
Stress (Pa = N/m²)	
1 lbs/in² (psi) = 6.895 kPa	1 kPa = 0.145 lbs/in² (psi)
1 kips/in² = 6.895 MPa	1 MPa = 0.145 kips/in²
1 lbs/ft² (psf) = 47.88 Pa	1 Pa = 0.021 lbs/ft² (psf)
1 kips/ft² = 47.88 kPa	1 kPa = 0.021 kips/ft²
Moment	
1 lb-in = 112.98 N-mm	1 N-m = 0.7375 lb-ft = 8.851 lb-in
1 lb-ft = 1.3558 N-m	
Energy	
1 ft-lb = 1.3558 Joule	1 Joule = 0.7375 ft-lb
Acceleration	
1 ft/sec² = 0.3048 m/sec²	1 m/sec² = 3.2808 ft/sec²
	1 cm/sec² = 0.3937 in/sec²
	= 0.032808² ft/sec²

Some convenient numbers and relationships

1 G (gravitational acceleration) = 9.81 m/sec² = 981 cm/sec² = 981 gals = 32.18 ft/sec²

1 kg force = 1 kg (mass) × 9.81 m/sec ² = 9.81 Newton =9.81 × 10^{-3} kN

γ_w (unit weight of water) = 9.81 kN/m³ = 62.4 lb/ft³

CIVIL ENGINEERING

SOIL MECHANICS FUNDAMENTALS

While many introductory texts on soil mechanics are available, most are either lacking in their explanations of soil behavior or provide far too much information without cogent organization. More significantly, few of those texts go beyond memorization of equations and numbers to provide a practical understanding of why and how soil mechanics work.

Based on the authors' more than 25 years of teaching soil mechanics to engineering students, ***Soil Mechanics Fundamentals*** presents a comprehensive introduction to soil mechanics, with emphasis on the engineering significance of *what soil is, how it behaves,* and *why it behaves that way.* Concise, yet thorough, the text is organized incrementally, with earlier sections serving as the foundation for more advanced topics. Explaining the varied behavior of soils through mathematics, physics, and chemistry, the text covers:

- Engineering behavior of clays
- Unified and AASHTO soil classification systems
- Compaction techniques, water flow and effective stress
- Stress increments in soil mass and settlement problems
- Mohr's Circle application to soil mechanics and shear strength
- Lateral earth pressure and bearing capacity theories

Each chapter is accompanied by example and practice problems that encourage readers to apply learned concepts to applications with a full understanding of soil behavior fundamentals. With this text, engineering professionals as well as students can confidently determine logical and innovative solutions to challenging situations.

Cover photo:
Kansai International Airport during Phase II construction in 2003.
Photo courtesy by Kansai International Airport Land Development Co.

K12080

ISBN: 978-1-4398-4644-5
90000
9 781439 846445

CRC Press
Taylor & Francis Group
an **informa** business
www.crcpress.com

6000 Broken Sound Parkway, NW
Suite 300, Boca Raton, FL 33487
270 Madison Avenue
New York, NY 10016
2 Park Square, Milton Park
Abingdon, Oxon OX14 4RN, UK

www.crcpress.com